TREATMENT OF COLLAPSIBLE SOIL USING ENCASED STONE COLUMNS

By

Nesreen Al-Obaidy

A thesis submitted to
the University of Birmingham
for the degree of
DOCTOR OF PHILOSOPHY

School of Engineering
College of Engineering and Physical Sciences
The University of Birmingham
March 2017

UNIVERSITY OF BIRMINGHAM

University of Birmingham Research Archive

e-theses repository

This unpublished thesis/dissertation is copyright of the author and/or third parties. The intellectual property rights of the author or third parties in respect of this work are as defined by The Copyright Designs and Patents Act 1988 or as modified by any successor legislation.

Any use made of information contained in this thesis/dissertation must be in accordance with that legislation and must be properly acknowledged. Further distribution or reproduction in any format is prohibited without the permission of the copyright holder.

ABSTRACT

Stone columns are widely used as structural elements to transfer loads from the superstructure to the underlying soil strata. They are preferred in many loading situations due to the simplicity, short duration, and cheap cost of their construction. However, their performance is mainly affected by the lateral support exerted by the host ground. Unless they are encased, they are largely not applicable for treating some types of soil, such as collapsible deposits (which could lose the required confinement upon load or inundation). A search of the literature revealed few studies that focused on the behaviour of a granular column installed into metastable soil, and the impact of its encasement. Also, employing electrical resistivity survey, which may offer a useful mapping tool to monitor the hidden subsurface of the composite cell of the column and the surrounding soil and detect any local changes in such a system, has not been considered previously. This study examined the failure mechanism and stress-settlement characteristics of a footing-type foundation resting on untreated soil (US), soil treated with an ordinary stone column (OSC), and soil treated with an encased stone column (ESC) into artificial loess deposits subjected to inundation. The investigation was carried out by means of conventional geotechnical laboratory work and the electrical resistivity tomography method. In addition, an analytical solution using a MATLAB script was presented to determine the load carrying capacity of the reinforced foundation and to validate the experimental results.

A scaled-down model of a typical encased stone column in an artificial loess matrix was constructed in the lab (dimensions of the column: 40 mm diameter x 360 mm length; dimensions of the soil bed cell: 349 mm diameter x 360 mm depth). The experimental model was subjected to a series of conventional and unconventional load tests, in the presence and absence of resistivity measurements, under controlled soaking conditions. One dry and two partially saturated cases of the soil bed (introducing 2.73 and 6.15 L of water), and two wetting scenarios, were investigated before any increment of load and after a stress of 100 kPa.

The outcomes of the physical model in the three test chambers demonstrated the efficiency of using an encased stone column over the ordinary stone column and the untreated collapsible soil. Both the ultimate bearing capacity and the reduction in compressibility increased when using the encased stone column. The improvement was related to the degree of saturation of the host soil; the higher the degree of saturation, the greater the improvement achieved.

The results of the resistivity tomography system offered a valuable window into the soil-column interface, subjected to varying loads and saturation conditions. The soil conductivity was very sensitive to load-induced and moisture-induced variations during collapse.

The analytical model illustrated that the enhancement in the ultimate bearing capacity of the reinforced column is influenced in proportion to variations in both the degree of saturation and matric suction. Also, it increases when increasing the tensile strength of the geotextile and the angle of internal shear resistance of the column fill material. However, it decreases when the diameter of the column expands. The theoretical results strongly agreed with the experimental data.

DEDICATION

To the loving memory of my father

To my beloved mother, who was always so patient and understanding, it would not have been possible without her prayers and motivational words

To my wonderful brothers, sisters, and their families for all their love, support, and encouragement

To my lovely husband, Assad and my kids, Ahmed, Zahraa, and Ali, I am entirely thankful for having you in my life and for all the acceptance, backing, and inspiration that you gave me, and the sacrifices that you made during the challenging period of my study

ACKNOWLEDGEMENTS

First of all, I would like to express my deep and sincere gratitude to my supervisor, Professor Ian Jefferson, for his unconditional enthusiasm, inspiration, and guidance throughout the entire study; without his support the work of this PhD would have been very difficult to tackle. Also, I would like to gratefully acknowledge my co-supervisor Dr Gurmel Ghataora for his supervision, assistance and encouragement.

I cannot fully express my gratitude to Professor Nigel Cassidy for all his support, patience, and regulations regarding the geophysical model.

I am particularly very grateful to the laboratory technician Mr Sebastian Ballard for his enormous effort, creativeness, and invaluable assistance in the laboratory.

I would also like to convey my great thanks to Dr Thomas Günther for providing BERT software.

My special thanks to the reviewers, Professor David Chapman and Dr Alexander Royal, for their valued feedbacks at the annual progress review meetings during the three year period of my study.

I would like to gratitude all the technicians at the Civil Engineering Laboratories for their unconditional support.

Many thanks to all my friends for their support and encouragement and to my colleagues in the Department of Civil Engineering especially: Omar Abubaker, Saif Alzabeebee, Anna Faroqy, Christopher Shaw, Jabar Rasul, Atiku Sadiq , Maliha Samin, Sahand Moshirian, Roxana Amini, and post-doctoral researcher Giulio Curioni for their support, discussions and sharing literature.

My thanks to my friend in Chemical Engineering Shahad Al-Najjar who always gives her kind wishes and supportive words.

Also, Mr Sam Birch is acknowledged for his assistance in proofreading.

Finally, I would like to present my profound thanks to the Iraqi Ministry of Higher Education and Scientific Research for sponsoring this work and to the University of Thi-qar for awarding the study leave. The staffs of the Iraqi Cultural Attaché in London are greatly acknowledged, specifically the Administrator, Mr Ali Al-Rubaie.

TABLE OF CONTENTS

ABSTRACT…… I
DEDICATION ……....III
ACKNOWLEDGEMENTS…….. IV
TABLE OF CONTENTS…….. ..V
LIST OF FIGURES…… XII
LIST OF TABLE……..XVIII
ABBERAVATIONS…….. ..XX
CHAPTER ONE……...1
1 INTRODUCTION.....1
1.1. Introduction.....…… ...1
1.2. Background...…… …..1
1.3. Geophysical Testing in Monitoring the Performance of Stone Columns…..…….. 4
1.4. Problem Context and Research Questions……...…….……4
1.5. Research Aim and Objectives 5
1.6. Anticipated Contribution.....6
1.6.1 Key Gaps in Existing Literature.....6
1.6.2 What is the Focus on 7
1.6.3 What Contribution to Fill the Gaps 7
1.7. Thesis Outline 8
1.8. Summary 9
CHAPTER TWO...…….....10
2 LITERATURE REVIEW OF STONE COLUMNS…….....10
2.1. Introduction.....10
2.2. Ordinary Stone Columns (OSC) 10
2.2.1. Historical Background…….....11
2.2.2. Methods of Construction.....11
2.2.3. Factors Affecting the Behaviour of a Single Stone Column 13
2.2.3.1. Properties and Type of Soil...…… .13
2.2.3.2. Properties of Stone Column Material…… 14
2.2.3.3. Stone Column Geometry...…… 15
2.2.3.4. Loading Type and Arrangement...……..16
2.2.4. Factors Affecting the Behaviour of a Group of Stone Columns……... .16
2.2.4.1. Spacing...…… 17
2.2.4.2. Arrangement...…….....18

2.2.4.3. Loading Area...……...19
2.2.5. Load Transfer and Failure Mechanism…….…..19
2.2.6. Unit Cell Concept….....20
2.2.7. Special Improvement of Stone Columns.....21
2.2.8. Studies on Stone Columns 21
2.2.8.1. Model Studies……..…21
2.2.8.2. Geophysics……..…22
2.3. Encased Stone Columns (ESC).....25
2.3.1. Installation Technique for Encased Stone Columns 25
2.3.1.1 Displacement Method……..…25
2.3.1.2 Replacement Method……..….26
2.3.2. Factors Affecting Performance of Encapsulated Stone Columns and Failure Mechanism...28
2.3.3. Ultimate Carrying Capacity 29
2.3.4. Settlement 30
2.3.5. Previous Laboratory Studies on Reinforced Stone Columns 30
2.3.5.1. Type of Host Soil…….....31
2.3.5.2. Fill Material……...31
2.3.5.3. Geosynthetics Used……. ...32
2.3.5.4. Soil Bed Formation…….....32
2.3.5.5. Column Construction…….....32
2.3.5.6. Loading Arrangement…….....32
2.3.5.7. Modelling Inundation in Previous Studies..……..….33
2.3.5.8. Laboratory Modelling of Encased Stone Column Acting on Collapsible Soil…… ..33
2.4. Summary 43
CHAPTER THREE ……..…….....45
3 MODELLING THE HOST GROUND……. 45
3.1. Introduction.....45
3.2 Modelling the Meta-Stable Soil in the Laboratory 45
3.3 Previous Methods and their Feasibility in Producing a Large Specimen 46
3.4 Selecting the Method and the Material Used in this Study 49
3.5 Materials 49
3.6. Sample Preparation 52
3.7 Single and Double Oedometer Collapse Tests.....53
3.8 Errors in Laboratory Tests 53
3.9 Repeatability of the Collapse Test 54
3.10 Experiments on Soil (A) and ECC 54

3.10.1 Index Properties, Specific Gravity, and Particle Size Distribution Curves for Different Mixtures……..54
3.10.2 Compaction Tests.....57
3.10.3 Effect of Clay Content on the Specimen of Ground Silica after Allowing Air Drying 58
3.10.4 Identifying the Preparation Water Content 63
3.10.5 Effect of Clay Content on the Specimen of Ground Silica with Oven Drying (5 hours).....65
3.10.6 Effect of Clay Content on the Specimen of Ground Silica with Oven Drying (20 hours).....68
3.10.7 Effect of Void Ratio 70
3.10.8 Results of Double Oedometer Tests for Soil (A) 71
3.11 Experiment on Soil (B) and ECC.....72
3.12 Mixture Used as Host Ground 74
3.13 Shear Strength Parameter of Soil Selected as Host Ground 75
3.14 Soil Water Characteristic Curve of Soil chosen as Host Ground.....77
3.15 Summary 78
CHAPTER FOUR.....79
4 MODEL FOOTING, EXPERIMENTAL PROCEDURES, AND TESTING PROGRAMME….....79
4.1. Introduction.....79
4.2. Selection of the Encased Stone Column Footing Model 79
4.2.1. Loading Arrangement 79
4.2.2. Rigidity of the Footing.....80
4.2.3. Dimensions of the Test Cell and the Pile Geometry 81
4.2.4. Scaling Down the Material 81
4.2.5. Representing Underground Water Movement 81
4.3 Materials 82
4.3.1. Soil 82
4.3.2. Fill Material 82
4.3.3. Geotextile.....83
4.3.4. Sand.....84
4.3.5. Gravel.....85
4.3.6. Casting Powder 85
4.3.7. Nylon String.....85
4.4 Lab Equipment and Apparatus.....85
4.4.1. Test Cells and Their Accessories 85
4.4.2. Loading Frame and Axial Loading System 85
4.4.3. Dial Gauges.....86
4.4.4. Mixer.....86

4.4.5. Auger Drilling 87
4.4.6. PVC Circular Plate 87
4.4.7. Compaction Tools 87
4.4.8. Water Reservoir 88
4.5. Formation of the Soil Bed 88
4.5.1. Formation of the Filter Layer 88
4.5.2. Greasing the Inner Faces of the Test Cell 89
4.5.3. Mixing the Soil 89
4.5.4. Compacting the Soil inside the Test Tank 89
4.5.5. Sealing the Compacted Sample 91
4.5.6. Drying Process 91
4.6. Construction of Ordinary Stone Column (OSC) 92
4.7. Construction of Encased Stone Column (ESC) 93
4.8. Testing Programme 94
4.9. Running the Test 95
4.10. Strategy for Wetting the Deposits inside the Test Cell 97
4.11. Detecting the Shape of Failure of OSC and ESC 98
4.12. Feasibility Test 100
4.13. Repeatability of Main Tests 102
5.10. Summary 103
CHAPTER FIVE 104
5 DESIGN, CONSTRUCTION, CALIBRATION, AND TEST RUNNING OF THE AUTOMATED MULTI-ELECTRODE RESISTIVITY CELLS 104
5.1. Introduction 104
5.2. Electrical Resistivity Tomography (ERT) 104
5.2.1. Concept of Electrical Resistivity 104
5.2.2. Factors Controlling Resistivity Magnitudes 105
5.2.3. Advantages of ERT Over Other Geophysical Techniques 107
5.2.4. Recent Related Studies 107
5.2.5. Electrical Resistivity Method in Loess Soil 107
5.2.6. Circular Resistivity Cell Calibration 112
5.3. Configuration of the Current Resistivity System 113
5.4. Design and Construction of the Multi-Electrode Resistivity Cells 116
5.5. Data Acquisition System 118
5.5.1. Resistivity Meter 118
5.5.2. Power Source 118

5.5.3. Laptop Computer 118
5.5.4. TIGIMG Control Software.....119
5.6. Inversion Technique.....119
5.7. Calibration of the Cylindrical Test Cells 120
5.7.1. Calibration of the Hanna Conductivity Meter.....121
5.7.2. Measuring Resistivity Using the Calibrated Hanna Probe.....121
5.7.3. Measuring Tap Water Resistivity Using the Acquisition System.....122
5.8. BERT and Imaging the Resistivity of Tap Water 124
5.9. Experimental Geometric Factors 126
5.10. Conductivity of Water to Introduce to the Test Soil 129
5.10.1. Identification of Water Resistivity Using a Calibrated Hanna Probe 129
5.10.2. Selecting an Appropriate Salt Concentration for the Required Conductivity 130
5.10.3. Effect of Increasing the Conductivity of Tap Water on General Geotechnical Properties ..132
5.11. Running the Loading Test while Taking Resistivity Measurements of the Tested Cells 133
5.12. Measurement Errors.....136
5.13. Summary 137
CHAPTER SIX……..……...138
6 RESULTS AND DISCUSSIONS.....……138
6.1. Introduction.....138
6.2. Results of the Physical Model.....138
6.2.1. Tests 1, 2, and 3 (Dry State).....138
6.2.1.1. Aim of Tests and General Description (Dry State).....138
6.2.1.2. Checking the Homogeneity of the Deposit (Dry state) 138
6.2.1.3. Time-Settlement and Stress-Settlement Characteristics of the Foundation (Dry State)139
6.2.1.4. Deformation of the Soil Surface (Dry State).....141
6.2.1.5. The Horizontal Deformation of the Tank (Dry State).....142
6.2.1.6. Investigating the Soil Surface after Completing the Tests (Dry State) ..……142
6.2.1.7. Investigating the Failure Profile of the Column after Completing the Tests (Dry State)..……...143
6.2.2. Tests 4, 5, and 6 (Wetting the Test Cell with 2.73 L of Water: Wetting Prior to Loading)…144
6.2.2.1. Aim of Tests and General Description (Wetting with 2.73 L of Water).....144
6.2.2.2. Checking the Homogeneity of the Host Ground (Wetting with 2.73 L of Water).....144
6.2.2.3. Admitting Water (Wetting with 2.73 L of Water) 145
6.2.2.4. Time-Settlement and Stress-Settlement Characteristics of the Foundation (Wetting with 2.73 l of Water) 145
6.2.2.5. Deformation of the Soil Surface (Wetting with 2.73 L of Water) 148

6.2.2.6. Deformation of the Tank (Wetting with 2.73 L of Water).....149

6.2.2.7. Investigating the Soil Surface after Completing the Tests (Wetting with 2.73 L of Water) ... ……. 150

6.2.2.8. Investigating the Water Profile after Completing the Tests (Wetting with 2.73 L of Water) ....……..……..151

6.2.2.9. Investigating the Failure Profile of the Column after Completing the Tests (Wetting with 2.73 L of Water)……..152

6.2.3. Tests 7, 8, and 9 (Wetting the Test Cells with 6.15 L of Water: Wetting Prior to Loading) ..……...……...153

6.2.3.1. Aim of Tests and General Description (Wetting with 6.15 L of Water)……...153

6.2.3.2. Checking the Homogeneity of the Host Ground (Wetting with 6.15 L of Water)…….153

6.2.3.3. Admitting Water through the Soil Deposits (Wetting with 6.15 L of Water)……154

6.2.3.4. Time-Settlement and Stress-Settlement Characteristics of the Foundation (Wetting with 6.15 l of water)…….……...…….154

6.2.3.5. Deformation of the Soil Surface (Wetting with 6.15 L of Water)…….155

6.2.3.6. Movement of the Tank (Wetting with 6.15 L of Water)……....156

6.2.3.7. Investigating the Soil Surface after Completing the Tests (Wetting with 6.15 L of Water).....……...157

6.2.3.8. Investigating the Water Profile after Completing the Tests (Wetting with 6.15 L of Water)...……..... 157

6.2.3.9. Investigating the Failure Profile of the Column after Completing the Tests (Wetting with 6.15 L of Water)…….158

6.2.4. Tests 10, 11, and 12 (Wetting the Test Cells with 6.15 L of Water: Wetting after Loading) ……159

6.2.4.1. Aim of Tests and General Description (Soaking after Stress of 100 kPa)……159

6.2.4.2. Checking the Homogeneity of the Host Ground (Soaking after Stress of 100 kPa) …...……..…….....159

6.2.4.3. Admitting Water through the Soil Deposits (Soaking after Stress of 100 kPa).....160

6.2.4.4. Stress-Settlement Characteristics of the Foundation (Soaking after Stress of 100 kPa) .....……160

6.3. Results of the Geophysical Survey.. 162

6.3.1. Circular Configuration. 162

6.3.1.1. General Trend of the Measurement of the Three Chambers.....162

6.3.1.2. The Data Corresponding to the Area Surrounding the Column of the Three Chambers …...……..……...166

6.3.1.3. Test 13 (Resistivity Measurements of the Test Chamber of Untreated Soil)……167

6.3.1.4. Test 14, Resistivity Measurements for the OSC Test Chamber……..171

6.3.1.5. Test 15, Resistivity Measurements for the ESC Test Chamber……..174

6.3.2. Vertical Arrays 178
6.4. Summary 181
CHAPTER SEVEN 183
7 THEANALYTICAL MODEL 183
7.1. Introduction 183
7.2. The Adopted Analytical Model 183
7.3 Basic Theory behind the Derivation of the New Analytical Model 183
7.4 MATLAB Code 186
7.5 Sensitivity of the Analytical Model 186
7.5.1. Influence of the Tensile Strength of the Geotextile on the Ultimate Bearing Capacity of the Encased Foundation 188
7.5.2. Influence of the Stone Column Diameter on the Ultimate Bearing Capacity of the Encased Foundation 190
7.5.3. The Influence of the Angle of Internal Shear Resistance of the Column Material on the Ultimate Bearing Capacity of the Encased Foundation 191
7.6. Validation of the Experimental Results 193
7.7. Summary 194
CHAPTER EIGHT 195
8 CONCLUSIONS AND RECOMMENDATIONS 195
8.1. Introduction 195
8.2. Conclusions 195
8.2.1. Conclusions from Material Development 195
8.2.2. Conclusions from the Physical Model 196
8.2.3. Conclusions from the Geophysical Survey 197
8.2.4. Conclusions from the Analytical Model 198
8.3. Recommendations for Future Work 199
REFERENCES 201
APPENDIX (A) 214
APPENDIX (B) 228
APPENDIX (C) 254
APPENDIX (D) 259
APPENDIX (E) 265

LIST OF FIGURES

Figure 1.1: Load transfer mechanism for (a) a rigid inclusion (b) a stone column (redrawn from Hughes and Withers 1974), where: σ_v: ultimate load; τ: shear stress; σ_b: end bearing stress; and σ_r: radial stress 2
Figure 1.2: Percentages of studies regarding encased stone columns in different types of soils 4
Figure 2.1: (a) Dry-top feed method and (b) Dry-bottom feed method (c) Wet-top feed presented by Taube et al. (2002) 12
Figure 2.2: Improvement factor against area ratio for different angles of internal friction, ϕc (Priebe, 1995) 14
Figure 2.3: A typical layout of stone columns (a) Triangular Arrangement, (b) Square Arrangement, (c) Hexagonal Arrangement (redrawn from Balaam & Poulos, 1983), where: d_e: effective diameter of the composite cell; and S: spacing between two stone columns. 18
Figure 2.4: Modes of failure of stone columns (redrawn from Barksdale and Bachus, 1983) 19
Figure 2.5: Unit cell idealisations (redrawn from Barksdale and Bachus, 1983), where: d_e: effective diameter of the composite cell; d: diameter of stone column; l: length of stone column; σ_s: Stress acting on soil; σ_c: Stress acting on the column 20
Figure 2.6: Displacement method (Alexiew et al., 2005) 26
Figure 2.7: Replacement method (Gniel & Bouazza, 2010) 26
Figure 2.8: Installation of partially encased stone column in the field (Lee et al., 2008) 27
Figure 2.9: Inserting a geogrid net into a pre-bored and partially constructed stone column (Lee et al., 2008) 27
Figure 2.10: Construction of a partially encased stone column in soil (Lee et al., 2008) 28
Figure 3.1 : Comparison of the collapsibility of the undisturbed Malan loess from China and the reconstituted air fall method samples by Assallay et al. (1997) 48
Figure 3.2: Flow chart representing the schematic procedure to produce a reconstituted sample and a compacted sample of collapsible soil (Jotisankasa, 2005) 48
Figure 3.3: Compaction curves of the three soils, (a) Soil A, (b) Soil B, (C) ECC 51
Figure 3.4: Soil sample preparation using the wet paste method 52
Figure 3.5: Particle distribution curve of the artificial loess for different silica to China clay mixture in comparison to limits of natural loess 56
Figure 3.6: Compaction test results for different mixtures of Soil (A) and China clay ((a) Gs=2.65 and (b) Gs=2.64) 57
Figure 3.7: The typical time settlement curve for loading, soaking, and reloading the soil specimen 60
Figure 3.8: The collapse upon wetting with respect to time 61
Figure 3.9: Series of single oedometer tests on specimens of ground silica at different clay mixing ratios, soaking at 200 kPa 62
Figure 3.10: Clay content versus collapse potential for samples with 48 hours air drying 63
Figure 3.11: Hydro-collapse test, 8% water content (Collapse Test No. 4) 64
Figure 3.12: Hydrocollapse test, 15% water content (Collapse Test No. 5) 64
Figure 3.13: Initial water content versus collapse potential 65
Figure 3.14: Clay content versus collapse potential for samples dried for 5 hours 66
Figure 3.15: Series of single oedometer tests on specimens of ground silica at different clay mixing ratios (5 hours drying) 67
Figure 3.16: Clay content versus collapse potential for samples after drying for 20 hours 68

Figure 3.17: Series of single oedometer tests on specimens of ground silica at different clay mixing ratios, after drying for 20 hours 69
Figure 3.18: Single oedometer test for two different initial void ratios 70
Figure 3.19: One dry and one soaked artificial sample after loading is completed in the double oedometer test 71
Figure 3.20: Double and single oedometer tests results for a specimen with 85% ground silica, 15% China clay, and 12% initial water content after 48 hours air drying 71
Figure 3.21: Double and single oedometer tests results for a specimen with 80% ground silica, 20% China clay, and 12% initial water content after 48hours air drying 72
Figure 3.22: : Dry unit weight versus liquid limit (taken from Das, 2014) 73
Figure 3.23: Single oedometer results of specimens (A) and (B) with 20% water content 73
Figure 3.24: Single oedometer results of this study for artificial specimens (A) and (B), compared to natural loess soil from the Star Lane site, Essex (tested by Miller, 2002) 74
Figure 3.25: Shear stress versus shear displacement of compacted artificial loess 76
Figure 3.26: The failure envelope of the compacted artificial loess 77
Figure 3.27: SWCC of the compacted artificial loessial soil 78
Figure 4.1: The set up and model geometry (drawing is not to scale) 80
Figure 4.2: Sieve analysis for stone used as a fill material 83
Figure 4.3: Sieve analysis of the Leighton Buzzard Sand used 84
Figure 4.4: The loading frame and the experimental setup 86
Figure 4.5: The PVC plate placed over the test cell used for load eccentricity 87
Figure 4.6: Compaction of the sand layer on top of a gravel layer, using a wooden rod 89
Figure 4.7 (a): The level of the plate is checked with a spirit level, (b): Compaction process using hammer 90
Figure 4.8: Checking the layer level (a) Using a spirit level (b) Using a measurement rule 91
Figure 4.9: The three cells covered with three well-sealed nylon sheets after compacting 91
Figure 4.10: Auguring the hole and compacting fill material to construct the ordinary stone column ..92
Figure 4.11: The ordinary stone column constructed at the centre of the test cell 93
Figure 4.12: Wrapping the geotextile around the steel tube 93
Figure 4.13: Stitching the geotextile to form a cylinder encasement 94
Figure 4.14: Ensuring the load lined up with the centre of the test cell 96
Figure 4.15: Left: Vacuuming aggregate from the stone column hole; Right: collecting the vacuumed aggregate in the storage container 98
Figure 4.16: Left: Mixing the cast powder with water; Right: Mixing the cast paste with the vacuumed aggregate 99
Figure 4.17: The cast paste was poured into the empty hole in the centre of the host ground 99
Figure 4.18: The cast column is ready to be studied for its failure shape after removing the surrounding soil 99
Figure 4.19: Water content profile of the soil deposit 101
Figure 4.20: Dry unit weight through the soil layers in three bore holes 101
Figure 5.1: Popular electrode configrations used in resistivity surveys and their geometric factors (Loke, 1999) 105
Figure 5.2: Examples of changing the water content profile with respect to time (Jackson et al., 2002) 108
Figure 5.3: The positions of the horizontal rings of the electrodes on the test cell 113
Figure 5.4: Different electrode configurations for the circular cell 115

Figure 5.5: Typical vertical electrode configurations 116
Figure 5.6: Fixing electrodes into holes: (a) View from outside of the test cell (b) View from inside the test cell 117
Figure 5.7: The resistivity cell after installing the wiring 118
Figure 5.8: The acquisition system 119
Figure 5.9: The three grids of inversion for a 2D problem: (a) Parameter mesh (b) Secondary mesh (c) Primary mesh (Günther et al., 2006) 120
Figure 5.10: Measuring the resistivity of tap water using the Hanna meter probe and the thermometer 122
Figure 5.11: Measuring the resistivity of tap water using the acquisition system 123
Figure 5.12: Resistant measurements for rings in Tank 1 123
Figure 5.13: Resistant measurements for rings in Tank 2 124
Figure 5.14: Resistant measurements for rings in Tank 3 124
Figure 5.15: Parameter mesh showing the 212 electrodes, 192 electrodes of the six rings and 20 electrodes of the vertical arayes, their positions in the xy plane, and the geometry of the tank 125
Figure 5.16: The secondary mesh 125
Figure 5.17: Inversion by BERT showing apparent resistivity of tap water of 111 Ohm.m 126
Figure 5.18: Typical inversion results for tap water (input data is resistance measurement) 126
Figure 5.19: Experimental geometric factors of the six rings in Tank 1 for 768 readings 127
Figure 5.20: Experimental geometric factors of the six rings in Tank 2 for 768 readings 127
Figure 5.21: Experimental geometric factors of the six rings in Tank 3 for 768 readings 128
Figure 5.22: Typical geometric factors for one ring 128
Figure 5.23: Resistivity and conductivity of tap water at different temperatures 129
Figure 5.24: Resistivity and conductivity of tap water + 0.03 g NaCl at different temperatures 130
Figure 5.25: Resistivity and conductivity of tap water + 0.04 g NaCl at different temperatures 130
Figure 5.26: Resistivity and conductivity of tap water + 0.05 g NaCl at different temperatures 131
Figure 5.27: Resistivity and conductivity of tap water + 0.06 g NaCl at different temperatures 131
Figure 5.28: Resistivity and conductivity of tap water + 0.07 g NaCl at different temperatures 131
Figure 5.29: Resistivity and conductivity of tap water + 0.08 g NaCl at different temperatures 132
Figure 5.30: Changes in resistivity with respect to variations in temperature for different NaCl concentrations 132
Figure 5.31: Collapse characteristics for different salt concentrations 133
Figure 5.32: Aspects of sample preparation for the resistivity cells 134
Figure 5.33: Providing the experiment with an inundation source and fixing the dial gauges in their positions 135
Figure 5.34: Connecting one ring to the acquisition system and taking resistivity measurements 136
Figure 6.1: Time-Settlement curve of the foundation resting on untreated collapsible soil and treated with both ordinary and encased stone columns (dry state) 140
Figure 6.2: Stress-settlement curve of the foundation resting on untreated collapsible soil and treated with both ordinary and encased stone columns (dry state) 140
Figure 6.3: Collected readings of two dial gauges placed on left)D.G1) and right (D.G2) of the foundation, on the top soil surface, for untreated collapsible soil US, soil treated with OSC, and soil treated with ESC (dry state) 141
Figure 6.4: Lateral movement of the side wall of the test cells with respect to the vertical stress of the ordinary and encased stone columns (dry state) 142

Figure 6.5: The mode of failure on the surface of the load cells (a) US, (b) OSC, (c) ESC, on left the original photo and on right the cracks are highlighted....143
Figure 6.6: No bulging was observed for either OSC or ESC columns 144
Figure 6.7: Time-settlement curve (wetting with 2.7 L) 145
Figure 6.8 : Untreated soil (on right) and OSC (on left) under stress of 400kPa 146
Figure 6.9: Untreated soil (on right) and OSC (on left) under stress of 800 kPa 146
Figure 6.10: OSC (on right) and ESC (on left) under stress of 400 kPa 147
Figure 6.11: OSC (on right) and ESC (on left) under stress of 800 kPa 147
Figure 6.12: The stress-settlement curve of the foundation resting on untreated collapsible soil and treated with both OSC and ESC (wetting with 2.73 L) 148
Figure 6.13: The collected readings of two dial gauges placed on left D.G1 and right D.G2 of the foundation, for untreated collapsible soil US, treated with OSC, and treated with ESC (wetting with 2.73 L of water)..149
Figure 6.14: Lateral movement of the side wall of the test cell with respect to the vertical stress of the ordinary and encased stone columns (wetting with 2.73 L)....149
Figure 6.15: cracks observed after completion of loading on untreated soil US and before removing the foundation, on left the original photo and on right the cracks are highlighted 150
Figure 6.16: Cracks observed after completion of loading on untreated soil US and removing the foundation and sand layer, on left the original photo and on right the cracks are highlighted 150
Figure 6.17: Very fine cracks around the foundation resting on the OSC, on left the original photo and on right the cracks are highlighted 150
Figure 6.18: The change in water content after completing the test (initial wc=9.1%) 152
Figure 6.19: Failure profile under soaking with 2.73 L of water for (a) ESC (b) OSC (c) OSC with dimensions 153
Figure 6.20: The time-settlement curve (soaking with 6.15 L) 154
Figure 6.21: Stress-settlement behaviour (wetting with 6.15 L) 155
Figure 6.22: Readings from observation points on the soil surface at different distances from the foundation 156
Figure 6.23: The lateral movement against vertical stress of the tanks associated with the OSC and ESC ..157
Figure 6.24 : Water content profile after digging out....158
Figure 6.25: Failure profile under soaking with 6.15 L of water for (a) ESC, (b) OSC, (c) OSC with dimensions 159
Figure 6.26: Different soaking patterns (test cell of untreated soil) 161
Figure 6.27: Different soaking pattern (test cell of OSC) 161
Figure 6.28: Different soaking patterns (test cell of ESC) 161
Figure 6.29: Inversion results for test tank with untreated soil at different loading stages 163
Figure 6.30: Inversion results for test tank with the OSC at different loading stages 163
Figure 6.31: Inversion results for test tank with the ESC at different loading stages....164
Figure 6.32: Vertical slice through the inversion results for the tank of untreated soil under loading up to 300 kPa....165
Figure 6.33: Vertical slice through the inversion results for the OSC tank under loading up to 300 kPa 165
Figure 6.34: Vertical slice through the inversion results for the ESC tank under loading up to 300 kPa 166
Figure 6.35: Inversion results of Ring 1 for tank filled with untreated soil only under different loading stages 168
Figure 6.36: Inversion results of Ring 2 for tank filled with untreated soil only under different loading stages 168

Figure 6.37: Inversion results of Ring 3 for tank filled with untreated soil only under different loading stages 169
Figure 6.38: Inversion results of Ring 4 for tank filled with untreated soil only under different loading stages 169
Figure 6.39: Inversion results of Ring 5 for tank filled with untreated soil only under different loading stages 170
Figure 6.40: Inversion results of Ring 6 for tank filled with untreated soil only under different loading stages 170
Figure 6.41: Inversion results of Ring 1 for tank filled with soil and OSC under different loading stages 171
Figure 6.42: Inversion results of Ring 2 for tank filled with soil and OSC under different loading stages 172
Figure 6.43: Inversion results of Ring 3 for tank filled with soil and OSC under different loading stages 172
Figure 6.44: Inversion results of Ring 4 for tank filled with soil and OSC under different loading stages 173
Figure 6.45: Inversion results of Ring 5 for tank filled with soil and OSC under different loading stages 173
Figure 6.46: Inversion results of Ring 6 for tank filled with soil and OSC under different loading stages 174
Figure 6.47: Inversion results of Ring 1 for tank filled with soil and ESC under different loading stages 175
Figure 6.48: Inversion results of Ring 2 for tank filled with soil and ESC under different loading stages 175
Figure 6.49: Inversion results of Ring 3 for tank filled with soil and ESC under different loading stages 176
Figure 6.50: Inversion results of Ring 4 for tank filled with soil and ESC under different loading stages 176
Figure 6.51: Inversion results of Ring 5 for tank filled with soil and ESC under different loading stages 177
Figure 6.52: Inversion results of Ring 6 for tank filled with soil and ESC under different loading stages 177
Figure 6.53: Resistivity values in the three chambers according to the configuration of the vertical arrays 179
Figure 6.54 : Resistivity of the three chambers under no stress and stress of 300 kPa (vertical arrays) 180
Figure 7.1: Unit cell model of encased stone column installed in collapsible soil (a) dry condition (b) partial saturation (c) full saturation 185
Figure 7.2: Bearing capacity of OSC and ESC for different degrees of saturation 187
Figure 7.3: Bearing capacity of OSC and ESC for different degrees of saturation 188
Figure 7.4: Bearing capacity of the foundation reinforced with a geotextile versus tensile strength of the geotextile (for different degrees of saturation).....189
Figure 7.5: Bearing capacity of the foundation reinforced with a geotextile versus tensile strength of the geotextile (for different suction) 189
Figure 7.6: Bearing capacity of the foundation reinforced with a geotextile versus degree of saturation (for different column diameters).....190
Figure 7.7: Bearing capacity of the foundation reinforced with geotextiles versus matric suction (for different column diameters).....191
Figure 7.8: Bearing capacity of the foundation reinforced with a geotextile versus degree of saturation (for different angles of internal friction of the stone column) 192
Figure 7.9: Bearing capacity of the foundation reinforced with a geotextile versus matric suction (for different angles of internal friction of the stone column) 192
Figure B.1: Liquid Limit curve of Soil (A) 229
Figure B.2: Liquid Limit curve of Soil (B) 230
Figure B.3: Liquid Limit Curve of English China Clay (ECC) 231
Figure B.4: Liquid Limit Curve of soil 100% ground silica M10 245
Figure B.5: Liquid Limit Curve of soil 95% ground silica M10 + 5% ECC.....245

Figure B.6: Liquid Limit Curve of soil 90% ground silica M10 + 10% ECC.....245
Figure B.7: Liquid Limit Curve of soil 85% ground silica M10 + 15% ECC.....246
Figure B.8: Liquid Limit Curve of soil 80% ground silica M10 + 20% ECC.....246
Figure B.9: Liquid Limit Curve of soil 75% ground silica M10 + 25% ECC.....246

LIST OF TABLES

Table 2-1: Requirements of different installation technique of stone columns and countries commonly employ them according to the literature (Nayak, 1987 and 1996; McKelvey & Sivakumar, 2000; Serridge, 2005; McCabe et al., 2009; Babu et al., 2012; Amini, 2014) 12
Table 2-2: Benefits and limitations of geophysical studies (Amini, 2014) 24
Table 3-1: Properties of Soil A, Soil B and ECC 50
Table 3-2: The severity of collapse according to the value of the collapse potential as presented by Jennings & Knight (1975) 53
Table 3-3: Index Properties ,specific gravity , grain size percentages of different mixtures of soil (A) and English China clay (ECC) 56
Table 3-4: Percentage of error for repetition of tests No. 1, 2, and 3 (see Section 3.9) 63
Table 3-5: Percentage of error for repetitions tests No. 4 and 5 (see Section 3.9) 65
Table 3-6: Percentage of error for repetition tests No. 6, 7, 8, and 9 (see Section 3.9) 66
Table 3-7: Percentage of error for repetition tests No. 10, 11, 12, 13, and 14 (see Section 3.9) 68
Table 3-8: Percentage of error for repeated test with initial void ratio of 1.33 (Test No. 15), see Section 3.9 70
Table 3-9: Percentage of error for repetition tests of double collapse test for two mixtures, ground silica with 15% and 20% clay content (see Section 3.9) 72
Table 3-10: Percentage of error for repeated collapsible test for soil (B) (see Section 3.9) 74
Table 4-1: Physical and mechanical properties of the soil 82
Table 4-2: Physical and mechanical properties of the crushed stone 83
Table 4-3: Properties and specification of geotextile 84
Table 4-4: The testing programme 95
Table 4-5: Time required to transfer the water from the reservoir to the soil tanks 98
Table 4-6: Average values of water content and dry unit weight 101
Table 4-7: The percentage errors of readings of settlement with loading for Tests 1, 2, and 3 (dry case) and their repetitions 102
Table 4-8: Percentage errors of readings of settlement with loading for Tests 4, 5, and 6 (wetting with 2.73 l) and their repetitions 102
Table 4-9: The percentage errors of readings of settlement with loading for tests 7, 8, 9, 13, 14, and 15 (normal cells and resistivity cells) 103
Table 5-1: Dimensions of the resistivity tanks used 117
Table 5-2: The full specifications of Hanna Conductivity Probe HI 8733 121
Table 6-1: The homogeneity of the soil extruded from the middle of the tank for an ordinary stone column or encased stone column in Test 2 and Test 3, respectively (dry state) 139
Table 6-2: The homogeneity of the soil extruded to form the stone column or encased stone column for Test 5 and Test 6 (wetting with 2.73 L) 144
Table 6-3: The homogeneity of the soil extruded to form the ordinary stone column or encased stone column for Test 8 and Test 9 (wetting with 6.15 L) 153
Table 6-4: The homogeneity of the soil extruded from the middle of the tanks with the OSC and ESC for Test 11 and Test 12 (soaking after stress with 100 kPa) 159
Table 6-5: The deviation from Archie's law for the soil in the three chambers 167
Table 7-1: Parameter values and symbols used in the MATLAB script 186
Table 7-2: Comparison between the experimental results and the theoretical calculations 193

Table B-1: Specific gravity of Soil (A) 228
Table B-2: Specific gravity of Soil (B) 228
Table B-3: Specific gravity of English china Clay (ECC) 228
Table B-4: Liquid Limit calculations of Soil (A) 229
Table B-5: Liquid Limit calculations of Soil (B) 230
Table B-6: Liquid Limit calculations of English China Clay 231
Table B-7: Plastic Limit calculations of Soil (A) 232
Table B-8: Plastic Limit calculations of Soil (B) 232
Table B-9: Plastic Limit calculations of English China Clay (ECC) 233
Table B-10: Compaction test data for Soil (A) 234
Table B-11: Compaction test data for Soil (B) 235
Table B-12: Compaction test data for English China Clay (ECC) 236
Table B-13: Technical Properties of Soil A (Ground Silica M10) 237
Table B-14: Technical Properties of Soil B (Ground Calcium Carbonate) 238
Table B-15: Technical Properties of English China Clay of type Puroflo 50 provided by WBB Devon Clays LTD 239
Table B-16: Specific Gravity of different mixture of Ground Silica M10 (Soil A) and English China Clay (ECC) 241
Table B-17: Calculations of liquid limit for different mixture of ground silica Soil (A) and (ECC) 242
Table B-18: Calculations plastic limit for different mixture of ground silica Soil (A) and (ECC) 247
Table B-19: Compaction test data for mixture of 95% ground silica M10 and 5% English China Clay (ECC) 249
Table B-20: Compaction test data for mixture of 90% ground silica M10 and 10% English China Clay (ECC) 250
Table B-21: Compaction test data for mixture of 85% ground silica M10 and 15% English China Clay (ECC) 251
Table B-22: Compaction test data for mixture of 80% ground silica M10 and 20% English China Clay (ECC) 252
Table B-23: Compaction test data for mixture of 75% ground silica M10 and 25% English China Clay (ECC) 253
Table D-1: The configuration of the thirty two electrodes over one ring, 128 measurements, C1 and C2: current electrodes, P1 and p2: Potential electrodes 259
Table D-2: The configuration of the thirty two electrodes over the two vertical arrays, 111 measurements, C1 and C2: current electrodes, P1 and p2: Potential electrodes 262

ABBERAVATIONS

τ	shear stress
Δ	total settlement of a stone column subjected to an external load and under inundation
γ	unit weight of soil
ϕ'	effective angle of shearing resistance of soil
ϕ'_c	effective angle of internal friction of the column material
σ'_{ro}	effective lateral soil stress
δ_1	elastic settlement of the column owing to the axial load
δ_2	settlement due to down drag force owing to consolidation of the nearby soil
δ_3	vertical settlement due to the lateral displacement of the column
δ_4	settlement of the soil strata located below the column‟s tip
ρ_a	apparent resistivity
σ_b	end bearing stress
σ_c	stress acting on the column
γ_{dry}	dry unit weight of soil
γ_{dry}	dry unit weight of fill material
$\gamma_{dry\ max}$	maximum dry unit weight of fill material
$\gamma_{dry\ min}$	minimum dry unit weight of fill material
Δe	change in void ratio
ρ_f	resistivity of fluid
σ_n-u_w	effective normal stress
σ_r	radial stress
σ_s	stress acting on soil
ρ_{sat}	resistivity of saturated soil
ρ_{sat}	resistivity of saturated soil
ρ_{unsat}	resistivity of unsaturated soil
σ_v	ultimate load
ΔV	difference in voltage between two potential electrodes
μ_s	Poisson's ratio of soil

2D	two dimensions
3D	three dimensions
4D	four dimensions
A	total area of the composite soil-column
a	an indicator of the tortuosity
A/A_c	area ratio
A_c	area of stone column
a_r	area replacement ratio
ave.	average
B	parameter
BERT	boundless electrical resistivity tomography
BRE	Building Research Establishment
c'	effective cohesion of soil
Cc	coefficient of curvature
C_p	collapse potential
CPT	cone penetration test
c_u	undrained shear strength
Cu	coefficient of uniformity
d	diameter of the stone column
D.O.T	double oedometer tests
D10	diameter of soil at which 10 percent of the soil particles are finer
D30	diameter of column material at which 30 percent of the material particles are finer
D50	diameter of soil at which 50 percent of the soil particles are finer
D60	diameter of column material at which 60 percent of the material particles are finer
D90	diameter of soil at which 90 percent of the soil particles are finer
DCPT	dynamic cone penetration tests
d_e	equivalent diameter of the composite cell of stone column and soil
d_e/d	spacing ratio
d_f	diameter of the fill material particle
d_t	depth of treatment
e	void ratio

E_c	modulus of elasticity of the column
E_c/ E_s	stone column-soil modular ratio
ECC	English china clay
e_o	initial void ratio
ERT	electrical resistivity tomography
E_s	modulus of elasticity of the soil
ESC	encased stone column
F	formation factor
F_i	factor of influence
F_{imp}	improvement factor
GPR	ground penetrating radar
G_s	specific gravity
h	soil depth
I	electrical current generated between the two current electrodes
k	geometric factor
k_o	coefficient of lateral earth pressure at rest
k_p	Rankine passive pressure coefficient for the column material
l	length of stone column
LL	liquid limit
m	soil parameter
m(i)	individual reading
n	porosity of the soil
OSC	ordinary stone column
PI	plasticity index
PL	plastic limit
R	electrical resistance of the ground
r_c	radius of the stone column
RD	relative density
S	columns spacing
s	degree of saturation
S.O.T	single oedometer tests
sd	Standard deviation

SPT	standard penetration test
SWCC	soil water characteristic curve
t	thickness of the geotextile
TDR	time domain reflectometry
T_s	tensile strength of geotextile
u_a-u_w	matric suction stress
US	untreated soil
w_p	water content of the filter paper
x	parameter that depends on the degree of saturation
α	resistivity temperature coefficient
γ_{sat}	saturated unit weight of soil
γ_w	unit weight of water
ΔT	change in temperature
ρ	resistivity after a change in temperature
ρ_o	original resistivity

CHAPTER ONE

INTRODUCTION

1.1. Introduction

Recent work has opened up the possibility of using stone columns in collapsible soils, soils prone to relatively rapid volume compressions that occur due to the action of load and/or increases in water content, by the use of encasement, thereby overcoming the problem of losing the lateral support of the soil itself when the collapse occurs. However, the full behaviour of this type of ground improvement in such soils, characterised by their metastable fabrics, is still unclear. This is mainly because of a noticeable deficiency in both related studies and the use of instrumentation that could detect invisible subterranean behaviour objectively and efficiently, such as those used in geophysics surveys.

Electrical resistivity tomography (ERT) is a geophysical technique that has been employed for many years in hydrogeological and geotechnical investigations (Loke, 2012). The resistivity method is relatively cost effective and less invasive, and the measured data can cover a larger volume of the specimen (Calamita et al., 2012). Although the technique has been applied to detect heterogeneity of soil, and it has proven successful, as confirmed by Borsic et al. (2005), the potential for using it in monitoring soil reinforced with a stone column has not been considered previously.

Therefore, in the present thesis a geotechnical study is integrated with a geophysical investigation to characterise the use of encased and uncased granular columns in an artificial loess deposit. The laboratory part of the study includes conducting a series of conventional and non-conventional load tests under control conditions, with and without taking resistivity measurements. Also, an analytical model has been developed in this research to determine the load carrying capacity of the foundation.

1.2. Background

Stone columns are widely used globally due to their versatility and relatively broad applicability in different soil and foundation situations. They are inexpensive and easy to construct. They essentially work by reinforcing the ground to increase the bearing capacity, control the rate of settlement, reduce total and differential settlement, improve slope stability and increase resistance to liquefaction (Hughes & Withers, 1974; Engelhardt & Golding,

1975; Balaam & Booker, 1981; Sondermann & Wehr, 2004). In addition to this, stone columns can now be considered environmentally satisfactory (McKelvey & Sivakumar, 2000), further details in Section 2.2.

Once stone columns are subject to loading, they transfer the load to the surrounding soil by shear stresses developed along the side interaction between soil and granular column, as well as end bearing at the column base. The leading mode of failure in stone columns is bulging into neighbouring soil, except when the column is very short (McCabe et al., 2007). This mechanism of transferring stresses distinguishes stone columns from rigid piles, as illustrated by Hughes & Withers (1974) and shown in Fig. 1.1. Stone columns obtain their load capacity from the confinement mobilised by the surrounding soil.

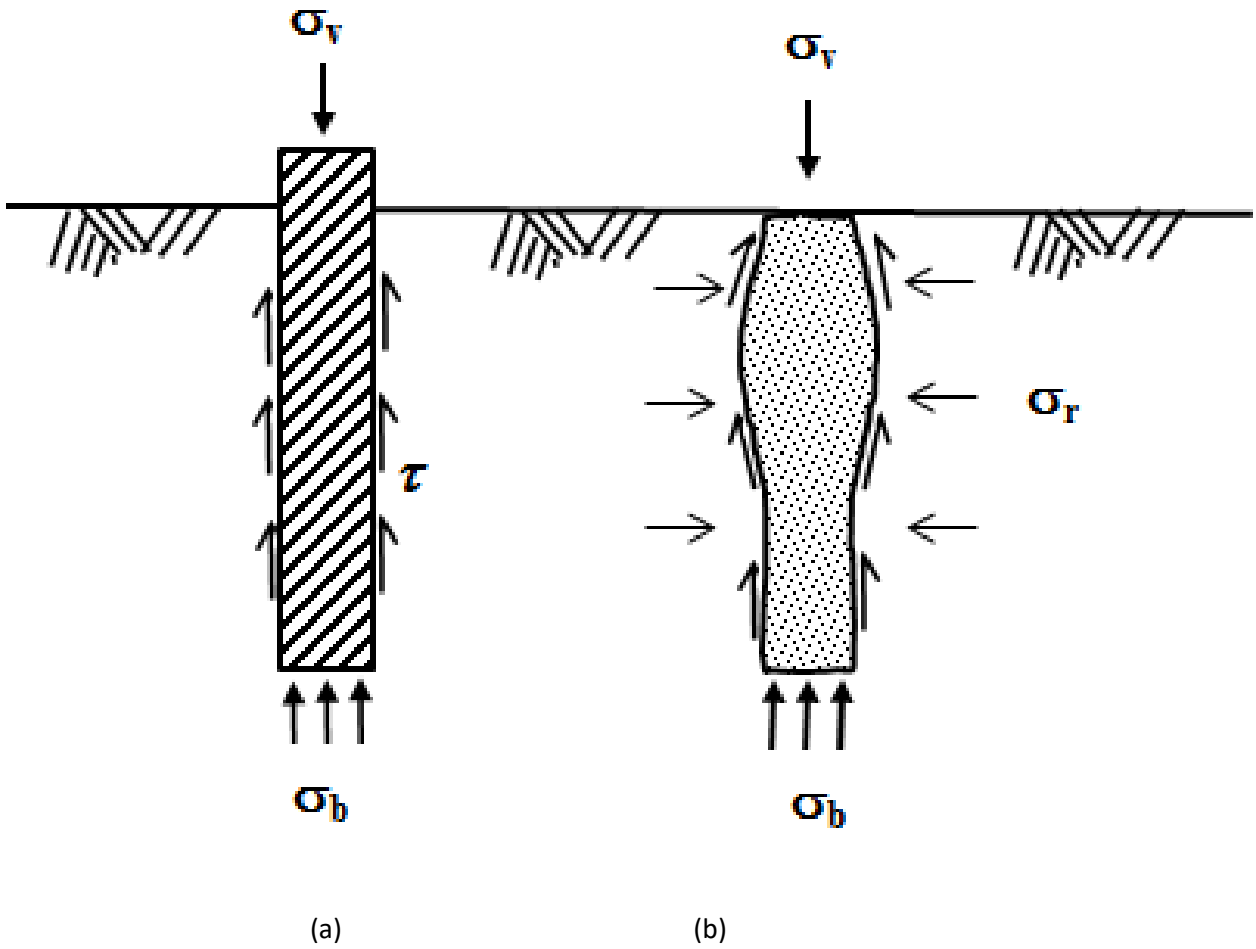

Figure 1.1: Load transfer mechanism for (a) a rigid inclusion (b) a stone column (redrawn from Hughes and Withers 1974), where: σ_v: ultimate load; τ: shear stress; σ_b: end bearing stress; and σ_r: radial stress

Similarly to very soft soils, the lateral confinement exerted by collapsible soils may not be sufficient. Consequently, the formation of the stone column itself may not be applicable. Casing individual stone columns with a suitable geosynthetic is one of the ideal solutions for solving this limitation (Ayadat & Hanna, 2005). The encasement makes the stone columns stiffer and stronger, further to the function of drainage that they preserve.

Early example of encased stone columns was introduced by Van Impe & Silence (1986). Case histories indicated a successful performance of this technique in soft soils such as examples given by Alexiew et al. (2005), Raithel et al. (2008) in Europe, and de Mello et al. (2008) in South America.

However, little field research on the use of encasement with stone columns to treat collapsible soils has been undertaken to date. Of the few examples presented, Araujo et al. (2009) who investigated the conduct of full scale load tests of geosynthetic- encased column installed into porous collapsible fine soil. Outcomes showed that encasing the sand column caused a significant increase in load capacity of the foundation, and water injection at the column‟s top prompted the soil collapse, influencing the behaviour of the column overall. These investigators pointed to the importance of a satisfactory soil bearing capacity at the column‟s base.

Ayadat (1990) was probably the first to use encasement to treat collapsible soil. He used a gap-graded mixture as a host collapsible ground consisting of 78% concrete sand, 10% Leighton Buzzard sand (less than 90 mm), and 12% speswhite kaolin clay. Based on his findings, the reinforced sand column with geosynthetics contributed to an increase in the ultimate bearing capacity of the sand column, and that was in proportion to the geosynthetic material stiffness. Also, a remarked decrease in the settlement was recorded. Ayadat et al. (2008) discussed the failure process of the ordinary stone column rested on a collapsible soil after soaking with water; they reported that the stone column was unsuccessful to reinforce collapsible loose soil because of the loss of the lateral confinement of such soil.

The majority of studies to date have focused on the performance of encased columns in clay or sandy soils. Very few studies have referred to the potential of employing this technique in reinforcing collapsible soil. Based on two hundreds published papers, pie chart in Fig. 1.2 shows statistical percentages of using encased stone columns in different types of soils. Thus,

the lack in relevant research makes the general behaviour of this treatment and it‟s applicability to treat collapsible soils are not thoroughly understood.

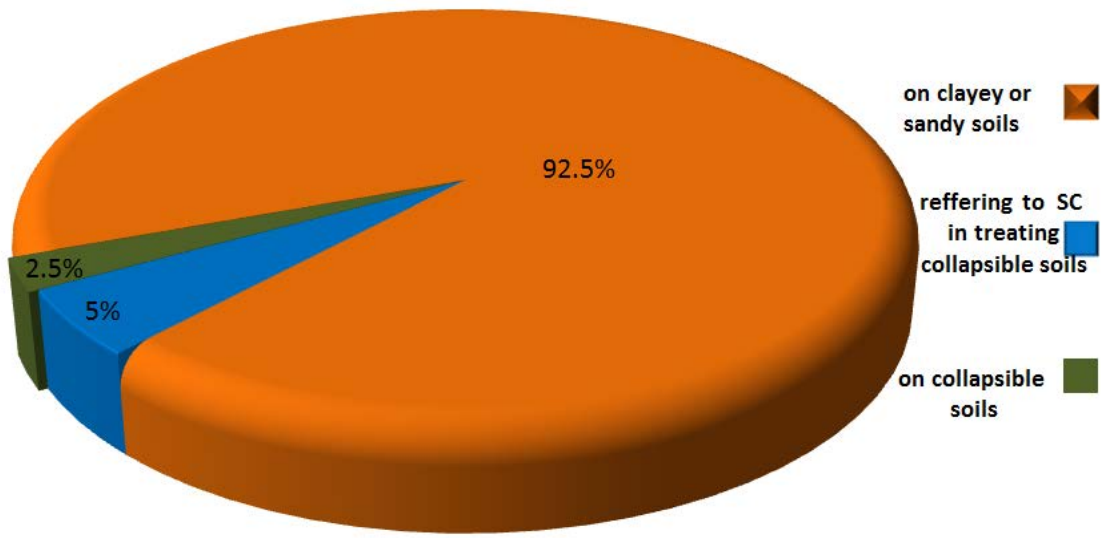

Figure 1.2: Percentages of studies regarding encased stone columns in different types of soils

1.3. Geophysical Testing in Monitoring the Performance of Stone Columns

Recent studies pointed to the potential of estimating the shear moduli of the stone column from the velocity phase obtained from the seismic wave test, a geophysical method (Redgers et al., 2008; Gazdek et al., 2011; Madun, 2012), but there were some limitations with applying such a method, specifically relating to the quantity of data collected, technique issues and the presence of water, as will be discussed in Section 2.2.8.2.

Electrical resistivity tomography (ERT) is a geophysical technique that has been proven to be a successful, cost effective 3D monitoring tool with many geotechnical applications, see further details and literature in Chapter Five. However, the potential for using this approach in monitoring soil reinforced with a stone column has not been considered previously.

1.4. Problem Context and Research Questions

Geotechnical engineers and designers are uncertain about the behaviour of stone columns in soils identified by their open structure. It is not clear whether they would still stand under inundation conditions, when the soil loses adequate lateral confining pressure. The mechanism of enhancement by wrapping the granular column in geotextiles is presented in the literature in the context of providing extra lateral stiffness through the geotextile hoops.

However, many aspects related to the treated collapsible soil itself, which may be considered of key importance, are not taken into account.

Key questions here include the following: what is the consequence of changing the degree of saturation of the host collapsible soil on the collapsibility of the treated ground? How then would that influence the ground improvement achieved by encapsulating the granular column? Is there any effect on the soaking pattern if the water flooding happens prior to or after the loading? How could the level to which the underground water is expected to rise through the soil influence the magnitude of the matric suction of the soil and its shear strength? Accordingly, how would it affect the overall behaviour of encased stone column in the context of bearing capacity, settlement and mode of failure under soaking with water at different levels?

In addition, it is important to ask whether there is any potential to use a geophysics survey in such a system for detecting the variations in geophysical properties, how the results of this could be integrated with the results of the physical model and what the limitations of electrical resistivity tomography (ERT) are in mapping the changes.

1.5. Research Aim and Objectives

The aim of this research is to provide a better understanding of the behaviour of the encased stone column when inserted into a collapsible soil using laboratory modelling and analytical predictions. The following objectives have been established to achieve this goal:

1. Finding gaps in current knowledge by conducting an intensive review of the literature for both ordinary stone column (OSC) and encased stone column (ESC).
2. Building a host collapsible ground of the column in the laboratory through simulating an artificial loess soil that behaves similarly to natural collapsible deposits in its overall manner.
3. Evaluating the improvement achieved in load-carrying capacity and settlement characteristics of the encased column foundation installed in an open-structure soil by testing the efficiency of encasing the column with a geotextile in the laboratory, in terms of two variables:

(a) The degree of saturation of the ground, to assess the worst case of inundation and how encased columns would perform.

(b) The soaking pattern; whether flooding with water prior to (or after) the loading would make the foundation behave differently.

4. Characterising the geophysical properties of the metastable soil, specifically for use in vibro-stone column foundations by developing an automated resistivity tomography system in the laboratory.
5. Establish a predictive method for the ultimate bearing capacity of an encased stone column resting on a collapsible fill, considering changes in the degree of soaking and matric suction and their effect on the shear strength of the soil.

1.6. Anticipated Contribution

1.6.1 Key Gaps in Existing Literature

Few field tests have been carried out previously to assess the load-settlement characteristics of columns reinforced with geosynthetics. Although they overcame the impact of the scale effect in comparison with laboratory testing, they were associated with difficulties in controlling the way in which the ground water was raised and introduced to the composite cell of the soil and the column. Therefore, evaluation based on these tests could be misleading, and not correctly represent the actual situation. These tests are also relatively costly and time consuming. This limitation is exemplified in the work undertaken by Araujo et al. (2009), which included soaking the system by introducing the water from the sand column‟s top into the column body, anticipating that water to spread out from the column body to the surrounding soil. In a similar case in Iraq, Salih (2003) flooded his field trial by adding water to the surface layer of both the soil and the confined stone column.

Regarding the laboratory work that has already been done in this area, it is not possible to install instrumentation along the system bodies of granular columns, whether surrounded by geosynthetics or not, due to their nature. So, the process of assessing the variations in stress concentrations, or the hydrological properties along the composite cell during loading is unfeasible. Alternatively, monitoring often occurs after completing tests and upon removal of loads from samples, which often introduces additional difficulties related to sample disruption and the consistency of the system as a depiction of the entire sample (Madun, 2012). Moreover, the process of the transformation of the sample could affect its initial water content (Zourmpakis et al., 2006).

In addition to this, collapsing soil texture in previous laboratory studies were modelled with relatively coarse, loose soil (see Ayadat (1990)), while fine soil, such as loess deposits, were not considered. The column itself almost was represented in the laboratory by a sand column rather than a stone column. On the other hand, in previous work researchers adopted an analytical model in which the undrained shear strength of the soil (c_u) is determined for the saturated case, as produced by Ayadat & Hanna (2005), while the impact of the severity of soil collapsibility and the effect of matric suction and degree of saturation on the shear strength of the treated collapsible soil after soaking with water have not been adequately addressed.

1.6.2 What is the Focus on

The research explores the function of a single encased granular column installed into a fine collapsible soil, using laboratory and analytical studies. The main focus is to evaluate the enhancement in load-carrying capacity, the reduction in settlement, and the shape of failure under loading and flooding with water. The applicability and limitations of employing geophysics imaging to detect the variations in the geophysical and hydrological properties of the system are studied.

1.6.3 What Contribution to Fill the Gaps

As concluded from previous sections, there is a necessity to conduct a detailed study highlighting key aspects that could impact the overall performance of this technique, and monitoring the hidden subsurface during loading and inundation effectively using a non-invasive, non-destructive tool. This would assist in understanding the mechanism of enhancement and as a result, knowledge gap related to this subject would be covered.

Intensive laboratory work, accompanied by an analytical study, has therefore been undertaken. The first challenge was producing an appropriate artificial collapse soil that would represent the soil treated with encased stone column. In this research, and for the first time, fine artificial loess was produced as a host collapsing ground. The work includes conducting a series of laboratory loading tests on foundation-type footings resting on untreated artificial collapsible soil and treated by encased and uncased granular columns. Underground water, rising from the base at different levels, is monitored; such observations have not been made previously for fine collapsible soil characterised by a relatively high capillary action. An automated electrical resistivity tomography (ERT) system is employed

for the first time as a powerful non-invasive tool for detecting the homogeneity and geophysical properties of the combined system (soil and column) under loading. The experimental programme is accompanied by an analytical prediction with using a Matlab code to determine the bearing capacity of the reinforced foundation and for validation purposes between experimental and theoretical results.

1.7. Thesis Outline

The thesis is presented in eight chapters, as follow:

Chapter Two reviews the literature relating to the topic in two main areas, ordinary stone columns and encased stone columns.

Chapter Three refers to the first part of the laboratory work, including the selection and preparation of the artificial loess bed that is used for the successive test series as a host ground for the granular column. The chapter starts with a brief review of the relevant literature. Factors that could affect the collapse phenomenon, such as clay content, water preparation and drying time, are investigated through single and double oedometer tests.

Chapter Four presents the second test series (the physical model), which includes loading tests conducted on normal cylindrical tanks that have no electrodes on their sides. The main focus for those tests was monitoring the load-settlement characteristic and the mode of failure of the foundation under different soaking conditions, after filling the cells with the prepared collapse soil and constructing the encased and uncased stone columns at the middle. The geotechnical properties of the material used, apparatus for testing, soil bed preparation, construction process for the encased and cased granular columns, strategy for inundating the system, testing programme and procedures for running the tests, and feasibility tests are all presented.

Chapter Five presents the third test series with resistivity measurements (the geophysical model), including the design of the resistivity cells developed and the full progress of the test procedure, including calibration with tap water, data processing and the inversion technique.

Chapter Six displays the results of both the physical and geophysical models, which are analysed, compared to results from the literature and discussed in detail.

Chapter Seven includes the development of the analytical procedure and the MATLAB code for calculating the bearing capacity of the system. Model sensitivity results are produced based on the influence of the matric suction of soil and the degree of saturation of soil for different geotextile and column properties that are likely to affect the response of the encasement.

Chapter Eight contains conclusions and gives recommendations for future work.

1.8. Summary

Chapter One provided an introduction to the concept of covering the granular column with geosynthetic for providing extra confinement, which is required when installing the column in collapsible soil. The background to the topic is presented, as are associated attempts in geophysical practice. The gaps in current knowledge pertaining to this subject and the description of the research problem are highlighted, which inevitably support the necessity of conducting this study to investigate the system and gain a better understanding of its function under loading, both with and without the presence of water. The scope of this study is stated, followed by the objectives to fulfil its aim via laboratory testing and analytical study. In the end, the structure of the thesis is outlined to present information in a logical order and focus the study on its research objectives.

CHAPTER TWO

LITERATURE REVIEW OF STONE COLUMNS

2.1. Introduction

This chapter provides an overview of both ordinary stone columns OSC and encased stone columns ESC, and follows this with brief reviews of the literature concerning the collapsible deposits and electrical resistivity tomography in Chapters Three and Five, respectively, as these form the main focus of the research work undertaken as discussed previously in Chapter One.

2.2. Ordinary Stone Columns (OSC)

Stone columns are a common ground improvement method employed to treat soft soils, and act as reinforcement elements to reduce settlement and increase bearing capacity (Hughes & Withers, 1974; Balaam & Booker, 1981; Sondermann & Wehr, 2004).

In some seismically active areas, they also reduce the liquefaction potential (Engelhardt & Golding, 1975; McKelvey & Sivakumar, 2000).

In addition to this, stone columns can now be considered environmentally satisfactory especially in the UK owing to largely use of dry feed method over the wet feed method and using recycled aggregate instead of primary aggregate (Serridge, 2006).

Stone columns are widely used in many loading situations, such as small isolated footings, strip footings, raft foundations, and very common large loads such as embankments, bridges, and other types of structure (Hughes & Withers, 1974; Hughes et al., 1975; Serridge, 2013; Killeen & Mccabe, 2014).

The historical background of stone columns; methods of installation; factors that affect the behaviour of a single and a group of stone columns; load transfer and main modes of failure; the unit cell concept; special improvements, including reinforcing by geosynthetics; and studies on stone columns, including geophysical investigation, are reviewed in the following sections of this chapter.

2.2.1. Historical Background

Reinforcement of soil through the use of stone columns is an old technique, for example was used by the ancient Iraqis since probably the 2nd or 3rd century BC. During archaeological investigations of Hatra (in northern Iraq), holes were found filled with uniform pieces of rock, covered with lime as a connecting material. In addition, rock discs were recognised, with diameters equal to the diameter of the stone column; these discs were arranged at different distances along the body of the stone column (Al-Obaidy 2000).

Later, stone columns were used in France in 1830 by French military engineers to support the heavy foundations of the ironworks at the artillery arsenal in Bayonne (Babu et al., 2013).

In 1937, the stone column technique was employed in Germany to densify loose sands for a government building in Berlin (Burland et al., 2012). Since then, this technique of soil improvement had been widely adopted in many construction projects (McKelvey & Sivakumar, 2000) and an early UK example was about 1991)Serridge, 2006).

2.2.2. Methods of Construction

Stone columns are constructed either by ramming or vibrofloatation technique. The latter includes vibro-displacement (dry-bottom feed method) and vibro-replacement (wet-top feed or dry-top feed method).

The selected technique is mainly depends on loading range, soil conditions (soil type and undrained shear strength of the soil c_u) and depth of the required improvement d_t as shown in Table 2-1 which is deduced from previous studies and it shows countries of construction.

Ramming and top feed methods include adding unconsolidated fill materials, such as stones or gravel, to a pre-bored hole in a number of increments and then compacting the fill materials either by a heavy falling weight if the ramming technique is employed or by means of vibration using air or water pressure in case of adopting the top feed method.

In bottom feed method, the stone material is supplied at the bottom of the hole via the vibrating poker (McCabe et al., 2009). Many texts provide full details of stone column construction e.g. Sondermann & Wehr (2004) and Mitchell & Jardine (2002). Figure 2.1 shows the dry-top feed, dry-bottom, and wet-top feed methods presented by Taube et al. (2002).

Table 2-1: Requirements of different installation technique of stone columns and countries commonly employ them according to the literature (Nayak, 1987 and 1996; McKelvey & Sivakumar, 2000; Serridge, 2005; McCabe et al., 2009; Babu et al., 2012; Amini, 2014)

Installation Method		Loading range	Soil conditions	Depth of treatment (d_t) and water presence	Countries of construction
Vibrofloatation	Dry top feed	light to heavy	It is rarely used for soft cohesive soil; instead, it is suitable for coarse and capable deposits, $c_u > 30$ kPa	shallow to medium depths, typically 10 m could be extended	America, Europe, and the UK
	Wet top feed	extraordinarily moderate to high	soft cohesive soil	medium to deep treatment up to 30 m below the water	America and Europe
	Dry bottom feed	different ranges of load	water-bearing and soft cohesive deposits, c_u = 15 to 50 kPa	$d_t > 15$ m; it is not influenced by the presence of ground water	America, Europe, and the UK
Ramming System		higher than that of vibrofloatation	soft cohesive soil	it is considered uneconomical if $d_t >$ 12-15 m	India

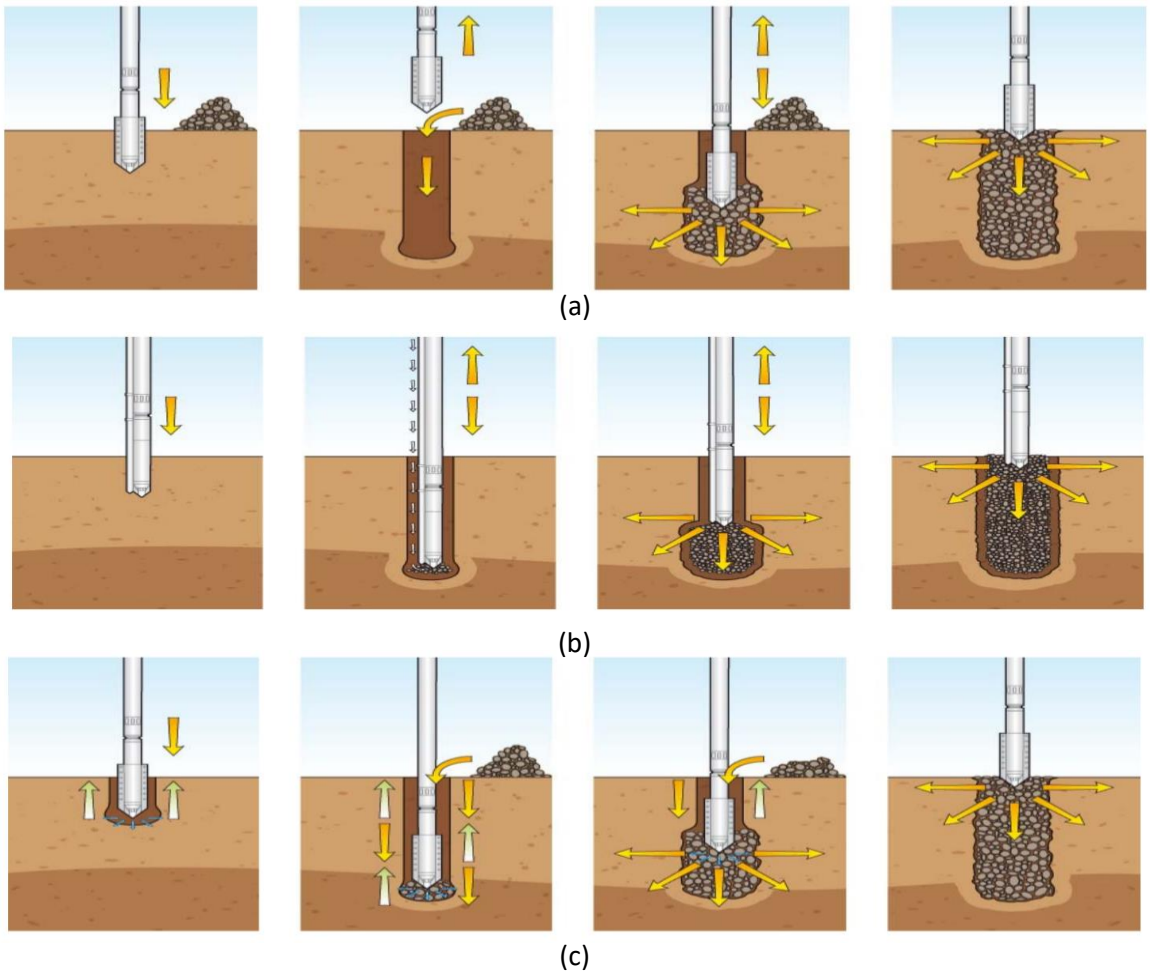

Figure 2.1: (a) Dry-top feed method and (b) Dry-bottom feed method (c) Wet-top feed presented by Taube et al. (2002)

2.2.3. Factors Affecting the Behaviour of a Single Stone Column

The properties and type of soil; the properties of the stone column material; the geometry of the stone column; and the loading arrangement mainly control the behaviour of individual stone columns. Each will be reviewed in turn in the following sections (2.2.3.1 to 2.2.3.4).

2.2.3.1. Properties and Type of Soil

The effect of soil on stone columns is controlled by undrained shear strength of the soil c_u, the in situ lateral stress in the soil, and the radial pressure deformation features of the soil (Hughes et al., 1975). For example, when granular columns are inserted into very soft soil, they may not derive significant load carrying capacity owing to low lateral confinement. The value of the undrained shear strength of the surrounding soil represents a guide to deciding the feasibility of the treatment. Although Wehr (2006) gave a lower bound of c_u ranging from 5-15 kPa, most studies reported a c_u more than 15 kPa is required to provide an adequate lateral captivity. However, stone columns are unsuitable when c_u exceeds typically 50 kPa or more due to the high resistance of the penetrating when trying to form the column (Barksdale & Bachus, 1983).

Some types of soil need careful treatment to guarantee successful functioning, for instance, organic soils. Stone columns are typically installed in such soil with a plasticity index (PI) less than 40%. However, in some circumstances vibro stone columns have successfully improved soils that have a PI greater than 40% (McCabe et al., 2007). Other soil conditions where stone columns are used include recent clay fills where stone column allow acceleration of settlement but without reducing the amount of settlement, whilst in some cases they may be advantages, the acceleration of settlement in young fills that have been in place for less than 10 years is not recommended due to its unpredictable behaviour (McCabe et al., 2007).

A soil type receiving increasing attention includes collapsible soils which lose lateral confinement upon inundation resulting in a sudden settlement (Mitchell & Jardine, 2002). Jefferson et al. (2000) confirmed based on literature that there is a potential to use stone columns in treating collapsible loess deposit of depth 1.5 m to 10 m, they stated that stone columns are inexpensive in comparison to conventional piles, but high caution in site control and assessment are required. Ayadat (1990) through his laboratory study improved the ordinary stone column embedded in collapsible soil by wrapping the stone by geotextile to overcome the problem of losing the lateral support of the host ground. However, the

enhancement achieved by this treatment to collapsible soils is not understood, specifically in the range of fine soils.

Soil characteristics such as undrained shear strength, in situ lateral stress, radial pressure deformation characteristics, plasticity index, and type of soil have a considerable influence on the success of stone columns. However, further characteristics, such as the collapsibility of the soil, have not been reported in any details.

2.2.3.2. Properties of Stone Column Material

The fill material of stone column must possess an adequate shearing resistance so that it can withstand stress concentrations (Jefferson et al., 2010). Properties such as internal angle of shearing resistance ϕ'_c and modulus of elasticity E_c of the fill can play a significant role in the manner in which stone columns perform.

Most previous studies suggested constructing stone columns by using materials with high angles of internal friction to achieve maximum bearing capacity. Figure 2.2 shows the relationship between the improvement factor $F_{imp.}$ and the area ratio (total area of the composite soil-column A to the area of column A_c) with respect to the angle of internal friction ϕ'_c for a typical soil with a Poisson's ratio μ_s of 1/3, according to the design chart presented by Priebe (1995).

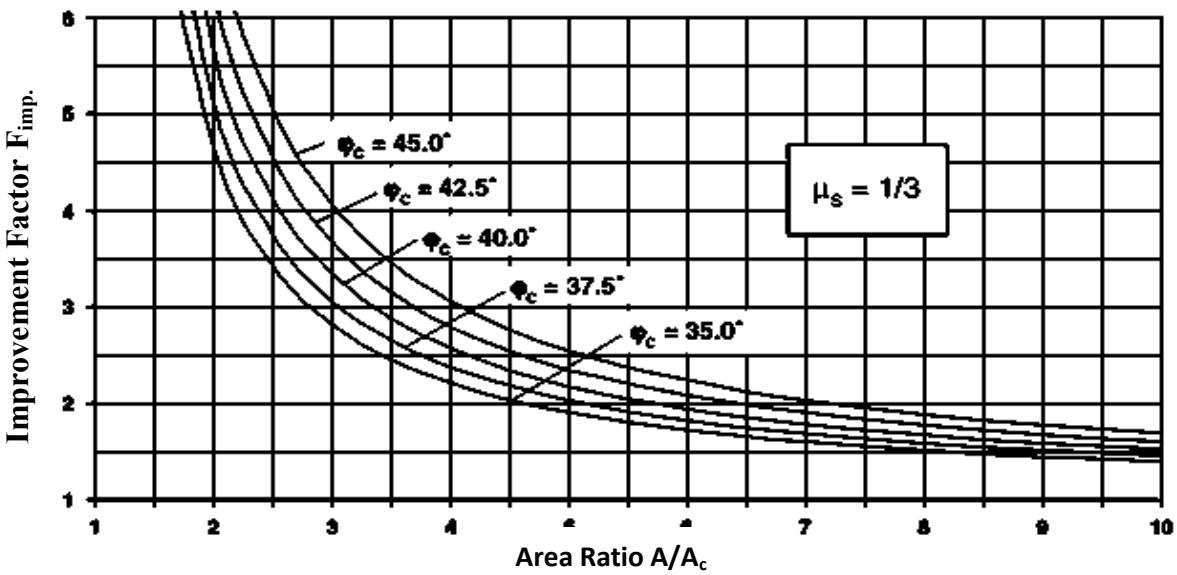

Figure 2.2: Improvement factor against area ratio for different angles of internal friction, ϕc (Priebe, 1995)

Regarding E_c, results showed that, for a given spacing of stone columns, as the stiffness ratio (modulus of elasticity of the stone column to that of the surrounding area) increases, stone columns take a greater proportion of the applied load. Through this, an increase in the stress concentration factor occurs (Ambily & Gandhi, 2007).

In addition to the mechanical properties of the stone column material discussed earlier in this section, their suitability is decided based on their particles shape, grain size distribution and absence of organics or impurities (Amini, 2014), also on their availability and economy (Babu et al., 2013). The ratio of the diameter of the column to the diameter of the fill material particles (d/d_f) is usually a value between 12 and 40, because in practice, granular columns are constructed at typical diameters (d) of 0.6-1 m, while stone particles have typical particle sizes (d_f) of 25-50 mm (Wood, 2000). The maximum size of the aggregate is limited to 40 mm in the case of adopting the bottom feed installation method in order to avoid blockages (Greenwood & Kirsch, 1983).

2.2.3.3. Stone Column Geometry

Hughes et al. (1975) defined the critical column length as the shortest column that is able to carry the maximum load, regardless of the settlement. Many investigators have stated no improvement beyond this length in terms of load-carrying capacity, but longer stone columns may be needed to manipulate the settlement (Babu et al., 2013).

The diameter of the stone column also plays a major part in increasing the bearing capacity and reducing the corresponding settlement of the stone column (Greenwood, 1975). Accordingly, the volume of soil replaced by granular columns (which can be expressed as area replacement ratio (a_r), defined as the ratio of the area of the stone column to the total area of the composite cell of the stone column and the surrounding soil) has a significant effect on the degree of improvement accomplished (Shahu et al., 2000).

The effect of geometry is very pronounced in identifying the failure mode of stone columns, thus if the length to diameter ratio is less than four, the stone column will fail due to end bearing failure, rather than bulging failure (Hughes & Withers, 1974). A column length to diameter (l/d) ratio of a minimum 6 is required to induce the full restraining axial stress on the column (McKelvey et al., 2004).

2.2.3.4. Loading Type and Arrangement

The stress concentration ratio at the ground surface (which represents the share of stress on the soil to the total stress of the composite cell of the column and surrounding soil) is high if the load of the composite ground is applied through a rigid foundation, as compared to a flexible foundation (Barksdale & Bachus, 1983).

In addition, the stone column-soil modular ratio (Modulus of Elasticity of column material E_c/ Modulus of Elasticity of soil E_s) can increase the rate of consolidation under a rigid raft, but not under a flexible raft (Balaam & Booker, 1981).

Stone columns subjected to static loads have proven the efficiency of increasing the load carrying capacity and reducing the compressibility of the soil, however, less attention has been paid to the behaviour of the system under cyclic loading, specifically on transport branches such as railways. Ashour (2015) stated that the presence of stone columns subjected to cyclic loading in clayey soil contributed to reducing the threshold stress and pore water pressure by providing a drainage path.

It is reported that previously adopted analytical models are unable to represent the influence of cyclic loading (Basack et al., 2016), while later investigators developed a finite-difference model, adopting a modified Cam clay theory to analyse the response of stone column-reinforced soft soil under cyclic loads. The presented model was validated through field and laboratory testing.

Loading arrangement in the field includes the entire composite area of the stone column and the treated ground to be subjected to loading from the superstructure.

2.2.4. Factors Affecting the Behaviour of a Group of Stone Columns

Foundations may consist of a group of stone columns installed fairly close together with a granular layer of sand or gravel is usually placed over the top of the stone columns. This granular layer or sand bed acts as a drainage layer and also distributes the stresses coming from the embankments (Mitchell & Huber, 1985).

The load bearing behaviour of a group of columns is different from a single column, with a particularly clear indication of this being provided in the shapes of the deformed columns (Hu, 1995).

Once columns are arranged with narrow spaces between them, at the centre of the group, it is expected that the attempt of one column to bulge will be resisted by the similar attempts of the adjacent columns (Wood, 2000).

The effect of stone column groups, when loaded, is to increase the ultimate load capacity of each of the single columns, resulting in less bulging compared with a single stone column. In the case of embankments, however, although strengthened by a group of stone columns, failure often occurs (Madun, 2012). This failure happens due to failure in the untreated soil outside the treatment zone when the soils move laterally outward from the column area toward the non-reinforced soil. This phenomenon is called 'spreading', which causes greater settlement (Tavena et al., 1979 after Madun, 2012).

Moreover, greater stress can be noticed at the top of the granular columns, while there is less stress in the interaction area between the column and the surrounding soil (Wood, 2000).

When placing a stone column in a group, further parameters should be taken into consideration such as spacing, arrangement and loading area; these now will be considered in turn.

2.2.4.1. Spacing

Stone columns placed as a group should be spaced such that the bearing capacity of the group piles should be equal to or greater than the sum of the bearing capacities of an individual stone column. Spacing between two stone columns (S) is usually measured centre to centre; see Fig. 2.3 in the next section (2.2.4.2) which includes more details about spacing and stone column‟s arrangement. Spacing (S) should not be less than 2.5 stone column diameters apart (Al-Mosawe et al., 1985).

If the spacing ratio (d_e/d, defined as the ratio of the equivalent diameter of the composite cell of stone column and soil to the diameter of stone column) is equal to or more than 5, the reduction in settlement due to the stiffness of the stone columns would be negligible (Balaam & Booker, 1985).

Also, Hughes and Withers (1974) reported that only the surrounding clay within a distance of 2.5 times the diameter of the stone column was affected by the applied load.

2.2.4.2. Arrangement

There are three possible ways stone columns may be arranged; these are an equilateral triangle, a square, or a regular hexagon (Balaam & Booker, 1981; Balaam & Poulos, 1983), see Fig. 2.3.

The model tests of Al-Mosawe et al. (1985) showed that the triangular footing is better at carrying loads when compared with the other types of footing.

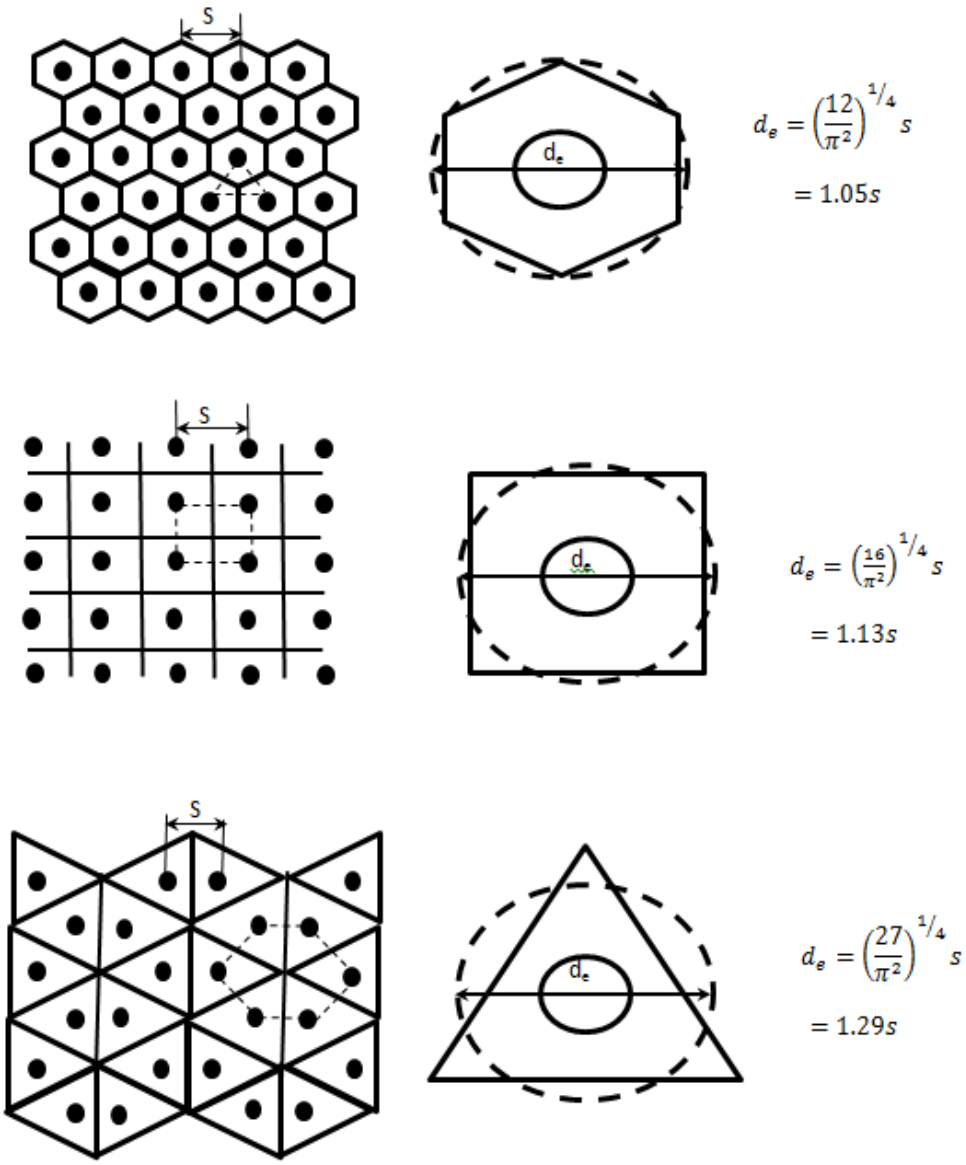

Figure 2.3: A typical layout of stone columns (a) Triangular Arrangement, (b) Square Arrangement, (c) Hexagonal Arrangement (redrawn from Balaam & Poulos, 1983), where: d_e: effective diameter of the composite cell; and S: spacing between two stone columns.

2.2.4.3. Loading Area

Stone columns can be employed in a small group if small loaded areas such as pads or strip footings are to be treated, while a large group of stone columns are used in cases where there are wide loaded areas, such as embankments. It is noticeable that in smaller groups the bordering columns become more significant as they have a lower bearing capacity. Also, vertical stress beneath small loaded area deteriorates much more intensely with depth than that underneath a large foundation (Killeen & Mccabe, 2014).

2.2.5. Load Transfer and Failure Mechanism

During the loading process, shear stresses will be induced along the body of the stone column, in the area of interaction between the stone column and the surrounding soil. This occurs as a result of unequal vertical strain, which causes a relative movement between stone column and soil. Consequently, the axial stress on the stone column will decrease with depth as the axial load is transferred to the soil via shear (Goughnour & Bayuk, 1979). Three modes of failure outlined by Barksdale & Bachus (1983) are commonly noticed; (a) Bulging Failure, occurs when the stone column is constructed through soft soil on a firm layer, with a length greater than 4-6 times the diameter,(b) General Shear Failure, observed when the column length is short and resting on firm strata, (c) Punching Failure, this mode of failure could be expected when the end bearing of the column is on a weak soil, and the length of the column is relatively short (length to diameter ratio is less than 2-3. For illustration, see Fig. 2.4.

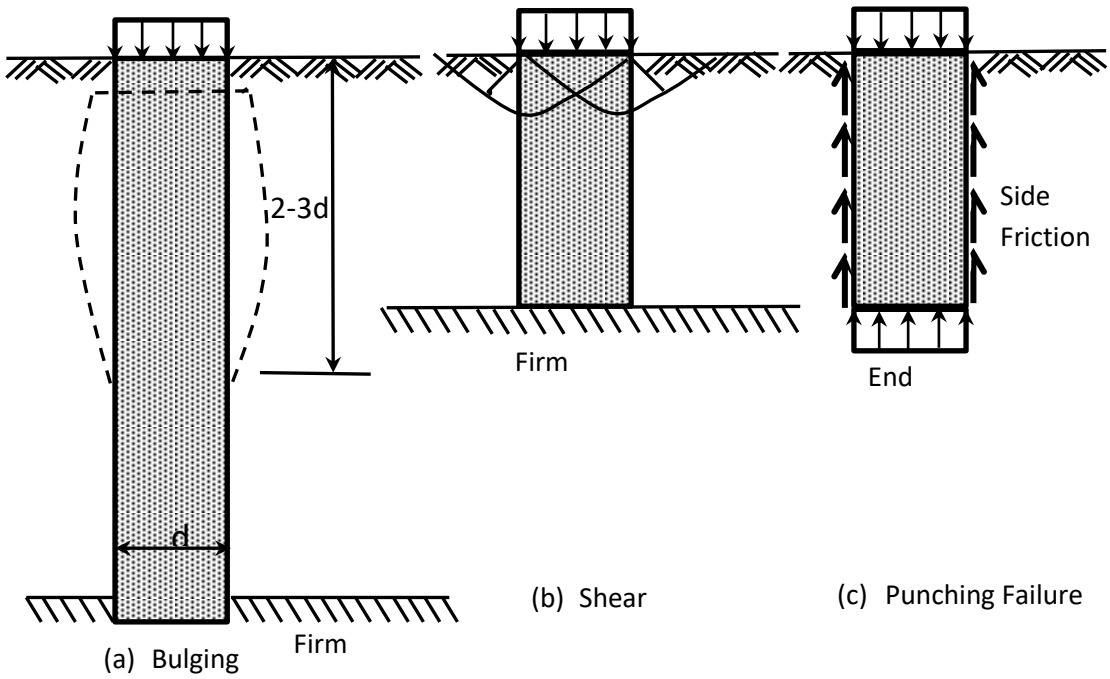

Figure 2.4: Modes of failure of stone columns (redrawn from Barksdale and Bachus, 1983)

2.2.6. Unit Cell Concept

To idealise a stone column installed in a soil, the composite cell of the stone column and the surrounding ground is represented using the unit cell concept, this assumes that stone columns are arranged in a particular geometric pattern, the influence of the boundary conditions is neglected, and the properties of the materials used are assumed identical (Balaam & Booker, 1981; McKelvey & Sivakumar, 2000). Balaam et al. (1978) suggested the unit cell concept, in order to represent a single stone column within a group through an equivalent diameter (d_e) of the column and the soil subjected to a uniform loading. d_e is proportional to the spacing (S), according to the arrangement patterns presented by Balaam & Poulos (1983), see Section 2.2.4.2. The unit cell can be physically modelled in the laboratory as a cylindrical-shaped chamber having a frictionless, rigid exterior wall symmetrically positioned around the stone column, see Fig. 2.5.

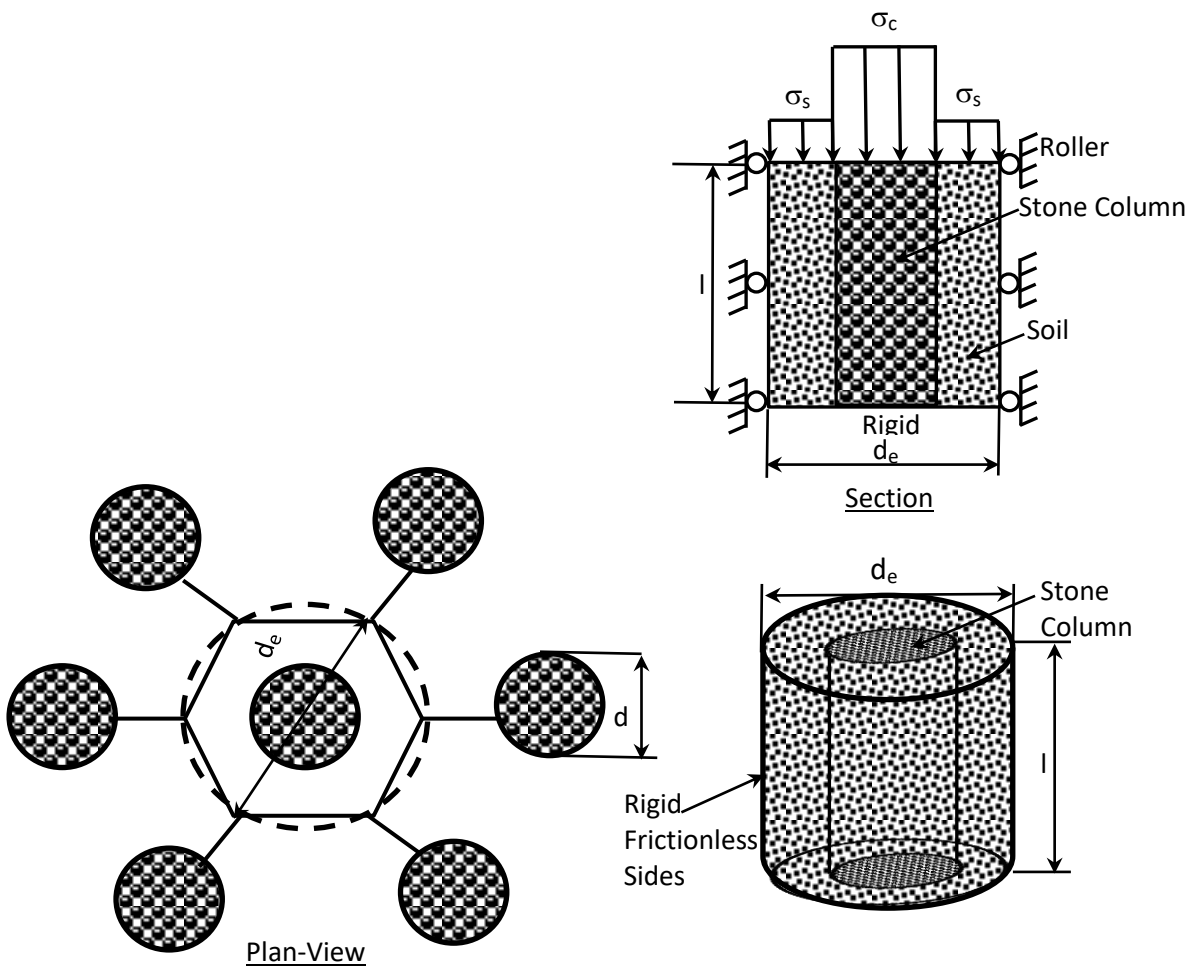

Figure 2.5: Unit cell idealisations (redrawn from Barksdale and Bachus, 1983), where: d_e: effective diameter of the composite cell; d: diameter of stone column; l: length of stone column; σ_S: Stress acting on soil; σ_C: Stress acting on the column

2.2.7. Special Improvement of Stone Columns

To enhance the performance of ordinary stone columns, especially in very soft soil, researchers presented four main methods:

1- Adding material such as cement or lime to the cohesionless material of the stone column. Thus, the stone column acts as rigid inclusion and the strength of the stone column increases (Dobson & Slocombe, 1982).

2- Internally reinforcing the stone column with horizontal elements, for example, see Al-Obaidy (2000) who added isolated concrete discs along the body of the stone column. Also, Sharma et al. (2004) introduced a laboratory model in which a number of geogrid rings were placed with varying spaces, arranged at specific depths, while Ayadat et al. (2008) presented an experimental study where horizontal wire meshes were added internally to granular columns. These wire meshes were made from different materials, including plastic, steel and aluminium. More recently, Prasad & Satyanarayana (2016) presented circular geogrid discs to enhance the function of the stone column.

3- Reinforcing the stone columns with vertical nails (small-diameter steel bars) driven along the circumference, as was suggested by Shivashankar et al. (2010).

4- Using an encasement such as geotextile, geogrid, or polymer sleeves. The encasement, as well as increasing the stiffness and strength of the stone column, stops the side squeezing of fill materials when the column is installed, even in extremely soft soils (Gniel & Bouazza, 2009). This is an approach that has been advocated by Ayadat (1990) to treat collapsible soil. Since the focus of the present study relates to improving the ordinary stone column by encasement, so Section 2.3 below and the following sections review the literature in this area.

2.2.8. Studies on Stone Columns

The nature of the previous conventional studies related to the subject (stone columns) and the respective geophysical studies are considered and discussed in Section 2.2.81 and Section 2.2.8.2 respectively.

2.2.8.1. Model Studies

The behaviour of stone columns under loading has been studied using different methods, including field observations, analytical solutions, and laboratory tests. Field studies represent a significant part of the overall verification of stone column design, and conventional load tests are commonly used in practice, so many researchers concentrated their attention on this

type of study (e.g. Engelhardt & Golding, 1975; Hughes et al., 1975; Goughnour & Bayuk, 1979; Datye & Nagaraju, 1981; Al-Obaidy, 2000).

Besides the field observations, a number of researchers have developed theoretical solutions for estimating the settlement and bearing capacity of soft soils reinforced by stone columns. Many researchers simulated their studies of stone columns using the finite element method (see Ambily & Gandhi, 2007; Elshazly et al., 2007; Elshazly et al., 2008; Fattah & Majeed, 2012; Frikha et al., 2013; Khabbazian et al., 2015), whereas others introduced their numerical models using the finite difference method (see; Han et al., 2007; di Prisco & Galli, 2011; Deb & Mohapatra, 2013). In most of the aforementioned studies, the soft soil is treated as an elastic material, and the column as an elasto-plastic material, and researchers adopted a unit cell concept to simulate a single stone column and its surrounding in situ soil.

Moreover, model experiments in the laboratory have been used to examine the behaviour of both a single stone column and a group of stone columns (see Sivakumar et al., 2004; Black et al., 2007; Cimentada et al., 2011). Model testing had been employed because of its simplicity and reasonable accuracy, although it suffers disadvantages due to the scale effect (McKelvey & Sivakumar, 2000). While many researchers used a circular or rectangular test tank, others employed a large-scale triaxial cell to cover the concept of a unit cell to represent both the stone column and the neighbouring soil. The soil bed in previous studies was prepared by either consolidation or compaction processes. Further details of the published work on reinforcing soft soil with stone columns between 1970 and 2012 are summarised by Najjar (2013).

2.2.8.2. Geophysics

Geophysical testing can be employed to monitor soil properties and corresponding deformation prior to ground improvement. However, the enhancement achieved post-soil treatment is difficult to assess, as a result of introducing the dense fills comprising the columns, which affect the treated area significantly (Esring & Bachus, 1991).

A measurement of surface shear wave velocity has been used by the Building Research Establishment (BRE) to predict vertical deformation and compare these estimations with that of conventional loading tests before and after treatment. The accuracy of such geophysical tools for the prediction of settlement characteristics was limited specifically for immediate and relatively short-term performance (Esring & Bachus, 1991).

Redgers et al. (2008) applied the continuous shear wave method to monitor variations in stone column stiffness before and after installation; the method proved to be more reliable over a large area than the popular standard field tests, standard penetration test SPT and cone penetration test CPT. The stiffness increased with time as a result of decreased pore water pressure from the drainage effect of the stone columns.

Jefferson et al. (2008) presented a spectral analysis of surface waves to assess variations in the soil properties after treating with vibro-replacement stone columns; the technique showed a good quality technique in lateral assessment. However, Madun et al. (2012) criticized the previous works as there were only limited data available for bench- mark observations and the locations of the sensors used and their influence on the data collected were not explored. In addition, the assumption used for analysis included that the soil behaves as laterally homogeneous and isotropic. Thus, the findings for a related wavelength represent the mean velocity of the entire horizontal layer.

Variations in embedded volume of stone and densification resulting from column installation were visualised through 2D compression P-wave refraction tomography by Gazdek et al. (2011). This method showed significant changes in soil profiling in the context of density and elastic properties before and after the intervention. However, the limitation by water presence needs reinterpretation in light of the measured data according to the actual state as was suggested by the authors.

Madun (2012) presented his study to evaluate the use of surface waves for detecting non-homogeneities in the properties of soil treated by vibro-stone column through an assessment of the stiffness profile gained by the survey; he determined the maximum and minimum frequencies that are useful for spectral analysis and transmission to maximize the signal-to-noise ratio. The maximum information on the soil properties was limited to half of the model depth, as the wavelength was short and did not cover the full size of the physical model. Furthermore, subsidiary findings of this approach indicated that there were boundary restrictions that must be eliminated, and also that there was insufficient sensor energy to continue along its direct path when a seismic wave propagates near the stone column, as some of the energy was reflected or refracted.

Alternatively, electrical resistivity tomography, which could offer an effective geophysical method to investigate ground characteristics and consistency and to evaluate the enhancement

achieved by the construction of the stone columns, has not been employed previously in monitoring such a system. This method used in many geotechnical applications and proved successes, it can provide a clear 3D image that can detect respective variations in water content or particle densification resulted from water movement or loading at any particular location of the tested soil. Amini (2014) summarised the advantages and disadvantages of geophysical surveys based on the literature related to seismic wave‟s studies in Table 2-2. Regarding the resistivity method, the table fit well the pros and cons mentioned except that the resistivity method can visualize the third dimension by using a proper inversion technique as that used in this study. The basic concept of this method, previous related work, and the inversion technique used are briefly explained in Chapter Five.

Table 2-2: Benefits and limitations of geophysical studies (Amini, 2014)

Advantages	Disadvantages
There are non-invasive, where physical tests are usually destructive.	
No sampling or drilling is required.	
Geophysical methods can cover a large area of treatment (Butcher and Powell, 1996).	However, they cannot visualise the three dimensions of the ground and require other tests and methods to provide both horizontal and vertical profiles (McDowell et al., 2002).
They are very fast methods of investigation, and are therefore cost effective.	However, various methods and equipment might be required to investigate different properties of the ground, which may therefore increase the cost of investigations (McDowell et al., 2002).
Measurements are in situ and the values measured are close to operationally determined ones.	Not enough data is available in many cases to evaluate the data collected from geophysical investigation (Madun et al., 2012).
Laboratory and numerical models usually deal with well-graded, idealised conditions, whereas most sites treated by ground improvement methods are brownfield sites, filled ground, and alluvial deposited sites (SivaKumar et al., 2004). Consequently, geophysical methods can measure performance regardless of idealisations and assumptions for various sites.	
Most physical tests do not take into account the long-term performance of Vibro Stone Column VSC (for instance pore water pressure dissipation after treatment is finished), whereas geophysical methods could be used to study these effects in the long term (Redgers et al., 2008).	

2.3. Encased Stone Columns (ESC)

As stated in Section 2.2.6, encasing stone columns with geosynthetics is one of the improvement schemes used to enhance the load-settlement conduct of stone column foundations. Upon encapsulation, the load carrying capacity of the system increases, while the generation of pore water pressure and compressibility decline (Najjar, 2013; Hosseinpour et al., 2016).

The sleeve hoop stress provides an additional confining pressure on the encased column, subsequently mobilising resistance to further deformation in a collaborative manner (Wu et al., 2009).

The geotextile also significantly enhances the drainage of the system and acts as a filter, so that it allows water to seep from the soil without any loss of fines in the long term (Malarvizhi & Ilamparuthi, 2004).

A brief introduction to the technique of encapsulation was given in Section 1.3. Details concerning the installation technique, factors controlling behaviour, and the failure mechanism of encased stone columns stabilising soft soil are reviewed in subsequent sections (2.3.1 and 2.3.2). Afterwards, calculations of the bearing capacity and settlement of encased columns remedying collapsible soil are presented. In the last section (Section 2.3.5), some related previous lab works on sleeved column foundations are discussed.

2.3.1. Installation Technique for Encased Stone Columns

Two main methods for installing encased stone columns (ESC) are described by Tandel et al. (2012). These are (1) Displacement Method, and (2) Replacement Method.

2.3.1.1 *Displacement Method*

In this method, a closed-tip steel tube is pushed down into the soft soil and then the cylindrical frame of geotextile and fills is inserted into the empty hole. After that, the tip opens, and the tube is pulled upwards under vibration. The method is usually recommended for very soft soils (for instance, c_u < 15 kPa). Figure 2.6 shows the displacement method presented by Alexiew et al. (2005).

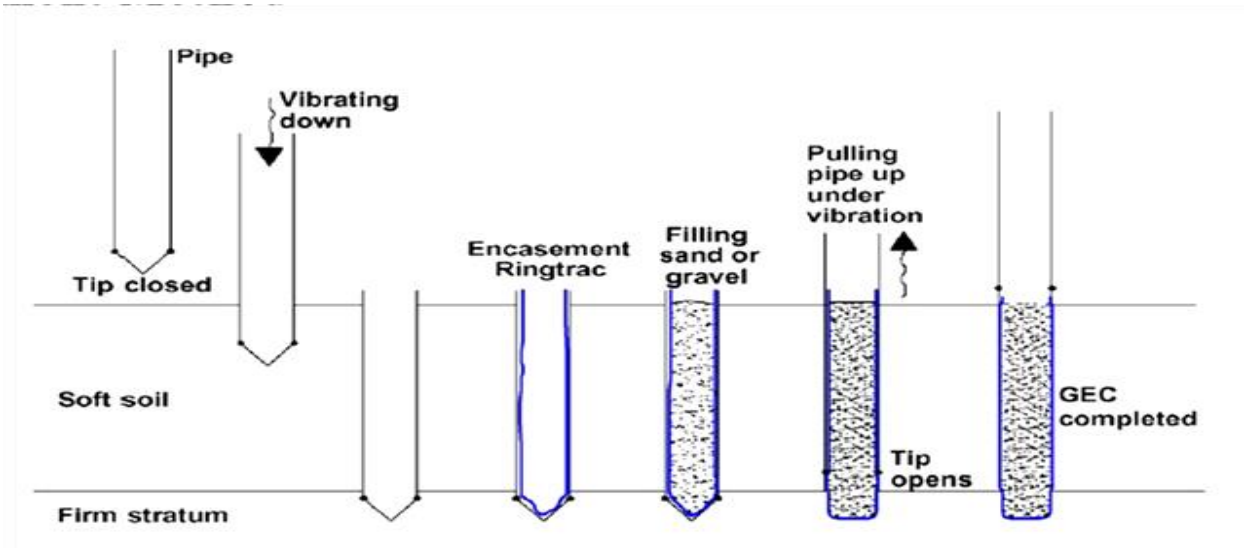

Figure 2.6: Displacement method (Alexiew et al., 2005)

2.3.1.2 Replacement Method

This method of installation has been adopted if there is the potential for vibration to influence adjacent buildings or the soil has a rather high resistance to penetration. An open steel pipe is installed into the soil until it reaches the hard layer, followed by the removal of the soil within the shaft via an auger boring. Figure 2.7 exhibits the replacement method produced by Gniel & Bouazza (2010).

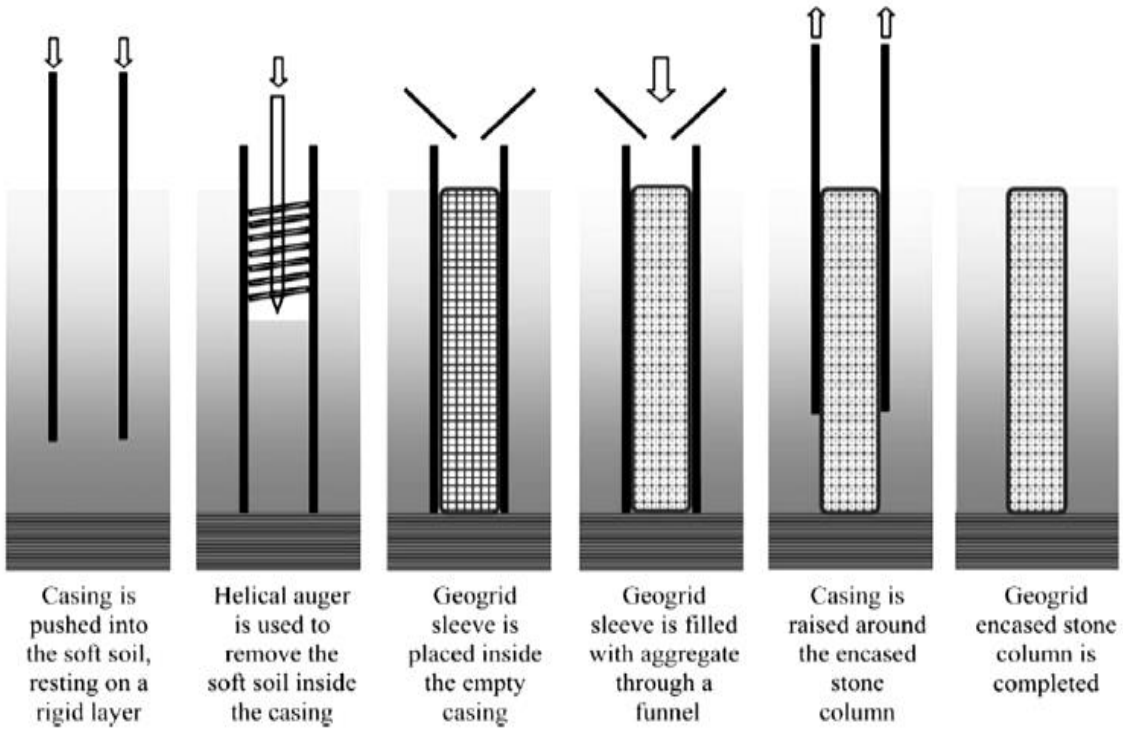

Figure 2.7: Replacement method (Gniel & Bouazza, 2010)

An additional method of construction is presented in the field by Lee et al. (2008). They performed a method of construction for partially encased stone columns. A polyester geogrid is used and designed to have the same diameter as the column to be constructed (0.8m) and lengths equal to two and three times the diameter, respectively. An auger is employed for drilling; after that a casing is installed and soil is removed as shown in Fig. 2.8. Then, stones of 25mm in diameter are inserted into the casing in layers and each layer is compacted until they form the shape of the stone column to the height where the geogrid has been designed to be placed. Finally, the cylindrical geogrid is implanted into the stone column and the stone column is built up to the ground surface, with a depth of 5.5 m. For illustration, see Figs. 2.9 and 2.10.

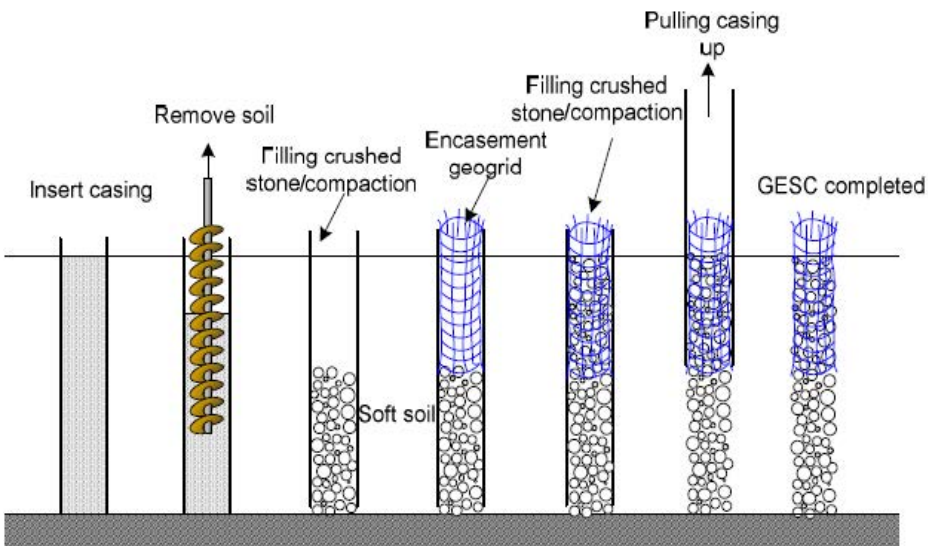

Figure 2.8: Installation of partially encased stone column in the field (Lee et al., 2008)

Figure 2.9: Inserting a geogrid net into a pre-bored and partially constructed stone column (Lee et al., 2008)

Figure 2.10: Construction of a partially encased stone column in soil (Lee et al., 2008)

2.3.2. Factors Affecting Performance of Encapsulated Stone Columns and Failure Mechanism

In comparison to an uncased column, an encased granular column increases the stress concentration on the column, thereby reducing the load on the soil, consequently reducing settlement (Malarvizhi & Ilampararuthi, 2007). Stress in an encapsulated granular column increases when reducing the column diameter, because of the mobilisation of higher confining stresses in a smaller diameter; this trend for stress is different from that of an ordinary granular column, which is not related to the diameter (Tandel et al., 2013).

Encasing stone columns is recommended in soft soils using stiff encasements and under moderate loads because, for high applied loads, the encasement reaches its tensile strength and does not provide any further improvement. Also, column encasement has a negligible effect for an elastic column and starts to be useful only after column yielding. Thus, no distinct sign of strength yield can be found in encased columns before the encasement reaches its yield strength (Hong, 2012).

The settlement reduction provided by the encasement does not depend on the area replacement ratio (Castro & Sagaseta, 2011). However, it depends significantly on the stiffness of the encasement, as shown in the laboratory work by Ayadat (1990), and more recently in the numerical study presented by Zhang & Zhao (2015).

Das & Pal (2013), in their laboratory study on two different types of soil (sandy silt soil and clay soil), distinguished the effect of the shear strength of the host ground on the amount of bearing pressure achieved by the encased system, but it was less than that of the unreinforced stone column.

Hataf & Nabipour (2013) distinguished a stiffer performance by encased columns with coarser fill material in the column, in comparison to using finer fill material.

For a certain settlement, the scale of bulging in an encapsulated stone column is far less than in an uncased stone column, regardless of the condition of the column at the end, whether floating or end bearing (Malarvizhi & Ilamparuthi, 2010). This general bulging failure occurred in such arrangement of installation and the small size of expansion of the wrapped column are also confirmed by Ghazavi & Afshar (2013). Since bulging of stone columns takes place only in the upper portion, due to the lack of lateral pressure, providing a geosynthetic in that portion may also be equally as beneficial as the entire length (Ali et al., 2010; Tandel et al., 2013). Bulging could occur at a different depth of the stone column; in the case of stone columns in layered soils, it can be seen that bulging occurred predominantly in weaker soil, due to the reduced lateral confinement offered by that soil (Das & Pal, 2013).

Regarding grouped stone columns, the failure mode observed was a combination of bulging and lateral deflection of the stone columns. In tests on a single stone column, because the column was placed at the centre of the loading plate, the bulging was axisymmetric and the stress in the stone column and surrounding clay bed was uniform. However, in tests on groups of stone columns, because the columns were not centrally located under the loading plate, the stresses around the stone columns were not similar (Ghazavi & Afshar, 2013).

2.3.3. Ultimate Carrying Capacity

The majority of the suggested design methods for encapsulated granular columns installed in soft soils simulate the influence of encasement by providing an extra lateral confining stress. The amount is generally estimated from values of the geotextile's properties (stiffness and thickness) and the value of the diameter of the column.

Ayadat & Hanna (2005) deduced the calculation of the ultimate carrying capacity of the encapsulated stone column inserted into a collapsible deposit. It is governed by the geosynthetics lateral resistance in addition to the lateral confining earth pressure of the surrounding soil based on works produced for the conventional stone column by Hughes & Withers (1974), Hughes et al. (1975), and Briaud (1991). However, the undrained shear strength of the soil is computed based on a saturated case, while the actual case of natural collapsible soil is partially saturated. Thus, variations in degree of soil saturation and the

associated matric suction were not included. The governed equation by Ayadat & Hanna (2005) and more details are presented in Section 7.3.

2.3.4. Settlement

Ayadat & Hanna, (2005) produced an equation to calculate the total settlement of an end bearing stone column inserted into collapsible soil subjected to an external load upon wetting. They considered that the total settlement under these circumstances consists of three components, which could be defined as follows:

$$\Delta=\delta_1+\delta_2+\delta_3 \qquad (2.1)$$

Where:

Δ: the total settlement of a stone column subjected to an external load and under inundation;

δ_1: the elastic settlement of the column owing to the axial load;

δ_2: the settlement due to down drag force owing to consolidation of the nearby soil; and

δ_3: the vertical settlement due to the lateral displacement of the column.

They relied on the analytical models for compressible piles introduced by Poulos & Davis (1975) and Hughes & Withers (1974).

In the case of a floating column, it should take a fourth component of settlement δ_4 into consideration. That component is due to the settlement of the soil strata located below the column‟s tip, and is a result of inundation.

2.3.5. Previous Laboratory Studies on Reinforced Stone Columns

Table 2-3 outlines the recent published work related to the encasement of granular columns that has been carried out in the laboratory. The table illustrates how researchers presented their models, what the geometry was, and what materials they used for the soil beds and column fills. Also, the table shows how the encasement fabrics were employed; how the encased stone columns were installed in the soil bed; how the overlapping of the encasement was achieved, if mentioned; and how loading was applied. Finally, the last column in the table gives the main conclusions that were drawn. The following sections will discuss the points mentioned above in this section in detail, so the methodology of this research can be built based on findings drawn from previous studies, and so the knowledge gap can be clearly

identified. Consequently, the construction of the model in the present study will be clearly outlined.

2.3.5.1. Type of Host Soil

According to the literature presented in Table 2-3, little research has been done without soil surrounding the granular column creating a load on the encased granular material (see Gniel & Bouazza (2010), Lee & Yoo (2011) and Miranda & Da Costa (2016). Authors stated that they still adopted the unit cell concept, but with full replacement of the soil, and according to this case, the area replacement ratio (a_r) had been chosen (1). Although these studies drew good conclusions regarding the overlapping effect, the influence of the confining soil on the overlapping was not taken into consideration, as their model neglected the presence of soil.

Most laboratory investigations mentioned studied clayey soil stabilised with an encased rammed stone column e.g. Sivakumar et al (2004), Murugesan & Rajagopal (2009), Najjar et al. (2010), Demir et al. (2013), and Demir & Sarici (2016). Some investigators worked with this remedy in sandy soil such as di Prisco & Galli (2011), Hataf & Nabipour (2013), sandy silt e.g. Das & Pal (2013), and sensitive deposits, as will be explained in more detail in Section 2.3.5.8. The treatment showed successful performance with all soil types, and specifically for extremely soft soil.

2.3.5.2. Fill Material

According to Table 2-3, fill materials were represented by sand or aggregate compacted in layers or pre-frozen. It is well known that stone column performance is affected by the stiffness ratio (stiffness of column/stiffness of soil). In the field, fill materials are typically chosen to be stiffer and coarser than the surrounding soil and within a limited range of d_f/d as illustrated earlier in this chapter. So the ideal representation of stone column materials could be simulated with coarser fills, such as stones, aggregates, and gravels, rather than sand unless the diameter of the stone column was very small. A study by Hataf & Nabipour (2013) showed that coarser material presents better performance over finer fills. However, some studies used sand for simplicity of construction and adopted the idea of considering a stone column as a sand drain by preserving the function of drainage. Using sand as a fill may be suitable when soil is clayey rather than sand.

2.3.5.3. Geosynthetics Used

According to Table 2-3, materials for encasement simulated by different sorts of geosynthetics, including those that were woven and non-woven. To achieve an adequate overlapping of the encasement material, they were glued or sewn. The size of the models ranged from medium to large scale models. Different area replacement ratios (a_r) and length to diameter (l/d) ratios were adopted. The main criteria for selecting a geosynthetic were adequate stiffness and ability to act as a filter, allowing water to drain from the soil while preventing the soil from squeezing inside the fill material. Higher stiffness geogrids or geotextiles perform better e.g. Gniel & Bouazza (2010) and di Prisco & Galli (2011).

2.3.5.4. Soil Bed Formation

The compaction technique seems to be the dominant soil formation technique used in previous trials, as shown in Table 2-3. In some studies, soil bed depositions were achieved by using consolidated slurry of Kaolin clay in a triaxial chamber (see Sivakumar et al. (2004) and Najjar et al. (2010)) or one-dimensionally large cells such as that presented by Gniel & Bouazza (2009) and Murugesan & Rajagopal (2009).

2.3.5.5. Column Construction

Replacement techniques for compacted or pre-frozen fills were the most common method of column construction, as shown in Table 2-3, (see Malarvizhi & Ilamparuthi, 2004; Gniel & Bouazza 2009; Najjar et al., 2010). Displacement methods were used in far fewer examples (see Black et al., 2007; Murugesan & Rajagopal 2009), but without applying any vibration energy.

2.3.5.6. Loading Arrangement

According to the literature presented in Table 2-3, loading was achieved using three main methods, as follows:

1- Loading the column only; although it gives an indication of enhancement, it still does not represent the load distribution in the field, as the soil‟s contribution to carrying the applied load is neglected (Murugesan & Rajagopal 2009; Ali et al., 2010; di Prisco & Galli, 2011; Kumar & Jain, 2013; Tandel et al., 2013; Demir et al., 2013); Demir & Sarici, 2016).

2- Loading the entire composite cell of the stone column and surrounding soil uniformly (Sivakumar et al., 2004; Gniel & Bouazza, 2009; Uttam et al., 2013) or by applying a surcharge to the entire area and axial load on the area of column (Ayadat & Hanna, 2005; Sivakumar et al., 2010). This arrangement could be considered closer to a field configuration. However, the boundary effect from the side of the test cell could become a serious source of concern.

3- Foundation-type loading through a plate that has a diameter that is larger than the stone column's diameter (SivaKumar et al., 2004; Malarvizhi & Ilamparuthi, 2004 and 2007; Black et al., 2007; Sivakumar et al., 2010; Kameshwar et al., 2011; Das & Pal, 2013; Ghazavi & Afshar, 2013; Hataf & Nabipour, 2013). The encased stone column was usually surrounded by a soil bed partly loaded inside the tank; instead of confining the loaded area of the composite cell with a rigid wall representing the interaction of grouped columns, it seems that this type of loading is the closest to the unit cell concept idealisation and consequently to the field conditions. On the other side, it also avoids the boundary effect. So in this study, this loading arrangement has been adopted.

2.3.5.7. Modelling Inundation in Previous Studies

The column-soil cell subjected to wetting was modeled in the lab by Ayadat & Hanna (2005) by raising the water level inside the chamber using a constant-head system (see Table 2-3), whilst work done by Sivakumar et al. (2010) included placing the test container inside a water tub to achieve the required level of inundation. Also, in the model of an encapsulated granular column installed in expansive soil used by Kameshwar et al. (2011), the required degree of saturation was achieved by using a perforated GI sheet as a wall tank. As can be seen, there has been little research done on inundation patterns, even though it is very important in the field to know the source of inundation and then adopt the correct guidelines for the design process.

2.3.5.8. Laboratory Modelling of Encased Stone Column Acting on Collapsible Soil

As mentioned in Section 2.4.5.1, tests confirmed the efficiency of implanting encased stone columns even in very sensitive soils, such as peat deposit (Black et al., 2007) and expansive soil (Kumar & Jain, 2013).

Moreover, Malarvizhi & Ilamparuthi (2004 and 2007) embedded their rammed foundation into clay with high plasticity (collected from an area of Yung geological deposits). The aim of the later study was to monitor the solution in a fine weak soil bed characterised by high

compressibility, but different degrees of saturation, which could play a significant role in performance, have not been taken into account. The study was done only for the value of water content; it confirmed the effect of higher geosynthetic stiffness on increasing foundation strength, regardless of the column type (floating or end bearing) for different l/d ratios.

A laboratory model was presented by Ayadat & Hanna (2005) in which the column material was represented by uniform sand, in spite of the surrounding soil being represented by gap-graded soil, which is characterised by a sand-size grain and fills ranging from 1.18-2.36 mm.

In the study of Sivakumar et al. (2010), soil bed formation was achieved by mixing Kaolin clay with well-graded medium sand, which again does not reliably represent fine collapsible soils in the field, such as loess.

In conclusion, the studies considering the treatment for fine grain like loess deposit was not considered. Also, it is worth noting that geophysical studies beforehand were not employed.

Table 2-3: Previous laboratory studies on encased stone columns

References	Soil type	Fill materials	Geosynthe-tics used	Dimensions of tank or box used	Soil bed formation	Method of installation	Loading arrangement	d	a_r	l/d ratio	Setup sketch	Main conclusions
Sivakumar et-al. (2004)	Kaolin clay	Sand (frozen)	Geogrids	A chamber of 100 mm in diameter and 200 mm (length)	Consolidation using triaxial apparatus	Replacement	1- uniform loading on the entire area of soil and column 2- foundation-type loading through a plate of 40 mm in diameter	32	0.100 0.640	3.75 6.25	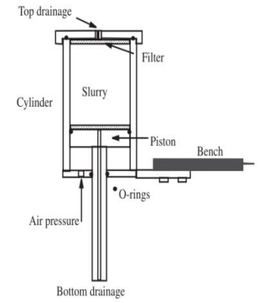	An increase of approximately 60% in encased column if compared with the ordinary sand column, and 185% if compared with the clay specimen without treatment. Shorter columns showed no increase in capacity, authors suggested this was due to the comparatively smooth surface features of the geogrids used.
Malarvizhi & Ilamparuthi (2004)	Marine clay of high plasticity	Granite chips compacted in layers	Nova curtain, Netlon square mesh, and Netlon CE121 (stitched)	A tank of 300 mm in diameter and 280 mm in height	Compaction in layers	Replacement	Foundation-type loading through a plate of 72 mm in diameter	30	0.174	9.33 7.50 5.00	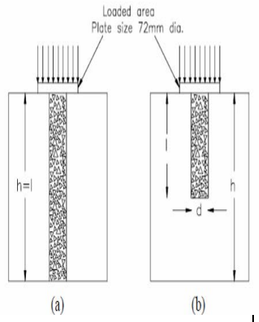	An increase in load carrying capacity irrespective of whether the column is end-bearing or floating. In the case of floating columns, the l/d ratio has less effect on the capacity of column for the lengths considered in this study. On the other hand, the modular ratio in end-bearing columns increases with increased settlement, regardless of the type of encasing material.
Malarvizhi & Ilamparuthi (2007)	Clay collected from a geological-ly young area	Granite chips (compacted in layers)	Nova curtain, Netlon square mesh, and Netlon CE121 (stitched)	A tank of 300 mm in diameter and 280 mm in height	Compaction in layers	Replacement	Foundation-type loading through a plate of 2.3 d in diameter	30	0.174	Various l/d	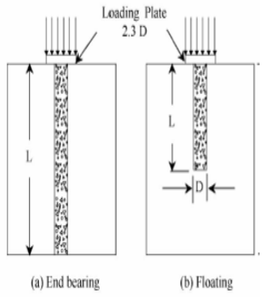	Bulging is distinguished at the top 4D of the column‟s length. Effectiveness of the encased stone column is higher if the column material is compressed well; as l/d ratio increases, settlement reduction ratio is reduced, but it is effective up to l/d=7.5, contrary to l/d=10 in a conventional stone column.

References	Soil type	Fill materials	Geosynthe-tics used	Dimensions of tank or box used	Soil bed formation	Method of installation	Loading arrangement	d	a_r	l/d ratio	Setup sketch	Main conclusions
Ayadat & Hanna (2005)	Collapsible soil	Coarse, uniformly graded sand (compacted)	Terram fabrics	A chamber of 390 mm in inner diameter, 407.5 mm in outer diameter, and 520 mm in depth	Compacting the soil inside the chamber in layers around a hollow aluminium tube at the centre of the chamber	After soil compaction, the tube at the centre was filled by sand which was compacted in layers successively	Surcharge on the entire area and axial load on footing of 40 mm diameter; wetting by raising the water level inside the cell using a constant-head system	23	0.330	10.87 13.04 17.82	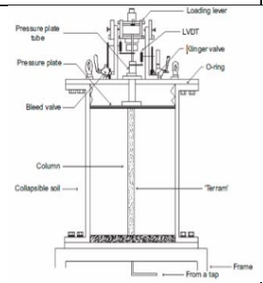	In such treatment, an increase in bearing capacity and reduction in settlement were noticed. Also, the encapsulated technique exposed a safe transfer of the load.
Black et al. (2007)	Peat sandwiched between two sand layers	Aggregate	Tubular wire mesh	A large steel-framed wooden box 1500 mm x 700 mm x 700 mm	Forming the soil bed first and then installing the stone column, but no vibration is represented	Displacement	Load was applied through a 145 mm diameter circular plate	80	0.300	9.00	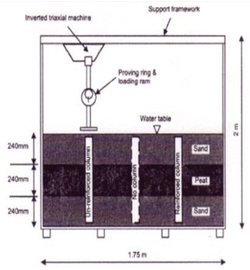	The method worked adequately as column bulging is restricted as a result to the further restraint delivered by the mesh, and a considerable improvement in load and settlement response is achieved.
Gniel & Bouazza (2009)	Kaolin clay	Frozen sand column	Fibreglass & Aluminium mesh (10 mm overlap resin curing)	A chamber of 260 mm x 540 mm	Enlarged consolidation cell, consolidating the slurry to the consistency of very soft clay	Replacement	The total area of soil bed and column were loaded through the piston provided with the cell	51	0.110	6.00	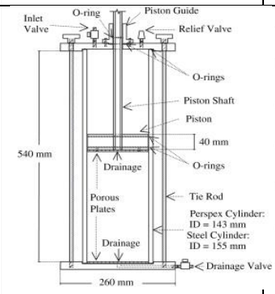	A substantial radial bulging was noticed directly below the base of the encasement. For partially encased columns, the bulging took place along the full length of the non-encased section and it was bound to a length of about 2 column diameters.
Gniel & Bouazza (2010)	No soil	Full-scale typical aggregates	Geogrid with a nominal amount of circumfere ntial overlap	Dimensions of unconfined compression machine	No soil	Filling the sleeve with aggregates	A constant displacement technique of loading was adopted rather than static loading, due to time constraints	240	1.000	3.58	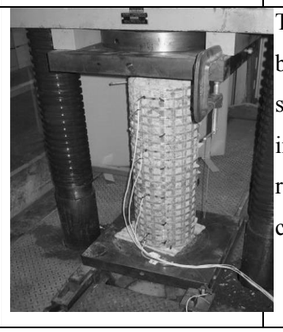	The outcomes indicated that biaxial geogrids are the best suited to the system. The increase in encasement stiffness resulted in increased column capacity and column stiffness.

References	Soil type	Fill materials	Geosynthe-tics used	Dimensions of tank or box used	Soil bed formation	Method of installation	Loading arrangement	d	a_r	l/d ratio	Setup sketch	Main conclusions
Murugesan & Rajagopal (2009)	Clay was obtained from a lake bed	Granite chips	Woven and non-woven geotextiles (stitched)	A tank of 210 mm in diameter and 500 mm in depth	Consolidating the slurry clay in laboratory-controlled conditions	Displacement	Loading only the stone column through a plate that has the same column diameter	50, 75, and 100	1.000	10.00, 6.66, and 5.00	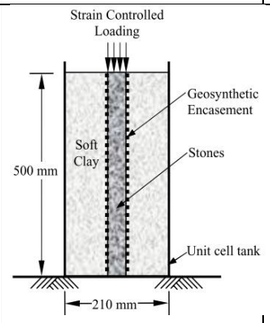	The failure mostly showed a linear trend without demonstrating any disastrous failure, which can be noticed in the conventional stone columns. Regarding the effect of column diameter, superior performance is noticed for columns with smaller diameters.
Sivakumar et al. (2010)	Loess soil (kaolin and well-graded medium sand at a ratio of 1:9)	Crushed basalt	Geogrid woven thread reinforcing mesh	One-dimensional chamber of 200 mm in diameter and 250 mm in height	Compaction in layers	Replacement	A constant surcharge mounted on the fill surface; the diameter of the footing was 50 mm, and load subjected upon wetting	32	0.41	7.81	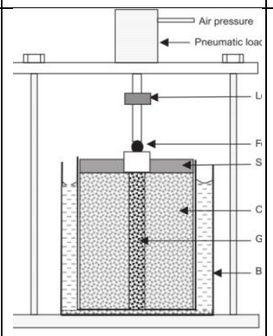	Using granular columns resulted in a significant reduction in bearing capacity, and caused considerable wetting-induced settlement, whilst the presence of geogrids contributed to increasing the bearing pressure and decreasing induced settlement.
Ali et al. (2010)	Kaolin clay	Stone chips	Geosynthe-tics	A cylindrical tank of 300 mm in diameter and 600 mm in depth	Compacted in layers	Replacement method	Loading the column only through 50 mm diameter loading plate	50	1.00	6.00		Encasing the granular column increased the bearing pressure many times over. Smaller columns showed affectivity over larger ones. Bulging of stone columns was noticed in the upper zone, so providing geosynthetics for that portion may be adequate.
Najjar et al. (2010)	Kaolin clay	Sand	Geosynthe-tics	Triaxial cell	Consolidation	Replacement method for the frozen sand column	Specimens were consolidated under effective confining pressures 100, 150, and 200 kPa and ; sheared at a strain rate 1%	20 & 30	≈0.080 & 0.180	3.55 5.30 7.10, & 2.30 4.60	CU tests with pore pressure measurement setup	Strain hardening behaviour was observed for fully penetrating encased columns only. This behaviour was resulted in an insignificant drop in the pore-water pressure; was more noticeable for higher a_r.

References	Soil type	Fill materials	Geosynthe-tics used	Dimensions of tank or box used	Soil bed formation	Method of installation	Loading arrangement	d	a_r	l/d ratio	Setup sketch	Main conclusions
di Prisco & Galli (2011)	Loose sand	Sand (compacted)	Non-woven & woven geotextile of polyethy-lene (glued & sewn)	A rigid caisson 400 mm x 800 mm x 200 mm	Pluvial deposition method to obtain a loose sand stratum (DR < 40%)	Compaction/ extraction procedure	The vertical load was applied on the top of the column by means of a rigid circular loading plate with a diameter of 40 mm	40	1.000	10.00	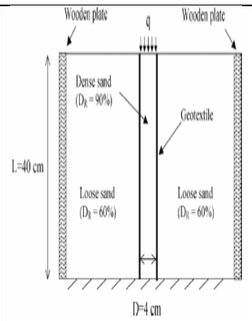	Once vertical load has adequately increased, a locking behaviour could be reached. On other hand, the average stiffness of unloading-reloading cycles is not influenced by either the mechanical properties of the geosynthetics or the stress level, although the amplitude of the cycles intensely impacts the reloading stiffness.
Kameshwar et al. (2011)	Inorganic clay under soaking conditions	77% black cotton soil, 15% fine sand & 8% lime	Two types of geosyntheti c with different bearing capacities	A tank of 100 mm in diameter and 300 mm in length	Compaction in layers	Replacement	A rigid M.S. plate equivalent to the diameter of the unit cell under consideration is placed on top of the stone column concentrically	25, 20, and 15	0.062	various	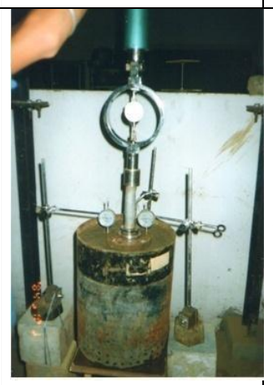	The percentage of decline in settlement indicated a greater amount with larger diameters and longer lengths of stone columns. The dual techniques of using treated material for the granular column and wrapping it with a geosynthetic are beneficial in developing additional load carrying capacity compared to an ordinary stone column.
Lee &Yoo (2011)	No soil	Compacted crushed stone	Two polyester geogrids (overlap)	A medium-scale unconfined compression frame	Filling with crushed stones	Compacting the stones inside the geogrid tube in three batches	Compression testing machine	250	1.000	3.20	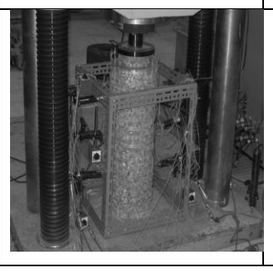	The overlap is an important fact-or governing conduct when an overlap is achieved.

References	Soil type	Fill materials	Geosynthe-tics used	Dimensions of tank or box used	Soil bed formation	Method of installation	Loading arrangement	d	a_r	l/d ratio	Setup sketch	Main conclusions
Ghazavi & Afshar (2013)	Clay	Crushed stone	Two types of nonwoven polypropylene geotextile 15 mm, overlapping	A large test box with plan dimensions of 1200 × 1200 x 900 mm	Clay bed prepared in layers (compaction)	Replacement	Loading single stone column through rigid plate (200 mm) Loading the triangle group with rigid plate 2.3 d (260 mm)	60, 80, and 100 60	0.053	5.00	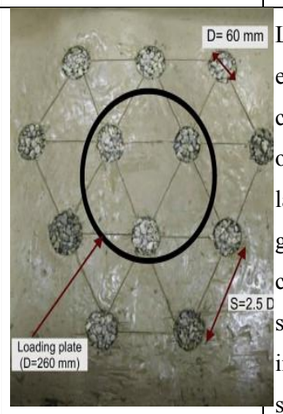	Lateral bulging decreases in encapsulated columns in comparison to conventional ones, as a result of the extra lateral confinement provided by geosynthetics. The ultimate capacity and stiffness of the stone columns increase when increasing the length and stiffness of the reinforcing encasement.
Uttam et al. (2013)	Weak deposits	Sand	Woven and non-woven geotextiles and geogrids (sewn and glued)	A tank of size 500 mm × 500 mm × 450 mm	Compaction with layers	Displacement	Loading on entire tank	50 and 75	0.010 0.010	8.00 and 5.33		The efficiency of a smaller diameter sand column is superior to that of bigger diameter ones. An encasement up to four times the diameter of the sand column may be adequate.
Das & Pal (2013)	Two soils, sandy silt and clay soil	Crushed stone aggregates	geotextile sheet	A cubic tank (height 450 mm, 320 mm × 320 mm	Compaction of soil and aggregates simultaneously		Load applied mechanically in a compression testing machine	50, 60, 70, 80, 90, and 100	1.000	6.00, 5.00, 4.28, 3.75, 3.33, and 3.00		The load capacity of encased columns is slightly more reliant on the strength of the surrounding soil compared to uncased stone columns. The strength of the encasement increases and the lateral stresses transmitted to the surrounding soil decrease.

References	Soil type	Fill materials	Geosynthe-tics used	Dimensions of tank or box used	Soil bed formation	Method of installation	Loading arrangement	d	a_r	l/d ratio	Setup sketch	Main conclusions
Kumar & Jain (2013)	Weak deposits of expansive soil	River sand	Nova net (stitched)	Tanks of 250, 325 and 400 mm heights and157.5, 204. 75, and 252 mm diameters	Compaction in layers	Replacement	Load applying to the stone column through a plate with a diameter the same as the column diameter	50, 65, and 80	Various	8.00, 6.15, and 5.00	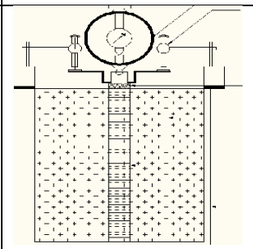	An obvious boost in carrying capacity when reinforcing the stone column. This capacity increases significantly with respect to increases in the diameter of the granular column.
Tandel et al. (2013)	Clay	Sand	Nova curtain, non-woven and woven geotextiles (epoxy-resin)	A steel cylindrical tank of 260 mm in diameter, 600 mm in height;	Compaction in layers, the depth of the clayey bed was 450 mm	Displacement	Through a rigid loading plate with a diameter equal to that of the stone column, placed over the stone column	50 and 75	1.000	9.00 and 6.00	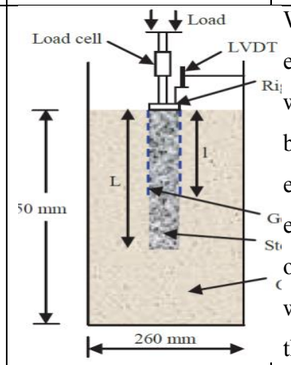	Wrapping the granular column enhanced the behaviour, whether the column was end bearing, floating, or partly encased. The stiffness of the encasement material has an obvious influence. The wrapping up to the top part of the stone column can considerably increase its load carrying capacity.
Demir et al. (2013)	Clay	Crushed stone	Geogrids	A circular test cell of 400 mm in diameter and 400 mm in height	Compaction soil in layers around an empty casing pipe	The pipe at the centre was filled with stones into batches	Loading on column only through plate of the same column diameter	50 and 100	1.000	8.00 and 4.00	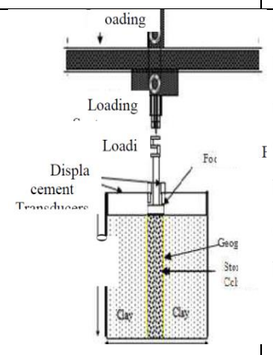	Smaller diameter stone columns have lower bearing capacity than larger diameter ones. Geogrid encasement increases bearing capacity of stone column because bulging behaviour of stone column is limited.
Hataf & Nabipour (2013)	Two, cohesive soil (clay) and granular soil (sand)	Different size of aggregates	An encasement	Cylindrical container of 100 mm in diameter and 100 mm in height	Compaction soil in layers around an empty casing pipe	The pipe at the centre was filled with stones into batches	The static loading system applied on circular foundations resting on a stone column		1.000	Not mentio-ned		Stone column reinforced with geosynthetic is more active in cohesive soils compared to granular soils. Also, coarser aggregates have better behaviour in comparison to finer ones. Reinforcing half of the column‟s length, particularly in clay, is the optimal encasing length.

References	Soil type	Fill materials	Geosynthe-tics used	Dimensions of tank or box used	Soil bed formation	Method of installation	Loading arrangement	d	a_r	l/d ratio	Setup sketch	Main conclusions
Afshar & Ghazavi 2014)	Clay	Crushed stone	Nonwoven polyprop-ylene geotextile	Large test box with plan dimensions of 1,200 mm x 1,200 mm	Compaction	Replacement	Rigid steel loading plate with a diameter of 200 mm and a thickness of 30 mm	60, 80, and 100	0.300, 0.400, and 0.500	5.00	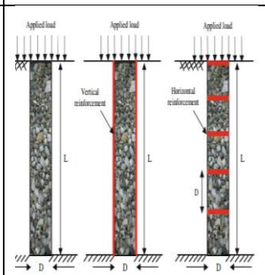	The study proved the effectiveness of a column reinforced with a cage of geotextile or geocell discs. However, the investigators suggested additional tests are required to investigate the load carrying performance of both columns with the same area ratio of replacement.
Fattah et al. (2016)	Clayey silty soil	Crushed stone	Pars mesh polymer type SQ12	Steel container of 1,500 mm length, 800 mm width, and 1,000 mm depth	Putting in the wet soil in 11 layers by light tamping	Replacement	Footing-type foundation under embankment resting on grouped stone column; load is applied by a hydraulic system	70	Varying spacing between columns 2.5d, 3d, and 4d	5.00 and 8.00	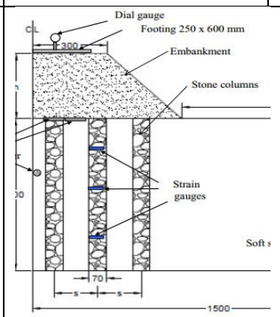	An embankment model, resting on soft soil reinforced with a group of encased stone columns, was tested. The results indicated that the bearing ratio of the system (for a particular height of embankment) increased with decreased spacing distances between the stone columns.
Demir & Sarici (2016)	Soft clay	Crushed stone	Polypropyl ene	Cylindrical tank of 600 mm diameter and 600 mm height was used	Compaction	Replacement	Load was applied on a steel circular plate of 50 mm diameter and 25 mm thickness	50	1.000	10.00	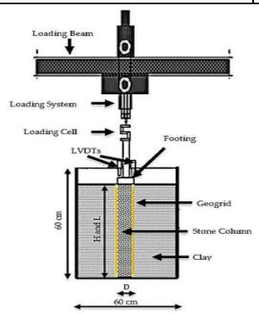	Performance was affected by encasement length. It was observed that for different encased lengths, bulging occurred roughly below the encasement.
Miranda & Da Costa (2016)	No soil	Uniformly graded limestone gravel	Polyester threads and Robutec woven fabrics (glued)	Triaxial samples 200 mm high x 100 mm in diameter		Freezing and thawing (two different relative densities of the gravel, 50% and 80%)	CD test was employed and confining pressures of 25, 50, 150, and 300 kPa were chosen for the tests; afterward, the sample was axially loaded	100	1.000	2.00		This improvement is more significant for low confining pressures at both densities. For a certain axial strain, the effect of the geotextile is noticeable as a result of the volume change of the sample during the defrosting

References	Soil type	Fill materials	Geosynthe-tics used	Dimensions of tank or box used	Soil bed formation	Method of installation	Loading arrangement	d	a_r	l/d ratio	Setup sketch	Main conclusions
												operation, and the isotropic consolidation stage, which makes the diameter of the sample without encasement to some extent smaller than that with encapsulation.

2.4. Summary

An intensive review of the literature concerning stone columns with and without encapsulation with geosynthetics has been performed. The literature showed ordinary stone columns have failed to treat collapsible soil, because the latter was not able to deliver the required strength upon inundation. The encasement of the column with geosynthetics has been offered as a successful technique to enhance its behaviour in such collapsible fill. The significant effect of the shear strength of the host soil on the improvement achieved by the stone column has been addressed by previous researchers. However, the effect of collapse potential of the soil itself upon a change in the degree of saturation of the collapsible soil has not been dealt with before.

Previous conventional research in this topic included field, laboratory, and theoretical studies but recent work used a geophysical method (seismic wave method) to assess the performance of the reinforced foundation after the treatment. The method showed a potential to find the shear modulus profile of the treated ground but was associated with some restrictions such as the lack of comparative data, technical issues, the need to reinterpret the results in the existence of water, and the fact that it could provide two dimensions image only.

Electrical resistivity tomography (ERT) is a powerful, inexpensive technique used recently and applicable in many earthwork projects. Further literature is reviewed in Chapter Five. ERT is 2D or 3D imaging tool, the latter it can provide both horizontal and vertical profiles. However, using this method in observing treated soil with a stone column and knowing the geophysical properties of the system have not been considered previously.

Also according to the literature, the calculation of the ultimate carrying capacity of the encased stone column inserted into a collapsible deposit is controlled by the geosynthetics stiffness and the lateral confining offered by the surrounding host soil. However, the shear strength of the soil is determined according to the saturated case, not the actual dry or partially saturated case. Thus, changes in degree of saturation and the associated matric suction of the soil were not involved. So, producing an equation to compute the shear strength of unsaturated case is needed.

Majority of laboratory studies of using encased stone column had been performed to date using clayey or sandy soil as the host. The treatment showed successful performance with all soil types, and specifically for extremely soft soil. Fill materials were represented by sand or

aggregate compacted in layers or pre-frozen. The main criteria for selecting a geosynthetic were adequate stiffness and ability to act as a filter, allowing water to drain from the soil while preventing the soil from squeezing inside the fill material. Higher stiffness geogrids or geotextiles perform better. The compaction technique seems to be the dominant soil formation technique used in previous trials. Replacement techniques for compacted or pre-frozen fills were the most common method of column construction. The footing type foundation is the closest to the unit cell concept idealisation and consequently to the field conditions. The inundation patterns to simulate rising ground water through the soil layers have not been studied in any detail and the linked available studies are very few. Collapsible fine soils such as loess have not been considered in this context.

In summary, all above points from literature has been considered and they have helped to build the physical, geophysical, and analytical models used in this study and covering the knowledge gap in this field (see later chapters of this thesis). The review indicated the need to conduct this study as a result of a clear lack of studies on stone columns acting on fine collapsible soil, under changeable soaking and loading conditions, specifically using an electrical tomography system that can monitor the buried soil-column profile successfully.

CHAPTER THREE

MODELLING THE HOST GROUND

3.1. Introduction

This chapter describes the method used to prepare the artificial soil used to provide a controllable collapsible loessial deposit. Samples were formed in the laboratory, by compacting the soil at dry-of-optimum water content and then leaving the compacted sample to dry to allow bonds to form, see Miller (2002) for further details. This method was shown to be a good process for creating a large uniform loess model. The silt and clay particles of the natural collapse soil were modelled by mixing silica flour type M10 with different percentages of English China clay (ECC).

A series of single and double oedometer tests have been conducted to examine the collapse behaviour. The aim was to find out the collapse potential ranges obtained and how the artificial soil mimics the behaviour of natural deposits. From this, the right mixture and method for developing the host soil of the stone column tests were made.

This chapter provides the basic in selection the host collapsible soil used throughout this work (see Chapters Four and Five).

3.2 Modelling the Meta-Stable Soil in the Laboratory

With collapsible soils, sample extraction process even by thin-walled tubes can compress the soil notably, giving a new void ratio that is different from that of natural conditions (Houston et al., 2001). The sampling of the undisturbed samples is complicated in both dry and wet collapsible deposits such as loess; accordingly that is why controlled laboratory tests are often used (Bally, 1988).

However, many artificial soil models may not fully duplicate natural soil behaviour (Medero et al., 2009). Importantly, therefore is to find a balance between sample control and reliable duplication of natural behaviour. Thus, forming an artificial loess model in the laboratory requires making a model soil, which represents the natural loess under loading that exhibits a certain collapse potential under inundation. The key importance here is the way of representing the sedimentation of the deposits, and selecting the material used to simulate the silt particles and clay bridges (Miller, 2002).

3.3 Previous Methods and their Feasibility in Producing a Large Specimen

One of the methods for the preparation a lossic deposit model is the air-fall method, presented by Assallay et al. (1997) who provided a satisfactory sample of collapsing loess. The procedure for producing the sample included sieving the silt particles, and leaving them to fall from a certain height (250-400 mm) onto the oedometer‟s ring, positioned above a porous stone disc. As a result, it can simulate the initial structure that is shaped when particles are primarily deposited in air-fall mode

However, there are some limitations to this method. One of the disadvantages is the inconvenience caused by the dust pollution during air fall mode, especially in cases where a large sample of soil is formed, in addition to the exaggeration of the recorded collapse potential when comparing the results of the undisturbed samples with those of artificially created samples, as shown in Fig. 3.1. Also, there is a difficulty in controlling the corresponding target water content. Dibben (1998) used a steaming method; the specimen was positioned over a boiling container of water, and the steam was forced through the small specimen until the whole sample was wetted. Obviously, the steaming method could only suit the preparation of small samples, but when a big sample of multiple layers is steamed, the lower layers may collapse under the weight of the higher material due to the higher water content produced lower down the sample (Miller, 2002).

Some previous investigators have adopted various strategies by forming slurry of soil at 1.5 times the liquid limit, which is hydrated for weeks, then consolidated under a specific stress to produce a reconstituted sample e.g. Cunningham et al., (2003). Others dehydrated this slurry to form a stiff product that is ground and then compacted later on to produce a compacted collapsible sample e.g. Assallay (1998). Jotisankasa (2005) used both procedures with the slurry, and presented reconstituted and compacted collapsible samples based on those previous studies, as illustrated in Fig. 3.2. Jiang et al (2012) used disturbed natural loess samples after drying them for period of two weeks and then crushing them before adding 0.6% calcium oxide CaO. The material compacted in oedometer and triaxial cells and submerged into de-aired water to change the added CaO into calcium hydroxide $Ca(OH)_2$. The later would change to $CaCO_3$ by maintaining an internal pressure of the sample of 200 kPa for 24 hours when the cell was subjected to Carbon dioxide (CO_2) gas. This was followed by air –drying process for obtaining the required water content. Indeed, those procedures following the slurry creation or applying a gas for stimulating chemical reactions

are time consuming making this method not applicable for modelling a large volume of collapsible soil.

Recently, Langroudi & Jefferson (2013) used Leighton Buzzard sand to produce their target loess model weighting 150 g. The sand was mechanically crushed by a high-energy disc mill and then graded to a silt-sized range by sedimentation techniques. The mix of 70% silt, 10% kaolinite and 20% carbonates mixed thoroughly and settled into a standard oedometer ring by a nozzle from a vertical distance of 400 mm, then distilled water was successively added using a spray over the top surface of each layer of 2 mm thickness. Once more, this method can suit small specimens, rather than large ones.

However, other researchers investigated the wet paste method as an alternative to the previous methods above, which could suit a large sample (Miller, 2002). This approach includes compacting samples of differing clay contents by the same static load, then samples are left to dry out for bond formation satisfying a wet-dry cycle. Miller (2002) used this method as well as other methods and showed a good result when the comparison between the created sample and the natural loess deposit is made for the oedometer‟s ring size sample, after assessing the collapse potential for different mixtures through the oedometer size samples and as the corresponding triaxial samples obtained their maximum stiffness for a dryness period of two days. She chose to compact the ground silica HPF4 at dry of optimum after mixing with 30% clay to prepare her large sample. Soil compaction was carried out in a medium size perspex box with dimensions of (490 mm x 400 mm) in seven layers; each layer had been left for two days before the next layer was compacted on top, so the soil was allowed to dry and the bonds to form.

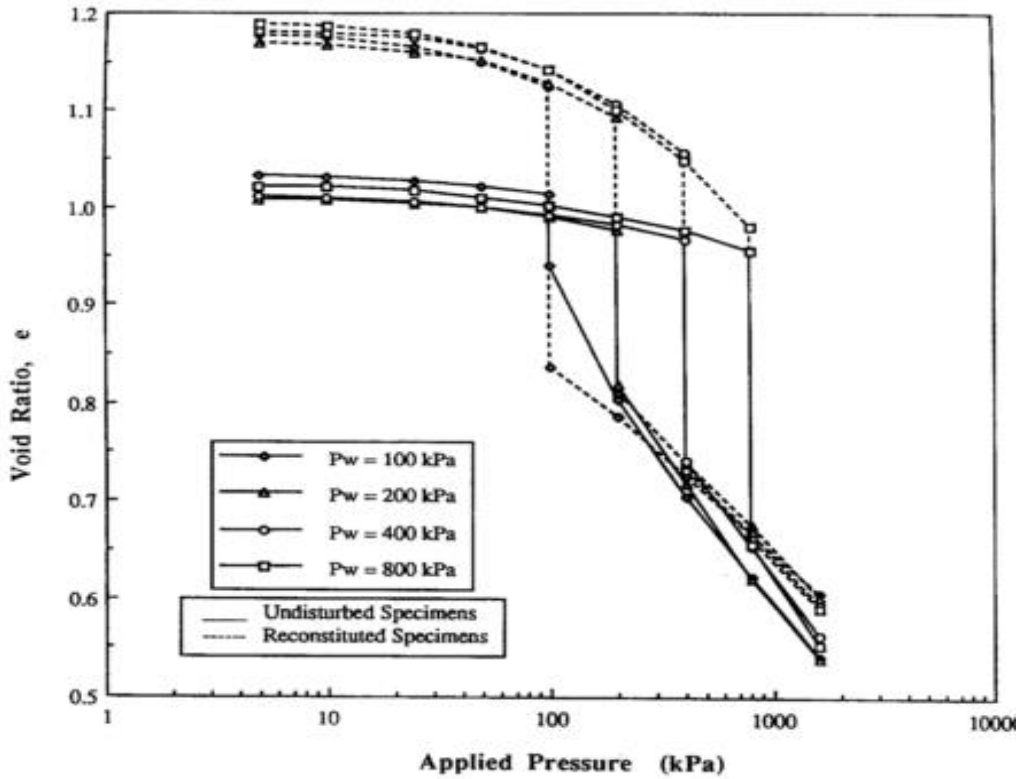

Figure 3.1 : Comparison of the collapsibility of the undisturbed Malan loess from China and the reconstituted air fall method samples by Assallay et al. (1997)

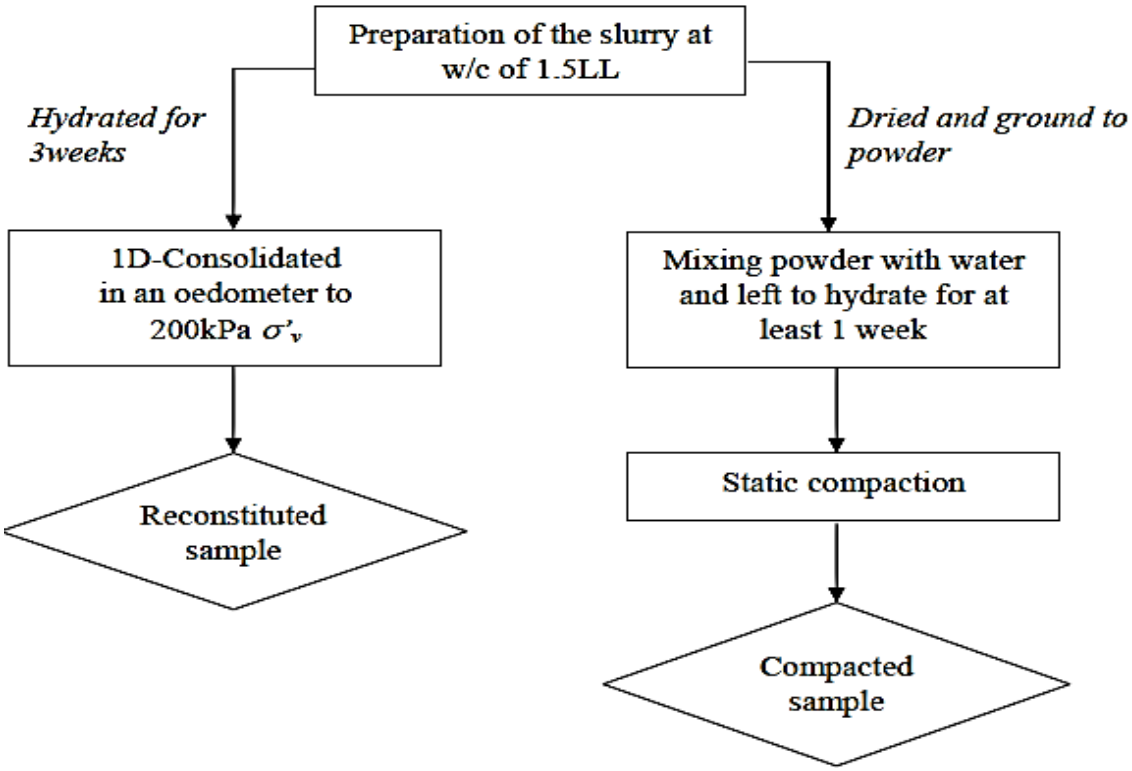

Figure 3.2: Flow chart representing the schematic procedure to produce a reconstituted sample and a compacted sample of collapsible soil (Jotisankasa, 2005)

3.4 Selecting the Method and the Material Used in this Study

It appears that the wet paste method presented by Miller (2002) for her large footing model is the most applicable method to produce the metastable loess model. However, the HPF4 ground silica employed in her study is no longer available in the material markets, so it has been necessary to find an alternative material that can simulate the size of the particles.

The following sections present the work to simulate a loess deposit using M10 silica flour, taking into account factors that can play a role in its collapsibility such as changing clay content, initial water content, initial void ratio, and drying period. Also, this will be used as a guide for researchers to focus on the source of the material as an attempt to test another soil from different geologic origin has failed in producing the target collapsible soil although it has almost the same range of soil particles.

3.5 Materials

In this investigation, three types of soils were tested; Soil A, Soil B, and ECC. Soil A and Soil B are alternately used to simulate the silt particles of the artificial loess while ECC is used to simulate the associated clay bridges.

Table 3-1 summarises the descriptions and properties of the three soils. The relationship between optimum water content and maximum dry density for the three tested soils is shown in Fig. 3.3; compaction was conducted using Light Compaction Method (2.5 kg compaction rammer falling from a height of 300 mm) according to BS 1377: Part 4 (BSI, 1990).

The corresponding calculations of the specific gravity, liquid limit, plastic limit, and compaction tests for the three soils are summarised in the tables and figures shown in Appendix (B), see Table B-1 to Table B-12 and Fig. B.1 to Fig. B.3. The technical details of all three selected materials were provided by the manufacturers and are illustrated in tables B-13, B-14, and B-15.

Table 3-1: Properties of Soil A, Soil B and ECC

		Soil A	Soil B	ECC	Notes or Standards
Description	Type	M10	S200	Puroflo 50	As provided by supplier
	Texture	Ground silica	Calcium carbonate powder	Clay	As provided by supplier
	Geologic origin	Sandstone	Limestone		As provided by supplier
	Colour	white	off-white	Yellow	
Properties	D10 in micron	4	3	<1	As provided by supplier
	D50 in micron	23	19	2	As provided by supplier
	D90 in micron	60	63	8	As provided by supplier
	Specific gravity G_s	2.65	2.65	2.61	Small pyknometer method Clause 8.3 of BS1377: Part 2 (1990)
	Liquid limit LL	28	24	58	Cone penetration method Clause 4.3 of BS1377: Part 2 (1990)
	Plastic limit PL	20	14	32	Clause 5 of BS1377: Part 2 (1990)
	Plasticity index PI	8	10	26	Clause 5 of BS1377: Part 2 (1990)
	Maximum dry unit weight in kN/m^3	15.1	17.5	14.6	BS1377: Part 4 (1990)
	Optimum water content %	20	13	28	BS1377: Part 4 (1990)

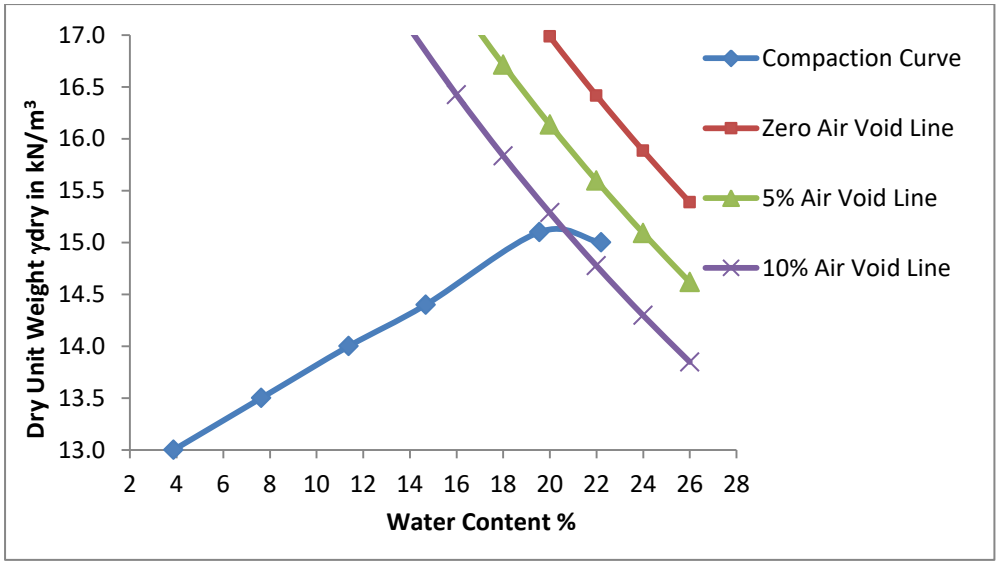

(a)

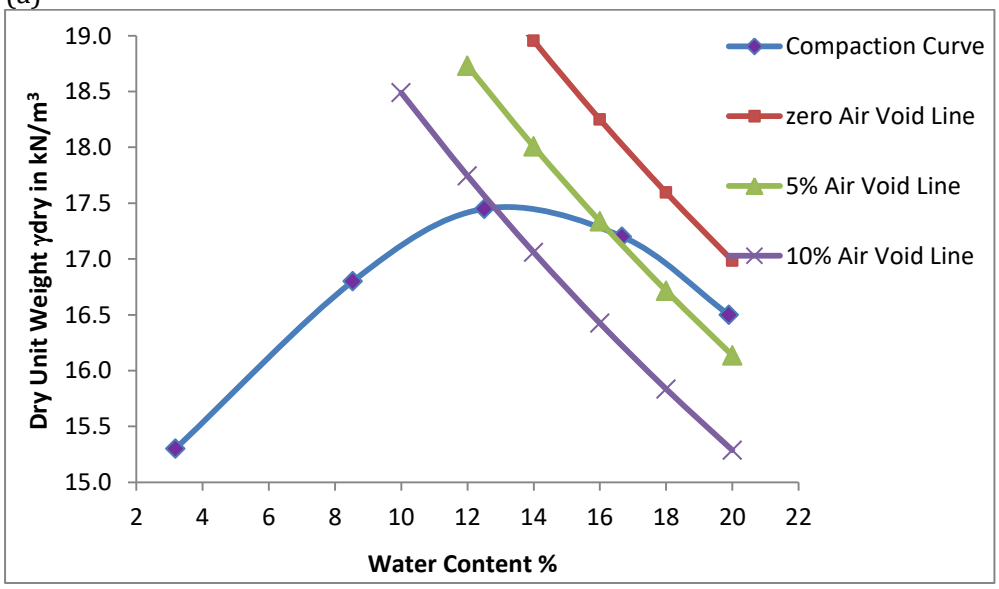

(b)

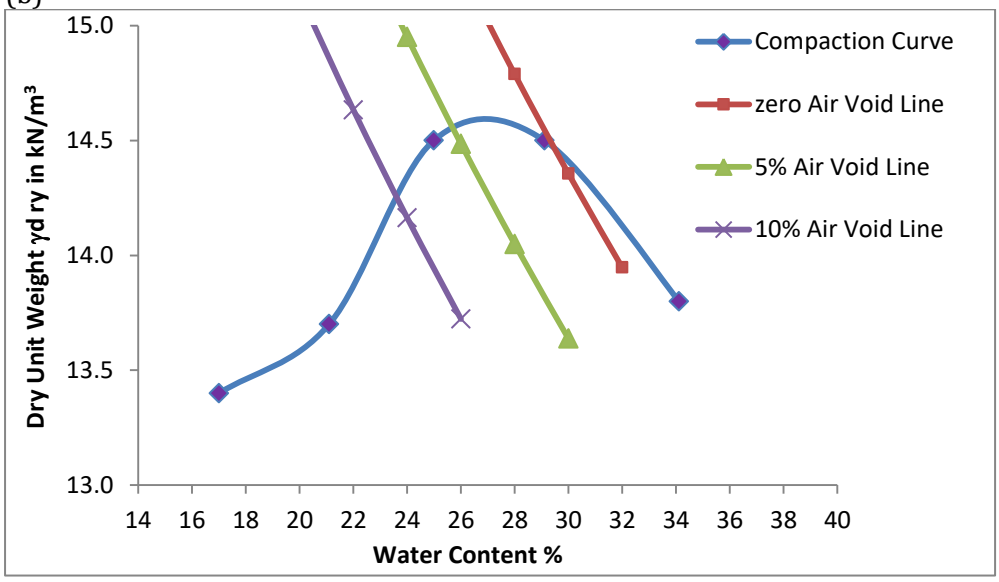

(c)

Figure 3.3: Compaction curves of the three soils, (a) Soil A, (b) Soil B, (C) ECC

3.6. Sample Preparation

This section describes the sample preparation for an oedometer size specimen to conduct the collapse tests that will be illustrated in Section 3.7. An empty oedometer ring (approximately 75mm diameter and 19 mm height) and a steel base (that has a diameter bigger than the ring diameter) have been both provided. The greased ring has been positioned on the base. Ground silica mixed with a percentage of China clay thoroughly for 4 minutes to ensure a uniform mix. The required water content was added and mixed as quickly as possible to eliminate the reduction in the water content owing to evaporation. This wet soil was compacted lightly with a steel rod of 25 mm diameter in three layers to achieve the target void ratio. Afterwards, each layer was compacted and the soil surface was scratched by a straight-edged knife for developing a proper bonding with the next layer. Aspects of the procedure are summarised in Fig. 3.4. The corresponding compaction effort required to achieve the target density was calculated as shown in Appendix (B). Once the compaction had been completed, the soil specimens were put in a sealed plastic bag and left for 24 hours to ensure equilibrium. As the wetting-drying process is crucial for developing clay bonds and producing collapse behaviour (Trofimov, 1990), after wetting with water, specimens were left to air dry for 48 hours while others were put in an oven at 105 ^{o}C for a specific time to investigate different drying off scenarios.

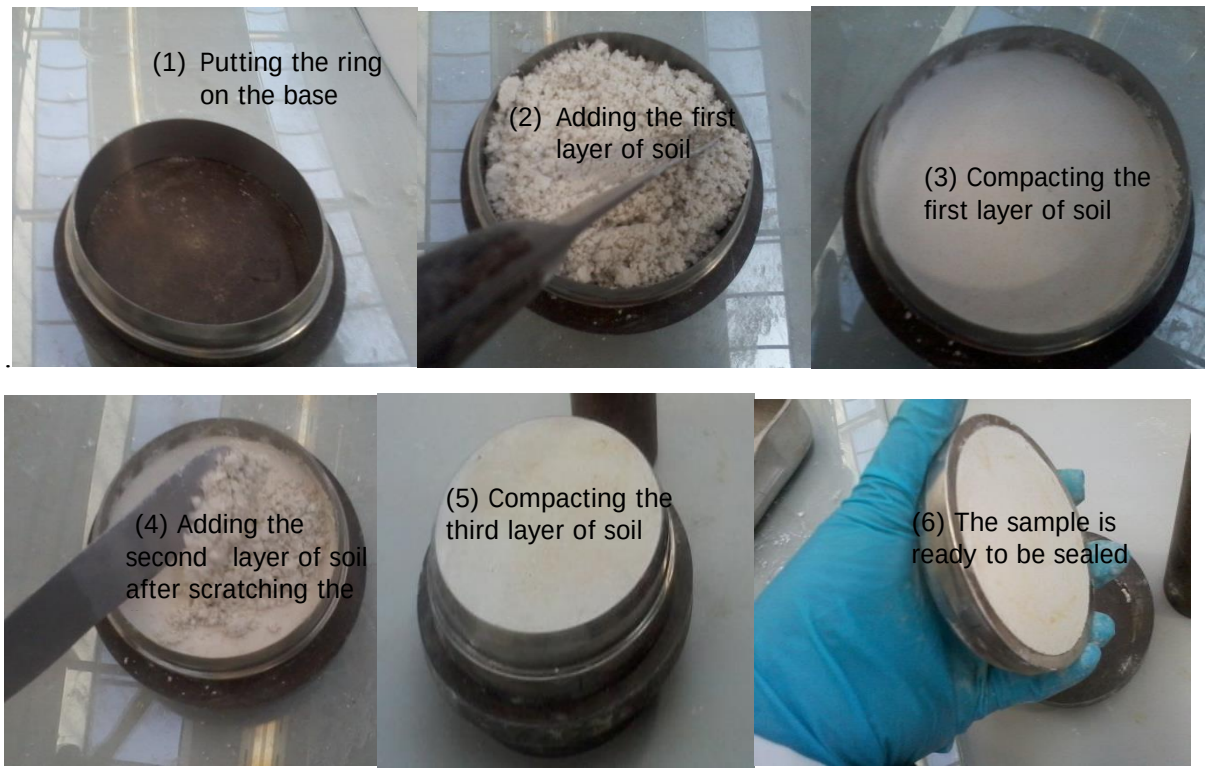

Figure 3.4: Soil sample preparation using the wet paste method

3.7 Single and Double Oedometer Collapse Tests

Series of single oedometer tests S.O.T and double oedometer tests D.O.T have been conducted to determine the collapse potential C_p. In S.O.T, a dry sample is typically loaded to 200 kPa, at which the sample is saturated and associated volume change measured. Subsequently, the sample is loaded up to 800 kPa. In D.O.T, two identical (as close as possible) samples; one dry and one saturated are tested (Abelev, 1948; Jennings & Knight 1957; Lutenegger & Saber, 1988). C_p from S.O.T or D.O.T is calculated using the following equation:

$$C_p = \Delta e / 1 + e_o \qquad (3.1)$$

Where in S.O.T, Δe is the change in void ratio upon soaking, and e_o is the initial void ratio while in D.O.T, Δe is the difference of deformation between the dry and saturated curves, and e_o is the initial void ratio from the dry curve. The severity of the collapse is assessed depending on the table proposed by Jennings & Knight (1975) as demonstrated in Table 3-2.

Table 3-2: The severity of collapse according to the value of the collapse potential as presented by Jennings & Knight (1975)

C_p	0-1	1-5	5-10	10-20	>20
Severity of collapse problem	No Problem	Moderate Trouble	Trouble	Severe Trouble	Very Severe Trouble

3.8 Errors in Laboratory Tests

In laboratory testing, equipment and human mistakes, temperature variations, or other changes in the laboratory environments can contribute to existing errors. The sources of error should be identified first to eliminate them as much as possible, devices should be standardised, and the uncertainty produced from different tests under the same conditions should be assessed (Taylor, 1979). Conventional tests were conducted as set out in appropriate standards and this incorporated produced recommendations for the number of repetitions required to give a reliable value with acceptable percentages of error (Head, 2006). So, in this research, index, compaction, and particle density tests have been conducted according to British Standards as was mentioned in Section 3.5. In collapse experiment, human errors such as the measurement of the dry density, the water content, or the specific gravity value used in computations could affect the calculated collapse potential. So, caution

was taken in performing the related experiment as mentioned in the standards. Also, S.O.T and D.O.T have been carried out in oedometer apparatus according to the procedures described in Section 3.7, and all suggestions to avoid expected errors from the literature are taken into consideration.

3.9 Repeatability of the Collapse Test

At least three trials of each collapse test have been performed to ensure the measurement of reliable and accurate values. The measurement at any certain load of three repetitions are averaged and computed by summing up the three values and then dividing them by three, as written mathematically in the following expression:

$$\text{average} = \text{ave.} = \sum_{i=1}^{3} m(i) \qquad (3.2)$$

The uncertainty in each individual measurement m(i) is determined by the standard deviation sd of the three measurements, as illustrated in the equation below:

$$sd = \sqrt{\frac{\sum_{i=1}^{3}(m(i)-\text{ave.})^2}{2}} \qquad (3.3)$$

The fractional error, which is the magnitude of the uncertainty divided by the average value, is then calculated (eq. (3.3)/eq. (3.2)) and multiplied by 100 to give the percentage error. The percentage indicates how much confidence should be placed in the measured value, for more details, see Taylor (1997). The equation of the standard deviation is valid for at least two repeated tests. Some researchers using the standard deviation method in error analysis, even for small data set when an experiment is repeated just twice or three times have showed a good representation for error bands, e.g. Amini (2014) and Ashour (2015). In this study each collapse experiment (of nine readings) was repeated three times only, the parcent error calculated was compared with the work done by Langroudi (2014) for similar collapse tests on loess samples and a good agreement was noticed.

3.10 Experiments on Soil (A) and ECC

3.10.1 Index Properties, Specific Gravity, and Particle Size Distribution Curves for Different Mixtures

The index properties and the specific gravity after mixing Soil A (M10 ground silica) with different percentages of China clay (ECC) are determined according to Clauses 4, 5, and 8.3 in British Standards BS1377: Part 2 (1990) respectively.

Particle size distribution curves for those mixtures and associated grain size percentages are determined from combining the related particle distribution curves for Soil A and ECC with respect to their shares in the mixture. Table 3-3 shows the values of index properties, specific gravity and grain size percentages of the mixtures and Fig. 3.5 represents the size distribution characteristics in comparison to the natural loess boundaries.

The Atterberg limits and the low plasticity index match very well the ranges of British loess presented by Derbyshire & Mellors (1988) such that ranges of the liquid limit and plastic limit lie between 28-46% and 17-23% respectively, also, values observed are very consistent with the range of the natural loess of Libyan and Chinese Loess presented by Assallay (1998) , Northern France loess by Muñoz-Castelblanco et al. (2012), and more recently Plateau loess in China tested by Zhen Liu et al. (2016).

The values of specific gravity are found to be very consistent with the work done by Miller (2002) for similar soil mixtures prepared with percentages of silica only or silica to Kaolin of 80/20 and 70/30.

Adding the China clay to the silica changed its grain curve. In comparison to upper and lower limits of natural loess of Lanzhou presented by Derbyshire & Mellors (1988), which has similarity with loess of UK in particle size distribution, fabric and mineralogy (Rogers et al,1994), the grain size distribution curves of those mixture were fit very well within the boundaries up to 0.005 mm , for less than 0.005 mm, pure silica , silica with 5% and 10% ECC showed little decreasing than the lower limit of natural loess as shown in Fig. 3.5.

However, in context of the artificial loess composition percentages, they are agreed with the natural depositions of loess reported in the literature e.g. Assallay, (1998), Kruse et al. (2007), Liu et al. (2016), sand sized grains have the percentages lies within the range 1.5% to 2%, silt particles form the dominant particle size between 80.25% to 92% and the greater percentage among them belongs to coarse silt from 39.25% to 52% , clay sized particle ranging between 6% and 18.25% , again see Table 3-3.

The respective calculations for index properties and specific gravity are summarised in Appendix (B) in Table B-16, Table B-17, and Table B-18; the liquid limit curves are also presented in the figures from Fig. B.4 to Fig. B.9.

Table 3-3: Index Properties ,specific gravity , grain size percentages of different mixtures of soil (A) and English China clay (ECC)

Soil mixture	LL %	PL %	PI	G_s	Grain size percentages				
					Sand% >0.063 mm	Silt %			Clay %
						Coarse 0.02–0.063 mm	Medium 0.0063-0.02 mm	Fine 0.0063-0.002 mm	
100% Soil A	28	20	8	2.65	2.0	52.00	25.00	15.00	6.00
95% Soil A + 5% ECC	28	20	8	2.65	1.9	49.45	24.65	15.55	8.45
90% Soil A +10% ECC	29	21	8	2.65	1.8	46.9	24.30	16.10	10.90
85% Soil A +15% ECC	29	21	8	2.64	1.7	44.35	23.95	16.65	13.35
80% Soil A +20% ECC	29	22	7	2.64	1.6	41.80	24.60	16.20	15.80
75% Soil A +25% ECC	29	22	7	2.64	1.5	97.25	23.25	17.75	18.25

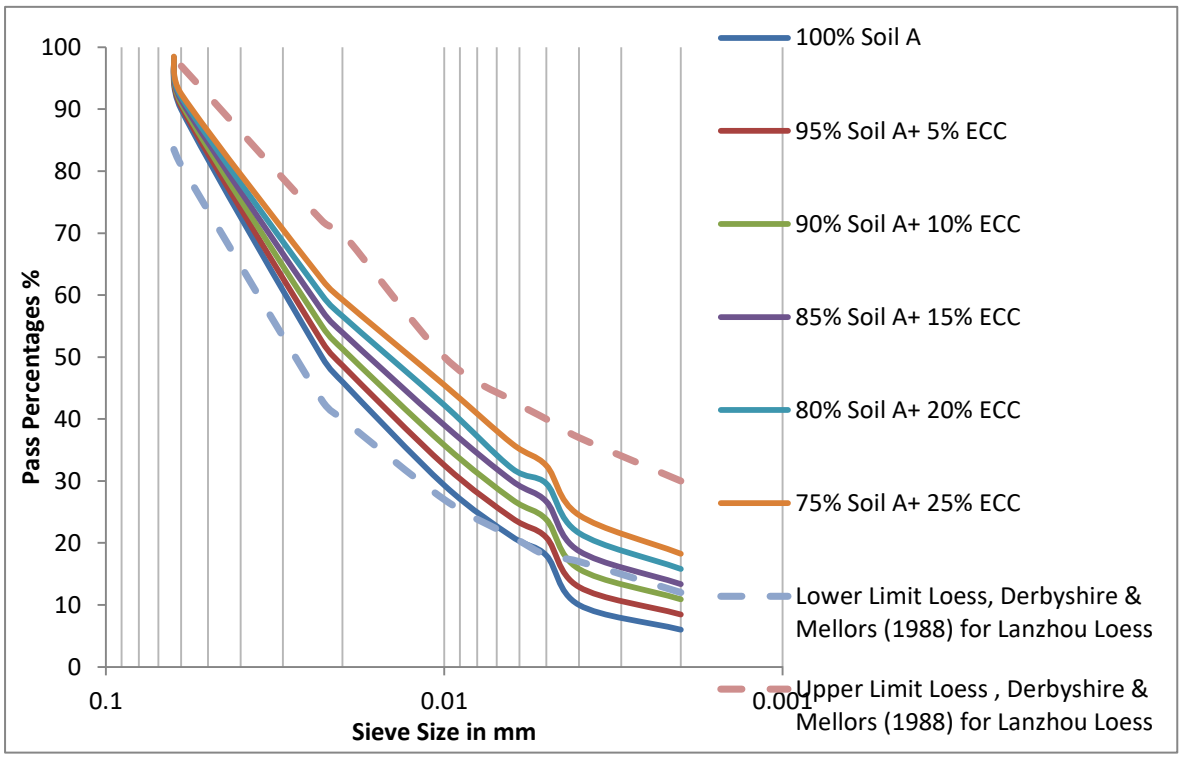

Figure 3.5: Particle distribution curve of the artificial loess for different silica to China clay mixture in comparison to limits of natural loess

3.10.2 Compaction Tests

The relationship between water content and dry unit weight for the different mixtures of ground silica and clay are determined by compaction test according to BS1377: Part 4 (1990). The results showed that the more clay, the higher the compaction curve, which could be as a result of the finest clay particles occupying the spaces between the coarser silt grains; the same compaction characteristic was observed by Dafalla (2013) for different mixtures of clay and sandy soil. The values of minimum dry density ranged from 13 kN/m^3 to 13.9 kN/m^3, which is close enough to fit the minimum dry density range reported by Costa & Baker (1981) i.e. 10.8-13.7 kN/m^3. The compaction curves and the relevant air void lines are represented for different mixtures in Fig. 3.6.

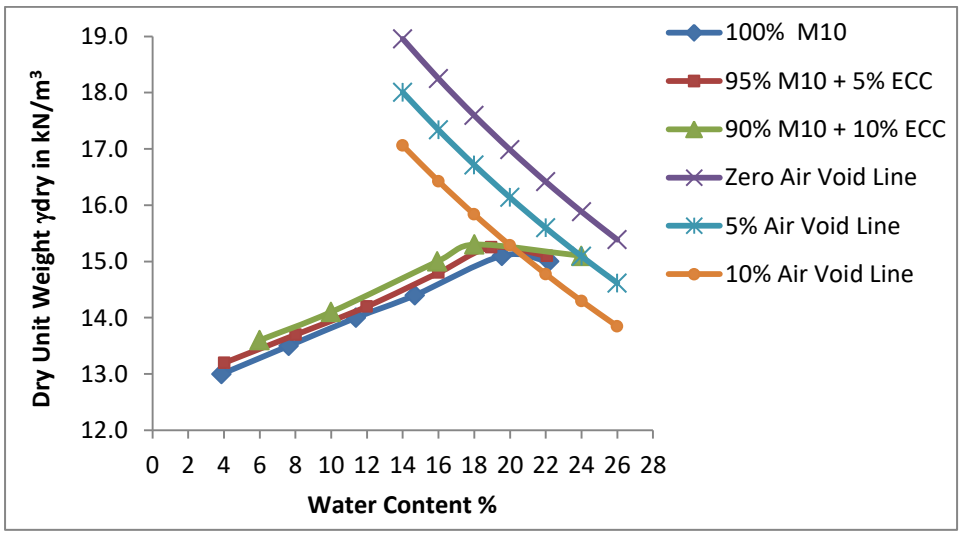

(a)

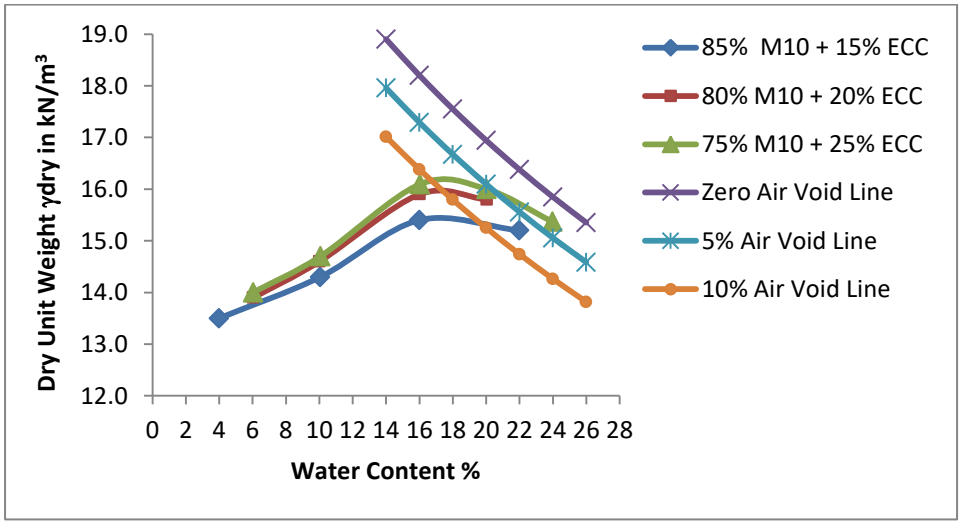

(b)

Figure 3.6: Compaction test results for different mixtures of Soil (A) and China clay ((a) Gs=2.65 and (b) Gs=2.64)

3.10.3 Effect of Clay Content on the Specimen of Ground Silica after Allowing Air Drying

Single oedometer tests were conducted on specimens of ground silica mixed with three different percentages of ECC clay: 15%, 20%, and 25%, as those mixtures showed to be a good representation of natural loess properties and composition as was discussed in Section 3.10.1. The samples were permitted to dry in air for 48 hours.

The initial void ratio was chosen relatively high, 0.93, to lie within the range in the natural deposit e.g. Gao (1996) and Assallay (1998), relying on the assumption of Derbyshire & Mellors (1988) by considering a soil to be susceptible to collapse if it has sufficient void spaces in its natural state to hold its liquid limit of water at saturation. The water content was selected to be 12%, which represents the ideal water content, as will be discussed in Section 3.10.4.

All samples were loaded up to 200 kPa before soaking with distilled de-aired water and resuming loading up to 800 kPa. The associated settlement readings have been recorded until deformation stopped or has slowed to less than 0.005 mm/hr., which is much lower than that typically used e.g. Lutenegger & Saber (1988).

During all loading increments, the majority of settlement is observed within the first hour of loading. The considerable compression occurs after flooding the specimen with water; see Fig. 3.7, which summarises the typical time-settlement curve for loading, soaking, and reloading. The later behaviour described as the results to the thickening water films as a result to increase of water content, which tends to lubricate the surrounding soil particles and induce them easily to be relocated and packed into a denser structure.

Regarding collapse upon wetting, approximately 67% of the collapse starts once the water has been introduced to the specimens and approximately 91% has been observed after the first 15 minutes from the introduction of water to record the first settle to collapse, then the settlement continued gradually with slower rate for the next hours, see Fig.3.8. Similar behaviour for natural loess is discussed by Rogers et al. (1994) where they recognised two type of settlement upon inundation; collapse settlement which forms 95% of the total settlement and occurs initially after wetting within the first 10 minutes and subsidence settlement which occurs after the collapse settlement and could last for hours. Langroudi (2014) noticed during his collapse experiment on artificial loess that the bulk of the collapse is typically seen within 5.5 min after inundation and then remained almost constant after 12

minutes (first collapse settle). An explanation for such a result is that, on the wetting path, the soil structure collapses due to an increase in the thickness of the thinnest possible water film, which causes a decrease in matric suction under a relatively high, constant, super-imposed active force. Tadepalli & Fredlund (1991) also noticed a cessation of the decrease in total volume of the centre of the inundated sample, as the matric suction at this region approached zero.

In all samples, regardless the amount of clay content, it was observed that the void ratio decreased significantly upon wetting, as displayed in Fig. 3.9, which demonstrates the change in void ratio versus stress. The relationship between clay content and the collapse potential for those three mixtures is demonstrated in Fig. 3.10. The results shows that the severity of the collapse achieved is „moderately trouble" to „trouble", according to Table 3-2; higher collapsibility for the sample is observed when M10 ground silica is mixed with 25% China clay. The outcomes of these experiments are due to the particles being in a loose condition, and their temporary stability results from a combination of capillary forces and clay bridges at the contact points. Under wetting and loading, both of them will reduce, and the grains will tend to slip over each other. The percentage error linked with the repeated tests of this series is presented in Table 3-4.

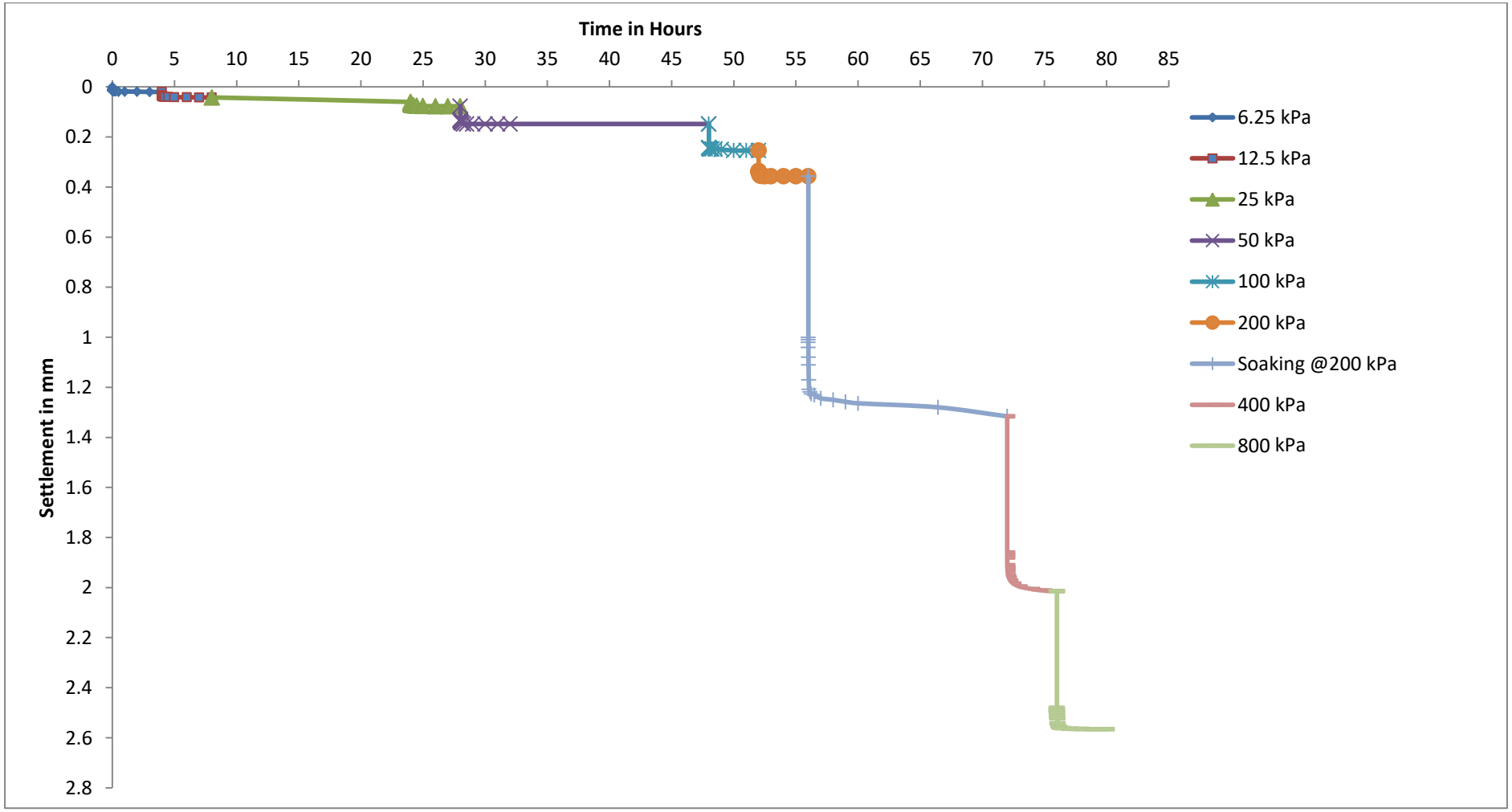

Figure 3.7: The typical time settlement curve for loading, soaking, and reloading the soil specimen

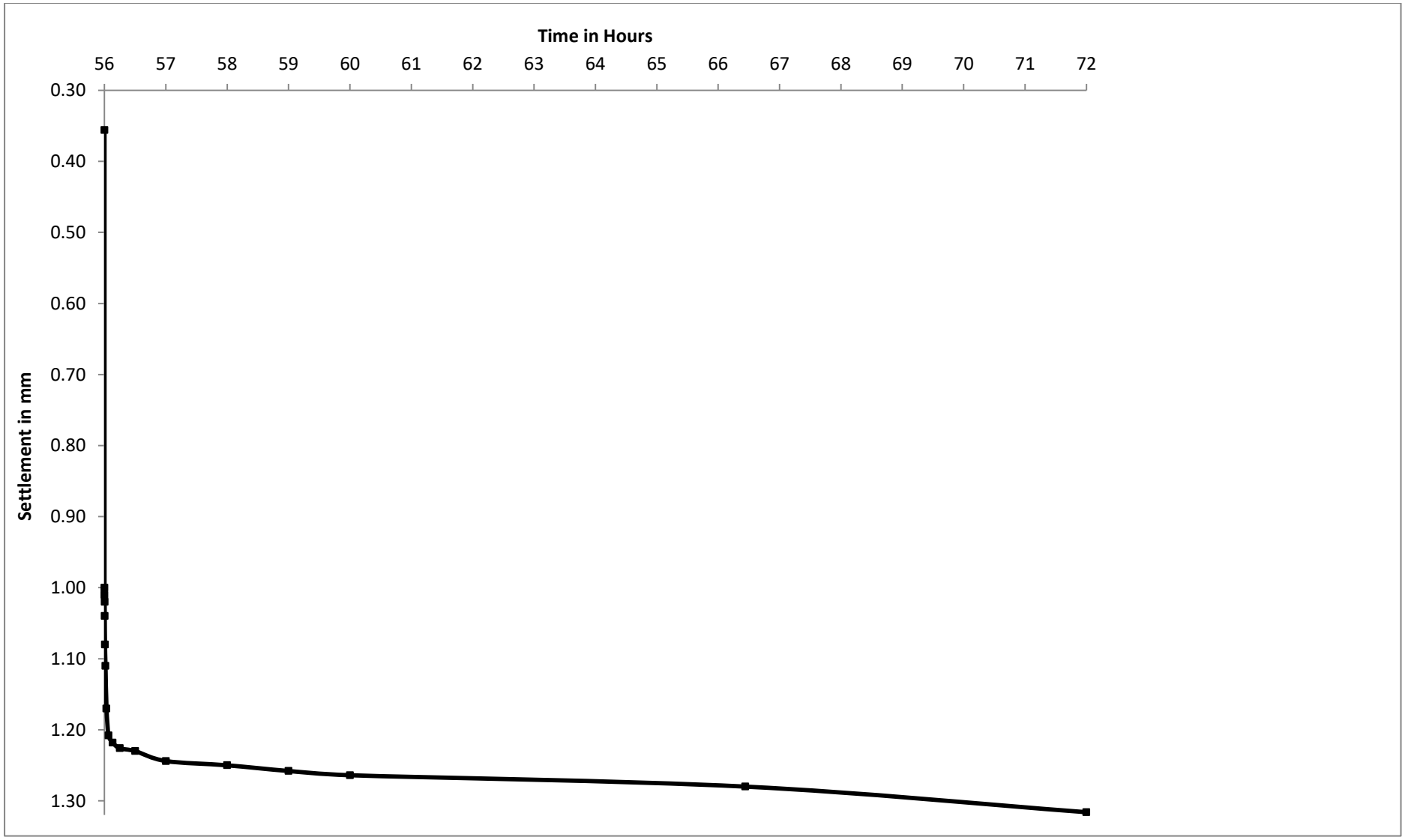

Figure 3.8: The collapse upon wetting with respect to time

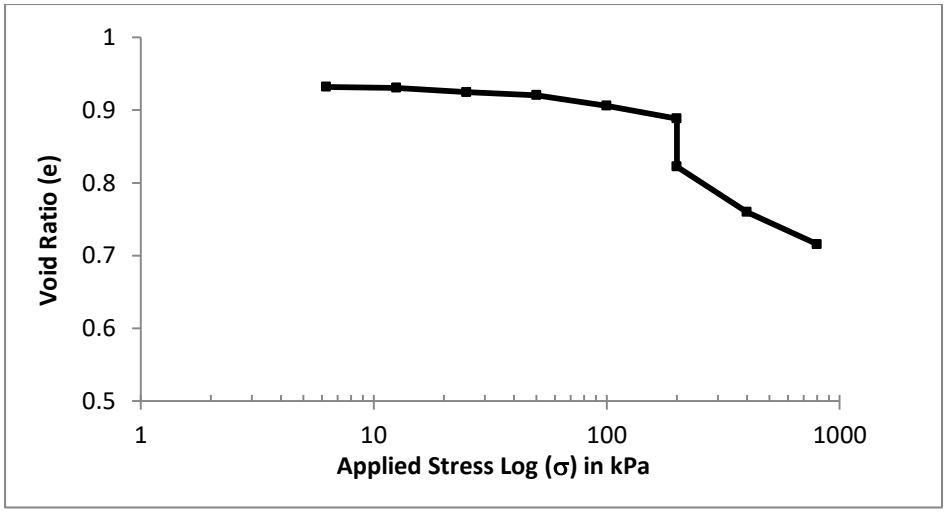

(a) Soil A with 15% English China clay (Collapse Test No. 1)

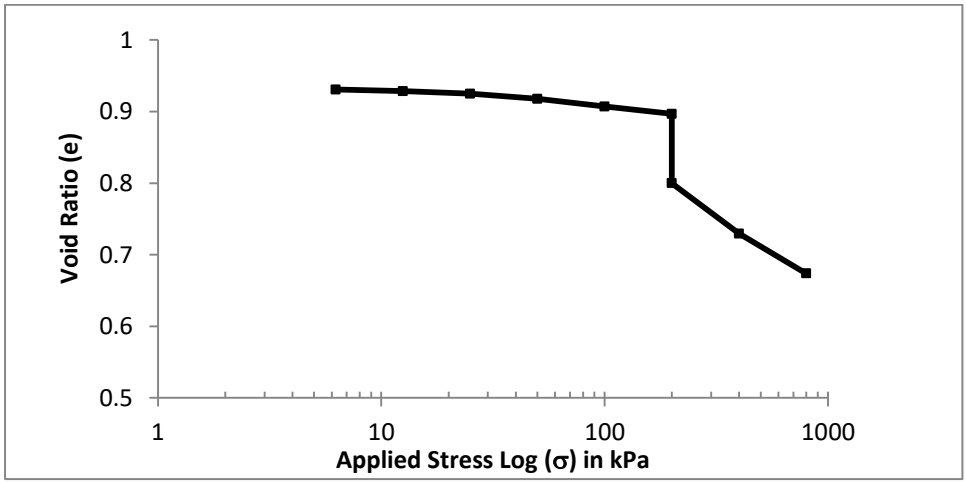

(b) Soil A with 20% English China clay (Collapse Test No. 2)

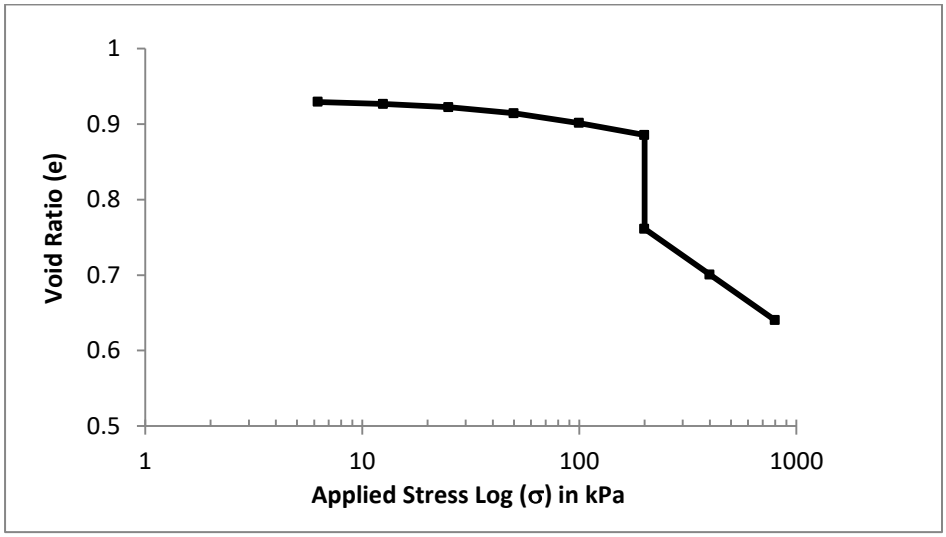

. (c) Soil A with 25% English China clay (Collapse Test No. 3)

Figure 3.9: Series of single oedometer tests on specimens of ground silica at different clay mixing ratios, soaking at 200 kPa

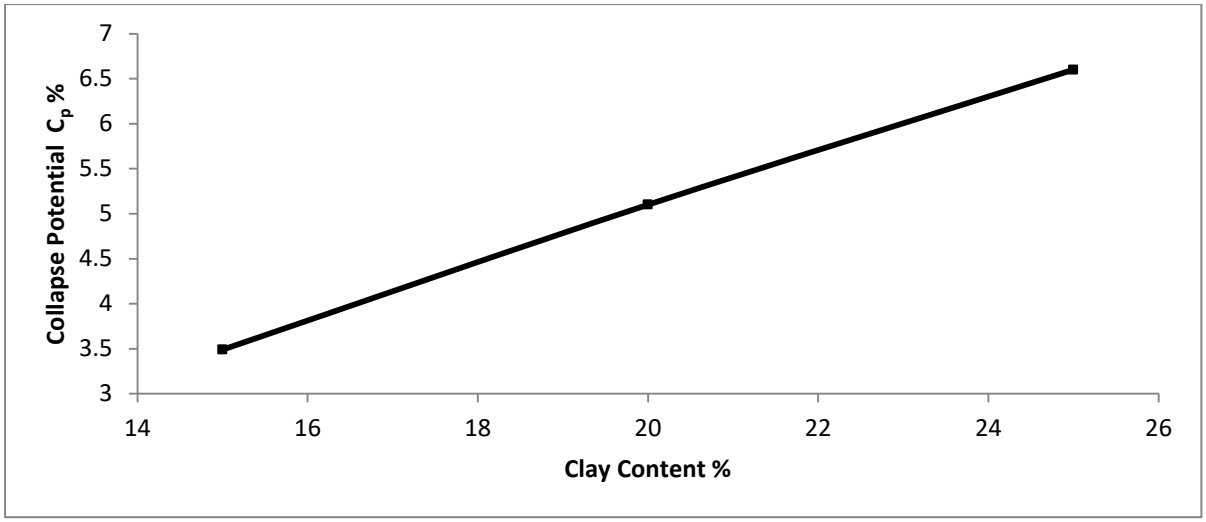

Figure 3.10: Clay content versus collapse potential for samples with 48 hours air drying

Table 3-4: Percentage of error for repetition of tests No. 1, 2, and 3 (see Section 3.9)

Stress in kPa	Percentage of Error %		
	Collapse Test No. 1	Collapse Test No. 2	Collapse Test No. 3
6.25	2.5	2.0	2.9
12.5	2.7	1.4	1.7
25	3.8	1.3	1.7
50	2.2	1.4	2.4
100	2.6	1.6	1.7
200 (before wetting)	1.8	1.1	2.7
200 (after wetting)	1.2	0.9	1.1
400	0.4	0.9	1.4
800	0.8	1.1	1.1

3.10.4 *Identifying the Preparation Water Content*

In the wet paste method, the soil, which consists of silt and clay particles, is usually mixed with a specific water proportion to form a paste. The paste should achieve two criteria: to be wet enough to produce the required bonding of the soil, and be dry enough to prevent shrinkage from occurring within the sample (Miller, 2002). Miller used 15% water content for most of her samples. In this study, three initial water content levels are chosen to investigate this effect: 8%, 12%, and 15%. The later percentage is selected based on the study by Miller (2002) and two lower percentages are chosen to lie within the natural soil e.g. Muñoz-Castelblanco et al. (2012). The clay percentage that was added to the ground silica was 15%, and the initial void ratio for all three tests was 0.93. The same void ratio is chosen here for comparison purposes. Figures 3.11 and 3.12 show the hydrocollapse of the specimens after 84 hours of air drying from single oedometer tests corresponding to 8% and

15% water content respectively. The percentages of corresponding error for the two tests are presented in Table 3-5. The collapse potentials of those mixtures with above the water content and that of Test No. (1), characterised by 12% water content for the same mixture and the same conditions, are shown in Fig. 3.13. This shows that adding 12% of water to this soil gives a higher collapse potential. Below this value, the bonding does not form properly, and higher than that could cause the sample to be softer and produce a low initial void ratio before soaking. So it was decided to choose 12% water content for preparing the samples that need to be dried in air for 48 hours.

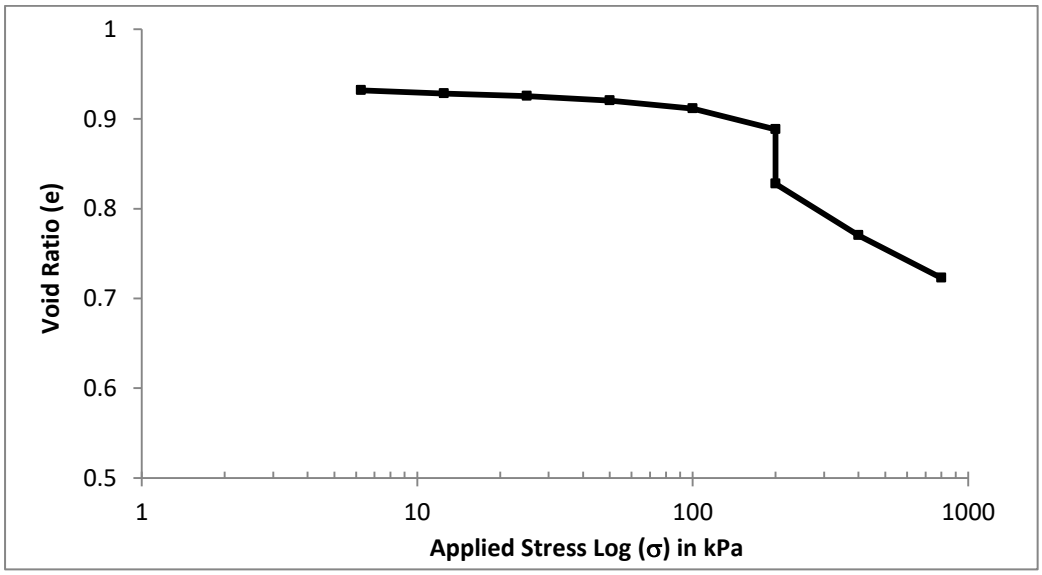

Figure 3.11: Hydro-collapse test, 8% water content (Collapse Test No. 4)

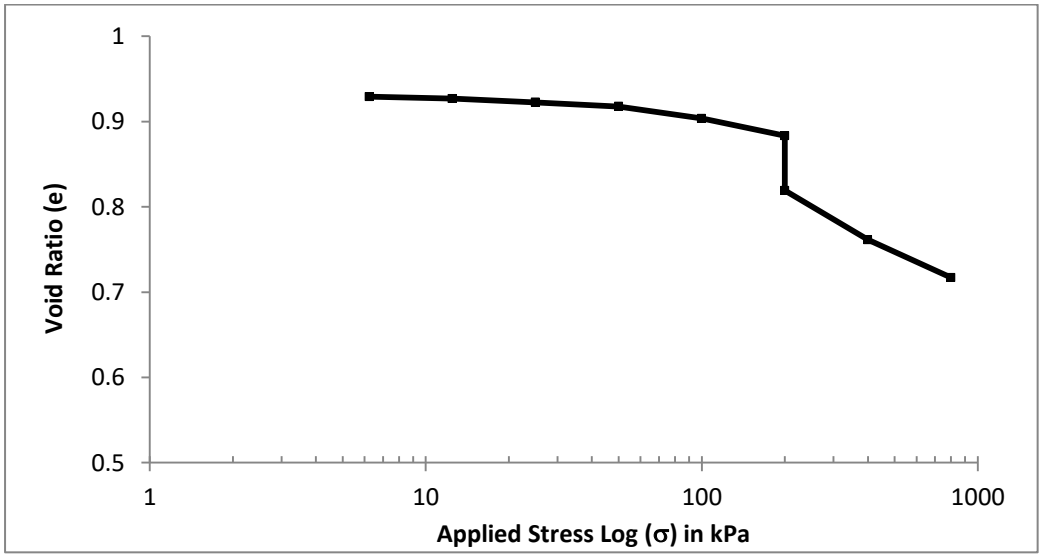

Figure 3.12: Hydrocollapse test, 15% water content (Collapse Test No. 5)

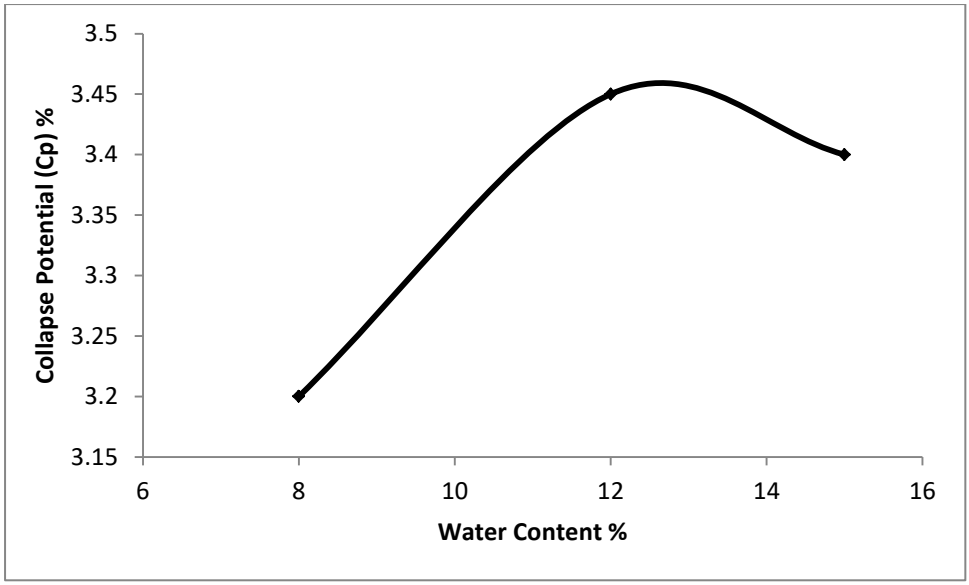

Figure 3.13: Initial water content versus collapse potential

Table 3-5: Percentage of error for repetitions tests No. 4 and 5 (see Section 3.9)

Stress in kPa	Percentage of Error %	
	Collapse Test No. 4 (8% wc)	Collapse Test No. 5 (15% wc)
6.25	2.2	3.4
12.5	3.6	3.0
25	2.8	3.4
50	3.3	3.3
100	2.5	3.6
200 (before wetting)	2.3	3.6
200 (after wetting)	2.3	1.9
400	1.7	1.9
800	1.9	1.3

3.10.5 Effect of Clay Content on the Specimen of Ground Silica with Oven Drying (5 hours)

The specimen of ground silica was mixed with different percentages of clay content after drying the samples for 5 hours in the oven at 105°C. Then samples are cooled down in a desiccator to prevent any change in water content. The water content and the initial void ratio are 15 % and 0.93 respectively. Figure 3.14 demonstrates the relationship between clay content and collapse potential; Table 3-6 shows the corresponding standard error; Fig. 3.15 shows the single oedometer results. Collapse severity was between „moderate trouble‟ and „trouble‟ with respect values between 4 and 5.28%. The greater collapse was for the sample containing 15% China clay. It is obvious the action of clay plates binder as bonds among silt grains. So if the clay was originally suspended in pore water, gradual evaporation would

cause the clay plates to retreat with the water into the menisci at inter-particle contacts, causing a collapse phenomenon according to Barden et al. (1973). It is worth mentioning here that although those specimens are almost dry, their collapsibility was not higher than that of the samples with 48 hours air drying, which have about 9.5 % water content after drying. That could mean gradual evaporation is better at producing a soil collapse model.

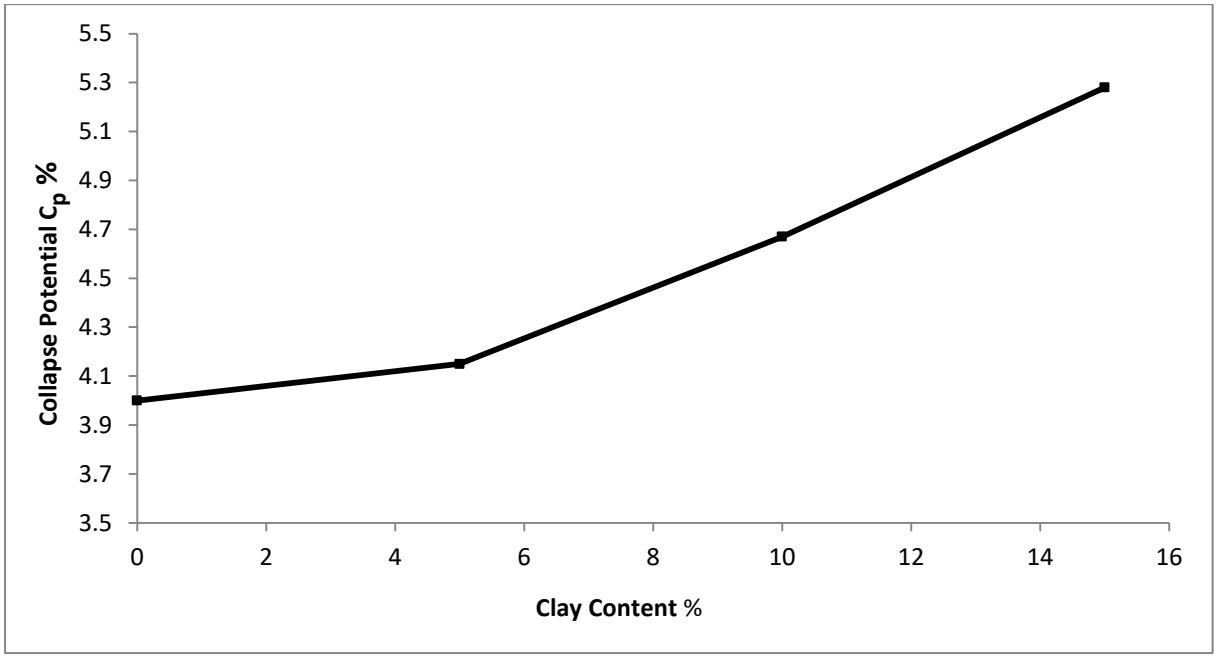

Figure 3.14: Clay content versus collapse potential for samples dried for 5 hours

Table 3-6: Percentage of error for repetition tests No. 6, 7, 8, and 9 (see Section 3.9)

Stress in kPa	Percentage of Error %			
	Collapse Test No. 6 (0% clay)	Collapse Test No. 7 (5% clay)	Collapse Test No. 8 (10% clay)	Collapse Test No. 9 (15% clay)
6.25	3.8	2.5	3.3	2.9
12.5	3.0	3.0	2.4	3.2
25	3.0	1.7	2.7	3.4
50	2.0	2.0	3.1	2.4
100	2.4	1.7	1.3	1.5
200 (before wetting)	1.5	1.5	1.6	1.2
200 (after wetting)	1.4	1.2	1.3	1.0
400	1.4	1.0	1.5	1.3
800	1.2	1.4	1.3	1.4

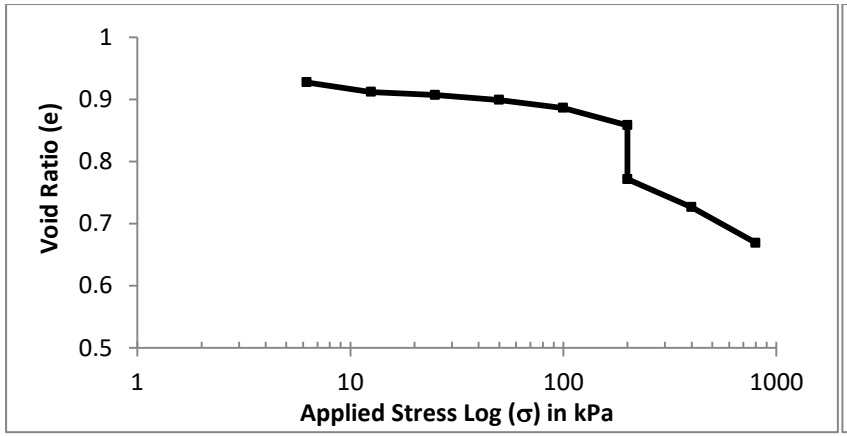

Soil (A) with 0% China clay (Test No.6)

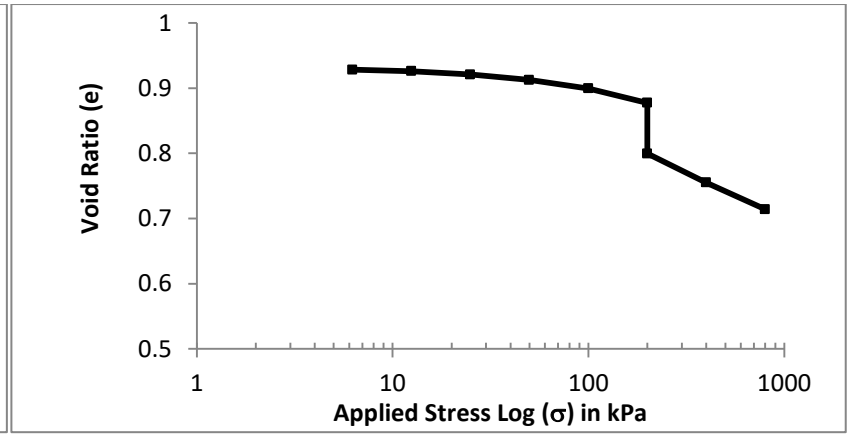

Soil (A) with 5% China clay (Test No.7)

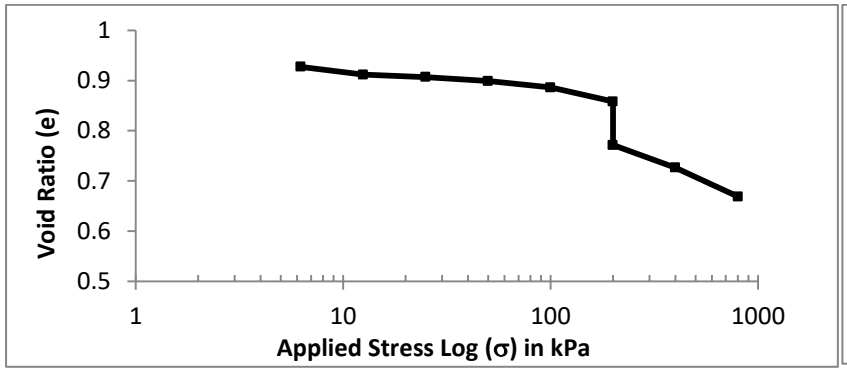

Soil (A) with 10% China clay (Test No.8)

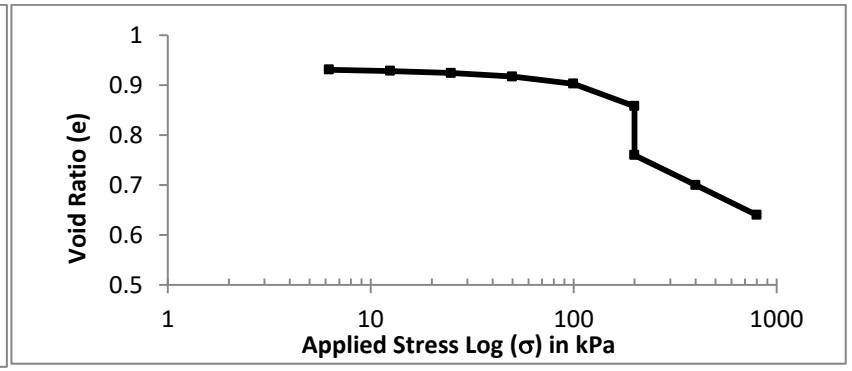

Soil (A) with 15% China clay (Test No.9)

Figure 3.15: Series of single oedometer tests on specimens of ground silica at different clay mixing ratios (5 hours drying)

3.10.6 Effect of Clay Content on the Specimen of Ground Silica with Oven Drying (20 hours)

This followed the same procedure as described in Section 3.10.5, except that the period of drying was longer, so the specimen was left in an oven for 20 hours; void ratio and initial water content were 0.93 and 15% respectively. The higher collapsibility was recorded for the sample containing 20% clay, with a collapse potential of 8.4%; see Fig. 3.16. Table 3-7 shows the consistency of the repeated tests. Figure 3.17 shows the results of three samples subjected to the single oedometer test.

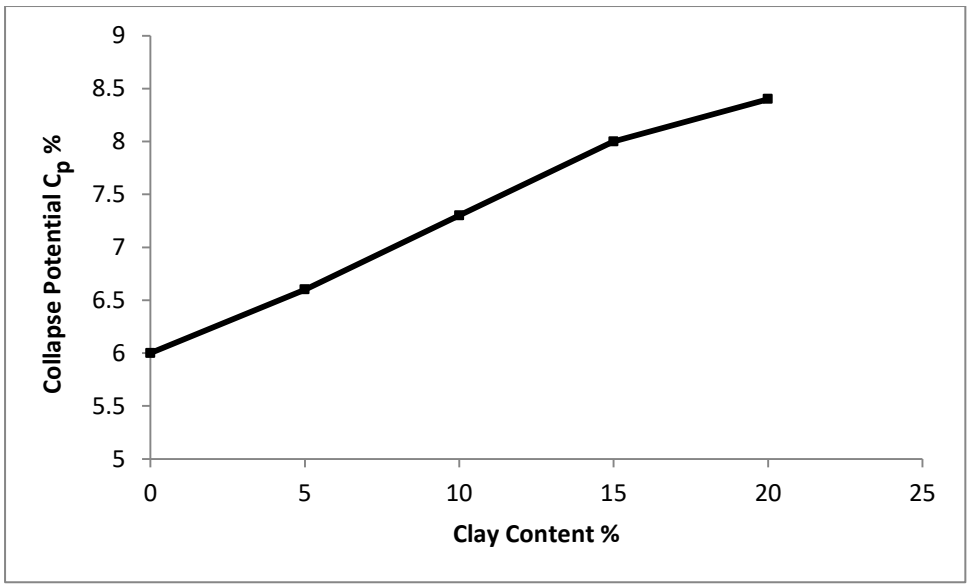

Figure 3.16: Clay content versus collapse potential for samples after drying for 20 hours

Table 3-7: Percentage of error for repetition tests No. 10, 11, 12, 13, and 14 (see Section 3.9)

Stress in kPa	Percentage of Error %				
	Collapse Test No. 10 (0% clay)	Collapse Test No. 11 (5% clay)	Collapse Test No. 12 (10% clay)	Collapse Test No. 13 (15% clay)	Collapse Test No. 14 (20% clay)
6.25	2.6	4.0	4.0	2.5	2.0
12.5	2.7	4.3	3.3	2.9	2.2
25	3.4	1.9	2.5	1.8	2.7
50	3.1	3.1	3.1	2.8	2.5
100	3.8	1.9	3.6	1.7	3.1
200 (before wetting)	2.9	1.8	1.8	3.7	2.5
200 (after wetting)	3.8	2.1	1.5	1.3	2.0
400	2.0	3.6	2.1	1.7	2.9
800	2.2	1.1	1.3	2.0	1.9

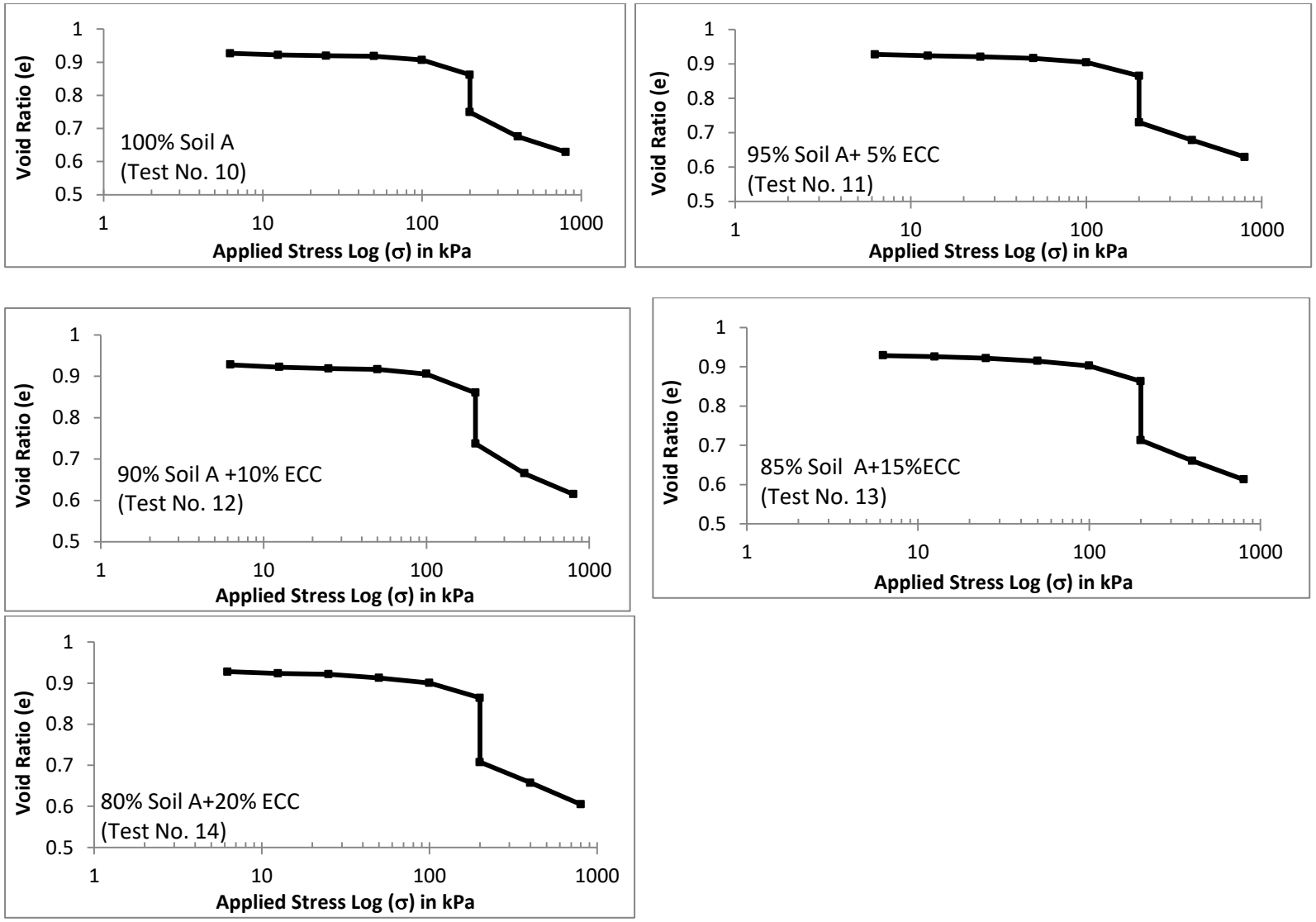

Figure 3.17: Series of single oedometer tests on specimens of ground silica at different clay mixing ratios, after drying for 20 hours

3.10.7 Effect of Void Ratio

Two different void ratios 0.93 and 1.33 were chosen to see their effect on the collapse. Figure 3.18 demonstrates the comparison of two varied void ratio curves of single Oedometer tests. The relationship between the collapse potential and the initial void ratio showed that the higher the initial void ratio, the greater the collapsibility. Before soaking, the decrease in void ratio with respect to load was higher in a higher void ratio. Results also showed that the soil with a higher initial void ratio (1.33) was the most collapsible upon wetting, 8.3%, in comparison to 5.28% for soil identified with the 0.93 void ratio. The deviation from the repeated test related to the void ratio of 1.33 is shown in Table 3-8.

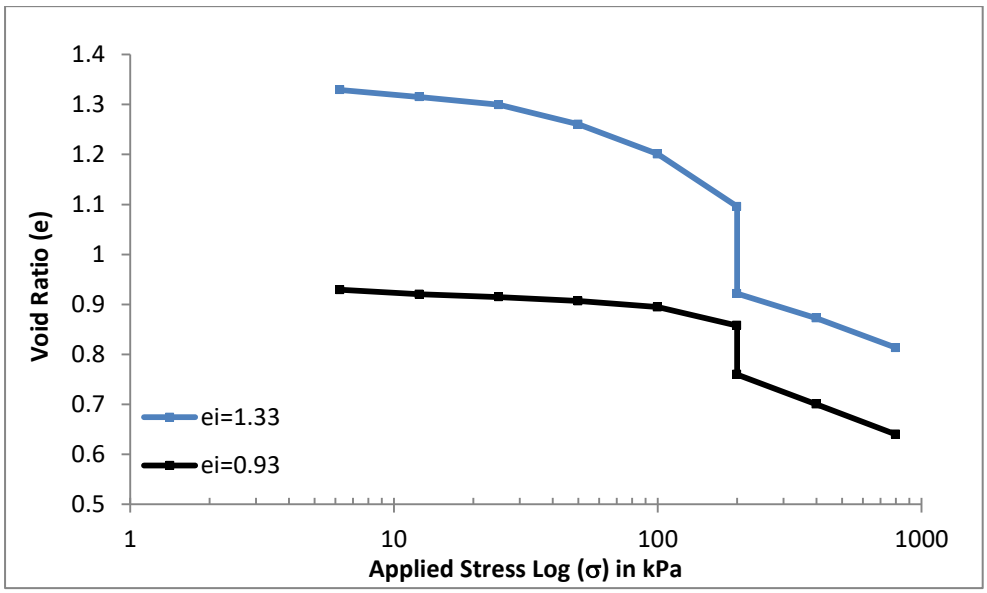

Figure 3.18: Single oedometer test for two different initial void ratios

Table 3-8: Percentage of error for repeated test with initial void ratio of 1.33 (Test No. 15), see Section 3.9

Stress in kPa	Percentage of Error %
	Collapse Test No. 15 (e_i=1.33)
6.25	2.0
12.5	3.9
25	4.2
50	3.4
100	2.7
200 (before wetting)	1.2
200 (after wetting)	1.3
400	1.7
800	0.9

3.10.8 Results of Double Oedometer Tests for Soil (A)

Two identical specimens were tested, following the procedure described in Section 3.7. It is obvious that with loading the wet sample experienced a considerable compression in comparison to the dry one. See Fig. 3.19. The data of the single oedometer test versus that for double oedometer test indicates a difference in the collapse potentials, as shown in Fig. 3.20 and Fig. 3.21, which refer to samples with 15% and 20% clay content respectively. It seems that the collapsibility measured by the double oedometer test is slightly higher than that of the single oedometer test. The results are reasonable according to Lutenegger & Saber (1988) who attributed such behaviour to the texture and properties of the soils being tested. Variations in repeated trials are illustrated in Table 3-9.

Figure 3.19: One dry and one soaked artificial sample after loading is completed in the double oedometer test

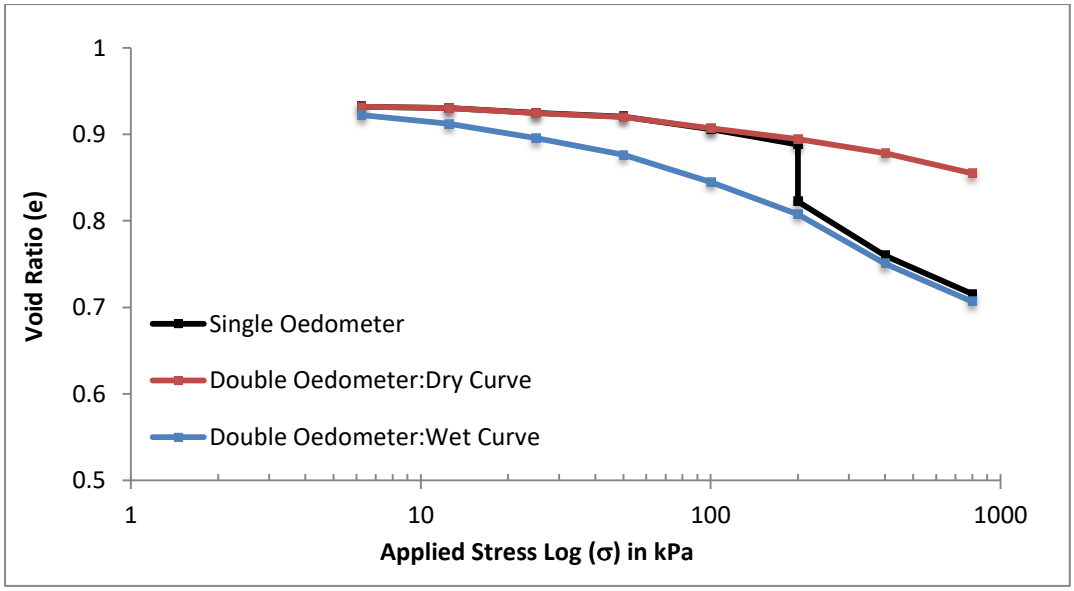

Figure 3.20: Double and single oedometer tests results for a specimen with 85% ground silica, 15% China clay, and 12% initial water content after 48 hours air drying

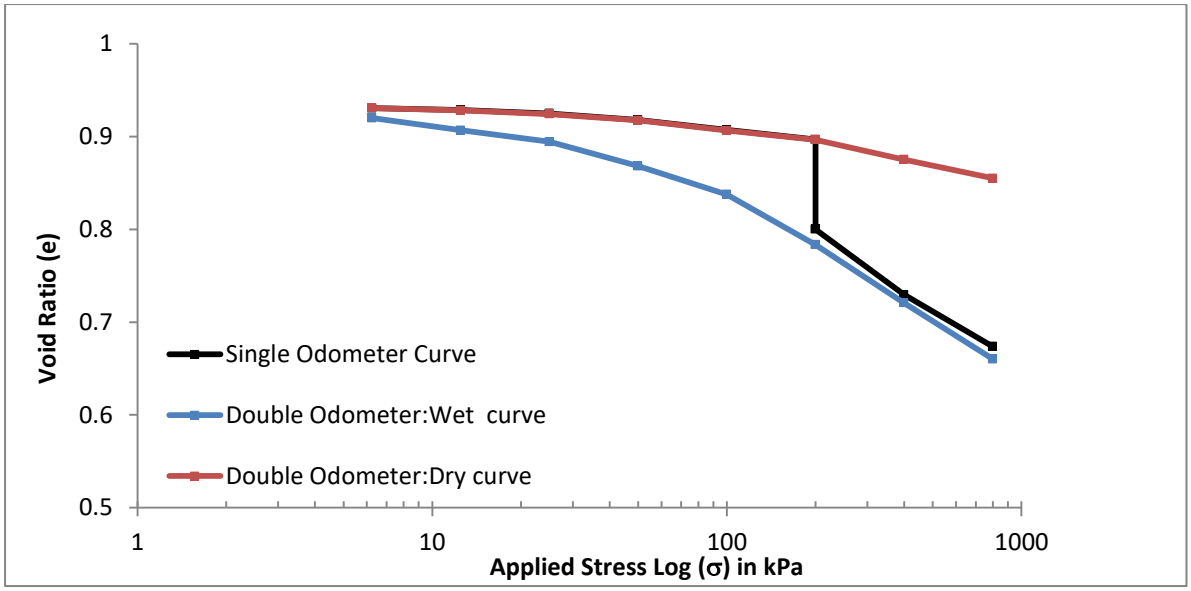

Figure 3.21: Double and single oedometer tests results for a specimen with 80% ground silica, 20% China clay, and 12% initial water content after 48hours air drying

Table 3-9: Percentage of error for repetition tests of double collapse test for two mixtures, ground silica with 15% and 20% clay content (see Section 3.9)

Stress in kPa	Percentage of Error %			
	Double Dry Test		Double Wet test	
	Collapse Test No. 16 (15% clay content	Collapse Test No. 17 (20% clay content)	Collapse Test No. 18 (15% clay content)	Collapse Test No. 19 (20% clay content)
6.25	2	1.5	1.9	1.4
12.5	3.6	1.8	2.6	1.1
25	1.9	2.5	3.5	1.3
50	1.2	1.3	1.6	1.2
100	1.6	2.3	1.4	0.9
200	1.7	2.6	1.3	1.4
400	1.6	1.8	1.4	1.2
800	1.2	1.0	1	1.1

3.11 Experiment on Soil (B) and ECC

Soil (B), with 20% clay, was tested following the same procedure as the single oedometer test in Section 3.8. The soil was air dried for 48 hours. The water content and the void ratio were chosen to be 12% and 0.93 respectively, so that a fair comparison with Soil (A) could be achieved. Soil (B) has the same collapse tendency as Soil (A). This probably as a result to values of the liquid limit and the natural dry unit weight of both prepared samples which lie within the zone in which loessial soil is likely to collapse according to Das (2014) as shown in Fig. 3.22. It was noted too that the collapse potential of Soil (B) is slightly higher than that

of Soil (A); although it has the same mixture and drying time, 6.7% versus 5.1%, Soil (A) is stiffer than soil (B) as the latter soil samples compressed significantly under loading in all loading increments, even before wetting, as shown in Fig. 3.23. Under such circumstances, Soil (A) is the closest to true natural collapsible soil, which, according to its definition, has a higher strength in a dry state, but loses strength upon wetting. Also, if we compare the oedometer results conducted on a natural loess sample by Miller (2002) which as the tested soil has particle distribution lies within limits given by Derbyshire & Mellors (1988), we find that Soil (A) is the closest to this; see Fig.3.24. The percentage of error for repetition tests is shown in Table 3-10.

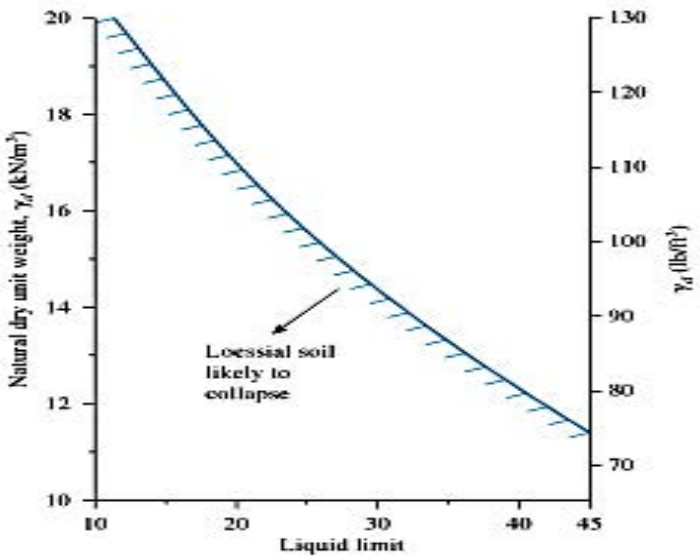

Figure 3.22: : Dry unit weight versus liquid limit (taken from Das, 2014)

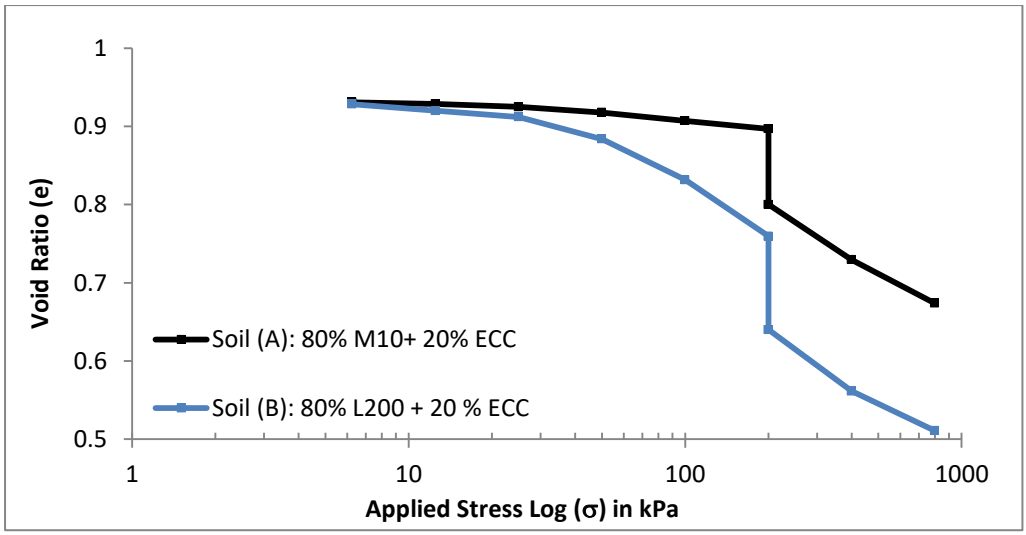

Figure 3.23: Single oedometer results of specimens (A) and (B) with 20% water content

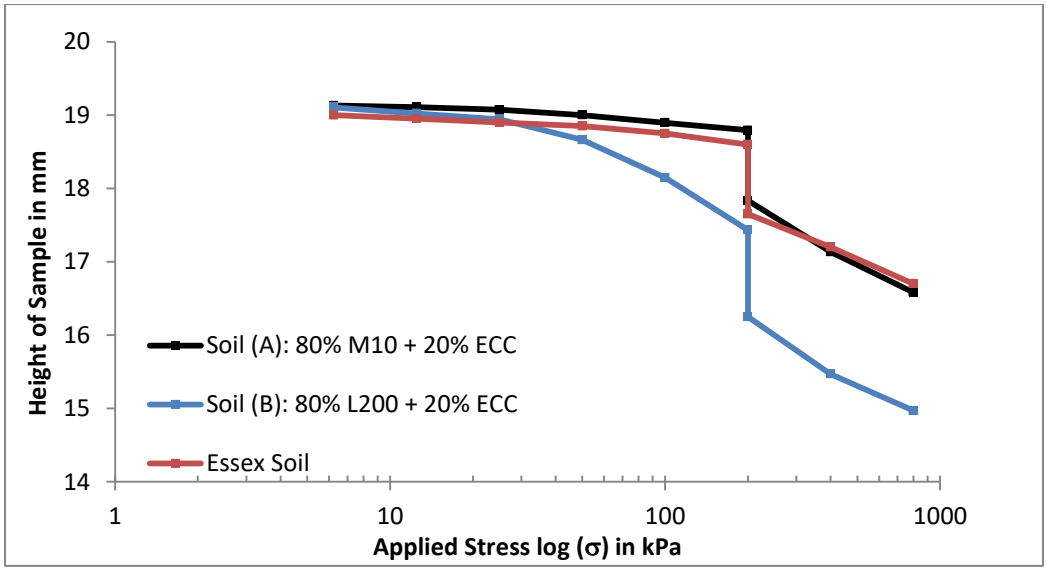

Figure 3.24: Single oedometer results of this study for artificial specimens (A) and (B), compared to natural loess soil from the Star Lane site, Essex (tested by Miller, 2002)

Table 3-10: Percentage of error for repeated collapsible test for soil (B) (see Section 3.9)

Stress in kPa	Percentage of Error %
	Collapse Test No.20 Soil B
6.25	3.7
12.5	1.7
25	2.4
50	2.4
100	1.8
200 (before wetting)	1.1
200 (after wetting)	1.1
400	1.0
800	1.0

3.12 Mixture Used as Host Ground

Factors that could play a role in collapse mechanisms, including clay content, initial water content, initial void ratio, and the period of drying, have been studied for different mixtures of M10 ground silica (Soil A has a sandstone geological origin) and English China clay through a series of single and double oedometer tests. It has been found that the collapsibility of Soil (A) increases with increasing clay content, void ratio, and period of drying. The severity of the collapse of this mixture ranges from „moderate trouble" to" trouble", whether the drying process takes place in air or oven. The ideal water preparation amount is 12%.

Soil (B), which has a limestone geological origin and almost the same size particles as Soil (A), was also tested. It produced a slightly higher collapsibility in comparison with Soil (A).

However, the overall performance of Soil (A) was the closest to the natural collapse deposit before and after soaking. It has been reported that considering loess particle size alone can cause a misleading and untruthful indicator of the collapse mechanism of a metastable soil. So, the key conclusion is to take the geological origin into consideration.

Based on the above conclusions, it was decided to use Soil (A) after mixing with 20% English China clay to construct the collapsible host ground for the stone column both with and without encasement, as will be described in the next chapter. The water content was chosen to be 12%. The shear strength parameter and the soil water characteristic curve for that mixture are described in the following two sections (3.13 and 3.14).

3.13 Shear Strength Parameter of Soil Selected as Host Ground

The effective shear strength parameters are determined using a small shear box apparatus which enables specimens of 100 mm square and up to 25 mm high to be tested. The two halves of the shear box are fixed first, then retaining, porous, and grid perforated plates are positioned. The soil (80% M10 and 20% ECC, mixed with 12% moisture) is compacted in three layers to achieve the required density. The specimen inside the shear box is sealed with plastic foil for at least 24 hours to ensure water distribution. Following this, the specimen is exposed to air to follow the drying procedure for 48 hours (the same time as for the oedometer specimens). Afterwards, the upper porous grid perforated plates and the loading pad are placed. The required sample height is calculated based on the height of the box, the main thickness of the plates, and number of ribs in each, following the calculation procedure mentioned in Head (1994). After structuring the soil sample, the shear box is installed in the shear machine and the sample is subjected to three stages: saturation, consolidation, and shearing. A similar procedure for loess soil is presented by Kalhor (2012).

First, distilled de-aired water is poured carefully into the shear carriage, such that it percolates slowly upwards through the specimen (the recommended procedure by Head (1994) when fine material, silt, or clay is to be tested). The sample is then left for 24 hours to ensure full saturation. The second stage is consolidation. In this stage, the selected vertical stresses are applied for 24 hours, and the minimum time of failure is estimated according to a value of t100 obtained from the square root time-settlement curve. The third stage is shearing. Three similar specimen are tested under different normal loads (50, 100, and 150 kPa) twice to ensure the reproducibility of the data. The samples are deformed at a strain rate of 0.1375

mm/min. Readings of horizontal displacement are taken every 0.20 mm where shear stress is recorded, as shown in Fig. 3.25.

The results indicate that the soil has a hardening strain behaviour, which is in agreement with the behaviour of the loess specimens with initial dry densities greater than 12.6 kN/m3 tested by Wen & Yan (2014). The hardening strain behaviour was observed because that once the soil has collapsed it will behave as though normally consolidated, as reported by Ayadat & Hanna (2005).

The peak shear at failure and corresponding normal stress are plotted to visualise the failure envelope as shown in Fig. 3.26, and consequently the effective apparent cohesion and angle of internal friction were found to be 8 kPa and 24.9^{o} respectively. The results were in agreement with the work done by Erol & EL-Ruwaih (1982), reported by Assallay (1998) (c'= 10 kPa and ϕ'=24°). The authors compared those results with the strength parameters under dry test, and stated that the angle of shearing resistance slightly decreased upon saturation because of the feasible lubrication influence of the water on the particle surfaces. Effective cohesion, however, noticeably decreases as a result of saturation.

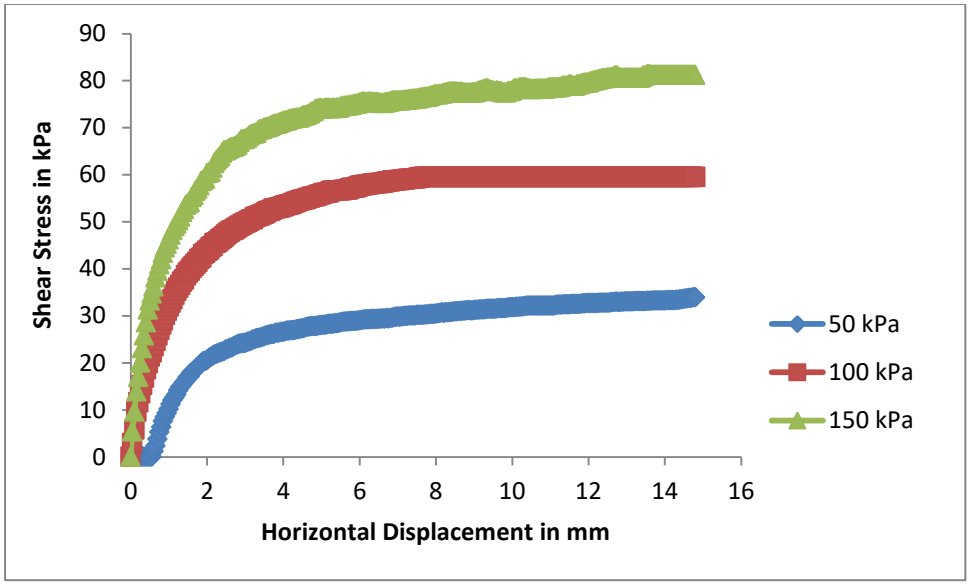

Figure 3.25: Shear stress versus shear displacement of compacted artificial loess

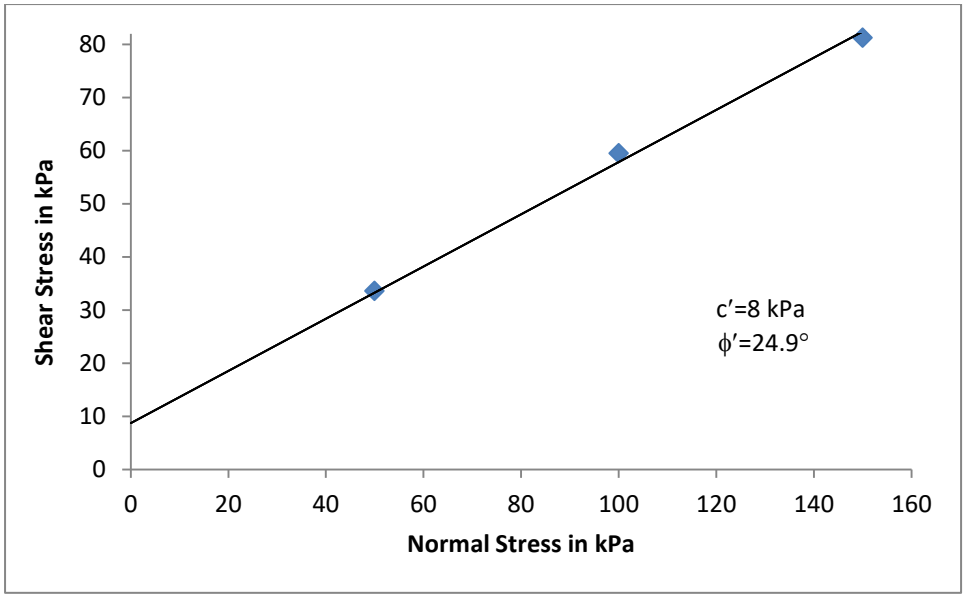

Figure 3.26: The failure envelope of the compacted artificial loess

3.14 Soil Water Characteristic Curve of Soil chosen as Host Ground

The water retention curve of the artificial soil has been determined using the filter paper method, after compacting two samples of soil (80% M10 and 20% ECC) with 12% water content. The samples were compacted in layers in the same way as described in Section 3.6, and then the samples were left for 24 hours in sealed bags, which were later removed to commence air drying for 48 hours. Afterwards, water was added to each of the samples which were covered by filter paper, using a syringe to ensure the homogeneity of the water distribution for each sample, as it was suggested by Muñoz-Castelblanco et al. (2012). The samples were sealed with plastic cling films for 24 hours. Following this, a set of three dry filters, of paper type No. 42, 55 mm in diameter, was sandwiched between two samples of soil. The upper and lower filter papers allowed drainage on both faces of the paper and ensured faster water transfer, keeping the middle paper clean. Both the samples and the filter papers are wrapped from the middle with insulation tape to keep a good contact between the paper and the soil. They are transferred to a glass jar which is wrapped with cling foil to ensure a good seal. Then, the samples were put in a constant temperature room and maintained for 10 days, for equilibrium purposes. The water content of the filter paper was determined after weighing it using a sensitive balance, putting it in an oven, and then reweighing; the balance used was named AG204 and is sensitive to 0.0001 g.

The matric suction corresponding to a certain moisture of the filter paper, w_p, was computed according to the following equation from Head (2006):

Matric suction=10^(4.84-(0.0622*w_p) if w_p <47%

Matric suction=10^(6.05-2.48*log w_p) if w_p >47%

The results for matric suction are shown in Fig. 3.27 and are in agreement with work done by Garakani (2013) for the soil water characteristic curve SWCC of collapsible loessial soil tested under zero pressure, as reported by Haeri & Garakani (2016). Also, the results agreed with those of Pereira & Fredlund (2000) for compacted collapsible soil.

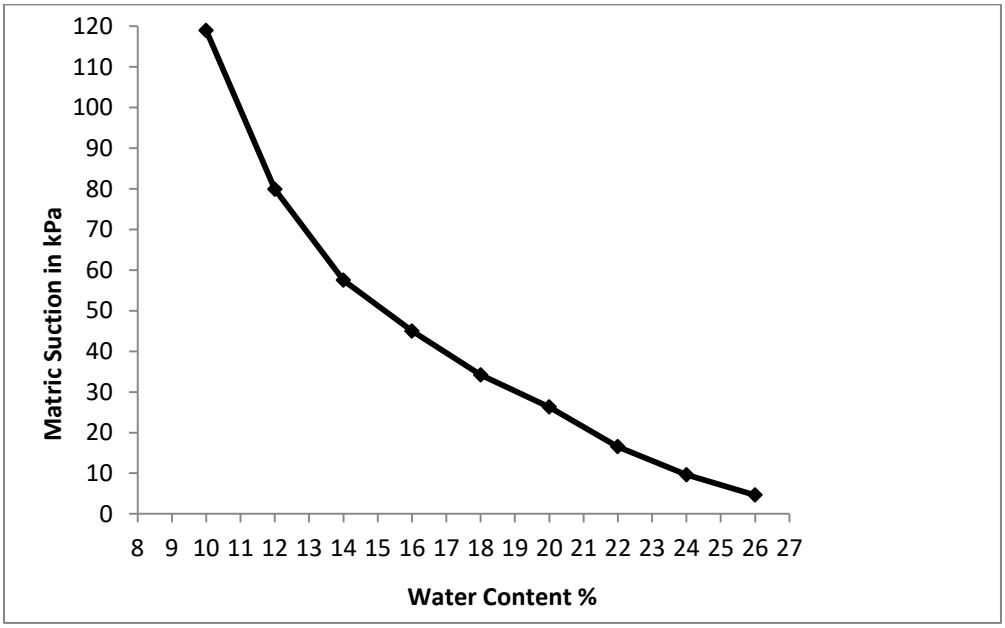

Figure 3.27: SWCC of the compacted artificial loessial soil

3.15 Summary

The material of host ground is selected based on the results of oedometer tests for different soil mixtures. It was decided to mix 80% M10 ground silica (Soil A) and 20% English China clay ECC at 12% water content. The apparent cohesion and angle of internal friction for that mixture were found from direct shear testing to be 8 kPa and 24.9^o respectively. Results of matric suction from the filter paper experiment showed good agreement with previous work done on loess soil.

CHAPTER FOUR

MODEL FOOTING, EXPERIMENTAL PROCEDURES, AND TESTING PROGRAMME

4.1. Introduction

This chapter presents the first series of laboratory work, which has been conducted on scaled-down models of ordinary stone columns (OSC) and encased stone columns (ESC) formed in the artificial collapsible bed (discussed in Chapter Three). The aim was to assess the general behaviour of this type of ground improvement in collapsible soils, under various conditions of suction and degrees of saturation. In Chapter Five, details of electrical resistivity will be discussed, from which a more detailed, understanding and evaluation of OSC/ESC will be achieved, see Chapter Six. This chapter first presents the selection of the footing model, material, and equipment used. Secondly, the full procedure to form the host soil bed and stone column are discussed. This is followed by an illustration of the testing programme and the approach of soaking the test cells with water, and an investigation of the column failure profile. Lastly, a feasibility test is described, along with the standard error of the repeated tests.

4.2. Selection of the Encased Stone Column Footing Model

Model testing had been employed because of its simplicity, repeatability and the fact that it provides a reasonable level of accuracy, although it has disadvantages associated with the scale effect (McKelvey & Sivakumar, 2000). Moreover, model testing allows the level of control required to achieve the research objectives. In this study, the selection of the loading arrangement, the dimensions of the test cell, the geometry of the stone column, the material (soil, fill, and geosynthetics), and the representation of the underground water will be discussed in the following sections (4.2.1 to 4.2.5).

4.2.1. Loading Arrangement

For this research and due to the time limitations, the performance of stone column foundation has been investigated for the stage of column‟s installation and early stages of foundation‟s loading. Therefore, it provides a reliable assessment of performance, as key changes (pore water pressure and column bulging) start at the time of installation, with load response occurring at a slow rate (Weber et al., 2006).

It is believed that loading the entire area of the stone column and the surrounding soil is the most appropriate model if the encasement is included (Ghazavi & Afshar, 2013). As with the confinement supplied by the sleeve hoops, the stress concentration will be increased on the stone column (Ghazavi & Afshar, 2013), and the application of the load on the column only will cause a premature bulging failure. Furthermore, loading the composite system would offer a more robust simulation of field situations, as the soil participates in carrying the load of the superstructure (Ambily & Gandhi, 2007). So, a foundation-type footing was chosen to rest on the artificial collapsed soil treated with a sleeved granular column.

4.2.2. Rigidity of the Footing

The rigidity of the footing (see, Fig. 4.1 for overall setup and model geometry) was checked under the assumption that it would be subjected to a uniform distributed load placed at the centre position, where the foundation is connected to the hydraulic jacks. Deflections were calculated for different load ranges and found to be very small in comparison to the deflection of the soil, which was predicted to be relatively high. Appendix (B) shows the key equation used and the corresponding calculations.

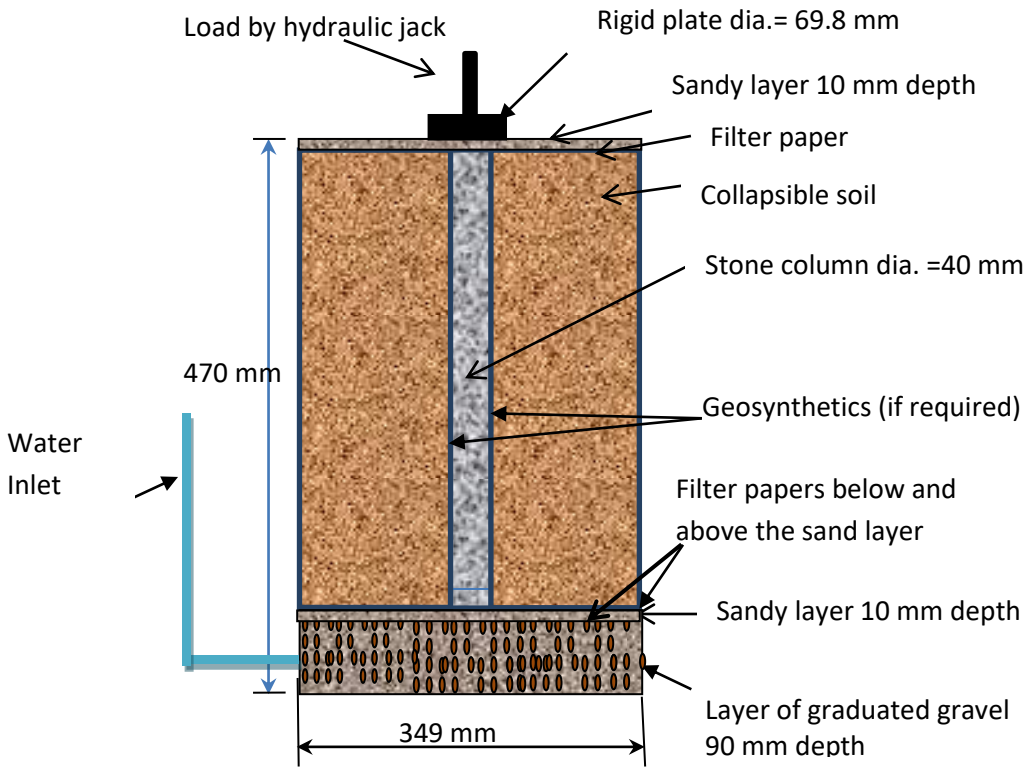

Figure 4.1: The set up and model geometry (drawing is not to scale)

4.2.3. Dimensions of the Test Cell and the Pile Geometry

The composite cell of the column and the metastable soil was modelled to a smaller scale than would be used in a practical situation, so all dimensions and stress conditions are scaled down accordingly. The soil and column were contained in a test cell with an inner diameter of 349 mm. Thus, the ratio of the soil bed diameter (349.0 mm) to the diameter of the foundation (69.8 mm) was equal to approximately 5, which is usually considered necessary to avoid boundary effects (Sivakumar et al., 2004).

The column diameter was chosen to be 40 mm, as the area replacement ratio which represents the ratio of the column area to that of the foundation area was approximately 33%; this is within the limits usually considered for conventional stone column systems (10% to 35%, as stated by Barksdale & Bachus (1983), and within the 30%-40% range recommended by Black et al. (2011) for controlling settlement. The length of the column was selected to be 360 mm, achieving an l/d ratio of 9. This is greater than the ratio of 6 that represents the minimum required to provide the full amount of limiting axial stress on the column, as reported by McKelvey et al. (2004). Thus the bulging failure zone can be monitored objectively.

4.2.4. Scaling Down the Material

The grain size of the modelled soil bed is not considered in this study as the behaviour of this particular size of soil particles, including clay bridges, is of key significance. There are of course limits to the similarity between the scaled models and a prototype constructed at full scale, as stated by Miller (2002). The artificial loess was modelled as presented in the previous chapter; the mixture and properties are presented in Section 4.3.1. The size of the fill material of the stone column and the tensile strength of the geotextile were chosen at a properly reduced scale, as will be described in Section 4.3.2 and Section 4.3.3 respectively.

4.2.5. Representing Underground Water Movement

As the upward motion of underground water is represented in this study, a filter layer consisting of gravel and sand was used as a transition medium to transfer the water from the inlet upwards through the soil strata. More details about the method of moistening and the amount of added water are illustrated in Section 4.10.

4.3 Materials

4.3.1. Soil

An artificial collapsible soil consisting of 80% ground silica M10 and 20% English China clay ECC was used as a host ground for the stone column footing models both with and without encasement. The soil was mixed at 12% water content. The mechanical and physical properties of the soil are found in Chapter Three, and are summarised in Table 4-1.

Table 4-1: Physical and mechanical properties of the soil

Properties	Values	Notes
Percentage of ground silica	80%	This particular mixture showed a close behaviour to natural loess as discussed in Chapter Three
Percentage of (ECC)	20%	
Specific gravity (G_s)	2.64	Small pyknometer method Clause 8.3 of BS1377: Part 2 (1990)
Liquid limit	29%	Cone penetration method Clause 4.3 of BS1377: Part 2 (1990)
Plastic limit	22%	Clause 5 of BS1377: Part 2 (1990)
Plasticity index	7%	Clause 5 of BS1377: Part 2 (1990)
Maximum dry unit weight	15.95 kN/m^3	BS1377: Part 4 (1990)
Optimum water content	18%	BS1377: Part 4 (1990)
Effective apparent cohesion (c')	8 kPa	Direct Shear Test, Head (1994), see Section 3.13
Effective angle of internal shear resistance (ϕ')	24.9^o	

4.3.2. Fill Material

Angular crushed stones with particle sizes in the range of 1-3 mm were used as fill material. The ratio of the diameter of the column to the diameter of the fill particles (d/dp) lies within the range 12-40, as this is the practical ratio used in the field, as recommended by Wood (2000). According to BS 5930:1999, particles are classified as very gravelly sand. Based on values of coefficient of uniformity (Cu) and coefficient of curvature (Cc), they are poorly graded. The poorly graded fill is used by many laboratory studies, e.g. Gniel & Bouazza (2009); Najjar et al. (2010); Dash & Bora (2013); and Fattah et al. (2016). The grain size

distribution curve is shown in Fig. 4.2 and all physical and mechanical properties are listed in Table 4-2.

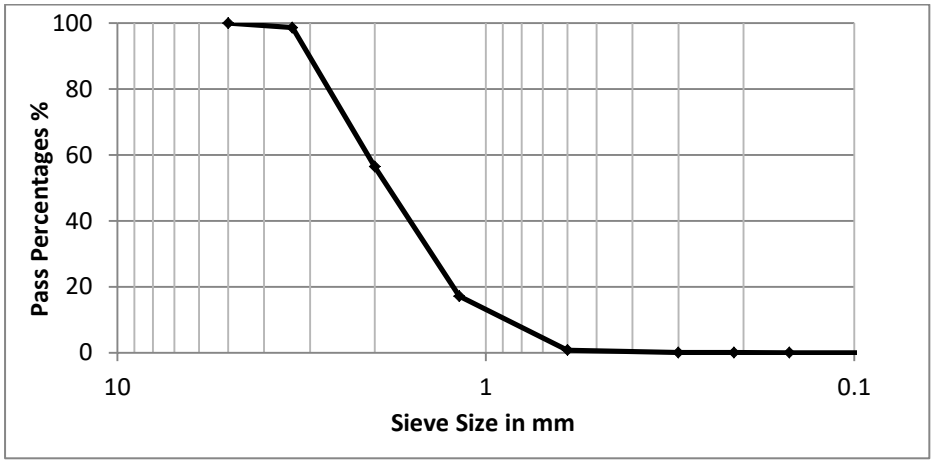

Figure 4.2: Sieve analysis for stone used as a fill material

Table 4-2: Physical and mechanical properties of the crushed stone

Property	Value	Notes
Maximum dry unit weight $\gamma_{dry\ max}$ (kN/m^3)	18.8	Clause 4.3of BS 1377: Part 4
Minimum dry unit weight $\gamma_{dry\ min}$ (kN/m^3)	15.8	Clause 4.5of BS 1377: Part 4
γ_{dry} at relative density (RD) of 70% in kN/m^3	17.8	RD=$(1/\gamma_{drymin}-1/\gamma_{dry})/(1/\gamma_{dry\ min}-1/\gamma_{dry\ max})$
D10 (mm)	1.00	BS 1377 Part 2
D30 (mm)	1.30	BS 1377 Part 2
D60 (mm)	2.05	BS 1377 Part 2
Coefficient of uniformity (C_u)	2.05	C_u=D60/D10
Coefficient of curvature (C_c)	0.82	$C_c=(D30)^2/(D10*D60)$
Angle of internal friction of the column material (ϕ_c')	39°	Direct shear test BS 1377: Part 7 (1990)

4.3.3. Geotextile

A woven polypropylene geotextile (Rhyno G8118) was employed to wrap the column with adequate overlapping so that no damage occurs within the formed geotextile column, using a stitching technique. A woven geotextile was preferred in this study to a non-woven one in order to prevent the loss of fine soil while preserving the drainage function of the system as recommended by Malarvizhi & Ilampararuthi, (2007). In the field, the tensile strengths of geosynthetics can be up to 400.0 kN/m, in order to wrap stone columns that have diameters of 400.0 to 1000.0 mm (Ghazavi & Afshar, 2013). In one example of this in a full-scale study of

Araujo et al. (2009), researchers used a geotextile of 200.0 kN/m to reinforce a stone column of 400 mm diameter installed into a loess soil. Since the scale of the dimensions and materials in a typical full-sized model of diameter 465 mm to that of the model chosen is approximately (1:0.086), a tensile strength of 17.2 kN/m is considered adequate to simulate the scale factor. The specifications of the geosynthetics, as provided by the supplier, are shown in Table 4-3.

Table 4-3: Properties and specification of geotextile

Specifications	Values	
Tensile strength (kN/m) BS EN ISO 10319	Warp	17.2
	Weft	11.5
Elongation at break (%) BS EN ISO 10319	Warp	15.0
	Weft	11.0
CBR Puncture Resistance (N)BS EN ISO 102236	1900	
Water flow normal to the plane ($1/m^2/sec$) BS 6906 Part 3	10	
Pore size 90% finer than (microns) BS 6906 Part 2	180	

4.3.4. Sand

A layer of 10 mm of Leighton Buzzard sand was used as a platform on top of the host ground and the stone column, in order to level the host ground surface and provide an even surface to facilitate the uniform loading of the system. Also, a layer of 10 mm was added on top of the gravel layer at the base of the test cylinder to create an even filter layer. The grain size distribution of the Leighton Buzzard sand used is shown in Fig. 4.3.

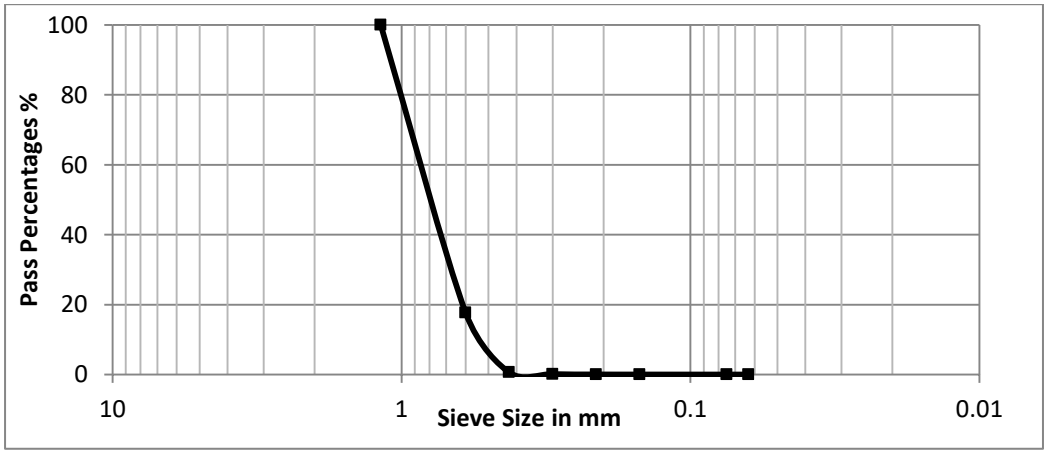

Figure 4.3: Sieve analysis of the Leighton Buzzard Sand used

4.3.5. Gravel

A layer of 90 mm of well-graded gravel of size up to 7 mm diameter was lightly compacted at the bottom of the test tank to allow a uniform distribution of water throughout the inundation phase. The gravel layer was followed by a thin layer of sand, as described in Section 4.3.4, and then covered with filter paper, the function of which was to act as a filter and prevents water from disturbing the soil particles.

4.3.6. Casting Powder

Casting was made by plaster of Paris to detect the shape of failure of encased and uncased stone columns. The full casting process is described in Section 4.11.

4.3.7. Nylon String

A braided nylon cord produced for Homebase Ltd. was used to sew the geotextile and form a cylinder with the same diameter as the stone column to be constructed (40 mm). The cord was very strong, as well as being flexible enough to sew easily.

4.4 Lab Equipment and Apparatus

4.4.1. Test Cells and Their Accessories

Three PVC cylinders with an inner diameter of 349 mm, outer diameter of 355 mm and height of 500-520 mm were used as test cells. The test cells had flanges that made them sufficiently rigid, and exhibited no lateral deformation during the preparation of the soil and during the test itself. Each tank was provided with a central water valve just above the tank base. The valve was connected to a water inlet reservoir by a clear plastic tube. The water reservoir (a plastic box) was fixed on a holding frame which was part of the loading frame itself, so the water flowed from the reservoir towards the bottom of the tank when inundation begins. This achieved the simulation of a rise in the underground water table through the soil layers.

4.4.2. Loading Frame and Axial Loading System

The loading frame is designed to transfer the required axial load to the test cells through a hydraulic system that consists of three hydraulic jacks, one in the middle and one on each side, which are used to apply the load to the untreated soil, soil treated with an ordinary stone column, and soil treated with an encased stone column. The maximum load that can be applied by the loading system is 5000 kg, which is much higher than the required maximum load of 320 kg (stress of 800 kPa) to be applied to the model footing. The load is applied to

the three cells at the same time and measured by Novatech load cell type E201T, with a capacity of 500 kg, connected to one of the hydraulic jack nozzles. The readings of the load cell are displayed via an electrical digital sensor (model LOAD-4-R-230A, manufactured by London Electronics Limited). The loading frame and the experimental setup is visualized in Fig. 4.4.

Figure 4.4: The loading frame and the experimental setup

4.4.3. Dial Gauges

High precision shockproof dial indicators with low measuring force and a 50 mm travel limit were used to measure the deformation of the foundation at the centre of each test cell. In addition, three strain indicators with a travel limit of 20 mm were used for each cell, fixed on the soil surface at different positions from the foundation, as will be described in Chapter Six. Two extra dial gauges with a travel limit of 20 mm were placed laterally on the side of the test tank to check the horizontal movement of the tank and its rigidity during the test. All dial gauges had a sensitivity factor of 0.01 mm per division.

4.4.4. Mixer

An electric mixer was used for the preparation of the soil samples, in which M10 ground silica and English China clay were mixed with distilled water. The amount of soil and water in the mixer was safe and did not overload the mixer. The duration of mixing was 12-15 minutes, to mix 2.617 kg of soil with 314 g of water used to achieve 12% water content.

4.4.5. Auger Drilling

In order to drill and form stone column vertically and centrally through the soil layers inside the test cell, a cross frame was used with a central hole to adjust the auger drill bit inside. This is illustrated in Section 4.6. A steel auger drill bit type Lewis style, 40 mm in diameter and 460 mm in length, was used to form the hole in which the stone column or the encased stone column is to be constructed, the tool was connected to a steel handle for easy control of the drilling. A steel tube with a diameter the same as the stone column model (40 mm) and a length of 500 mm was used to support the sides of the hole during construction when pouring stones in, to avoid any collapse of the soil into the hole.

4.4.6. PVC Circular Plate

A PVC plate was used, with holes at its perimeter; these holes coincided with the holes in the flange of the test cell. This plate was used to line up the test cell with the loading frame to ensure eccentricity and correct alignment, by exactly matching the holes in the plate with the holes of the tank flange. See, Fig. 4.5.

Figure 4.5: The PVC plate placed over the test cell used for load eccentricity

4.4.7. Compaction Tools

A PVC plate with a diameter of 333 mm was used in compaction to ensure the soil bed was evenly compacted. A 2.5 kg hammer was used to compact the soil in layers, as will be described in Section 4.5.4. A steel rod weighing 1.316 kg, with dimensions of 15.5 mm in diameter and 100 mm in length, was used to compact the stone fill, when stones charged to the hole in increments, see Section 4.6. Also, a wooden bar weighing 385 g, with a diameter of 23 mm and a length of 1.2 m, connected to thin steel plate with a diameter of 47 mm and a

thickness of 1.25 mm, was used to compact the gravel and sand layers at the bottom of the test soil. See Section 4.5.1.

4.4.8. Water Reservoir

Three plastic boxes were used as water reservoirs, two of which have dimensions of 410 x 310 x 225 mm, and one with dimensions of 410 x 280 x 245 mm. Each box was placed within the loading frame at a higher level than the test cell and was provided with a tap at the base, which was connected to a clear tube of 16 mm diameter, connected to the test cell. See the two blue boxes on sides and black box at the middle (Fig. 4.4).

4.4.9. Vacuum Cleaner

An electrical vacuum cleaner was used to extract the stone fill material from inside the hole at the centre of the test cell after completing the loading test and removing the foundation and sand layer from the soil surface. The aim was to refill the hole with stones after mixing with the plaster in order to discover the deformation shape of the stone column at failure. Further details are provided in Section 4.11.

4.5. Formation of the Soil Bed

The following procedure was followed to form the soil bed, again see Fig. 4.1.

4.5.1. Formation of the Filter Layer

Fourteen kilograms of well graded gravel, which had been washed and dried previously was poured into the base of one of the PVC cylinders mentioned in Section 4.4.1. The gravel layer was placed and lightly compacted by the wooden rod described in Section 4.4.7 to give a height of 90 mm. Afterwards, this was topped by a thin layer of Leighton Buzzard sand (the properties of which are given in Section 4.3.4) weighing two kilograms, and covered with filter paper which was tamped at the surface with the wooden rod. See, Fig. 4.6. The function of the filter layers was to allow a uniform distribution of water throughout the collapsible soil during inundation and prevent water from disturbing the contact soil particles. The total depth of the filter layers was 100 mm. The void ratio and the porosity of the gravel layer were 0.64 and 39% respectively, and the void ratio and the porosity of the sand layer were 0.27 and 22% respectively; see the corresponding calculations in Appendix (C).

Figure 4.6: Compaction of the sand layer on top of a gravel layer, using a wooden rod

4.5.2. Greasing the Inner Faces of the Test Cell

The inner face of the tank was wiped at a depth of 60 mm with a thin layer of grease before pouring the first increment of soil mixture into the tank. Although the accepted method to reduce friction between the inner walls of the test tank and the soil is to use two sheets of polythene with grease in between them as recommended by Tognon et al. (1999), this was impractical for the use of the electrodes of the resistivity cell. The greasing process was performed before compacting each layer of soil.

4.5.3. Mixing the Soil

80% silica flour and 20% China clay, in their dry state, were mixed thoroughly with a palette knife, until the colour of the mixture became homogenous. The percentages of the materials used were chosen based on the primary knowledge of the soil gained from the results of the oedometer tests mentioned in Chapter Three. 12% water content was added to this mixture, showing a hydrocollapse potential of 5.1%. For compacting one layer of the mixture three shares of soil, each one weighing 2.617kg was mixed in the electrical mixer and distilled water was added gradually to ensure a uniform water distribution within the mixture. The mixing duration was chosen to be 12-15 minutes. After mixing, the soil was poured into the tank without any delays, as that could cause undesired water evaporation.

4.5.4. Compacting the Soil inside the Test Tank

It is worth noting that vibratory compaction was not performed in this study, as this technique suits coarse-grained soil rather than fine particle soil. Also, the under-compaction method proposed by Ladd (1978), where by the compaction of the upper layers causes additional compaction of the layers underneath was also not used in this study. Although the latter

technique could achieve a uniform density for fine soils, making it applicable for this study, it needs a minimum of five sub-layers to be viable. In the current study, compaction was instead performed for each layer individually. Furthermore, pouring soil vertically from a high distance (the raining technique) was also avoided in this study because this could cause a reduction in the water content of the soil, which was already relatively low. Alternatively, the soil was scooped loosely from a very short distance, as performed by Ayadat (1990).

To provide more control over soil volume, and ensure a uniform distribution of the soil in each layer, the soil required for one layer was divided into three equal batches; each third was transferred and loosely levelled inside the tank. Then the soil was covered with a circular plastic plate with a diameter of 333 mm, see Section 4.4.7 and the level was checked using a spirit level, as shown in Fig. 4.7a.

The compaction of the soil layer was performed by using a 2.5 kg hammer on the plate, as seen in Fig. 4.7b. First, a very light compaction was achieved by letting the hammer fall from a close distance (20 mm) using 75 blows in a circular movement towards the tank's centre in a counter-clockwise direction in three layers. This was performed to avoid the production of dust that would have occurred if higher compaction were employed. Afterwards, compaction was performed for three layers from a fall distance of 125 mm with 75 blows per layer. The compaction effort is computed as illustrated in Appendix (C). Compaction achieved a void ratio, porosity, and dry density of 0.93, 48.3% and 13.7 kN/m3 respectively.

(a) (b)

Figure 4.7 (a): The level of the plate is checked with a spirit level, (b): Compaction process using hammer

The horizontal level of the soil layer surface was checked regularly with a spirit level, see Fig. 4.8a, while the vertical elevation was checked by a measurement ruler, see Fig. 4.8b.

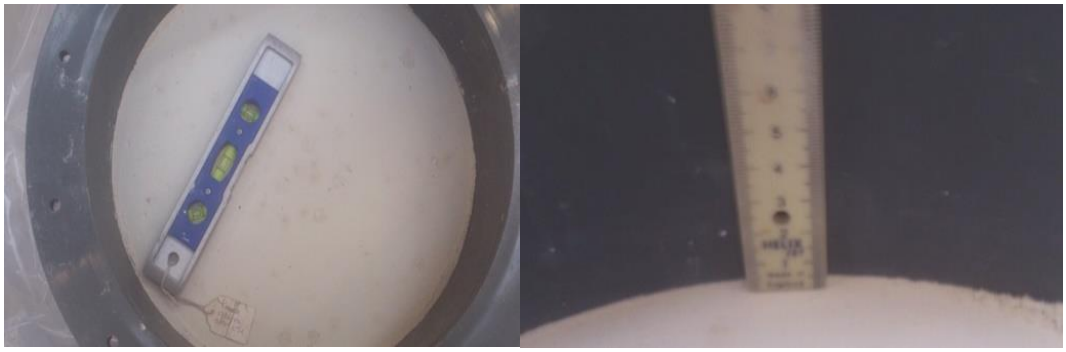

(a) (b)

Figure 4.8: Checking the layer level (a) Using a spirit level (b) Using a measurement rule

Then the surface of each compacted layer was lightly scratched using a palette knife to ensure good interaction between soil layers. Since the compacted samples were of relatively low water content, at a low degree of saturation, evaporation from the samples tended to happen relatively quickly. Care had to be taken during the compaction process to avoid any unnecessary evaporation.

4.5.5. Sealing the Compacted Sample

The mixed soil was kept covered with a plastic bag at all times during compaction and only opened when more material was required for a new layer. After the compaction of each layer and covering it with a nylon sheet, the whole tank was kept sealed with a nylon sheet for consistency purposes for 24 hours; Fig. 4.9 shows the three cells covered with nylon sheets after compacting one layer of soil.

Figure 4.9: The three cells covered with three well-sealed nylon sheets after compacting

4.5.6. Drying Process

After 24 hours, the nylon sheets were removed to leave samples to dry off in air for 48 hours, then the next layer of soil was added and the process was repeated.

4.6. Construction of Ordinary Stone Column (OSC)

Upon completing the final (6th) layer, the soil surface was checked in many directions with a spirit level to ensure it was level. At this point, the soil bed was ready for penetration by the ordinary stone column or encased stone column. The construction of the stone column included marking a centre point on the soil surface by fixing the cross frame in the centre, then inserting the auger bit (see Section 4.4.5), which had the same diameter as the required stone column (40 mm), into the cross frame, as shown in Fig. 4.10a. No collapse was observed in the hole formed. Afterwards, a steel tube with dimensions the same as the stone column model was placed in the hole to support the hole's sides and prevent any possible collapse from happening during the construction phase. Since the volume of the hole was known, the total weight of stone required to fill the hole was determined. The total weight of stone material was divided into six equal batches to fill up the hole. Each batch of stones was poured into the steel casing in six layers using a plastic funnel, as shown in Fig. 4.10b. Each layer of stones was compacted with the steel rod described in Section 4.4.7 with 30 blows, in order to achieve the required density of 17.8 kN/m^3; see Fig. 4.10c. Fig. 4.11 shows the stone column constructed in the middle of the test cell. The column material was compressed to a relative density of 70%, as the effectiveness of the encased stone column is higher if the column material is compressed well, according to Malarvizhi & Ilampararuthi (2007).

(a) The auger bit surrounded by the cross frame

(b) Steel casing topped by a plastic funnel to charge the stones inside the hole

(c) Compacting the stones inside the hole formed

Figure 4.10: Auguring the hole and compacting fill material to construct the ordinary stone column

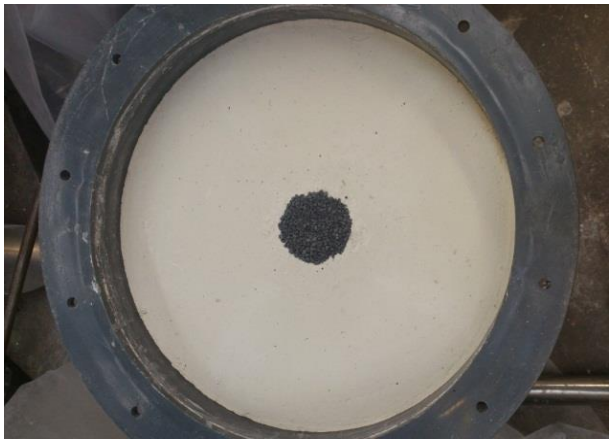

Figure 4.11: The ordinary stone column constructed at the centre of the test cell

4.7. Construction of Encased Stone Column (ESC)

To construct the stone column with encasement, first an impermeable layer (2 mm thickness) is placed at the hole‟s base. The function of that was to prevent water from spreading from the hole's centre towards the surrounding soil, because this could potentially increases the collapsibility of the soil, as was observed from a pilot experiment with a small-scale clear test cell. After this, an overlapping, sewn geotextile was wrapped as shown in Fig. 4.12 and then the same process as for the ordinary stone column, illustrated above, was followed. Figure 4.13 shows the stitching process to form the geotextile cylinder with a diameter equal to the hole diameter (40 mm).

Figure 4.12: Wrapping the geotextile around the steel tube

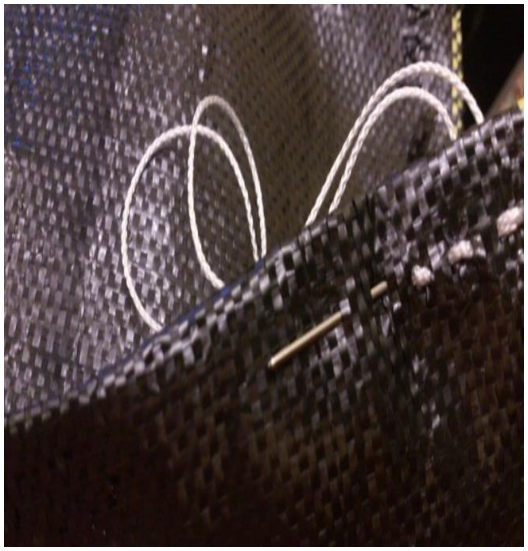

Figure 4.13: Stitching the geotextile to form a cylinder encasement

4.8. Testing Programme

In total, twelve tests were conducted using the physical model. In these tests, the soil bed was formed of six layers. Each layer of compacted soil, with an initial water content of 12%, was left in air for 48 hours for the formation of bonds; see Section 4.5. The tests included loading untreated soil (US), and soil treated with both ordinary (OSC) and encased stone columns (ESC), under specific cases of inundation. Different amounts of water were added to the soil deposits. In all tests, stone columns of 40 mm in diameter and 360 mm long have been used. The same encasement, with a tensile strength of 17.2 kN/m^3, was used. Two scenarios of soil wetting were followed. A full summary of the experimental programme is summarised in Table 4-4.

Table 4-4: The testing programme

Test No.	Treatment conditions	Inundation scenario	Inundation in litres*	Aim of installation
1	US	None (dry state)	None (dry state)	Monitoring the untreated soil loading behaviour under no wetting conditions
2	OSC	None (dry state)	None (dry state)	Conventional stone column efficiency under no wetting conditions
3	ESC	None (dry state)	None (dry state)	Encasing efficiency under no wetting conditions
4	US	Water soaking before loading	2.73	Collapse potential impact effect of inundation for the untreated soil
5	OSC	Water soaking before loading	2.73	Collapse potential impact effect of inundation for OSC
6	ESC	Water soaking before loading	2.73	Collapse potential impact effect of encasement
7	US	Water soaking before loading	6.15	Collapse potential impact effect of inundation for the untreated soil
8	OSC	Water soaking before loading	6.15	Collapse potential impact effect of inundation for OSC
9	ESC	Water soaking before loading	6.15	Collapse potential impact effect of encasement
10	US	Loading up to 100 kPa, then water was introduced	6.15	The effect of soaking after loading 100 kPa in case of untreated soil
11	OSC	Loading up to 100 kPa, then water was introduced	6.15	The effect of soaking after loading 100 kPa in the case of OSC
12	ESC	Loading up to 100 kPa, then water was introduced	6.15	The effect of soaking after loading 100 kPa in the case of ESC

Note: * The volume of water within the drainage lines is not included

4.9. Running the Test

Three test cells were tested at the same time; one contained the untreated soil, the second contained the ordinary stone column, and the third contained the soil treated with an encased stone column. Before transferring the three tanks to the loading frame, 2 kg of Leighton Buzzard sand was placed evenly on the soil surface of each tank (on top of filter layer) to ensure the uniform distribution of the load. The hydraulic jacks connected to the foundation model were lowered into position at the centre of the test cell. To ensure the centre of the test cell coincided with the centre of the model foundation, the circular PVC plate described in Section 4.4.6 was put on the test cell flange; see Fig. 4.14. Once the eccentricity and correct alignment were ensured, the jack height was adjusted to exert the required load.

Measurements of the vertical displacement of the foundation and the neighbouring soil surface were conducted using the dial gauges described in Section 4.4.3. The deformation of the tank sides for the tests of the ordinary stone column and encased stone column was monitored using dial gauges to ensure the rigidity of the tank. Once the dial gauges were set up to their zero readings, the experiment was provided with the source of the inundation (illustrated in the section below) and the loading proceeded according to the requirement of the testing programme. If the tests included soil resistivity measurement, the corresponding acquisition system illustrated in the next chapter was used. The load was gradually increased in doubled increments; each increment was maintained until the settlement observed did not change. Figure 4.4 in Section 4.4.2 shows the final setup of the first test.

Figure 4.14: Ensuring the load lined up with the centre of the test cell

4.10. Strategy for Wetting the Deposits inside the Test Cell

Water was transferred from the water inlets to the base of the test tanks via clear tubes. The valves were opened enough to allow a small amount of water to be added in a manner that ensured no air gaps between the gravel particles and no disturbance to the soil particles. An attempt was made to know the volume of water that fills the drainage lines and the filter layer consisted of the gravel and the sand; the water needed to fill the filter layer was found to agree with the calculations of the estimated void ratio, dry unit weight, volume, and height of the filter layer, as shown in Appendix (C). An initial estimation was made of the water required to fill the air voids of the soil, which occupied a certain volume; this did not represent the true degree of saturation of the soil, as capillary action and suction force will control that (see Chapter Six for further discussion). Theoretically, it was found that adding 6.15 l of water to the soil, saturated a soil column depth of 180 mm to give a degree of soil saturation for the whole tank of approximately 63%. However, adding 2.73 l of water to the soil will saturate 79.77 mm only, providing a degree of saturation of 40%; see the calculations in Appendix (C). Based on the above, the water needed to fill the air voids in the soil, which occupied a certain volume, and required to fill the drainage lines and the filter layer, was determined and added to the reservoir. The same quantity of water was added to each of the three test cells for each test. It was observed that the water was slowly drawn into the untreated soil deposit, and the entire quantity of water entered the tank, such that no water was observed in the tube at any level. The time recorded to transfer the water into the cells are illustrated in Table 4-5; even there is no guarantee that flow rate of water was the same for all of the tanks, the quantity of water entered to each tank was proportional with the type of deposit if it was treated or untreated with stone column at the middle. The presence of the stone column seemed to accelerate the saturation of the surrounding soil. After soaking, the soil was left for 24 hours to ensure saturation before the loading stage began.

Table 4-5: Time required to transfer the water from the reservoir to the soil tanks

Test No.	Foundation	Amount of the water added*	Time**
4	US	water for drainage lines +water for filter layer = (4.57 L) + (2.7 L)	45 minutes
5	OSC	water for drainage lines + water for filter layer = (5.1L) + (2.7 L)	25 minutes
6	ESC	water for drainage lines + water for filter layer = (4.57 L) + (2.7 L)	35minutes
7	US	water for drainage lines + water for filter layer = (4.57 L) + (6.15 L)	1 hour and 10 minutes
8	OSC	water for drainage lines + water for filter layer = (4.57 L) + (6.15 L)	35 minutes
9	ESC	water for drainage lines + water for filter layer = (4.57 L) + (6.15 L)	55 minutes

*The amount of the water added to the water reservoir

**Time required to transfer the water from the water box to the tank

4.11. Detecting the Shape of Failure of OSC and ESC

Once the loading of the column has been completed after each test, the column shape at failure was been investigated. First, the stones were vacuumed out and collected by the vacuum storage container, as shown in Fig. 4.15. After vacuuming, the empty column at the middle of the host ground was left inside the test cell.

Figure 4.15: Left: Vacuuming aggregate from the stone column hole; Right: collecting the vacuumed aggregate in the storage container

Fine cast powder (plaster of Paris) was gradually mixed with water in a ratio of 1 kg of powder to 750 ml water. After a creamy paste had formed, three quarters of the vacuumed

stone was added to the cast liquid and mixed thoroughly; see Fig. 4.16. Then, the paste was poured into the empty hole at the centre.

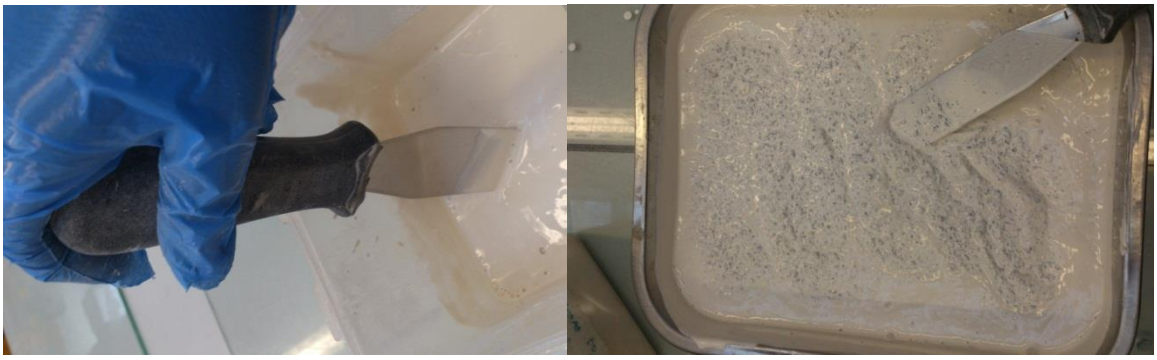

Figure 4.16: Left: Mixing the cast powder with water; Right: Mixing the cast paste with the vacuumed aggregate

Afterwards, the cast paste was added to the hole and compacted lightly with the steel rod, and then the cast mixture was left to rest for 24 hours; see Fig. 4.17. After 24 hours, when the cast liquid had set, the surrounding soil was cleaned out while the cast aggregate in the middle remained in the cell. The column's shape could then be studied; see Fig. 4.18.

Figure 4.17: The cast paste was poured into the empty hole in the centre of the host ground

Figure 4.18: The cast column is ready to be studied for its failure shape after removing the surrounding soil

In the case of the ESC experiments, after vacuuming the aggregates, the geotextile was removed from the empty hole to detect any damage to the geotextile itself or the sewing

cords. Then casting resumed with the geotextile presence and the same procedure as for the OSC was followed, in order to detect the shape failure of the ESC.

4.12. Feasibility Test

Before the main tests were carried out, a pilot test was conducted in order to refine the method for mixing the materials and compacting the soil layers, as well as to assess the feasibility of augering the soil and constructing the stone column hole without collapsing in order to find any possible problems before performing the real tests. This allowed the identification of the homogeneity of the soil deposits inside the tank, the initial water content of the soil in the tank, and the water content after 48 hours of drying. It also ensured the assessment of the feasibility of compacting the stone used as a fill, how many blows to use, and how much compaction was required to achieve the required relative density of stone.

The test tank was filled with soil layers in the same procedure described in Section 4.5, which was exactly the same as for the real tests. Soil was placed in layers in the tank; each layer was compacted with initial water content of 12% and left to dry in air for 48 hours. Afterwards, three bore holes were drilled using the auger bit, one at the centre and one each on the left and right, each one 60 mm away from the central hole. During the drilling process, the auger bit was pushed through the deposit to a depth equal to one layer of soil (60 mm); the extruded soil corresponding to this volume was weighed and then put into an oven to calculate both the dry density and the water content. Figure 4.19 shows the water content profile for the three positions in the deposit; it was noticed that the water content in the top layers and the bottom layers were lower than the middle layers, as evaporation was expected to occur on the top open surface, and on the bottom layer which was in full contact with the gravel layer. The average water content of the three bore holes exhibited values of 9.1%, 9.2%, and 9.1%; see Table 4-6. The error percent of the water content in the three bore holes, and for the six layers, ranged from 0.25-1.1%, which gives an acceptable consistency. Also, the dry unit weight values of the soil volume extruded from the centre, right, and left were very consistent and had average values of 13.71, 13.66, and 13.64, as shown in Fig. 4.20 and Table 4-6. The corresponding error band through the soil layers was 0.31-0.93%. The convergence in values of water content and dry unit weight indicates an acceptable homogeneity of the soil deposits. In general, it was observed that no problems occurred during the trial run, and no shrinkage of the deposit was witnessed; therefore, the main tests were undertaken as planned.

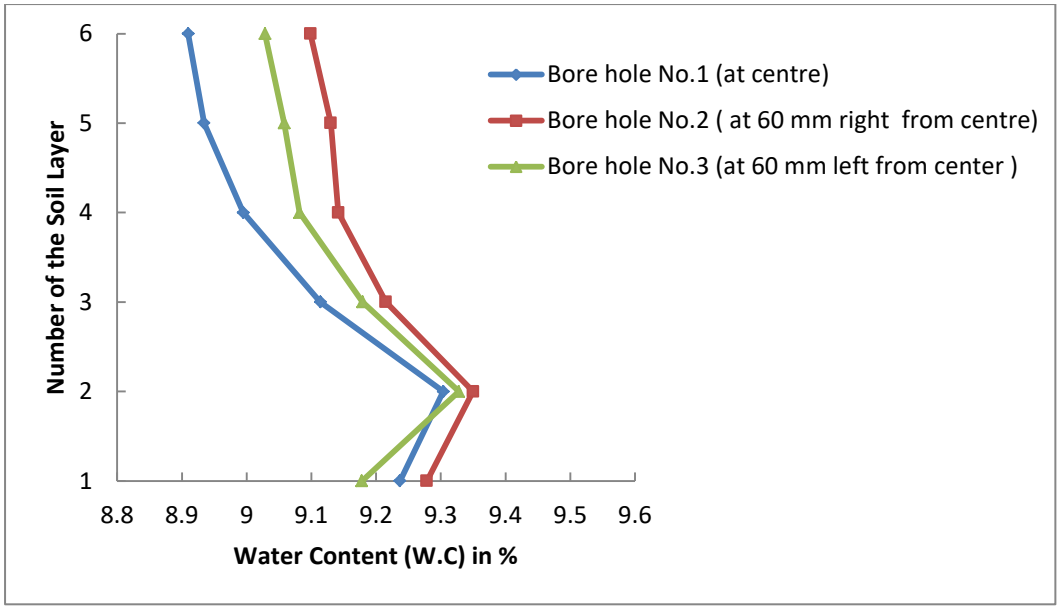

Figure 4.19: Water content profile of the soil deposit

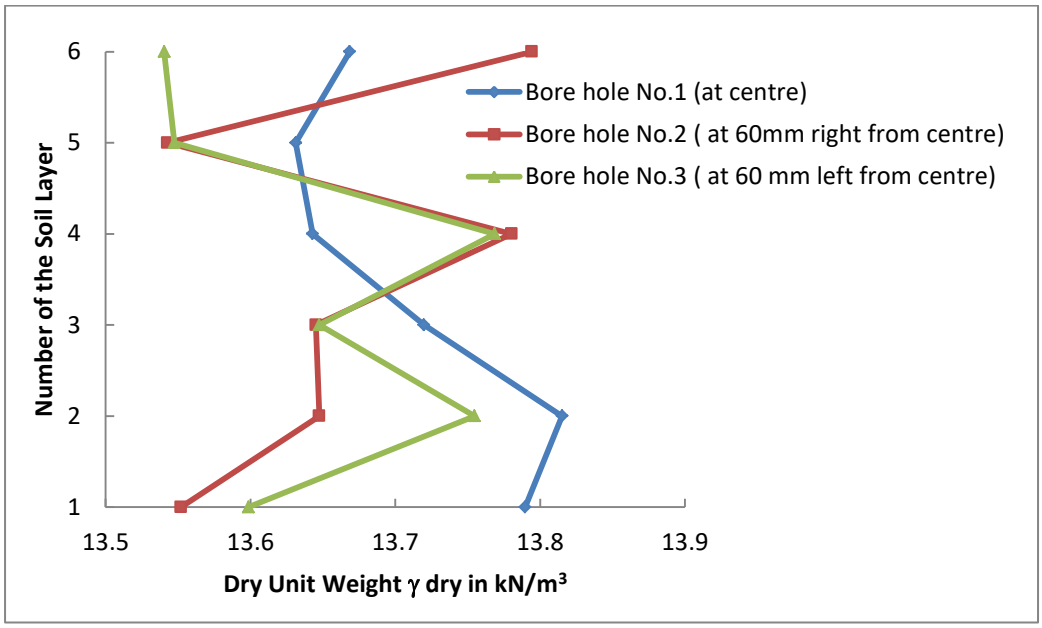

Figure 4.20: Dry unit weight through the soil layers in three bore holes

Table 4-6: Average values of water content and dry unit weight

Bore hole No.	Average water content (%)	Average dry unit weight kN/m^3
1 (at centre)	9.1	13.71
2 (60 mm right of centre)	9.2	13.66
3 (60 mm left of centre)	9.1	13.64

4.13. Repeatability of Main Tests

It is well known that a higher number of test repetitions provide more accurate and reliable results; however, in this research selected main tests have been repeated only once. The large scale of the test cells, the relatively long time required to form the soil bed and construct the stone columns, and the limited time dedicated for each task made it very difficult to repeat all tests multiple times. However, the first six tests, corresponding to the natural state, adding no water, and adding 2.73 l of water, were repeated. The following three tests, corresponding to soaking with 6.15 l of water, were compared to those under the same conditions in cells with electrodes. The percent uncertainty (error) was calculated for the nine main tests based on standard deviation from the average, using equation 3.3 presented in Section 3.6. The values from repeated tests show good agreement with those of the original tests; see Table 4-7, Table 4-8, and Table 4-9.

Table 4-7: The percentage errors of readings of settlement with loading for Tests 1, 2, and 3 (dry case) and their repetitions

Stress in kPa	Percent uncertainty (error) in experiment on untreated soil	Percent uncertainty (error) in experiment on OSC	Percent uncertainty (error) in experiment on ESC
12.5	3.4	3.4	2.3
25	2.3	2.3	2.8
50	2.8	1.7	2.9
100	1.9	3.6	3.2
200	3.2	3.1	2.9
400	2.9	1.6	2.7
800	1.9	1.5	1.5
Average error	2.6	2.5	2.6

Table 4-8: Percentage errors of readings of settlement with loading for Tests 4, 5, and 6 (wetting with 2.73 l) and their repetitions

Stress in kPa	Percent uncertainty (error) in experiment on untreated soil	Percent uncertainty (error) in experiment on OSC	Percent uncertainty (error) in experiment on ESC
12.5	3.4	3.4	3.4
25	3.3	2.7	3.2
50	3.5	3.6	3.4
100	3.1	3.3	3.4
200	1.5	1.7	2.2
400	1.4	2.0	2.0
800	1.0	1.2	1.2
Average error	2.5	2.6	2.7

Table 4-9: The percentage errors of readings of settlement with loading for tests 7, 8, 9, 13, 14, and 15 (normal cells and resistivity cells)

Stress in kPa	Percent uncertainty (error) in experiment on untreated soil	Percent uncertainty (error) in experiment on OSC	Percent uncertainty (error) in experiment on ESC
12.5	3.9	3.6	3.9
25	4.2	3.8	3.4
50	3.4	3.7	3.4
100	3.6	3.6	3.8
200	3.2	3.1	3.7
400	2.1	1.9	2.6
800	1.7	1.4	1.9
Average error	3.2	3.0	3.3

5.10. Summary

This chapter includes the parameters governing the selection of the footing model used. The properties of the soil bed, column fill, and geotextile were presented. The full processes for the setup and testing programme were described. The feasibility test results showed an acceptable deviation in water content and unit weight of soil at different locations within the sample.

CHAPTER FIVE

DESIGN, CONSTRUCTION, CALIBRATION, AND TEST RUNNING OF THE AUTOMATED MULTI-ELECTRODE RESISTIVITY CELLS

5.1. Introduction

Automated multi-electrode resistivity cells were developed in order to check the homogeneity across the inundated soil layers, before and after loading. Boundless electrical resistivity tomography (BERT) technology was employed to obtain a prominent 3D image of the electrical resistivity. The resistivity tomography image produced indicates any local changes in soil densification or volumetric water content of the subsurface for the three cells: untreated soil (US), ordinary stone column (OSC), and encased stone column (ESC).

The first section of this chapter provides a brief review of the electrical resistivity method. Following this, details of the design, construction, calibration, and test running of the new automated multi-electrode resistivity cells for the current laboratory tests are provided. Data acquisition and the control software package are also described.

5.2. Electrical Resistivity Tomography (ERT)

Electrical resistivity tomography (ERT), also known as resistivity survey, is a geophysical technique that has been employed for many decades in hydrogeological, mining, geotechnical, environmental, and hydrocarbon investigations (Loke, 2012). In the following sections (Section 5.2.1 to 5.2.6), the concept of electrical resistivity, its advantages over other geophysical surveys, the factors controlling resistivity magnitudes and some recent related studies are presented.

5.2.1. Concept of Electrical Resistivity

Electrical resistivity is a basic property that measures how strongly a given material faces the flow of electric current. An ERT survey involves the determination of the subsurface resistivity distribution by making measurements on the ground surface. First, an electric current is generated between two current electrodes, while the potential difference between two other potential electrodes is measured, giving the value of the resistance. Resistance is governed by Ohm‟s Law, as described in the equation 5.1:

$$R = \Delta V / I \qquad 5.1$$

Where R is the electrical resistance of the ground, ΔV is the difference in voltage between the two potential electrodes, and I is the electrical current generated between the two current electrodes. From the resistance, R, the value of the apparent resistivity (ρ_a) can be calculated as follows:

$$\rho_a = k.R \qquad 5.2$$

Where k is the geometric factor that depends on the electrode arrangement. Figure 5.1 indicates values of geometric factor corresponding to the popular electrode configurations used.

The apparent resistivity reflects the resistivity values for the corresponding homogenous ground for an identical electrode arrangement. To get the true resistivity, an inversion process should be undertaken. This inversion process involves finding a mathematical model of the ground section, which responds similarly to the real measured data. The model has a set of model parameters that represent the required physical magnitudes (Samouëlian et al., 2005).

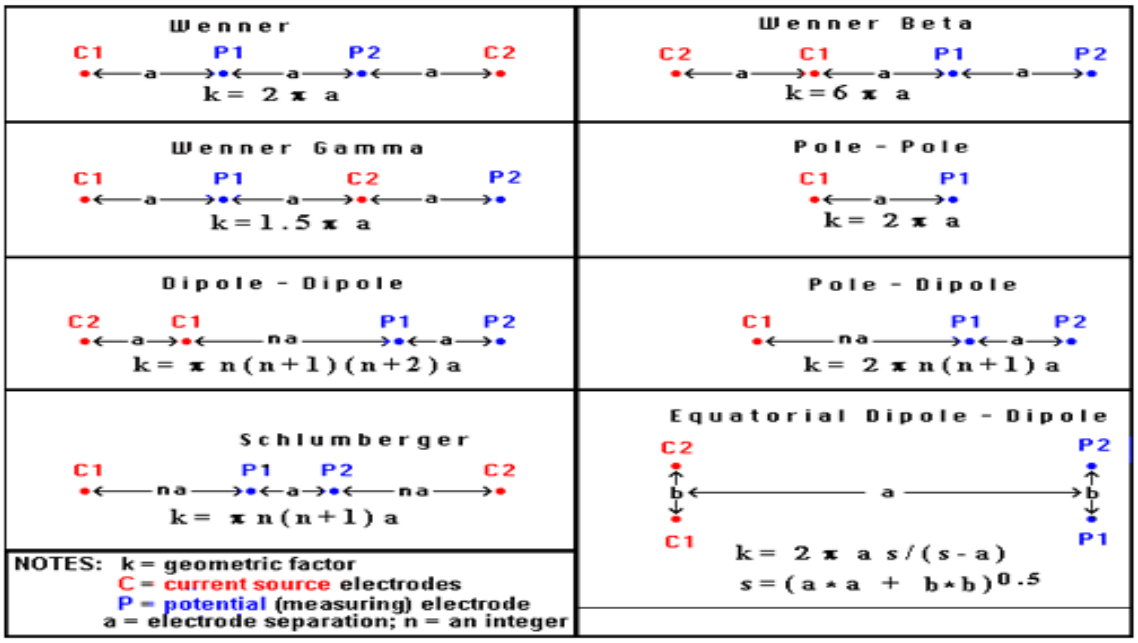

Figure 5.1: Popular electrode configrations used in resistivity surveys and their geometric factors (Loke, 1999)

5.2.2. Factors Controlling Resistivity Magnitudes

The electrical conductivity representing the reverse of the resistivity (1/ρ) of unsaturated soil has been explored by many researchers who deliberated its three phases (solids, air, and water) as parallel resistors. The air medium is an insulator. The solid particles are

nonconductive, and the electrical charge travels only in intergranular spaces occupied by water (bulk fluid). Consequently, the electrical conductivity of soils is noticeably reliant on the water content and the manner in which water is distributed (Kowalczyk et al., 2014).
Soil resistivity is clearly dependent on various geological parameters, such as clay content, porosity, degree of water saturation, and dissolved salt; its values range from 10 to just under 1000 Ω.m, while ground water resistivity lies between 10 and 100 Ω.m (Loke, 2011).

Archie (1942) presents an imperial relationship between the resistivity of clean sandstone saturated soil (ρ_{sat}) and the resistivity of fluid (ρ_f) as follow:

$$\rho_{sat} = F.\rho_f \qquad 5.3$$

Where F is the formation factor, which depends on the porosity of the soil (n) and can be calculated as follow:

$$F = a(n)^{-m} \qquad 5.4$$

Where a is an indicator of the tortuosity, ranging from 0.5 to 2.5 (Shihada et al., 2013), considered to be equal to 0.6 for sandstone, and m is a soil parameter, which is entirely dependent on the shape of the soil particles, varying from 1.2 for spherical particles to 1.9 for plated shell fragments (Jackson et al., 1978). Atkins & Smith (1961) reported that m equals 1.85 for kaolinite particles.

Archie (1941) also related the resistivity of unsaturated soil (ρ_{unsat}) to the degree of saturation (s) and the resistivity of the saturated soil (ρ_{sat}), in an approximated equation as follows:

$$\rho_{unsat} = \rho_{sat}.s^{-B} \qquad 5.5$$

Where B is a parameter that equals to 2.00 for sandstone and 1.64 for loess (Zha et al., 2010).

In addition to the above parameters, which influence the resistivity values, resistivity increases or decreases significantly with respect to temperature changes (Ward, 1971), see equation 5.6

$$\rho = \rho_o(1 + \alpha\Delta T) \qquad 5.6$$

Where ρ is resistivity after a change in temperature, α is resistivity temperature coefficient, ΔT is change in temperature, ρ_0 is original resistivity. If the temperature increases with a value of 1°C, the electrical resistivity declines by about 2%, as reported by Shihada et al. (2013).

5.2.3. Advantages of ERT Over Other Geophysical Techniques

In comparison with other techniques, such as time domain reflectometry (TDR), the resistivity method is relatively cost effective, less invasive, and less problematic because the electrodes are not inserted completely into the soil, thus making the readings easier and faster to perform. Moreover, the measured resistivity data can represent a larger size of the soil sample (Calamita et al., 2012).

For detecting water content, the resistivity method demonstrates good performance when compared with other electromagnetic methods such as neutron scattering, gamma ray attenuation, capacity sensors, ground-penetrating radar (GPR), and time domain reflectometry sensors (TDR), see Cosenza & Tabbagh (2004). The main concerns about these other techniques are related to the dielectric dispersion due to the water located within particle aggregations in clays when the water content in fine grained soils needs to be determined (Cosenza & Tabbagh, 2004). Moreover, the shear wave method also showed limitations regarding coverage of the entire area of the sample or in the presence of water, as discussed in Section 2.2.8.2.

5.2.4. Recent Related Studies

Recently, many investigators have presented resistivity tomography as a monitoring tool in many earthwork applications for imaging changes in water content or sample densification. Recent work has aimed to recognise early warning signs of inconsistent increases in moisture, such as heavy rain during seasonal cycles. For example Jackson et al. (2002) undertook experimental observations using an ERT survey performed in a laboratory on a core extruded from a road embankment constructed of tropical red soil in western Kenya. In this study, the resistivity process was also carried out on the uncased borehole wall at the site. The resistivity measurements were recorded over 18 months once soil compaction had been completed and before the construction of the pavement on the top layers of the compacted soil. The electrical surveys detected variations in water content with time, and also the water movement through the embankment layers were revealed (see Fig. 5.2). Consequently, the

geophysical image improved assessments of standard construction methods and delivered rapid assistance in finding out the optimum location.

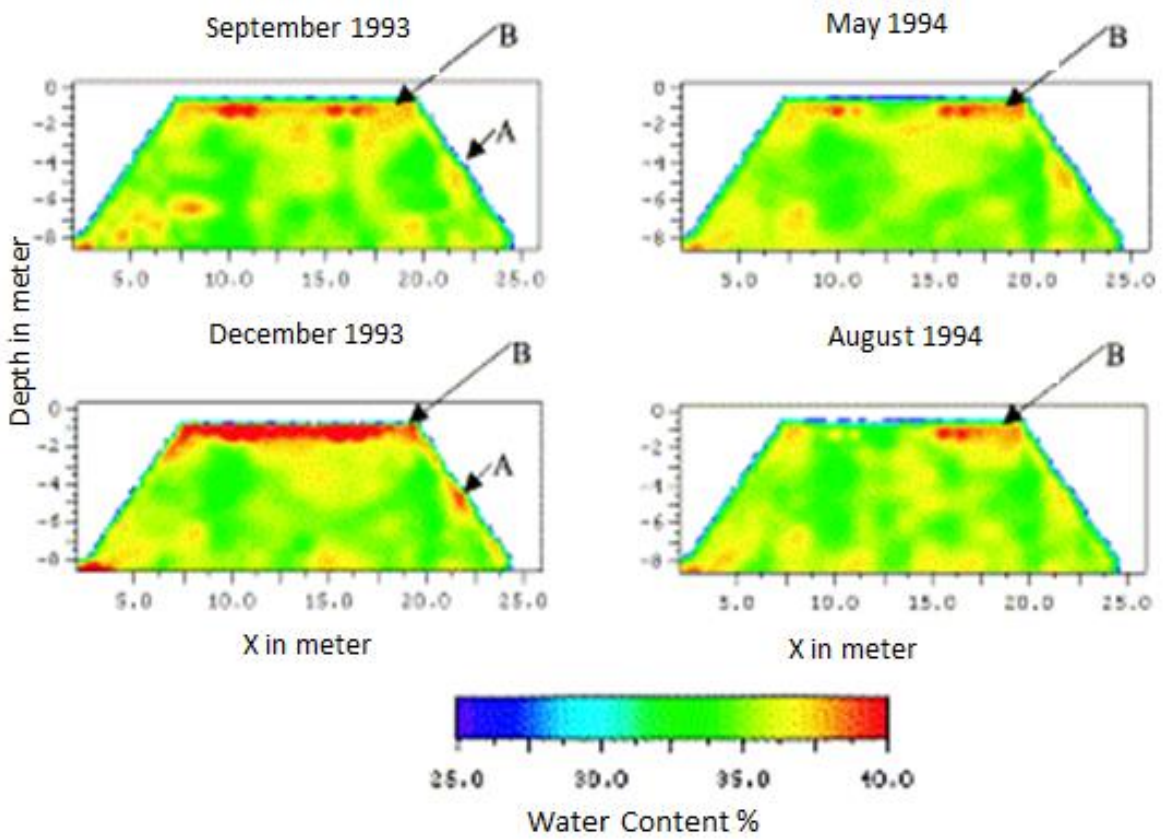

Figure 5.2: Examples of changing the water content profile with respect to time (Jackson et al., 2002)

Chambers et al. (2008) presented ERT in conjunction with conventional intrusive testing tools to explore a section of Victorian era embankment on the Great Central Railway. The integrated images from the ERT results and the intrusive sampling methods exposed both the spatial scope and water content changes, and were employed to consider the effect of an extraordinarily prolonged and heavy rainfall for the period of summer of 2007.

Chambers et al. (2014) added a correction to resistivity models to consider seasonal temperature variations, which enabled them to perform 4D electrical resistivity tomography monitoring of soil water dynamics in the same location as their previous study (an international railway embankment), in order to produce a 4D translation of subsurface resistivity distributions of water content based on the petro-physical relationships developed in the embankment material. Outcomes indicated that not only is water content a driver of instability, but pore water pressure is also a contributing factor. The development of this type of approach to asset monitoring provides the opportunity for upward trends in water content

to be analysed as they approach critical thresholds (e.g., the liquid limit), thereby providing the possibility of an early warning of potentially unstable embankment conditions. Although observations of the condition of this location did not cause serious concerns, the application of the methodology could extend to other more susceptible engineered earth structures.

The heterogeneities of soil composition were also studied using resistivity imaging tools. For instance, Borsic et al. (2005), who employed this tool to detect variations in porosity, grain size distribution, and clay content. The outcomes showed great potential for resistivity imaging in evaluating non-homogeneity throughout soil samples.

Comina et al. (2008) produced an innovative electrical resistivity oedometer cell; 42 electrodes were inserted in its internal boundaries. Electrical measurements were performed, along with seismic wave tests. The electrical measurements indicated that resistivity imaging can offer a powerful tool for the investigation of soil heterogeneities not detected by external measurements, demonstrating the potential and the limits of 3D electrical resistivity tomography for detecting both pre-existing and induced sample heterogeneities. Finally it is worth noting that experiments in the laboratory can provide a meaningful link with in-situ applications, where electrical resistivity tomography is currently used for site characterisation and the monitoring of several transient processes.

Sudha et al. (2009) integrated ERT measurements with data from standard penetration tests (SPT) and dynamic cone penetration tests (DCPT) at two different locations in a thermal power plant in Uttar Pradesh, India. The ERT data for transverse resistance was correlated with the soil properties (particle size distribution, cementation, porosity, and saturation). Findings indicated a linear relationship between transverse resistance and N-values, but this relationship relied on the site conditions and the soil characteristics mentioned.

Seladji et al. (2010) studied the impact of the compaction intensity of loamy soils on bulk soil electrical resistivity in the laboratory. They investigated agricultural and forest soils for three different densities (1.1, 1.3 and 1.6 g cm^{-3}). They concluded that increasing the compaction affect the soil resistivity regardless of the type of soil. Resistivity decreased with increasing soil density for samples with a typical water content of less than 25%. However, when water content was greater than 25%, the resistivity increased noticeably with increasing soil density.

Adli et al. (2010) focused on the improvement of resistivity data interpretation. They assessed the variations in resistivity measurements between field and lab trials for the same soil. They chose a rock formation in Penang, Malaysia, as the layers at this field site have a good connection. Then, samples under the same conditions as this site were tested in a laboratory. Measurements associated with the full-scale test indicated resistivity values lower than that of the laboratory test. The authors attributed such behaviour to the existence of underground water in voids and cracks in the subsurface rock.

Groundwater movement has been monitored by many authors; one example is the work that was done on an alluvium deposit by Saad et al. (2012) . The results showed that groundwater will lower the resistivity value, and silt will also lower the resistivity value more than the groundwater effect.

Yan et al. (2012) presented a linear relationship between the electrical resistivity and matric suction of Guangxi compacted expansive soil, based on laboratory test results. The resistivity technique saved considerable time and effort when determining the SWCC compared to the traditional laboratory methods. The authors connected the variation in the resistivity value to the magnitude of the formation factor.

Kibria et al. (2012) investigated the resistivity image technique with highly plastic clay; test results indicated that the average reduction in soil resistivity was 13.8 Ohm-m for an increase in water content from 10% to 20%. However, soil resistivity was almost constant above 40% water content. The study presented a correlation between the electrical property on one side and the water content and the unit weight of the clay on the other.

Calamita et al. (2012) examined the ability of the resistivity method beside the TDR for evaluating the spatial and temporal soil moisture variations in the Vallaccia catchment in Italy. Findings showed that the soil resistivity was proportional to the water content. If it is compared to TDR, the measurements of the resistivity method were easier and quicker and covered a bigger volume of soil.

Hassan (2014) focused on the resistivity behaviour of mechanically compacted clay soil. The resistivity was demonstrated to be very sensitive to water content, compaction, and compaction effort. In the case of the compaction of soil drier than optimum, the resistivity was found to be relatively high. Also, for a certain gravimetric water content, resistivity decreases with an increasing dry density and/or a decreasing void ratio. For the

characterisation of cracks in the tested soil, the outcomes revealed that cracks have irregular high resistivity that can be recognised from the rest of the soil bed, and altering the depth, length, width, and orientation of these cracks results in major variations in soil resistivity, as the cracks work as barriers that prevent the flow of electrical current.

Kowalczyk et al. (2014) studied the relationship between SPT and soil resistivity; the results demonstrated that a low N-value indicates low electrical resistivity. In granular soils, the electrical resistance of solids is very high, whereas it is very low for clays as a result of water adsorption along the clay platelets through the pore water within the aggregates.

In addition, the effect of the basic physical properties of soil on electrical resistivity has been studied by Abidin et al. (2014) under loose and dense conditions. It was established that the electrical resistivity value was highly influenced by the dissimilarities of the basic physical properties of the soil, particularly moisture content densities, void ratio, porosity, and particle grain fraction of soil.

5.2.5. Electrical Resistivity Method in Loess Soil

Zourmpakis et al. (2006) explored a meta-stable soil in the field, using the resistivity method and the shear wave method. A full-scale collapse experiment on a site of loess soils at Ospringe, Kent, UK was monitored through resistivity measurements. Their findings on two soil strata showed different trends, with a decrease in resistivity upon loading or inundation for the top strata, while the lower strata exhibited the opposite trend. The explanation for such behaviour was produced by Jackson et al. (2006) through the development of a conceptual clay-coating conduction model for analysing this field collapse trial. The important conclusion drawn was that soil resistivity is governed by its clay percentage and variations in lithology upon being subjected to stress or inundation. For the same site, Northmore et al. (2008) used three geophysical surveys (electromagnetic, resistivity, and shear wave velocity surveys) beside the conventional geotechnical investigations to highlight both the general and the precise information across the site. Authors argued that although, resistivity survey was more sensitive to resistivity variations between collapsible and non-collapsible loessic brickearth if it is compared to electromagnetic survey, and give the depth and the lateral extent of the collapsible loess layers, but still there is a need to have more details by performing the shear wave velocity method and comparing its profile to the geotechnical profile.

Another study on compacted loess using ERT was produced by Zha et al. (2010). The results based on this experimental research showed that soil electrical resistivity decreases with the increase of water content and degree of saturation. Once the water content goes beyond optimum water content, the impact of water content on the soil resistivity is insignificant while at lower water content, soil resistivity declines promptly with increasing water content. Also the study indicated that electrical soil resistivity decreases with the increase in temperature.

Munoz-Castelblanco et al. (2012) studied the effect of variations in water content on the electrical resistivity of natural unsaturated loess from northern France. The main observation is that a violation of Archie"s law was noticed at low degrees of saturation. The authors attributed this to the discontinuity of pore water within the clay share of the loess at low degrees of saturation. Furthermore, in dry conditions when the water content is under 7%, changes in resistivity magnitudes become too small to give a reliable accuracy in the approximation of the water content, but generally a slight increase in resistivity values has been observed for the densest specimens. In addition, the study showed the impact of porosity on the resistivity of the loess.

5.2.6. Circular Resistivity Cell Calibration

The analytical expression of the geometric factor (k) shown in Fig. 5.1 is related to simple configuration of a half-space infinite medium (flat layout). However, for a finite volume medium, such as a circular resistivity tank, boundary effects resulting from the 3D geometry of the cell have to be considered and a calibration process should be undertaken. Hassan (2014) summarised the two main methods of calibration based on previous studies.

The first is the laboratory calibration method, in which reference solutions such as KCl and NaCl are poured into the chamber to be tested, and then geometric factors are determined according to the known resistivity of those solutions and the known cell geometry. This experimental calibration is recommended to be carried out at 20° C; otherwise the temperature correction factor should be taken into consideration.

The second is the numerical calibration method. The calibration experiment in first method could be modelled numerically and geometric factors for the resistivity cell with a specific electrode configuration can be determined. In this study, the geometric factor is determined by numerical analysis using BERT, first computing the geometric factor for a homogeneous

medium occupying the same geometry of 1 Ω.m resistivity, and then correcting that value based on the resulting primary potential and the potential of the individual measurement. Calibration was also carried out using tap water to check the feasibility of gathering data and assessing the resistivity changes of the individual electrodes.

5.3. Configuration of the Current Resistivity System

A circular resistivity cell was used, due to the geometry of the test tank. Thirty two-equispaced electrodes were typically used in each horizontal plane, which represents one layer of the soil. The use of a 32-electrode configuration marginally improves the resolution, as suggested by Holder et al. (2004). Since there were six soil layers, six circular horizontal rings were designed at the middle of each soil layer; the vertical distance between two successive rings was 60 mm centre to centre. The first ring was positioned 130 mm above the base of the test tank, to be at the middle of the first layer of soil and the above the filter layer of gravel and sand. See Fig. 5.3.

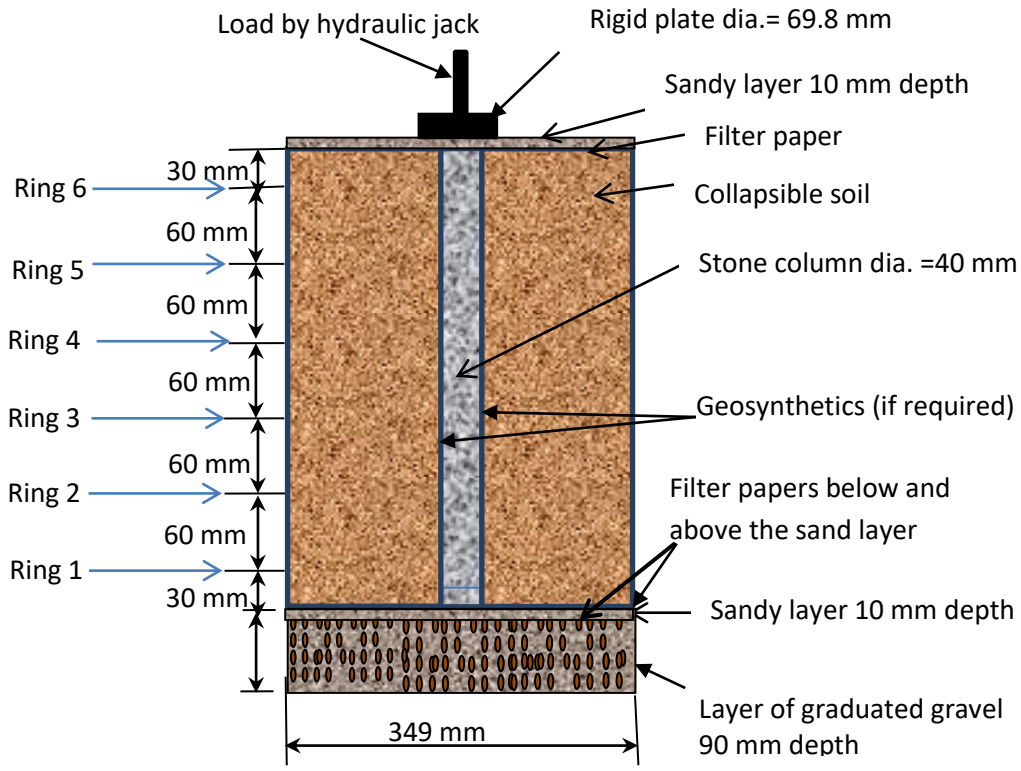

Figure 5.3: The positions of the horizontal rings of the electrodes on the test cell

Three tanks were instrumented to detect the resistivity changes of the untreated, treated with (OSC), and treated with (ESC) soil. A dipole-dipole electrode arrangement was employed to minimise the electromagnetic coupling problem, according to Loke (2012) and due to the

geometry of the test chamber in which current will not dissipate (Günther & Rücker, 2013). To take an individual resistivity reading, four electrodes were used; electrical current was generated between the first two electrodes, while voltage was measured between the third and fourth electrodes. A switching module was used to increase the efficiency and productivity of the collected data. The overlapping data levels are typically powerful enough to produce a high resolution. Also, two vertical electrode arrays were positioned on the sides of the test tank, each consisting of 16 electrodes to cover the area between each horizontal ring.

To get a better resolution, the experimental data have been collected using the following two main measurement protocols:

(1): Similarly to the procedure presented by Hassan (2014) for his dipole-dipole configuration, current was injected first into two adjacent electrodes on the cell perimeter, while potential differences were measured for the adjacent pair of electrodes. Then, the input current pair was switched in a clockwise direction and the same procedure repeated for the remaining electrode pairs. Afterwards, the spacing between the current electrodes was extended and the measured voltage electrodes followed the same procedure. The spacing between two electrodes was chosen as shown in Fig. 5.4. With this layout, 120, 6, and 2 linearly independent measurements can be collected from the 32 electrodes of the cell by considering electrode spacing to be 34.85 mm, 34.85x3 (104.55) mm, and 34.85x7 (243.95) mm respectively. Table D-1 in Appendix (D) shows the corresponding configuration of one ring.

(2): For the two vertical arrays, current was generated by a first pair of electrodes and potential differences were measured for the next two electrodes on the same side, then the current was generated on the opposite array between the two electrodes and the next electrodes above were measured, then swapping to the remaining pairs above, and so on. Afterwards, spreading the distance between the current source electrodes and measuring the potential electrodes. Then, the spacing between the input current and potential electrodes was extended, see Fig. 5.5. With this layout, 111 linearly independent measurements could be collected over the 32 electrodes of both vertical arrays; see Table D-2 in Appendix (D).

At each particular configuration for both rings and vertical arrays, each individual reading was repeated four times, as that provided a good resolution.

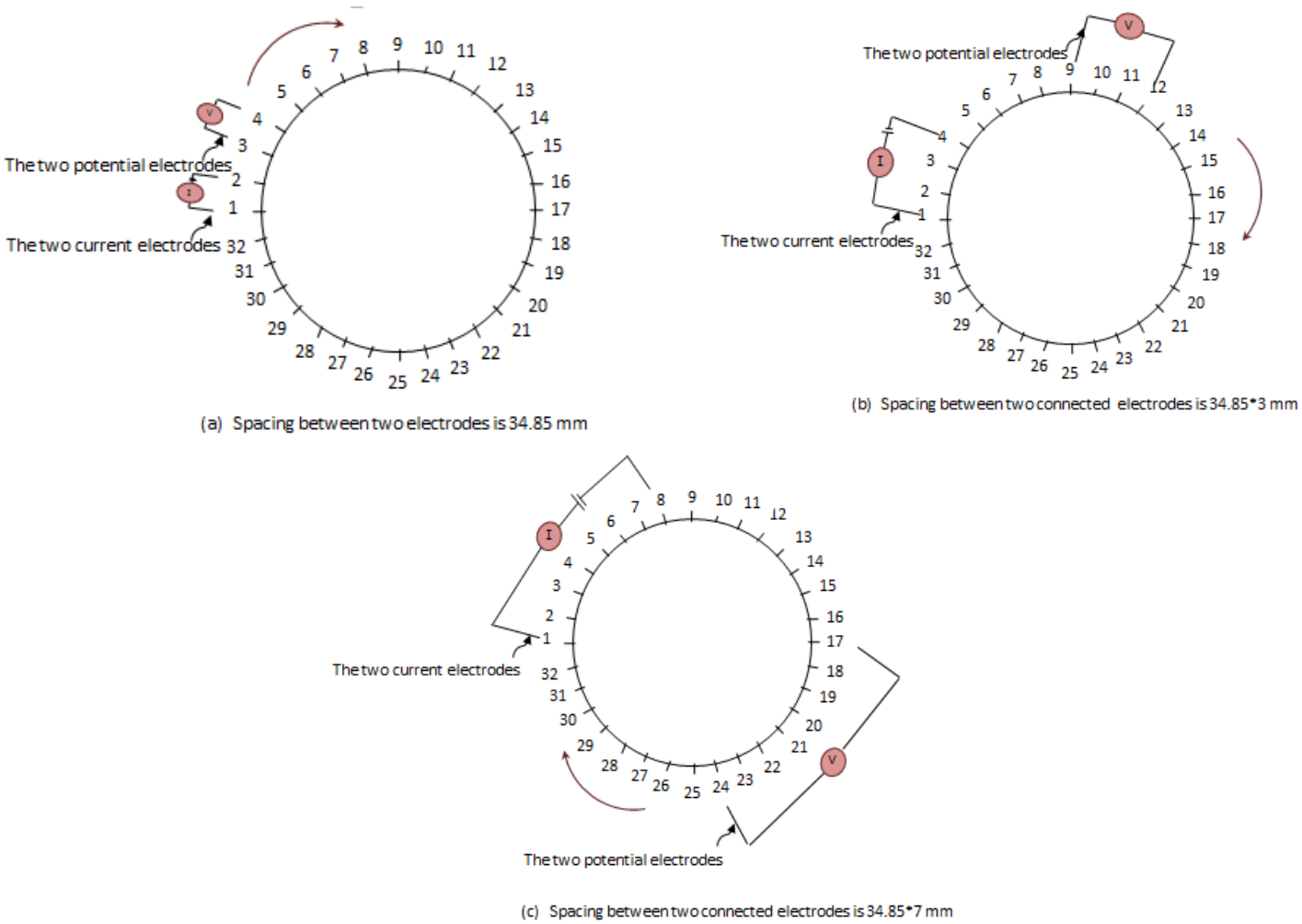

Figure 5.4: Different electrode configurations for the circular cell

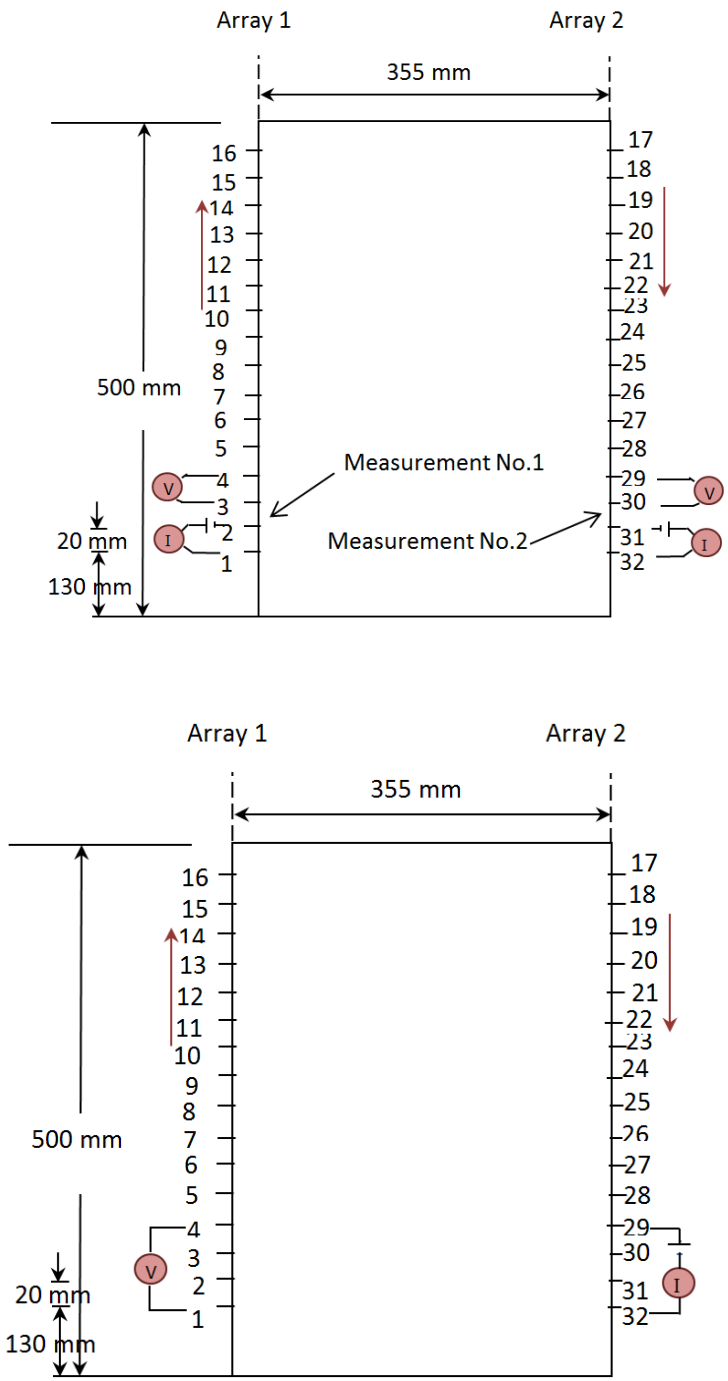

Figure 5.5: Typical vertical electrode configurations

5.4. Design and Construction of the Multi-Electrode Resistivity Cells

This study presents three multi-electrode cells, each one composed of 212 electrodes, in order to perform a cylindrical electrical resistivity tomography (ERT) measurement to investigate the heterogeneities resulting from the collapse of the loess soil caused by loading and inundation. The first cell was filled with the untreated metastable deposits, while the second

and third cells contained soil treated with an ordinary stone column and an encased stone column respectively. Three PVC tanks, which are approximately similar to the test cylinders without electrodes described in Section 4.4.1, were used; see Table 5-1.

Table 5-1: Dimensions of the resistivity tanks used

Tank No.	External Diameter in mm	Internal Diameter in mm	Height in mm
1	355	349	500
2	355	349	534
3	355	349	527

Firstly, the horizontal and vertical spacing between electrodes, according to the configuration mentioned in the previous section, were fixed around the test cylinder. Then, holes in the positions of the electrodes to be placed were drilled using a drill bit.

M4 threaded stainless steel rods, 50 mm long, were used as electrodes. Each hole was drilled and tapped to M4 thread. The electrodes extended into the test cylinder by approximately 6 mm and were tightened up using a washer and nut, after silicone sealant was applied to each electrode hole to ensure a watertight seal. Later, the sealant film was removed from inside the electrode by wiping. After fixing all electrodes in their positions, as shown in Fig. 5.6, the wiring to connect the cell electrodes with the acquisition system was installed and each electrode channel was named and marked; see Fig. 5.7.

(a) (b)

Figure 5.6: Fixing electrodes into holes: (a) View from outside of the test cell (b) View from inside the test cell

Figure 5.7: The resistivity cell after installing the wiring

5.5. Data Acquisition System

5.5.1. Resistivity Meter

A TIGRE resistivity meter shown in Fig. 5.8, was used in this study for data collection. It is capable of accurate measurements in a wide range of conditions. It has a maximum power output of 18 watts and the current can be set manually up to 200 mA. The screen of the device displays the selected current, the number of cycles (repetitions), and the resistivity connection. The device provided a range of measurements from 0.001Ω to 360 kΩ. More details can be found in the manual pdf, see "Tigre Manual Rev E 0506", 2006.

5.5.2. Power Source

To keep the acquisition system fully charged and ensure the charge did not drop below 13 volts (the operating voltage), two batteries were used alternately, with one used during measuring while the second was connected to the battery charger.

5.5.3. Laptop Computer

A laptop notebook, a Dell™ Latitude™ D830*, was selected due to its dual-core Intel processors with 64-bit support. The computer itself was dual booted to DOS and Windows; DOS is crucial for gathering the data and saving to the memory of the computer without any

loss, while Windows was used for easy access to transfer the data. The laptop computer was connected to the resistance meter using an R232 serial boot.

5.5.4. TIGIMG Control Software

Basic DOS software called TIGIMG was used to operate the computer and control the transfer of the collected data from the CAMPUS TIGRE. The software was loaded with parameter files that reflected the numbers of electrodes, the corresponding configuration, and the number of data. Figure 5.8 shows the computer, the acquisition system, the batteries, and the charger.

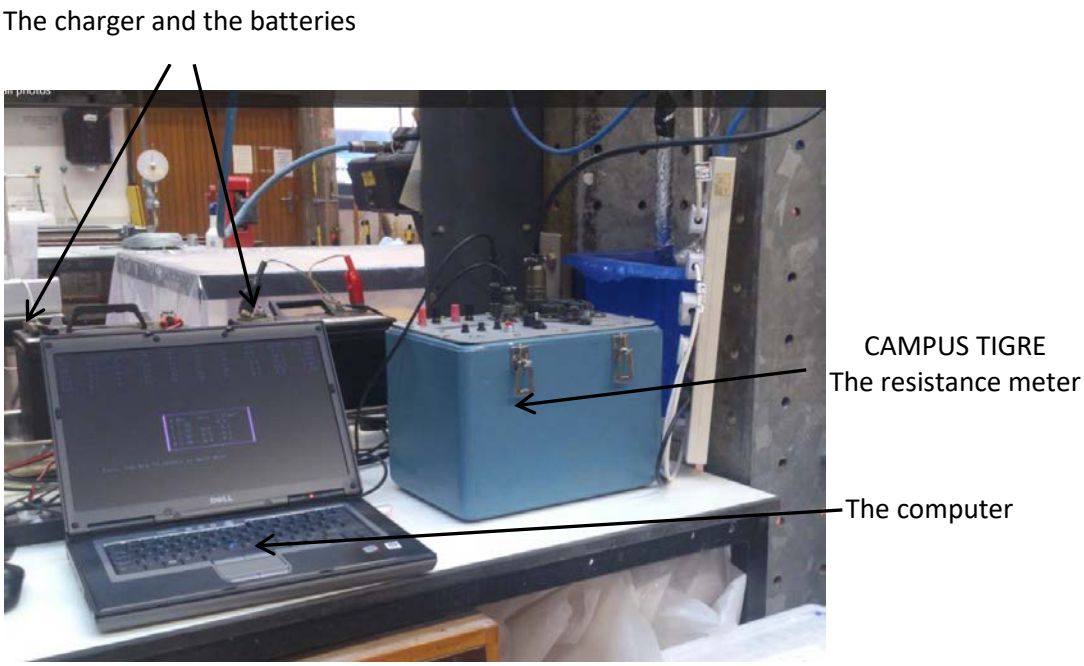

Figure 5.8: The acquisition system

5.6. Inversion Technique

The inversion process for getting the true resistivity was performed using a system called boundless electrical resistivity tomography (BERT). This technique is a powerful tool for generating mesh input, ERT modelling and inversion; see Günther and Rücker (2013). It is a distribution that uses unstructured finite element grids for forward calculation and for parameter identification. The use of tetrahedrons (3D) enables BERT to follow any geometry of the subsurface and satisfy the main advantage of working with arbitrary geometries. The inversion includes the generation of three meshes. The first mesh is a course mesh includes the parameters to be defined, while in the second mesh the forward calculation is performed through a global refinement of the parameter grid and prolongation to avoid the effects of

boundary conditions. The third mesh is called the primary mesh, and is used to calculate the primary potentials as needed for the secondary potential SP technique. An example of the three meshes in a 2D problem is shown in Fig. 5.9. The mesh requires a high refinement near the electrode locations to achieve the required accuracy. The geometric factors are deduced, indicating the apparent resistivity and the sensitivity matrix for the homogeneous case. Lastly, the real inversion is accomplished. The resistivity model is updated by an inverse sub-problem, and a forward calculation is carried out and checked against the data. The latter is done until the data are fitted well.

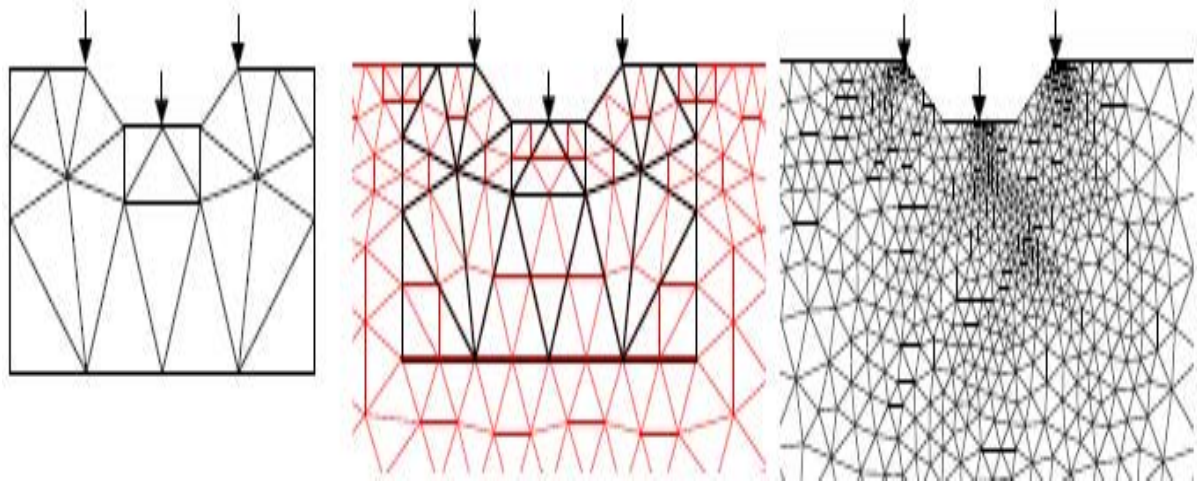

(a) (b) (c)

Figure 5.9: The three grids of inversion for a 2D problem: (a) Parameter mesh (b) Secondary mesh (c) Primary mesh (Günther et al., 2006)

5.7. Calibration of the Cylindrical Test Cells

The purpose of the calibration here is to enable a full assessment of the resistivity values for each individual electrode. Although caution was taken to ensure all electrodes and their wiring were identical, some slight variations may have existed, which need to be calculated and taken into account when the inversion process is carried out. So, it was decided that the system should be checked when the tanks were first filled with tap water, collecting the measurements and performing the inversion with BERT to see whether it is capable of producing a unified image reflecting the homogeneity of the water. To perform the calibration with tap water, prior knowledge of the value of the resistivity of the tap water used was required, before the resistivity measurements were taken. That was done using a calibrated Hanna Conductivity Probe, as will be explained in Section 5.7.2. Then, resistivity measurements were taken for the three cylindrical electrode cells after filling with tap water, as will be described in Section 5.7.3.

5.7.1. Calibration of the Hanna Conductivity Meter

A Hanna Conductivity Probe type HI 8733 was used in this study; the product specification, as provided by the supplier, is summarised in Table 5-2. A thermometer of the Brannan England RTD type was used to find out the temperature. The calibration was done with two reference solutions: HI 7033, which was used for conductivity measurements less than 84 µS/cm at 25°C, and HI 7031, which was used for conductivity ranges below 413 µS/cm at the same temperature. The probe and the thermometer were soaked with the reference solution, and based on the temperature, the probe was set to a certain value, shown on the bottle of the corresponding reference solution. Once the conductivity of the probe was calibrated, it was used to measure the water resistivity, as will be described in Section 5.7.2.

Table 5-2: The full specifications of Hanna Conductivity Probe HI 8733

Product Code	HI-8733
Range	0.0 to 199.9 µS/cm; 0 to 1999 µS/cm; 0.00 to 19.99 mS/cm; 0.0 to 199.9 mS/cm
Resolution	0.1 µS/cm; 1 µS/cm; 0.01 mS/cm; 0.1 mS/cm
Accuracy (@20 C^{o})	±1% F.S (excluding probe error)
Calibration	Manual, 1 point through EC knob
Temperature Compensation	Automatic, 0 to 50 C^{o} with 8 adjustable from 0 to 2.5%/C^{o}
Probe	HI-76302W, ATC, with 1 m cable
Power Supply	1x9V/ approx. 100 hours of continuous use
Environment	0 to 50 C^{o}; RH max 100%
Dimensions	145 x 80 x 36 mm
Weight	230 g

5.7.2. Measuring Resistivity Using the Calibrated Hanna Probe

The calibrated probe and the thermometer were soaked in tap water for each of the three test cells; see Fig. 5.10. Readings for conductivity at these particular temperatures (16°C to 18°C) were recorded. Since the resistivity equals the reciprocal of the conductivity, therefore the resistivity values of the tap water filling the three tanks were found. Consequently, those values assisted in the evaluation of the inversion by BERT in the next step.

Figure 5.10: Measuring the resistivity of tap water using the Hanna meter probe and the thermometer

5.7.3. Measuring Tap Water Resistivity Using the Acquisition System

The charged resistance meter (CAMPUS TIGRE) was connected to the computer through the RS232 serial port and to one of the 32-plug pin channels in each tank, whose resistivity was to be determined, by its cable; see Fig. 5.11. Parameter files had previously been created, displaying the number of electrodes and the particular electrode layout, as detailed in Section 5.5.4. First, the parameter file was loaded and the contact resistance was shown, then measurements were taken and saved. After all measurements have been taken for individual rings and the vertical array, the cable of the resistance meter was transferred to another channel. Figures 5.12, 5.13, and 5.14 show the collection of resistance data for the rings of Tank 1, Tank 2, and Tank 3 with respect to reading number, again see Appendix (D).

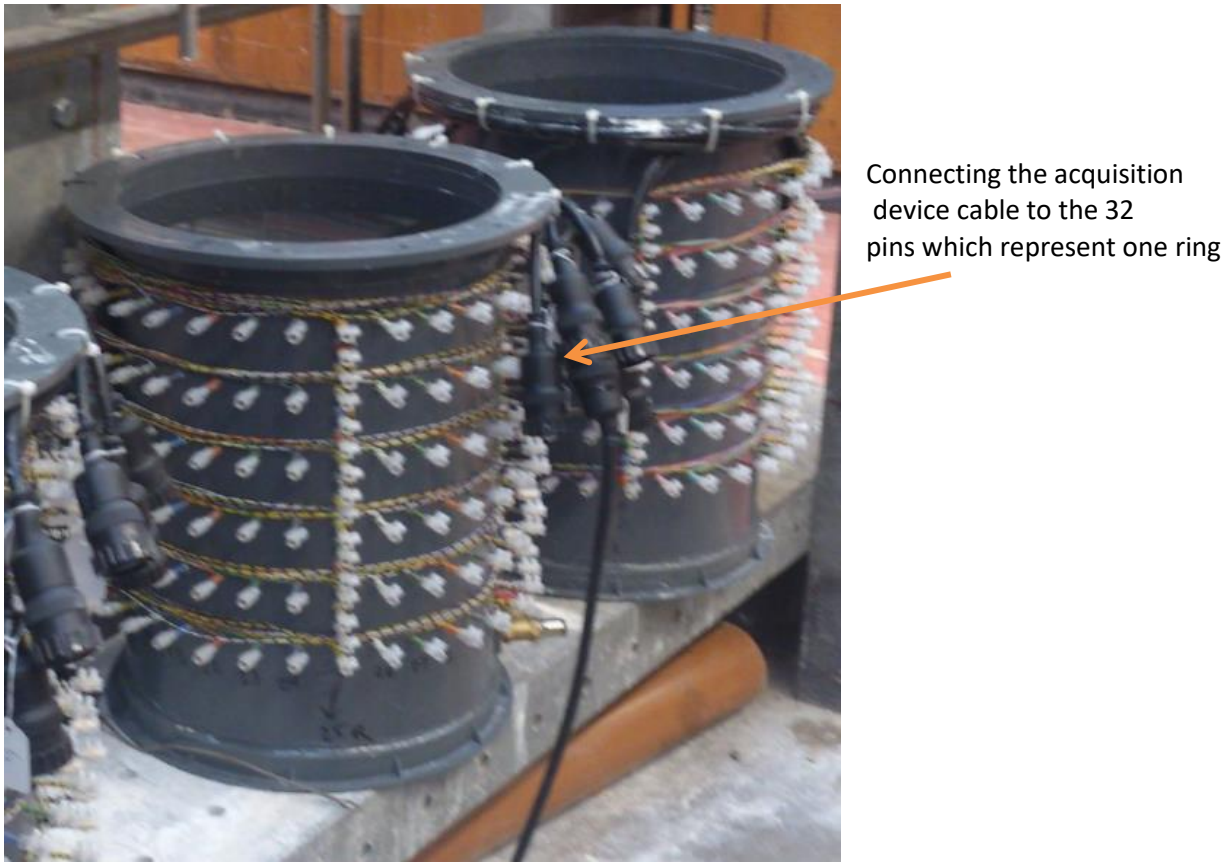

Figure 5.11: Measuring the resistivity of tap water using the acquisition system

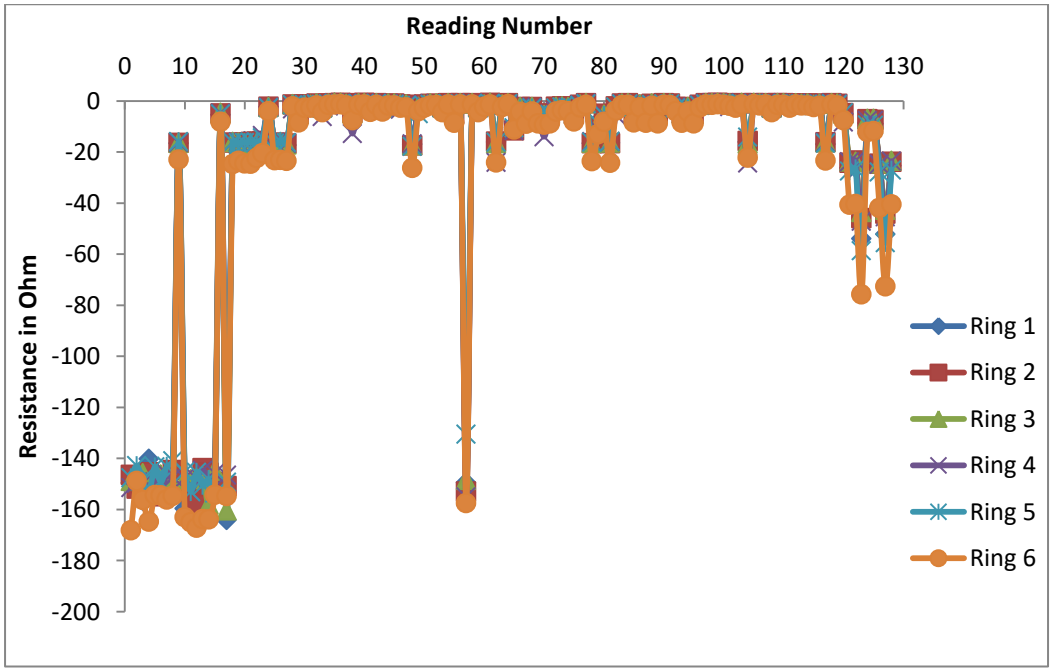

Figure 5.12: Resistant measurements for rings in Tank 1

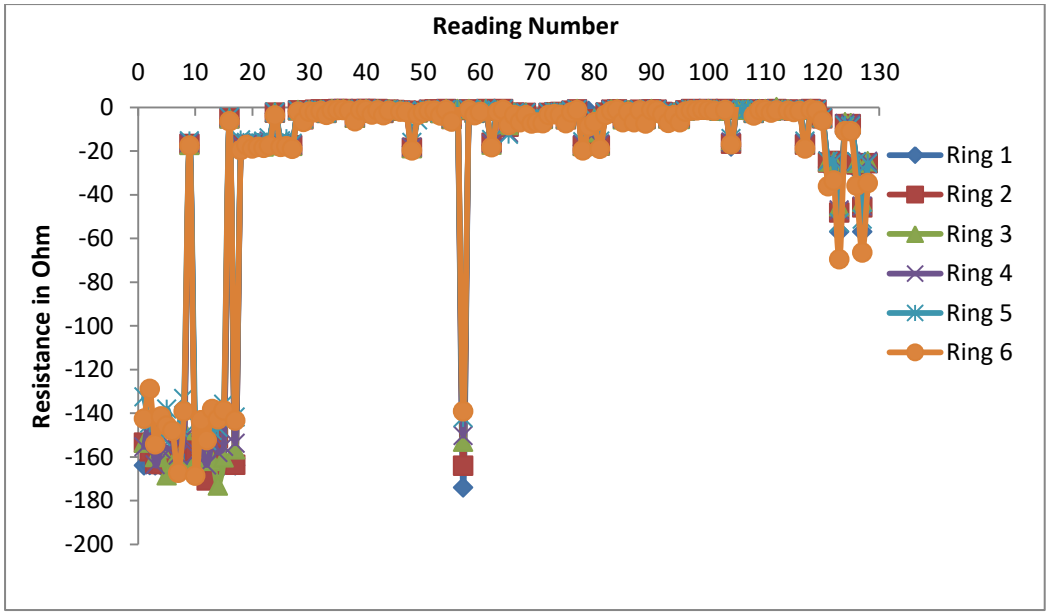

Figure 5.13: Resistant measurements for rings in Tank 2

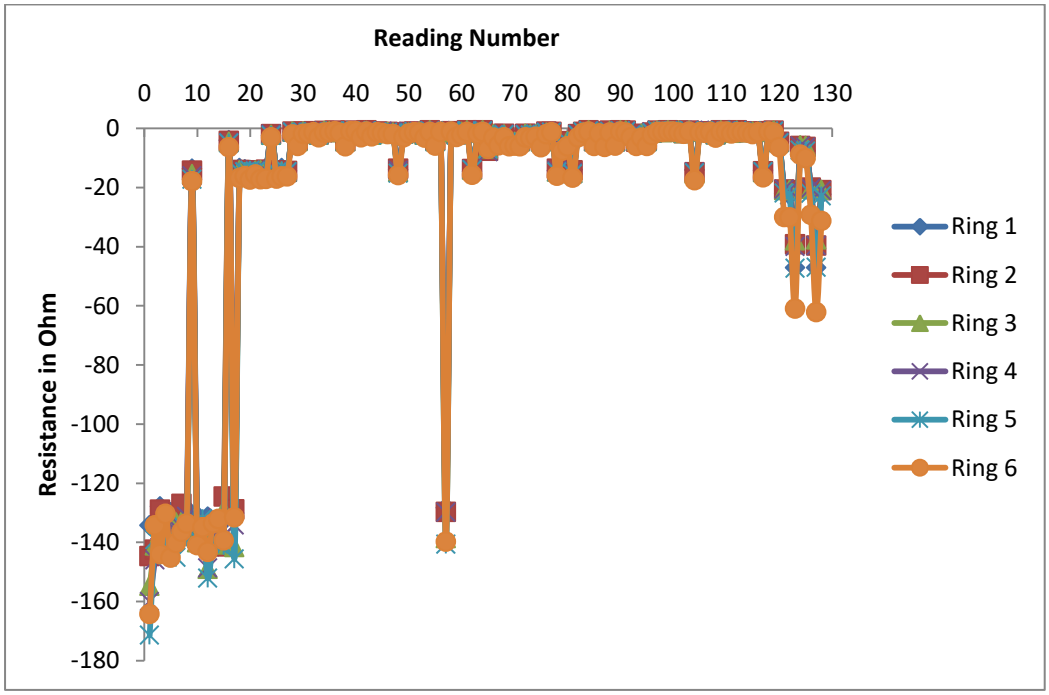

Figure 5.14: Resistant measurements for rings in Tank 3

5.8. BERT and Imaging the Resistivity of Tap Water

After collecting the data, the inversion was performed by BERT. Figure 5.15 displays the generated parameter mesh, which shows the geometry of the tank and the electrode layout. Fig. 5.16 illustrates the secondary mesh and the refinement near the electrodes. A numerical calibration was done to validate the performance of BERT in producing an accurate inversion; the data input was taken to be the same values measured by the Hanna probe for

tap water, by using a unified apparent resistivity value of 111 Ω.m as the input magnitude. Figure 5.17 demonstrates the inversion results, which were exactly equal to that value, 111 Ω.m, at all points around the tank. The resistance data gained from the acquisition system was inverted too, and it showed homogenous readings from all rings, consistent with the value measured by the Hanna probe, see Fig. 5.18.

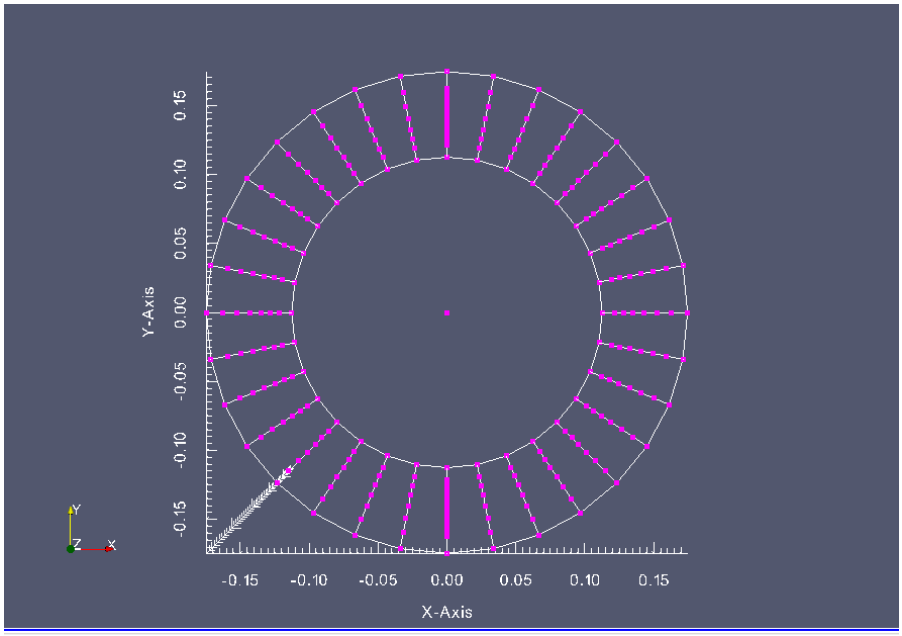

Figure 5.15: Parameter mesh showing the 212 electrodes, 192 electrodes of the six rings and 20 electrodes of the vertical arayes, their positions in the xy plane, and the geometry of the tank

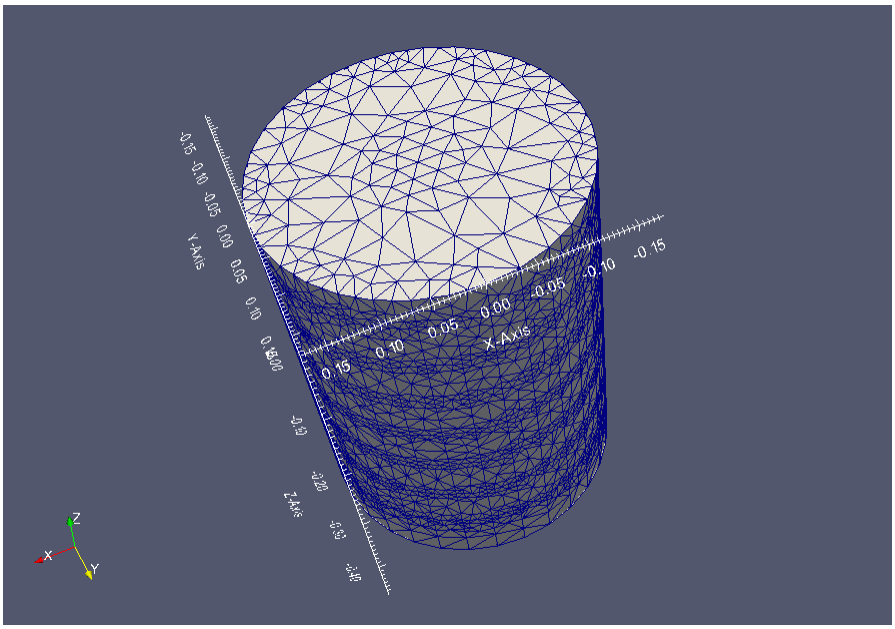

Figure 5.16: The secondary mesh

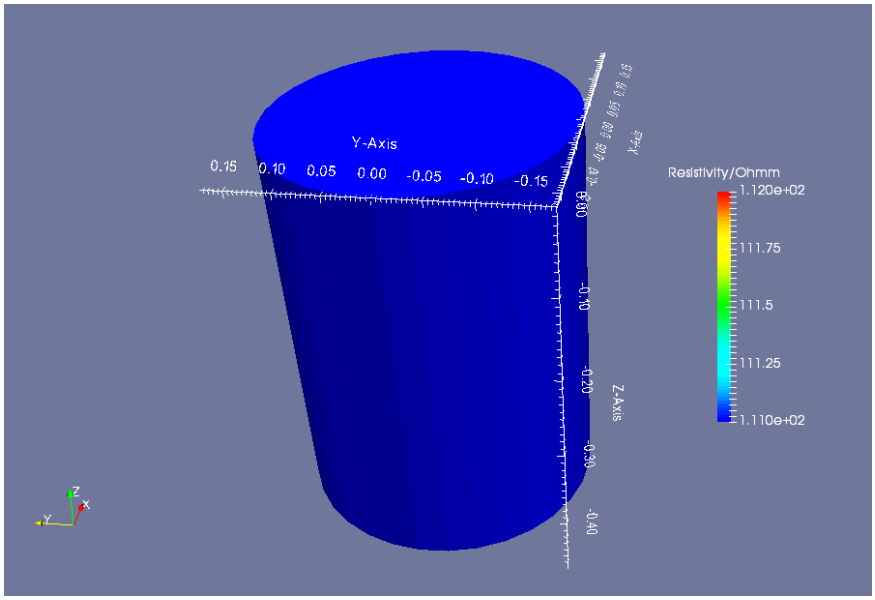

Figure 5.17: Inversion by BERT showing apparent resistivity of tap water of 111 Ohm.m

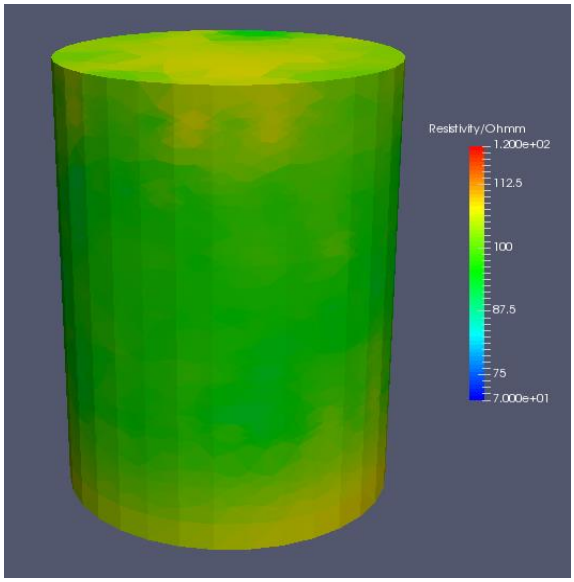

Figure 5.18: Typical inversion results for tap water (input data is resistance measurement)

5.9. Experimental Geometric Factors

The experimental geometric factors were obtained for each ring in the three tanks based on the resistance measurements from the acquisition system and the resistivity value of the Hanna probe. Figures 5.19, 5.20, and 5.21 demonstrate the corresponding geometric factors. These show the logic trend for the geometric factors which produced higher resistances for rings at the top and bottom of the tanks as a results of the boundary effect. The results for one ring, presented on a larger scale, as shown in Fig. 5.22, indicate that geometric factors are approximately equal for readings with the same configurations. For different electrode

arrangements, the configuration of a wider space between source and potential electrodes gives a higher geometric factor and consequently lower resistance.

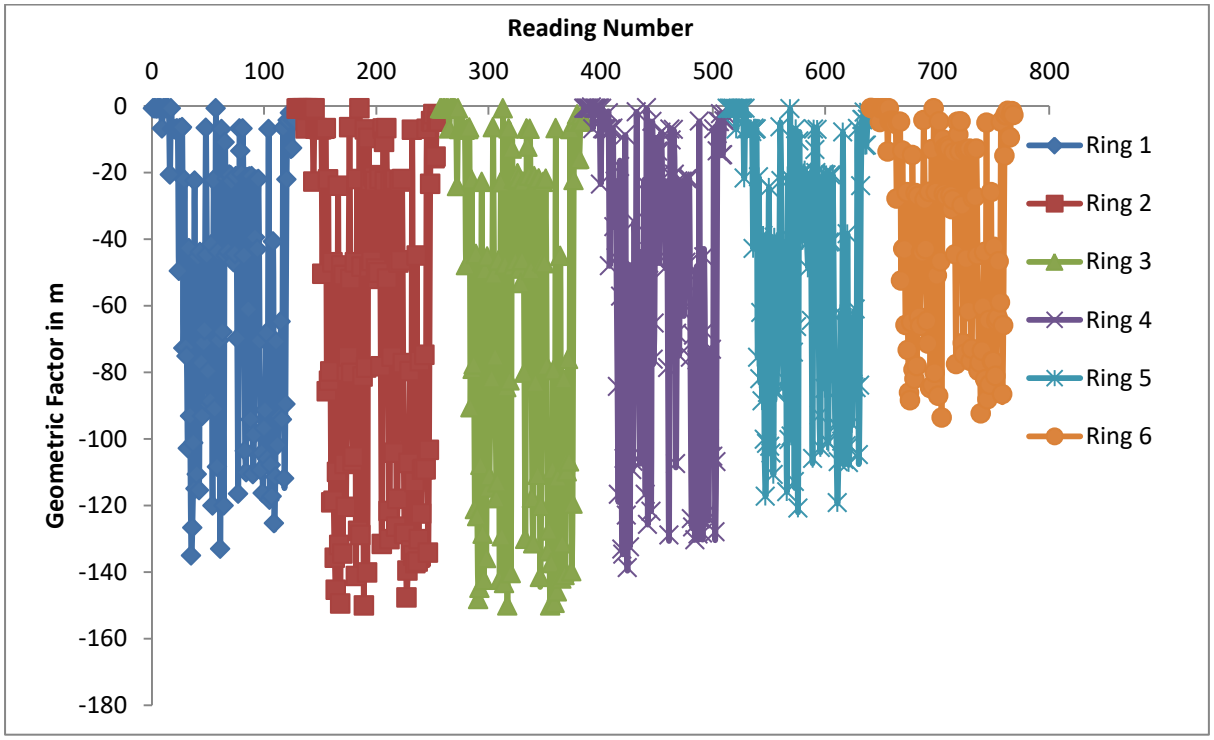

Figure 5.19: Experimental geometric factors of the six rings in Tank 1 for 768 readings

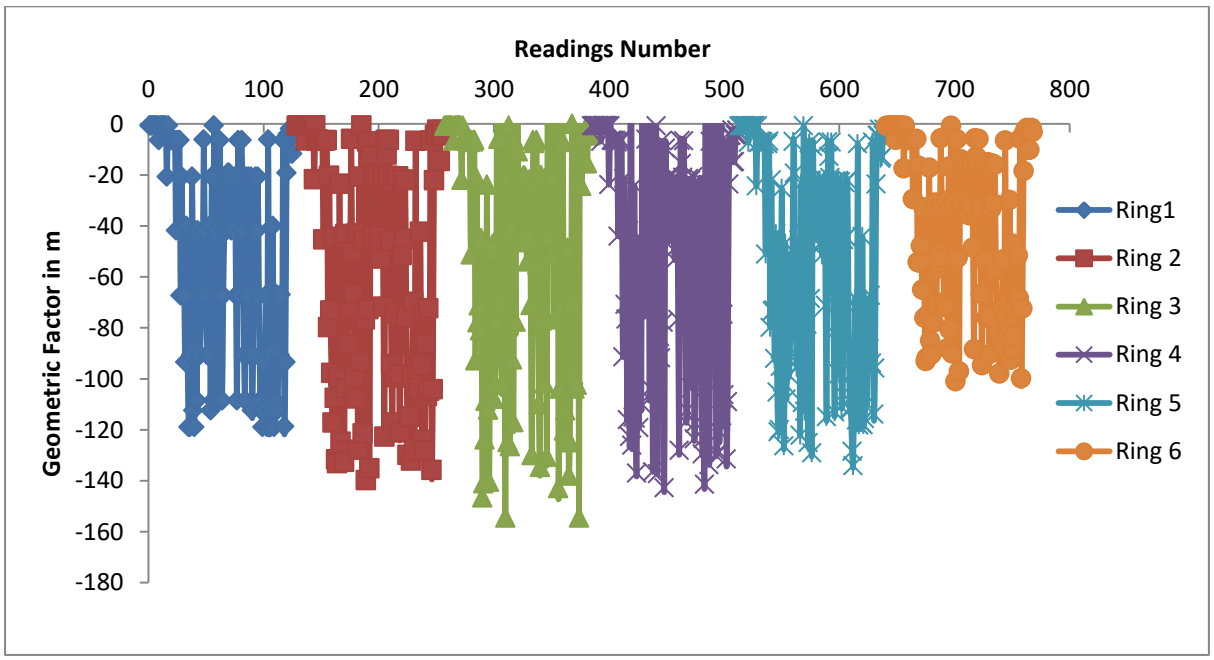

Figure 5.20: Experimental geometric factors of the six rings in Tank 2 for 768 readings

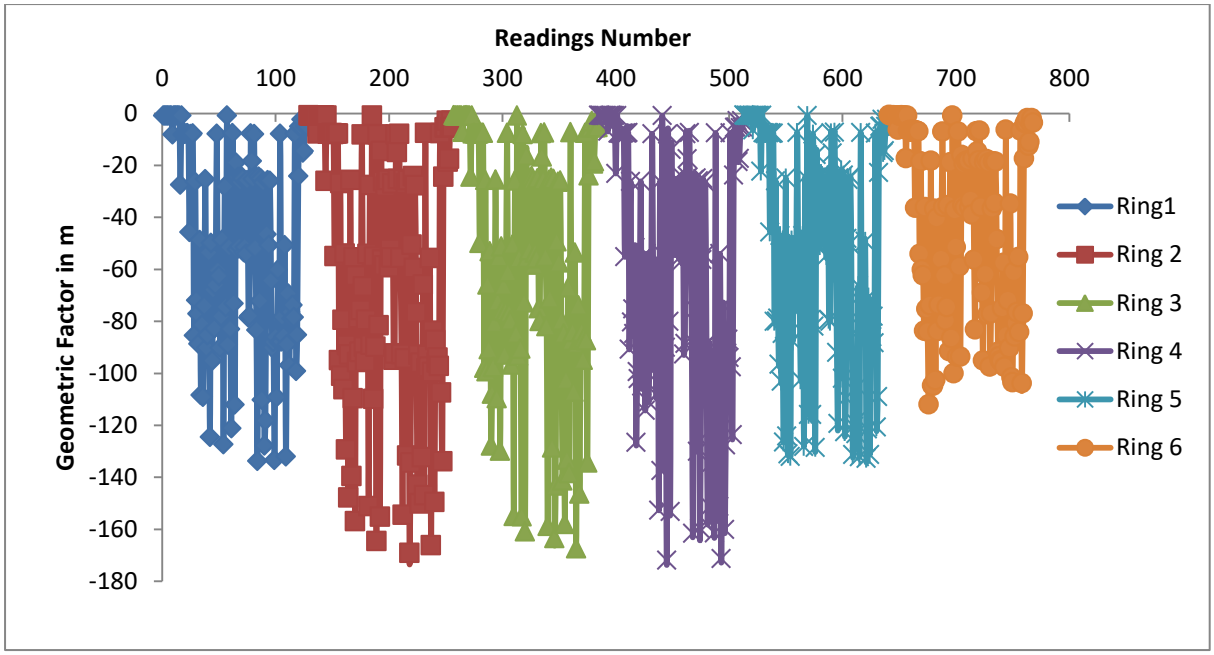

Figure 5.21: Experimental geometric factors of the six rings in Tank 3 for 768 readings

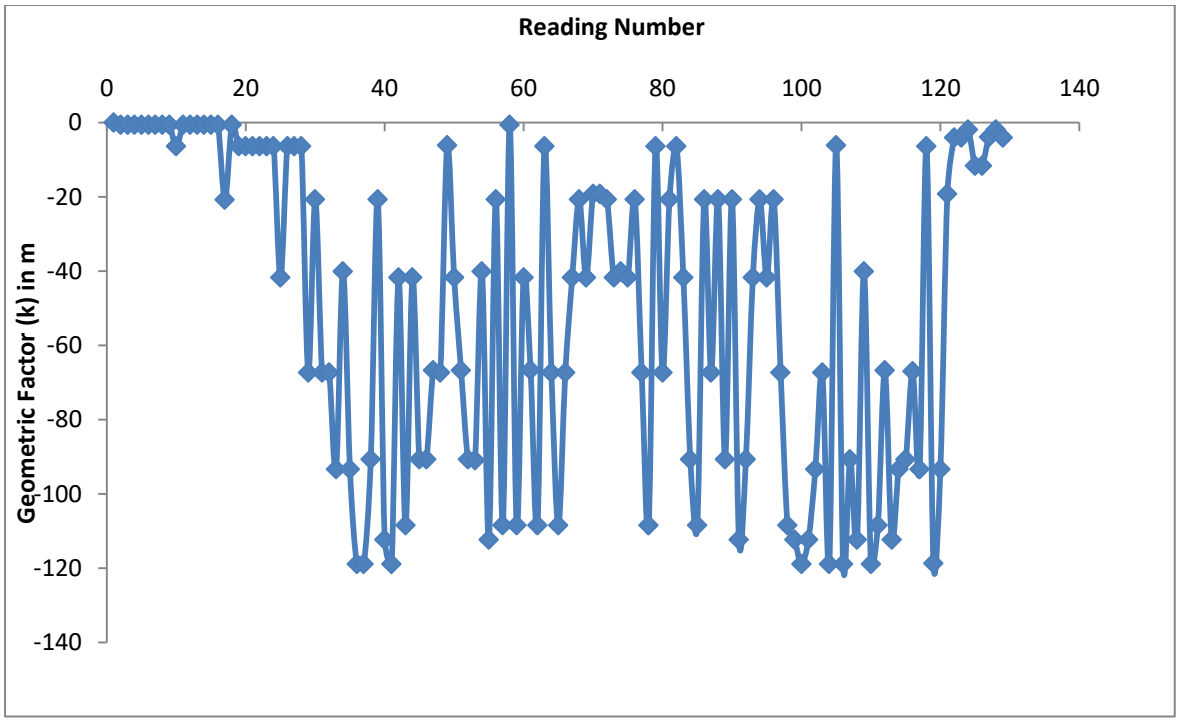

Figure 5.22: Typical geometric factors for one ring

5.10. Conductivity of Water to Introduce to the Test Soil

The following sections explain the procedure for choosing the proper conductivity of the water to be added to the test soil. The selection is based on two main criteria, the first is to gain a high resolution image of resistivity distribution, and the second is to get a good match with typical resistivity values for underground water in the field.

5.10.1. Identification of Water Resistivity Using a Calibrated Hanna Probe

Measurements for resistivity and conductivity were taken for different temperatures. The procedure was the same as for measuring the resistivity of the water in each tank using the calibrated Hanna meter and thermometer in Section 5.7.2, except that the volume of the water used this time was just 1 litre. The Hanna probe was calibrated with two reference solutions, HI 7031 and HI 7033. Figure 5.23 shows that the primary y-axis represents resistivity values in Ω.m, the secondary y-axis represents the conductivity of the water, and the x-axis represents the temperature of the water in degrees Celsuis. As observed from the collected data, it is obvious that the tap water used at this laboratory has a relatively high resistivity and low conductivity, although it requires a lower resistivity (higher conductivity) to ensure a clear inversion image and to accurately simulate the situation in the field. So, it was recommended that the value of resistivity was decreased to about 40 Ω.m, which improved the resolution of the image produced, but still lies within the range of the field resistivity, details discussed in Section 5.10.2.

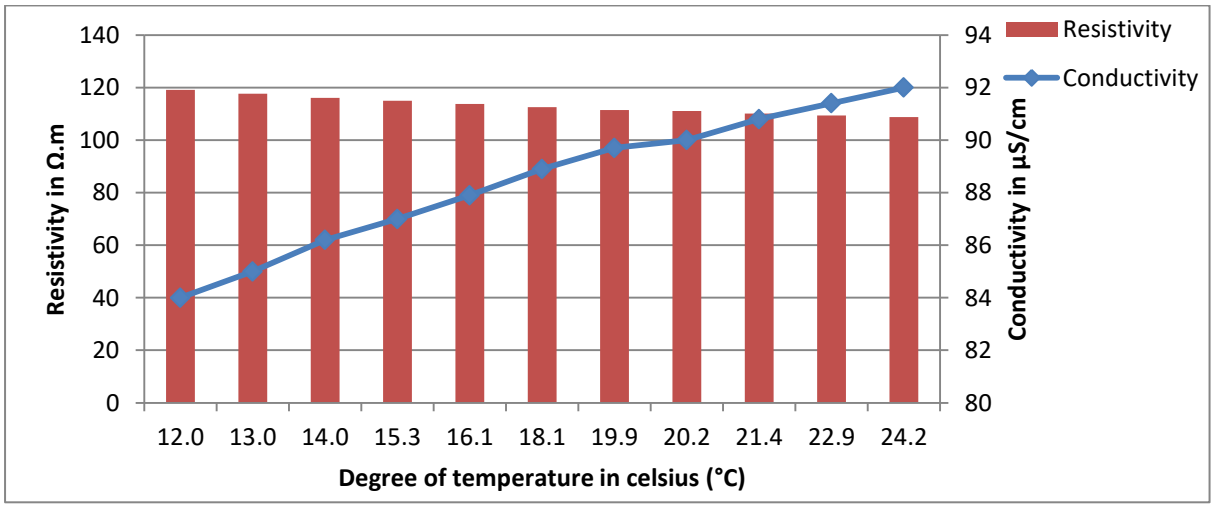

Figure 5.23: Resistivity and conductivity of tap water at different temperatures

5.10.2. Selecting an Appropriate Salt Concentration for the Required Conductivity

A range of different concentrations of NaCl salt (0.03 to 0.08 g/l) was added to the tap water and the effect on the water conductivity and resistivity was observed. The procedure included weighing an amount of NaCl salt and adding that amount to one litre of water. The salt was weighed using a sensitive balance; the balance used was the AG204, which is sensitive to 0.0001 g. Afterwards, the mixture of salt and water was mixed using a Fisherbrand electrical mixer, putting the magnetic stirrer bar inside the mixture container. Then, the calibrated Hanna probe and the thermometer were put into the water. Figs. 5.24 to 5.29 show the variations in conductivity and resistivity with respect to temperature for different concentrations of NaCl. Fig. 5.30 shows the full comparison of resistivity between those curves and the curve corresponding to tap water without additional salt.

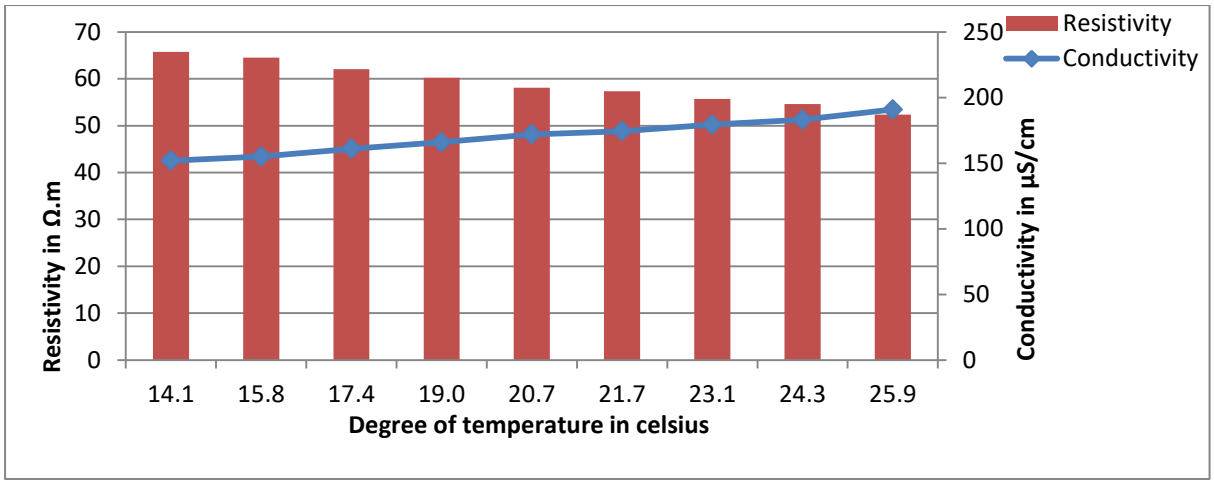

Figure 5.24: Resistivity and conductivity of tap water + 0.03 g NaCl at different temperatures

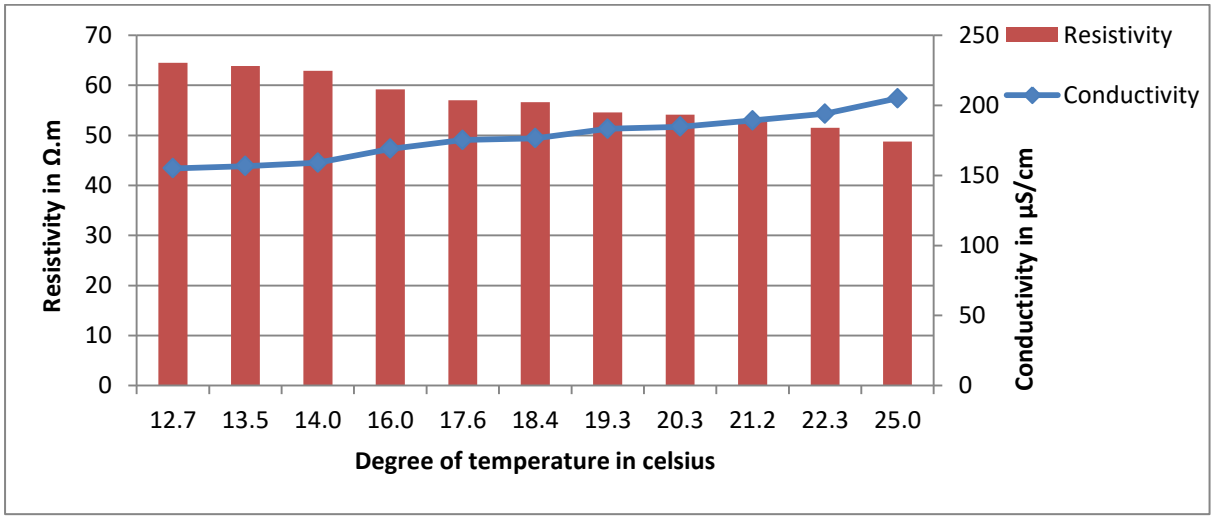

Figure 5.25: Resistivity and conductivity of tap water + 0.04 g NaCl at different temperatures

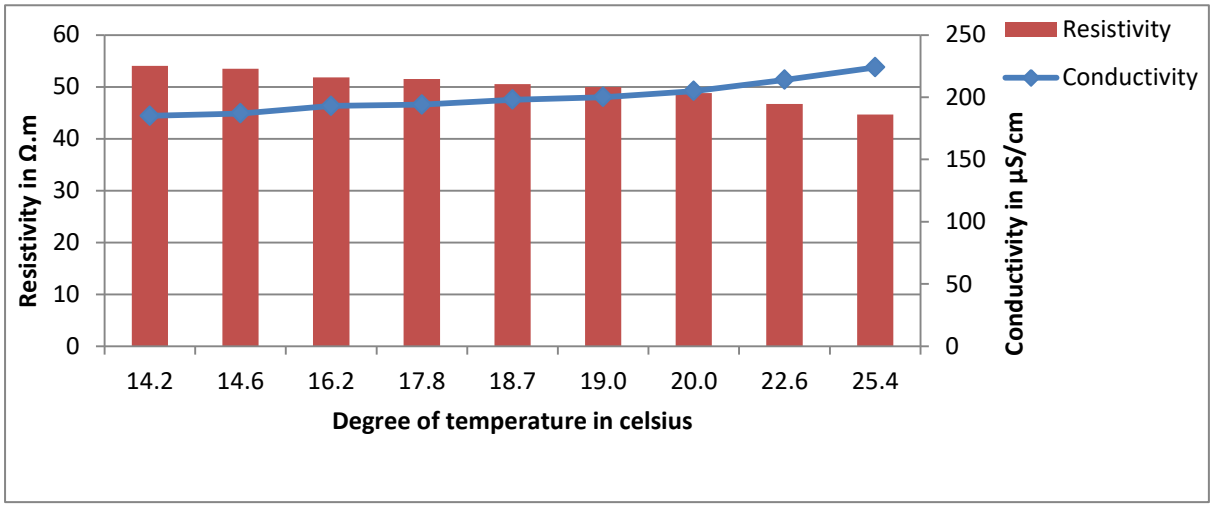

Figure 5.26: Resistivity and conductivity of tap water + 0.05 g NaCl at different temperatures

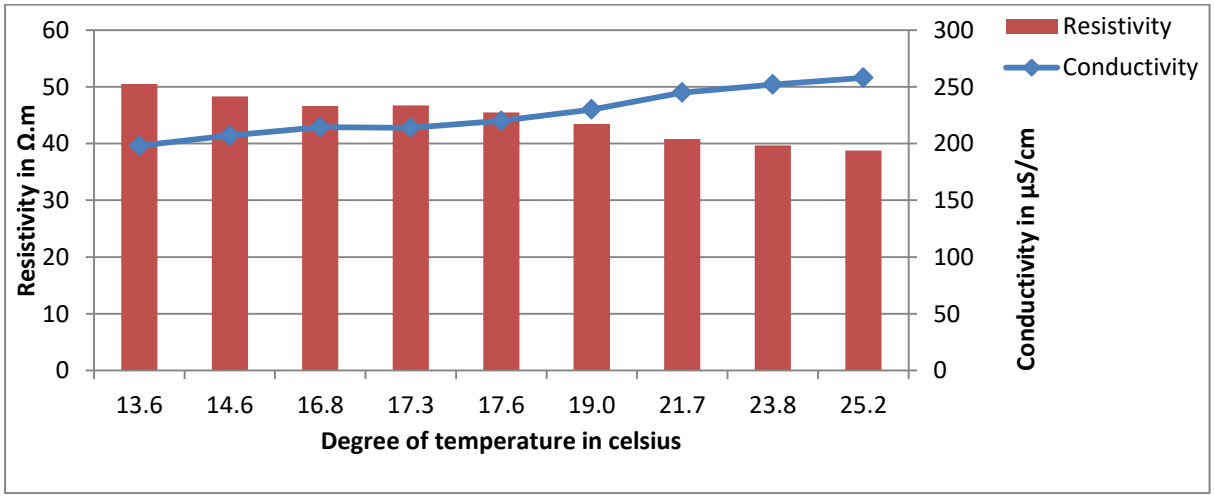

Figure 5.27: Resistivity and conductivity of tap water + 0.06 g NaCl at different temperatures

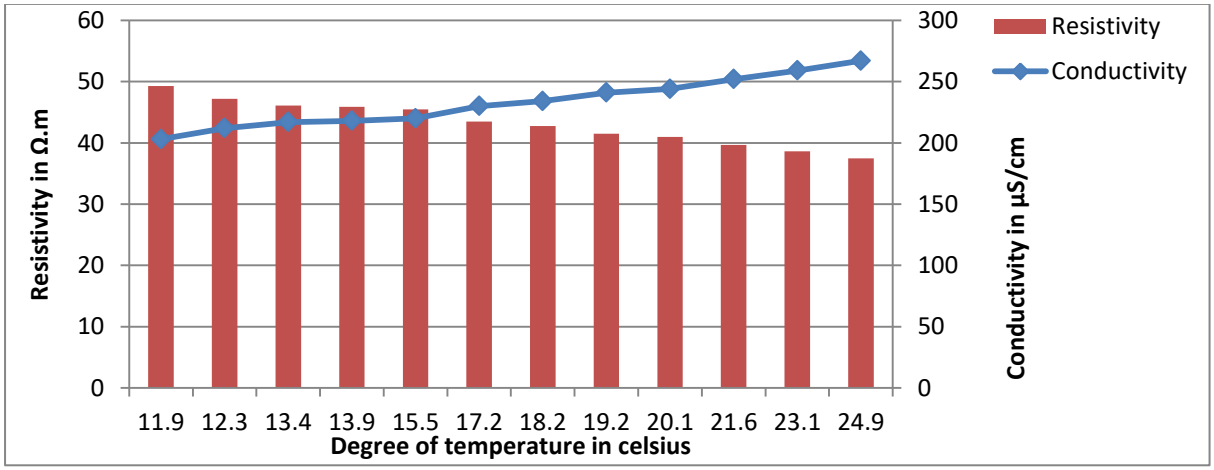

Figure 5.28: Resistivity and conductivity of tap water + 0.07 g NaCl at different temperatures

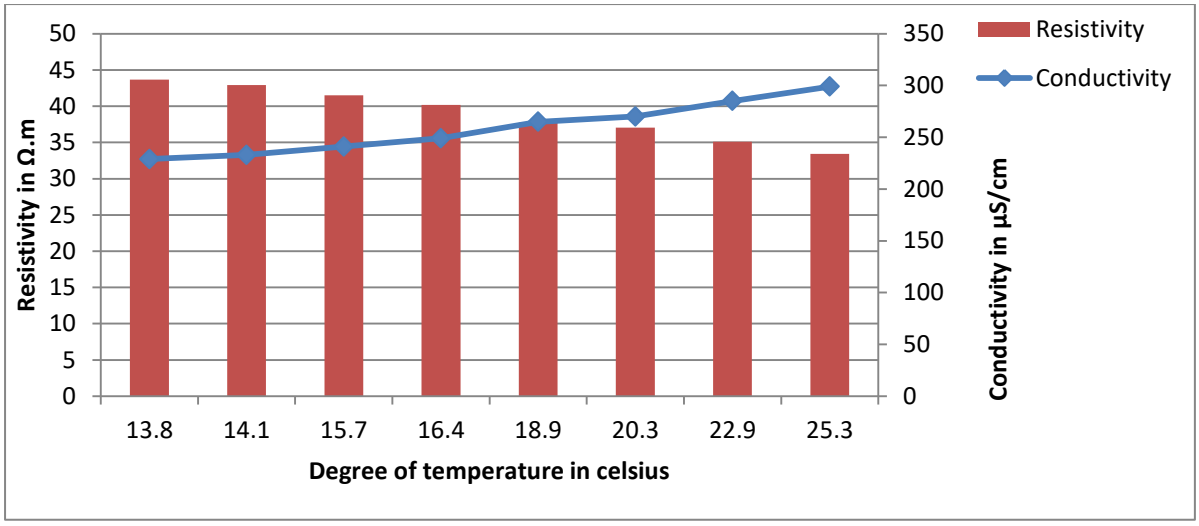

Figure 5.29: Resistivity and conductivity of tap water + 0.08 g NaCl at different temperatures

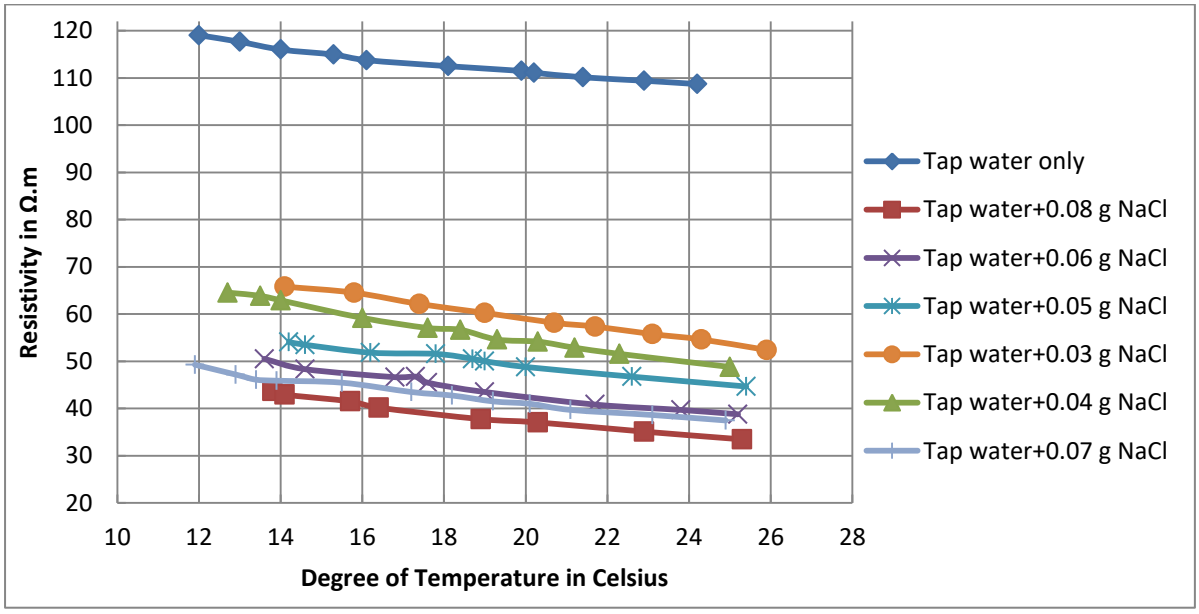

Figure 5.30: Changes in resistivity with respect to variations in temperature for different NaCl concentrations

5.10.3. Effect of Increasing the Conductivity of Tap Water on General Geotechnical Properties

To detect the effect of increasing the conductivity of the water and how that could affect the geotechnical properties of the soil, tests were performed to determine liquid limit, plastic limit, and collapse characteristics after adding 0.06, 0.05, and 0.04 g/l of NaCl to the water used to soak the sample. The plastic limit maintained at 22% as the same for samples without salt while little increase than 29.0 % (liquid limit of mixture without adding salt). The liquid limit values after adding 0.06, 0.05, and 0.04 g/L of NaCl were 29.7, 29.3, and 29.2

respectively. The collapse characteristics after adding the abovementioned salt concentrations were was consistent with those shown with no added salt, as shown in Fig. 5.31.

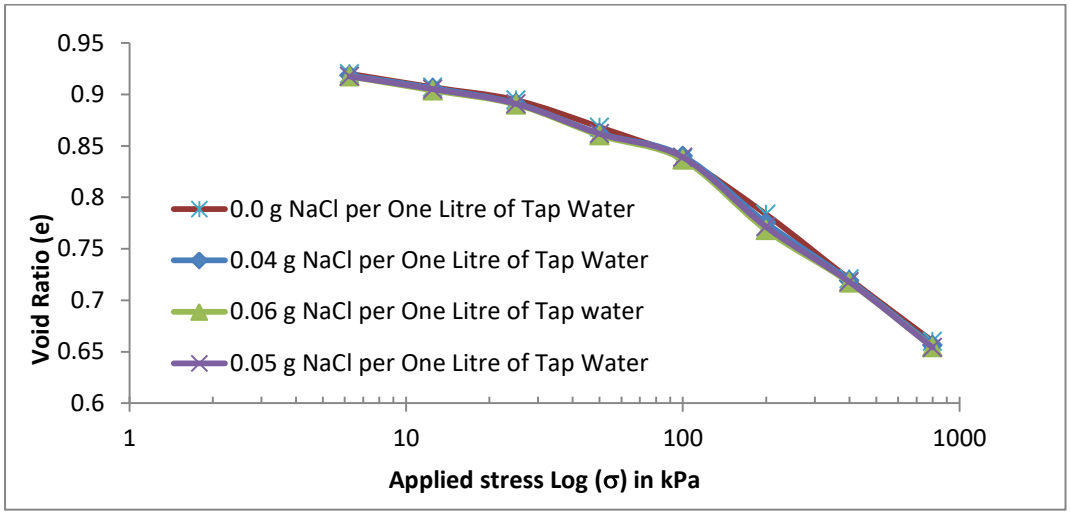

Figure 5.31: Collapse characteristics for different salt concentrations

5.11. Running the Loading Test while Taking Resistivity Measurements of the Tested Cells

The artificial collapse soil was compacted in the resistivity cells following the same procedure as for the normal cells without electrodes, described in Section 4.5. The columns were constructed at the middle of the tank, with and with encasement, following the processes described in Section 4.6 and Section 4.7. After topping the cells with a layer of sand, the cells were positioned inside the loading frame, while the hydraulic jacks were lowered into place. The load arm was applied centrally. Figure 5.32 shows some aspects of the experimental setup.

Before applying the first load increment, the cells are connected to the acquisition device in turn to check the homogeneity of the soil bed for each of the three cases: untreated soil, treaded with an ordinary stone column, and treated with an encased stone column. Starting with the first resistivity cell, the channel corresponding to a certain electrode ring was linked to the data acquisition unit. However, it was detected that there was no current through the soil and the sample behaved as a dielectric medium in a dry state; this could be as a result of the relatively high void ratio and low water content of the tested soil. Then, the conductive water (Tap water plus 0.06 g NaCl with resistivity 42 Ω.m , selected based on results in sections 5.10.2 and 5.10.3) was admitted to the samples of the three cells and dial gauges were fixed in their positions.

(a) Formation of the soil bed (b) Augering the column hole (c) Construction of untreated soil, OSC, and ESC

(d) Topping the test cells with the sand layer (e) Aligning the test cell centrally

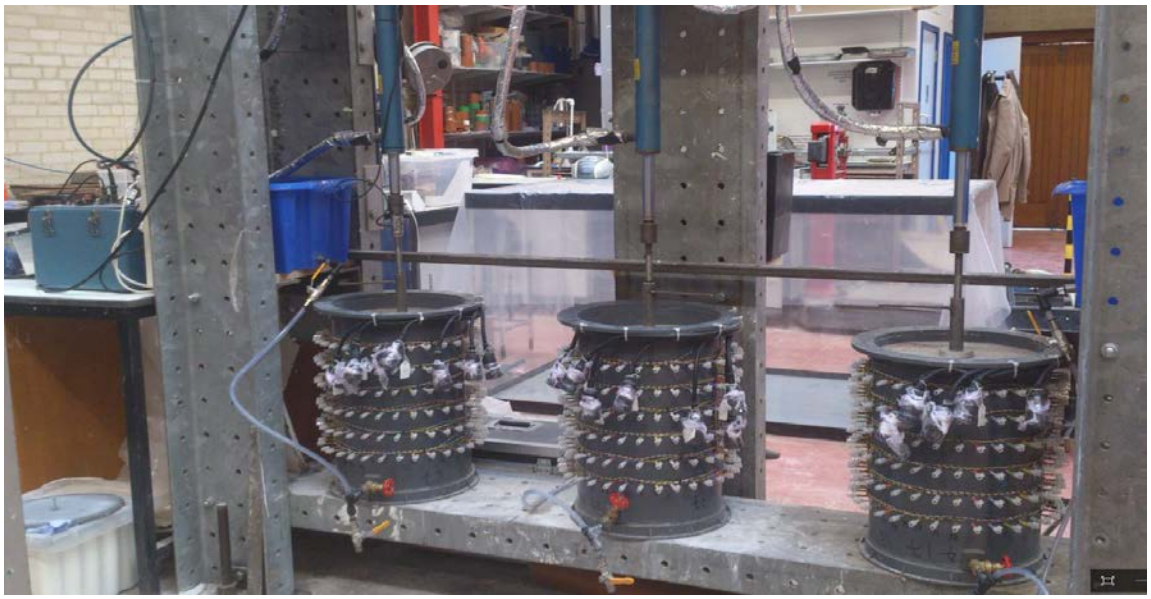

(f) The final setup of the three cells

Figure 5.32: Aspects of sample preparation for the resistivity cells

Figure 5.33 illustrates connecting one resistivity channel to the acquisition system, providing the experiment with a water source, and the setup of the dial gauges. The load was applied simultaneously to the three cells, while deformations were recorded in exactly the same procedure as followed for the normal test without electrodes, reported in Section 4.9. Thus, when a steady state of settlement was reached, the cells were connected to the acquisition system and readings taken for the three resistivity cells successively. Starting with first resistivity cell, the channel corresponding to a certain electrode ring was linked to the data acquisition unit and full apparent resistivity measurements were recorded; see Fig. 5.34. Complete measurements for one ring took approximately 55 minutes. Then, the data acquisition unit was connected to the next ring channel and measurements taken, and so on. Once resistivity measurements for the first test cell were completed, the readings for the second cell and then for the third cell were recorded. Then, loading was increased to next increment of load. Each increment was maintained until complete settlement was achieved and no more changes in physical conditions were expected. It is important here to consider that although ERT measurements could capture any time dependent changes in water content during the complete cycle of ERT measurement of each ring (during 55 minutes), it would do not influence the comparability of subsequent resistivity measurements, as they remain constant through time for each ring and taking measurements of the three tanks followed the same sequences and the comparison for each individual locations was assessed based on changing in load.

Figure 5.33: Providing the experiment with an inundation source and fixing the dial gauges in their positions

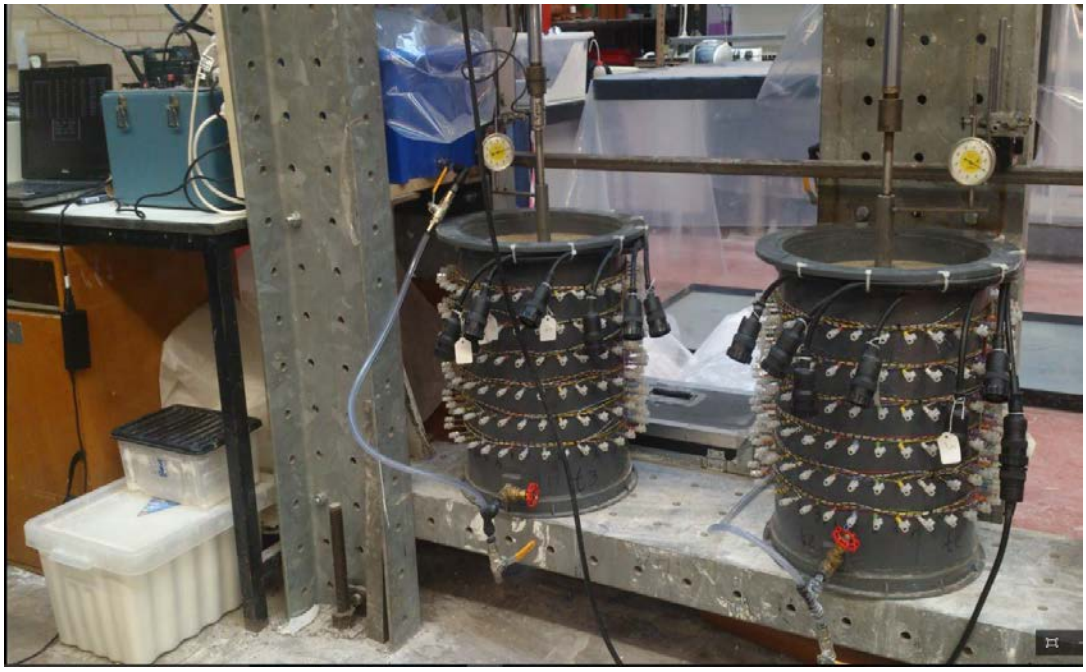

Figure 5.34: Connecting one ring to the acquisition system and taking resistivity measurements

5.12. Measurement Errors

Measured resistivity data are subject to error from different sources, such as instruments, polarisation, and poor electrode contact (Chambers et al., 2004). To avoid errors introduced by the instruments, the equipment in this study was tested and calibrated as described earlier in this chapter. Polarisation was prevented by choosing electrode spacing and using measurement scenarios to a avoid it. Poor electrode contact was checked regularly by the acquisition system and caution was taken to keep the electrodes as clean as possible during the preparation stages of the experiment.

In addition, errors resulting from two point measurements, which are common according to Heaney (2003), were avoided in this study through taking measurements from four points instead of two. Another source of errors could be as a result of the heating that accompanies the injection of current through the electrodes, so in the present system, the current was set to be very low to avoid such a heating effect.

The tests were repeated to obtain reliable measurements. Four readings were taken for each individual measurement and the corresponding calculated error percentages were included in the .dat file for the inversion procedure.

5.13. Summary

This chapter explained the concept of electric resistivity, some related studies, the design procedure of the resistivity cells used in the study, the selection of the conductive water used for inundation, and the calibration procedure. The geophysical survey (ERT) was begun prior to loading, after completing the construction of the ordinary and encased stone columns following the formation of the soil bed. The resistivity measurements, after integration with conventional geotechnical data, give a clear picture that ensures a fair comparison between untreated and soil treated with or without encasement. The aim is to understand the internal conditions of the hidden subsurface adequately and accurately, and understand how stress is distributed and moisture moves through the layers of the composite soil and stone column. Therefore, this can improve the assessment of the performance of the encased stone column inserted into metastable soil, as will be seen in Chapter Six.

CHAPTER SIX

RESULTS AND DISCUSSIONS

6.1. Introduction

In this chapter, the results and observations made during the testing procedure of the main experiments are presented. The outcomes are interpreted individually for two main series of tests: the first series associated with tests performed in the normal tanks without electrodes (the physical model) and the second series includes the results of the resistivity measurements. Data from both the conventional investigation and the geophysics survey are integrated and evaluated accordingly.

6.2. Results of the Physical Model

In the following sections, interpretations of twelve tests on the physical model with different soaking statuses and loading scenarios are discussed and compared with other published studies. However, the validation with the theoretical calculations will be presented in Chapter Seven, based on the analytical model presented in this study.

6.2.1. Tests 1, 2, and 3 (Dry State)

6.2.1.1. Aim of Tests and General Description (Dry State)

As described in Table 4-4, the aim of performing these tests was first to investigate the behaviour of the artificial collapsible untreated soil under loading in the absence of any source of inundation (Test 1) and then to find out the efficiency of using an ordinary stone column or a stone column encased with geotextiles in such dry conditions (Tests 2 and 3). The soil bed for these tests was formed by compacting each layer of soil with an initial water content of 12%, and leaving them for 48 hours afterwards for bonds to form, as described in Section 4.5.

6.2.1.2. Checking the Homogeneity of the Deposit (Dry state)

The homogeneity of the soil bed was checked by weighing, drying, and reweighing the extruded soil columns at the middle of the tanks in Tests 2 and 3. The outcomes showed a good level of consistency with those of the feasibility test in Section 4.12. Table 6-1 illustrates the values of water content and dry unit weight for the corresponding extruded samples.

Table 6-1: The homogeneity of the soil extruded from the middle of the tank for an ordinary stone column or encased stone column in Test 2 and Test 3, respectively (dry state)

Test No.	Bore hole No.	Location	Average water content %	Average dry unit weight in kN/m^3
Test 2	1	Centre of the test cell of the ordinary stone column	9.23	13.62
Test 3	2	Centre of the test cell of the encased stone column	9.27	13.79

6.2.1.3. Time-Settlement and Stress-Settlement Characteristics of the Foundation (Dry State)

Dial gauges with a travel limit of 50 mm, described in Section 4.4.3, were mounted to monitor the deflection of the foundation at the centre of each test tank. The load was gradually increased up to 800 kPa in doubled increments; each increment of load was maintained until no vertical movement was observed, as shown in Fig. 6.1. The load-settlement characteristics for the foundation rested on untreated soil, soil treated with an ordinary stone column OSC, and soil treated with an encased stone column ESC are demonstrated in Fig. 6.2. The load carrying capacity of the foundation, supported on untreated ground at a displacement of 7 mm (10% of the foundation diameter) in its natural state without soaking, was determined from the resultant curve. It showed a value of (740) kPa, which reflects a relatively stiff performance. Such behaviour was entirely expected and agreed with the results of the oedometer, see Chapter Three.

Under the final increment of load (800 kPa), both the OSC and ESC did not reach their settlement failure criteria, but it was observed that the ESC showed a remarked increase over the standard stone column in terms of a reduction in settlement, reaching a ratio of 230%, in comparison to only 150% for the OSC. The increase in bearing capacity of the encased stone column, in comparison to the ordinary stone column and untreated soil, was reported by many authors (for example Sivakumar, 2004).

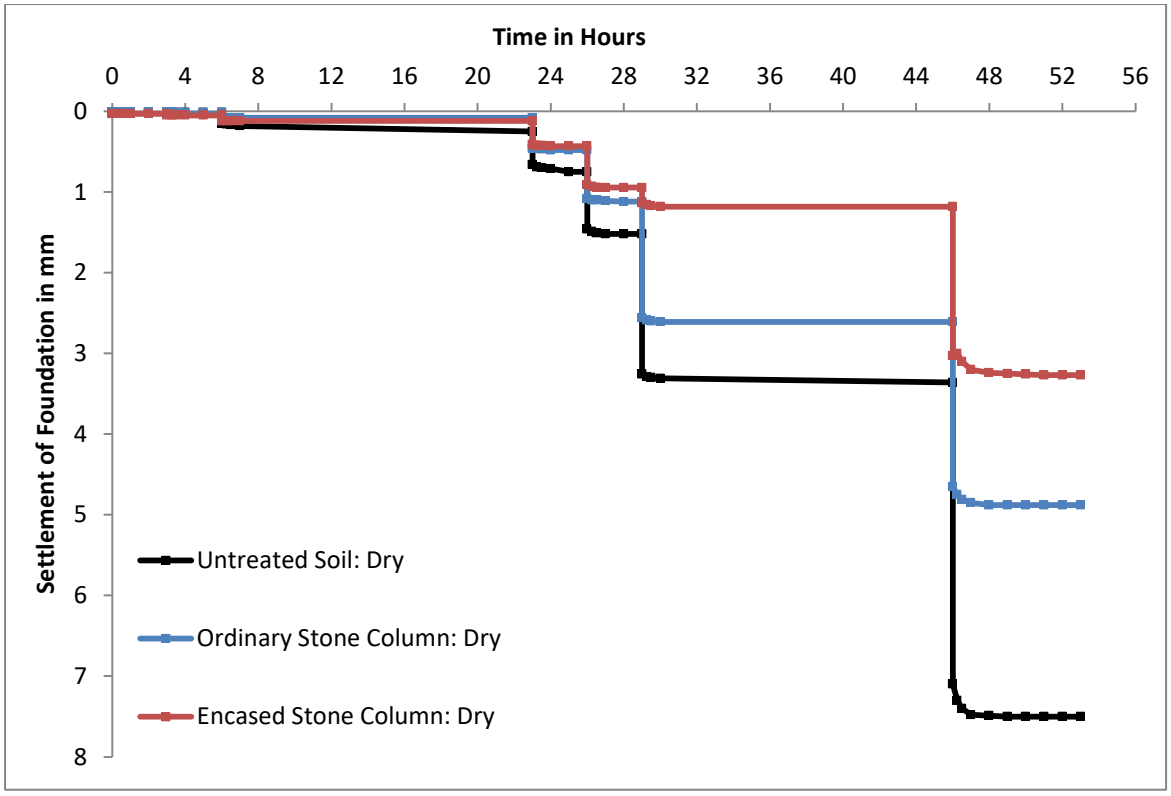

Figure 6.1: Time-Settlement curve of the foundation resting on untreated collapsible soil and treated with both ordinary and encased stone columns (dry state)

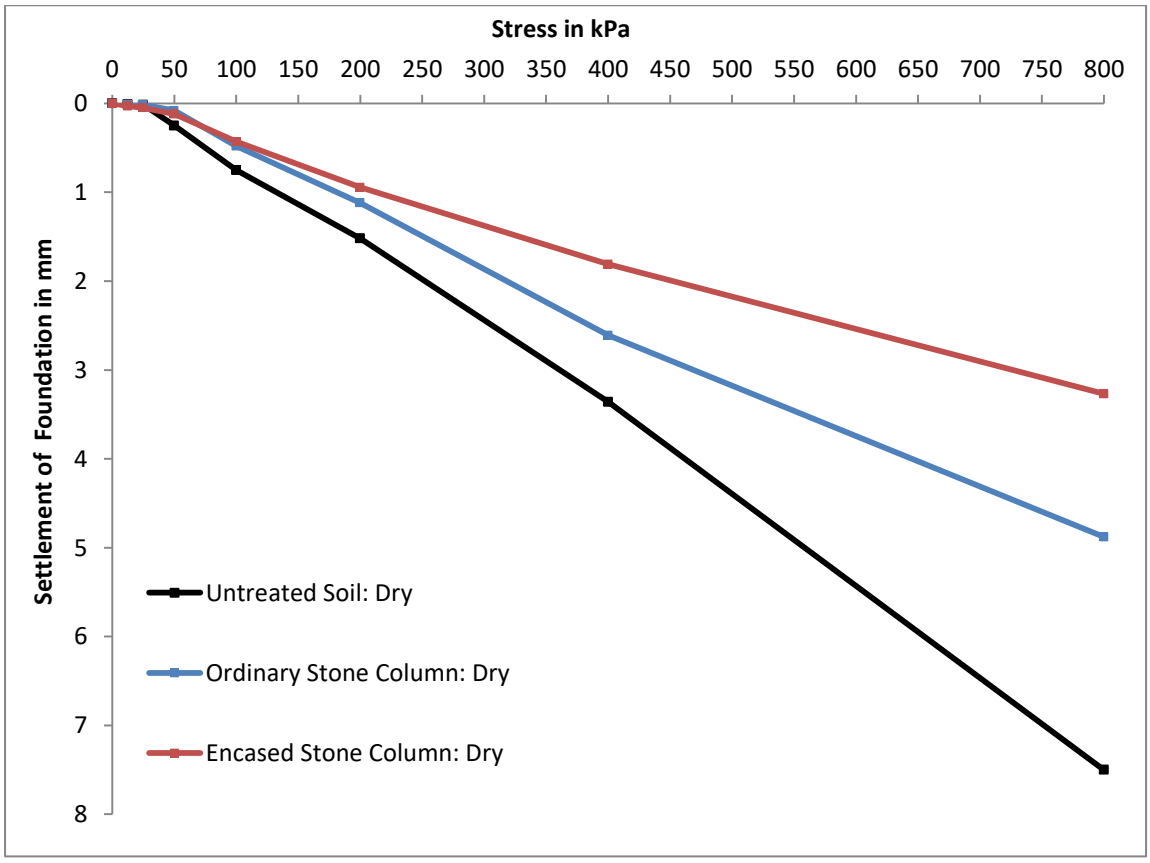

Figure 6.2: Stress-settlement curve of the foundation resting on untreated collapsible soil and treated with both ordinary and encased stone columns (dry state)

6.2.1.4. Deformation of the Soil Surface (Dry State)

Dial gauges with a travel limit of 20 mm, described in Section 4.4.3, were fixed on the soil surface at the approximate midpoint between the foundation and the side of the test tank on both sides of the foundation, in order to monitor the deformation of the neighbouring soil. Figure 6.3 shows the recorded deflection; it seems that the settlement of the soil surface at those points was relatively small in comparison to the total vertical deflection. The points next to the OSC recorded the biggest deflection. That could be as a result of the cracks that developed on the soil surface, which were relatively deep and clear in Test 2 (the test using the OSC), in comparison to Test 1 (the test using untreated soil only), as will be illustrated in Section 6.2.1.6. The observation points of the tank associated with encasement displayed the lowest readings, which confirmed the fact that stress concentrations increased on the stiffer encased stone column.

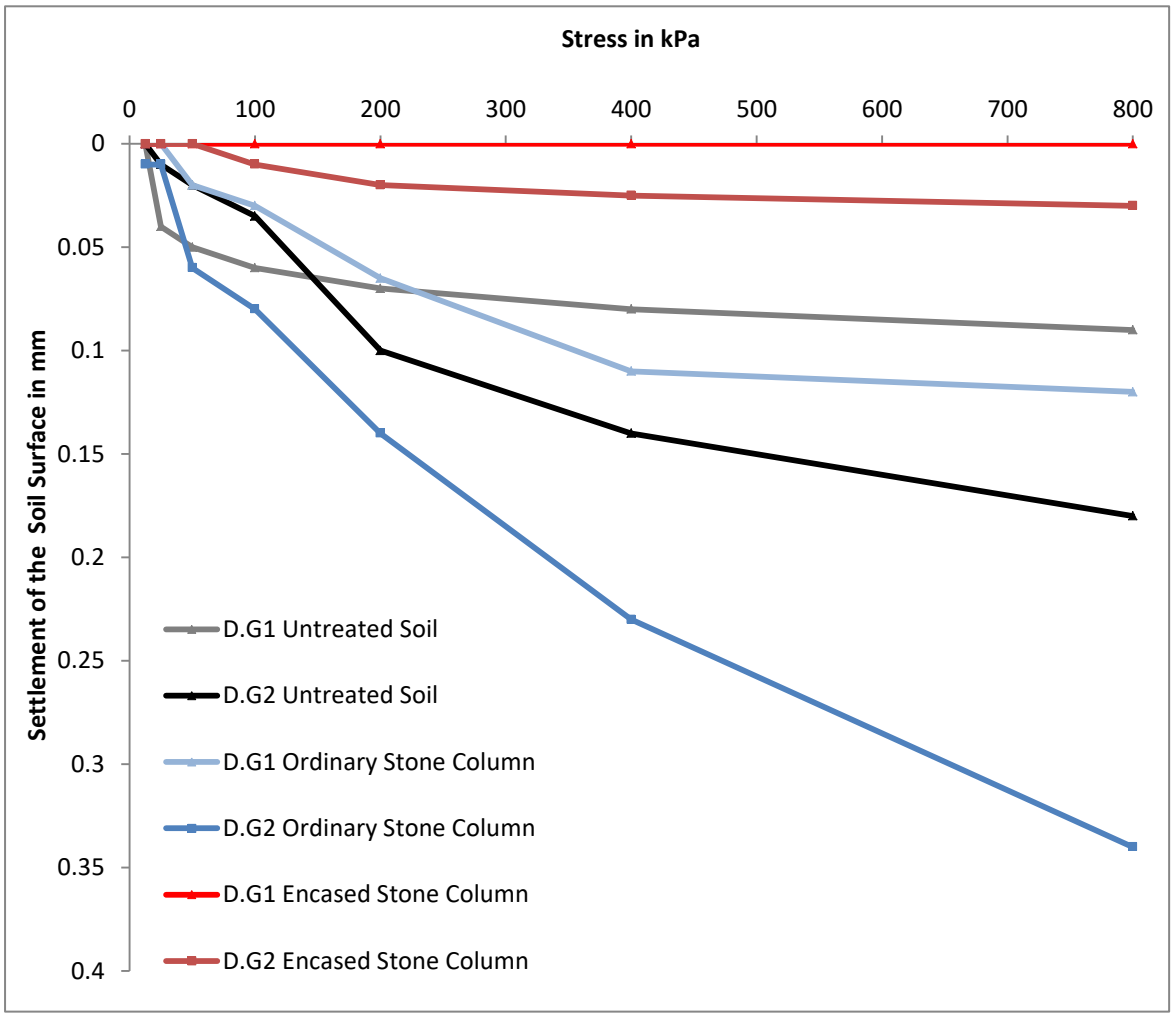

Figure 6.3: Collected readings of two dial gauges placed on left)D.G1) and right (D.G2) of the foundation, on the top soil surface, for untreated collapsible soil US, soil treated with OSC, and soil treated with ESC (dry state)

6.2.1.5. The Horizontal Deformation of the Tank (Dry State)

Sideways movement of the tank within the test chamber was observed by mounted horizontal dial gauges for the tests associated with stone columns (Tests 2 and 3). The deformation of the side of the tank was recorded while loading, as shown in Fig. 6.4. During Test 2, and under an applied stress of 50 kPa, the lateral displacement maintained a value of zero, but started to increase gradually afterwards, whereas lateral movement during Test 3 only started to record significant readings above zero under stress of 200 kPa. The maximum lateral displacement was reported at the final increment of loading (stress 800 kPa) for both ESC and OSC tanks, and reached values of 0.03mm and 0.04 mm respectively. That represents the resulting error that shows a variation from the assumption which considers lateral deformations in the soil at the boundary of the unit cell to be zero (according to the unit cell concept). However, those values are considered insignificant in comparison to the total recorded deflection of the tested soil and the possibility of noise occurring in the laboratory. No bulging of the sample occurred during either test, as will be discussed in Section 6.2.1.7.

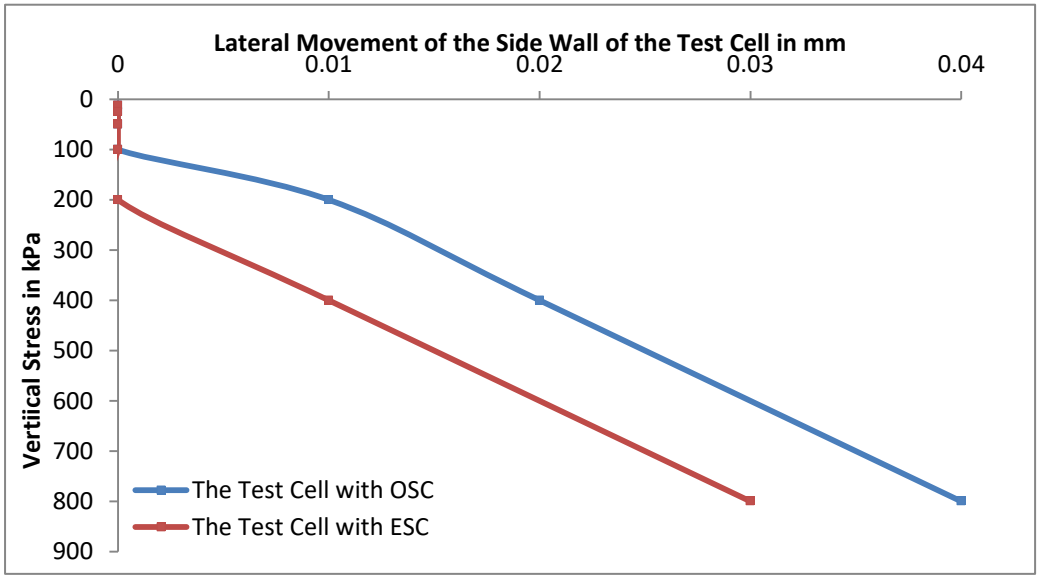

Figure 6.4: Lateral movement of the side wall of the test cells with respect to the vertical stress of the ordinary and encased stone columns (dry state)

6.2.1.6. Investigating the Soil Surface after Completing the Tests (Dry State)

At end of each test the sand layer on top was removed using a vacuum cleaner, in order to detect the failure mode of the surface in all three cells. It was noticed that the untreated soil indicated five radial cracks on the surface, while in the OSC cell, there were four cracks only. Although there were fewer cracks in the OSC tank than in that with the soil only, they were noticeably deeper. This may be a result of disturbance during the process of constructing the

stone columns. In the ESC tank, no cracks on the surface were observed, as it is believed the stress was concentrated on the encasement. Figure 6.5 demonstrates the cracks on the surface of the tested cells.

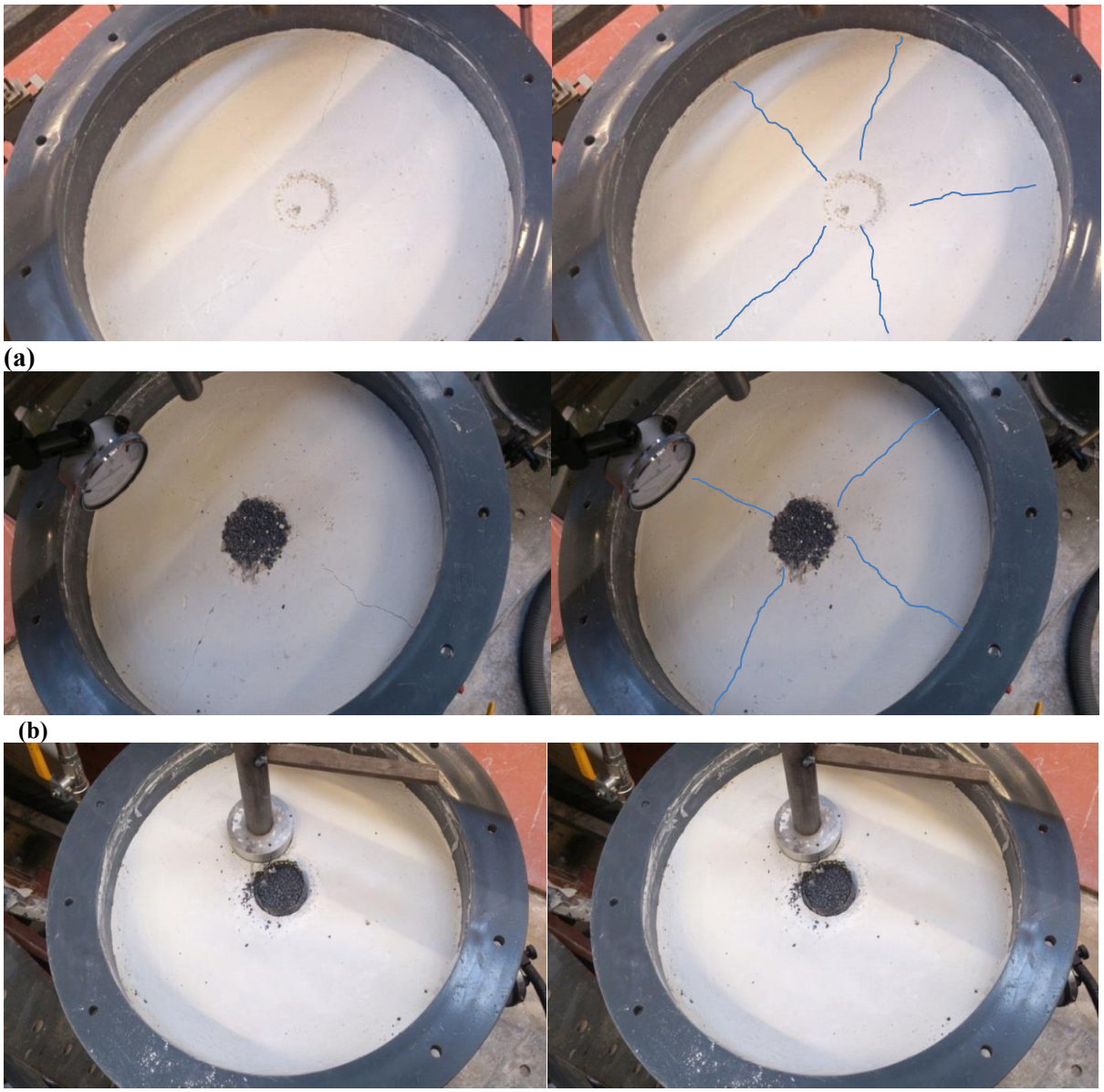

(a)

(b)

(c)

Figure 6.5: The mode of failure on the surface of the load cells (a) US, (b) OSC, (c) ESC, on left the original photo and on right the cracks are highlighted

6.2.1.7. Investigating the Failure Profile of the Column after Completing the Tests (Dry State)

Investigating the shape of bulging, following the procedure described in Section 4.11, showed that no bulging of the column was observed for both OSC and ESC. That may be due to the high stiffness of the host soil, which was enough to resist column expansion under loading. Also, no signs of damage were noticed on the geotextile itself or the stitching rods. Figure 6.6 shows the corresponding shape of the OSC and ESC after failure.

Figure 6.6: No bulging was observed for either OSC or ESC columns

6.2.2. Tests 4, 5, and 6 (Wetting the Test Cell with 2.73 L of Water: Wetting Prior to Loading)

6.2.2.1. Aim of Tests and General Description (Wetting with 2.73 L of Water)

The aim of these tests was to examine the behaviour of the untreated artificial meta-stable soil under loading and inundation with 2.73 L of water (Test 4) and then to discover the performance of using an OSC or ESC in such wetting conditions (Test 5 and Test 6). The soil bed for these tests was formed the same as for previous tests.

6.2.2.2. Checking the Homogeneity of the Host Ground (Wetting with 2.73 L of Water)

The homogeneity of the soil was checked through the extruded soil cores from the centres of the tanks for the OSC and ESC; they showed expected agreement with those of the pilot and previous main tests, described in Table 6-2.

Table 6-2: The homogeneity of the soil extruded to form the stone column or encased stone column for Test 5 and Test 6 (wetting with 2.73 L)

Test No.	Bore hole No.	Location	Average water content %	Average dry unit weight in kN/m^3
Test 5	1	Centre of the test cell of the stone column	9. 29	13.56
Test 6	2	Centre of the test cell of the encased stone column	9.35	13.67

6.2.2.3. Admitting Water (Wetting with 2.73 L of Water)

The wetting included soaking the soil in the tested cells with water before any load increment was mounted. The 2.73 L of water, in addition to the water required to fill the drainage lines and the filter layer, as described in Section 4.10, were admitted to each individual tank from the corresponding reservoir through the tube. The time required for all the water to penetrate into the soil was mentioned in Table 4-5 in Chapter Four. Then the inundated cells were left until the next day to complete the wetting process.

6.2.2.4. Time-Settlement and Stress-Settlement Characteristics of the Foundation (Wetting with 2.73 l of Water)

The dial gauges mounted on each foundation were observed and the corresponding data were collected. The foundation reached a value of 0.14mm from wetting when it was rested on soil only, while it recorded values of 0.04 mm and 0.05 mm when using the OSC and ESC, respectively. After wetting, the loads were added to the three cells at the same time, up to 800 kPa as in the previous tests. Each increment of load was maintained until no vertical movement was observed, as shown in Fig. 6.7.

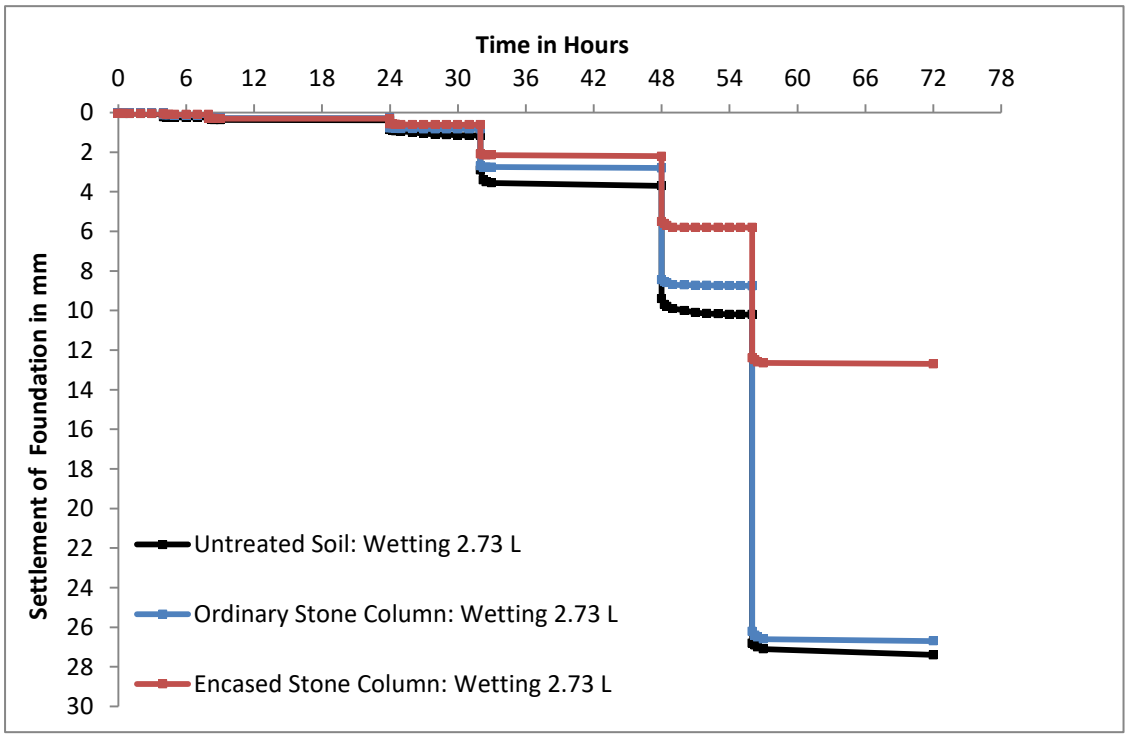

Figure 6.7: Time-settlement curve (wetting with 2.7 L)

The untreated soil was very sensitive to the change of water content, and this is expected as a result to the low plasticity index (Assallay, 1998).The behaviour of the OSC was very close

to that of the untreated soil and no significant improvement was observed, as both exhibited the convergence settlement during the loading stages. Figures 6.8 and 6.9 show the OSC and the untreated soil under stresses of 400 and 800 kPa respectively. The installed column clearly lost the required confinement from the host collapsed soil, as stated by Ayadat (1990) and Ayadat et al. (2008).

Also, the result indicates a good agreement with the advice given by Sivakumar (2010) that use of granular columns in compacted collapse fill upon inundation should be treated with caution. The authors reported that the improvement due to the use of a stone column was not significant in such fills unless mixing the column material with a small amount of cement. The encased stone column was affected by the shear strength of the surrounding soil, which was lower in the case of soaking with 2.73 L than in a dry state, the same observations as found by Das & Pal (2013).

Figure 6.8 : Untreated soil (on right) and OSC (on left) under stress of 400kPa

Figure 6.9: Untreated soil (on right) and OSC (on left) under stress of 800 kPa

However, the ESC showed a good performance and a significant decrease in settlement; see Fig. 6.10 and Fig. 6.11. That was in agreement with previous work done with encasement in

collapsible soil e.g. Ayadat & Hanna (2005) and Araujo et al. (2009). In comparison to the previous, the reason for the improvement is explained by Black et al. (2007), who stated that an encapsulated granular column functioned adequately, as bulging of the column is restricted as a result of the further restraint delivered by the encasement.

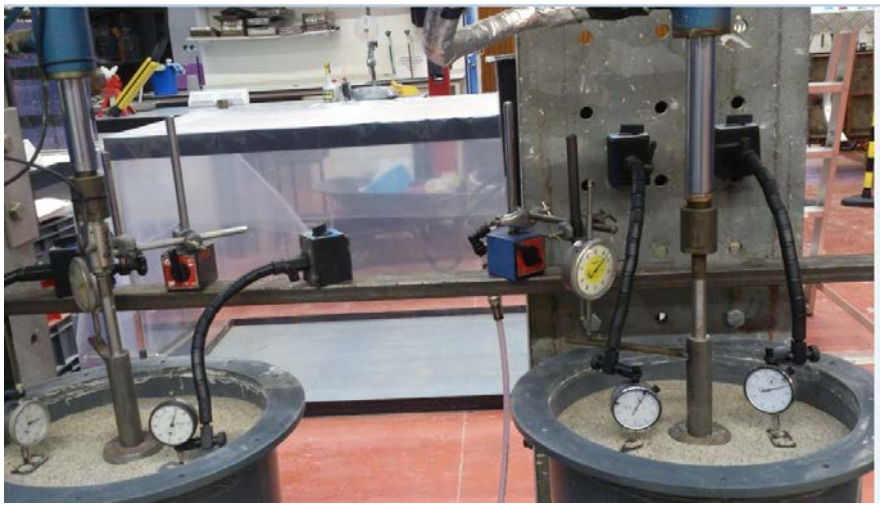

Figure 6.10: OSC (on right) and ESC (on left) under stress of 400 kPa

Figure 6.11: OSC (on right) and ESC (on left) under stress of 800 kPa

The stress-deformation curves of the foundation resting on untreated artificial loess soil, treated with an OSC, and treated with an ESC are demonstrated in Fig. 6.12. The outcomes showed that the maximum bearing capacity of the untreated soil and the OSC, corresponding at strain equals to 10% of the foundation diameter, is almost convergence at approximately 308 kPa and 350 kPa respectively, which means that there is no significant improvement when treating the soil with the ordinary stone column. However, encasing the stone column with geotextile indicated a maximum bearing capacity of approximately 460 kPa. Based on

that, the ESC provides an extra improvement with the ratio of 49% over the soil, while the improvement over soil by using OSC was just 14%.

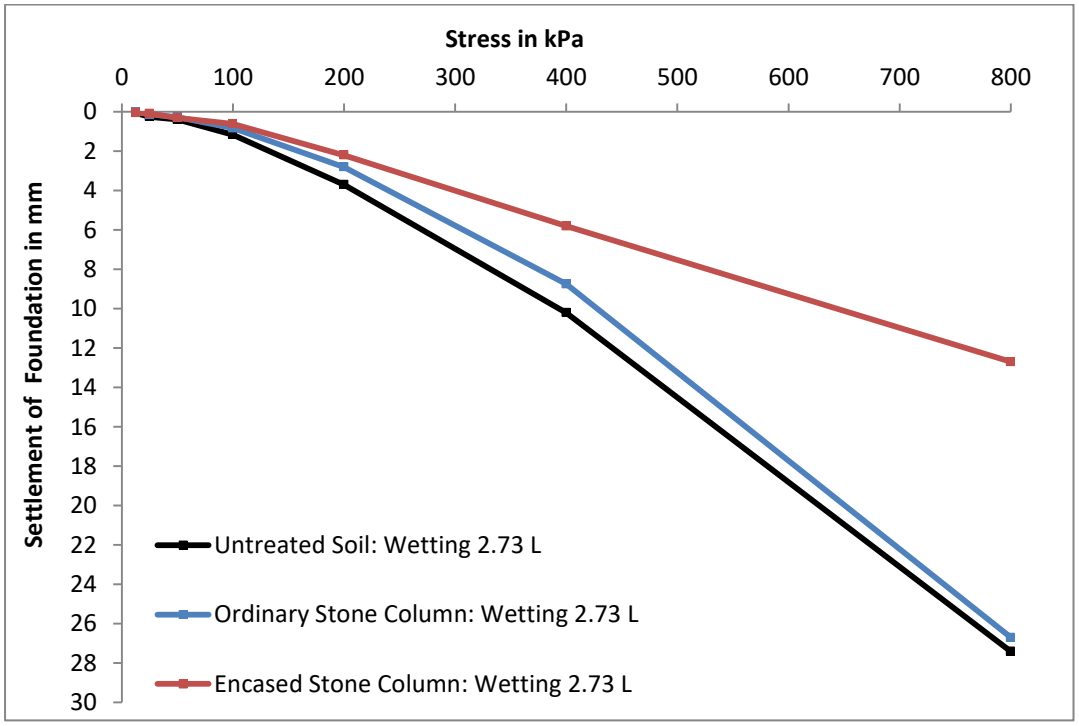

Figure 6.12: The stress-settlement curve of the foundation resting on untreated collapsible soil and treated with both OSC and ESC (wetting with 2.73 L)

The settlement corresponding to 800 kPa for untreated soil, OSC, and ESC was 27.4, 26.7, and 12.7 mm respectively, which reflects the high compressibility of the soil induced upon collapse. The settlement improvement factor (settlement of soil without treatment to settlement with treatment) at a stress of 800 kPa under soaking conditions with 2.73 L of water gave percentages of 216% for ESC, while it was only 103% for OSC.

6.2.2.5. Deformation of the Soil Surface (Wetting with 2.73 L of Water)

Figure 6.13 shows the deflection of the soil surface at points on the left and right of the middle, between the foundation and the boundary of the test tank. This showed that the settlement of the soil surface at those points recorded bigger values than that observed in previous tests, as a result of the presence of the water and resulting collapse. Variations in settlement for gauges on similar positions on both sides of the foundation (D.G1 and D.G2) for the tank that contained untreated soil showed a slight difference, which is expected as a result of the development of cracks, as will be seen in Section 6.2.2.7. The deflection of points next to the ordinary stone column recorded the biggest deflection of all observation points, which could be as a consequence of the bulging of the column. However, they showed

convergence values on both sides of the tank, which could show that the bulging was axisymmetric. Similar behaviour was observed when a single stone column was placed at the centre of the loading plate by Ghazavi & Afshar (2013). The smallest values were recorded for the gauges of the chamber associated with the ESC, which reflected the reduction in impact on the area around the column.

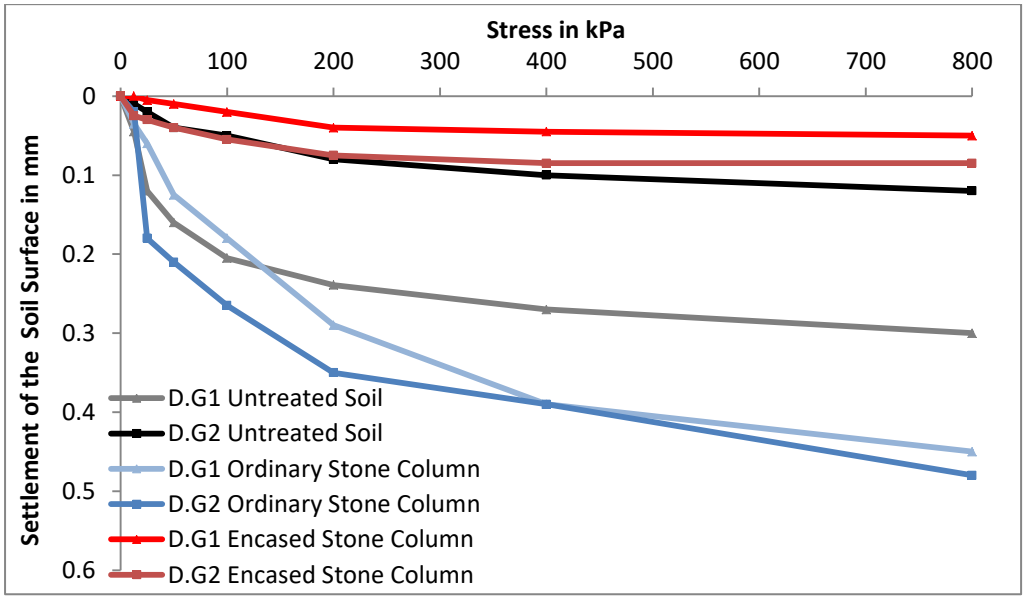

Figure 6.13: The collected readings of two dial gauges placed on left D.G1 and right D.G2 of the foundation, for untreated collapsible soil US, treated with OSC, and treated with ESC (wetting with 2.73 L of water)

6.2.2.6. Deformation of the Tank (Wetting with 2.73 L of Water)

Lateral movement showed no significant changes in readings in comparison to the previous tests during the progress of loading (maximum variation of 0.01 mm); this could reflect the rigidity of the tank and the applicability of avoiding the boundary effect. See Fig. 6.14.

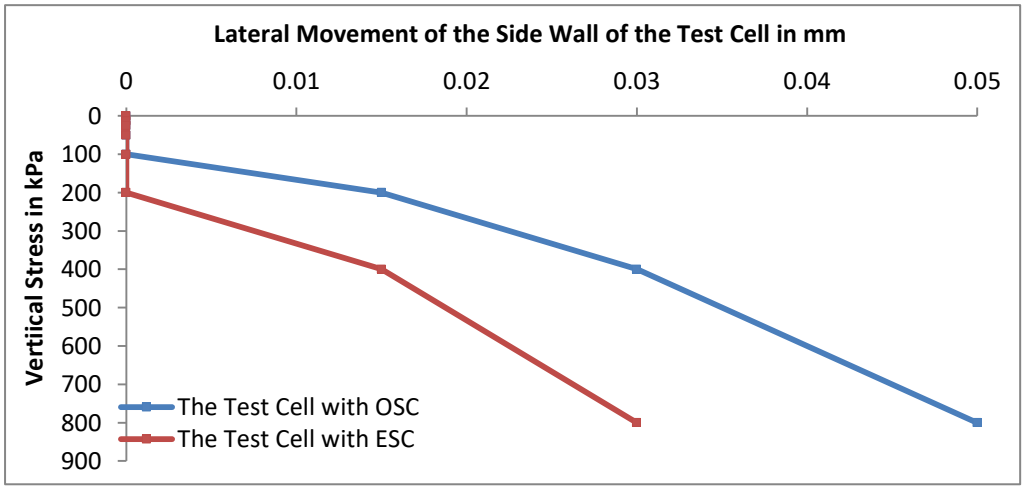

Figure 6.14: Lateral movement of the side wall of the test cell with respect to the vertical stress of the ordinary and encased stone columns (wetting with 2.73 L)

6.2.2.7. Investigating the Soil Surface after Completing the Tests (Wetting with 2.73 L of Water)

At the end of the three tests, the sand coats on the surfaces of the three chambers were detached in exactly the same way as done for previous tests, in order to see whether there were any fissures or cracks. It was noticed that the untreated soil (Test 5) indicated circular cracks, instead of the radial ones observed in the previous similar test (Test 2). Figures 6.15 and 6.16 show the status of the soil surface before and after removing the footing for the tank of the untreated ground. In the tank filled with soil and the OSC, there were only very fine cracks, as shown in Fig. 6.17. In the ESC tank, no cracks on the surface were detected, as it was believed the stress concentrated on the encasement, not on the soil.

Figure 6.15: cracks observed after completion of loading on untreated soil US and before removing the foundation, on left the original photo and on right the cracks are highlighted

Figure 6.16: Cracks observed after completion of loading on untreated soil US and removing the foundation and sand layer, on left the original photo and on right the cracks are highlighted

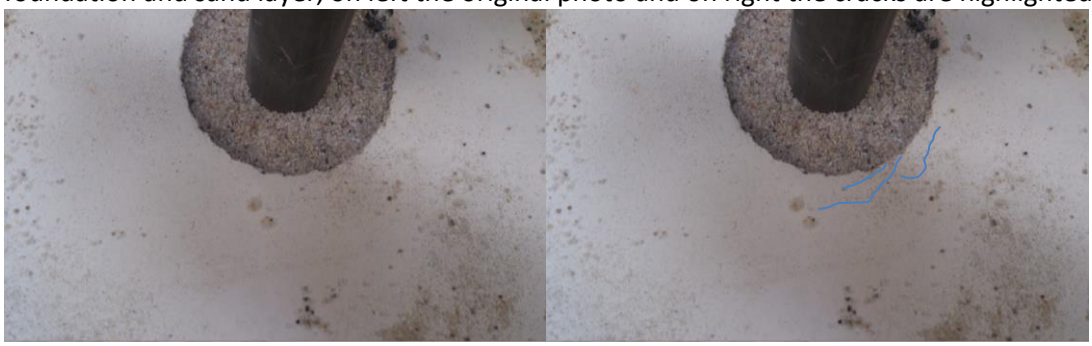

Figure 6.17: Very fine cracks around the foundation resting on the OSC, on left the original photo and on right the cracks are highlighted

6.2.2.8. Investigating the Water Profile after Completing the Tests (Wetting with 2.73 L of Water)

After the three tests were completed, the water content in the deposits was measured. Three samples were taken from each layer of 90 mm mid-way between the tank boundary and the footing plate at depths starting from the soil surface down to the tank base. The full profiles are shown in Fig. 6.18. It was observed that the values of water content in the deposit were bigger than the initial water content value of 9.1%. The water content increased with depth, from 13.9% at the top to 22.3% at the bottom. It is clear that although the amount of water added was small, the water rose through the whole depth of the soil, which reflects the capillary action of this particular soil. The capillary rise was related to the soil texture by Kuo (2014), and according to the values presented, silty soil, depending on its particle size, could reach a capillary height of 105.5-200.0 cm, which is higher than the height of the test cell. If the deposit of the untreated soil in term of saturation degree is traced, it is found that this water profile will give an average degree of saturation for the total deposit equal to 49.9%, while in theory, and as mentioned in Appendix (C) in Chapter Four, the value of saturation should be 40 % only. So this raises a question about the difference in the degree of saturation, but according to Miller (2002), an air gap usually occurred in all her similar tests, extending to the first third of the gravel layer. Because the test tanks were not transparent, this layer could not be seen; however, after the soil layers were completely removed, the level of water in the gravel layer decreased to settle down to the second lower half at the tank base. So if the increase of saturation is calculated by adding a third of the quantity of water that usually fills the gravel layer (3.57 L/3) as all the water added to the soil, that will give an extra degree of saturation which equals 7.15. So, if we add this to the theoretical value, the total degree of saturation will be 47.2% which is close to the measured value (49.9%). The important note here is that the water content at the base was not fully saturated, because the aforementioned air gap created free draining of the water within the soil particle layer at the bottom of the base, which means it will not reach saturation, as interpreted by Miller (2002). It was noted that the average degree of saturation of the soil surrounding the OSC was 50.7%, which is more than that without treatment, probably because of the radial movement from the column toward the soil subsurface, as was observed in the pilot test. Also, the soil treated with the encased stone column showed a higher average degree of saturation, 52.2%, which was due to the effect of the impermeable layer placed at the base of the ESC.

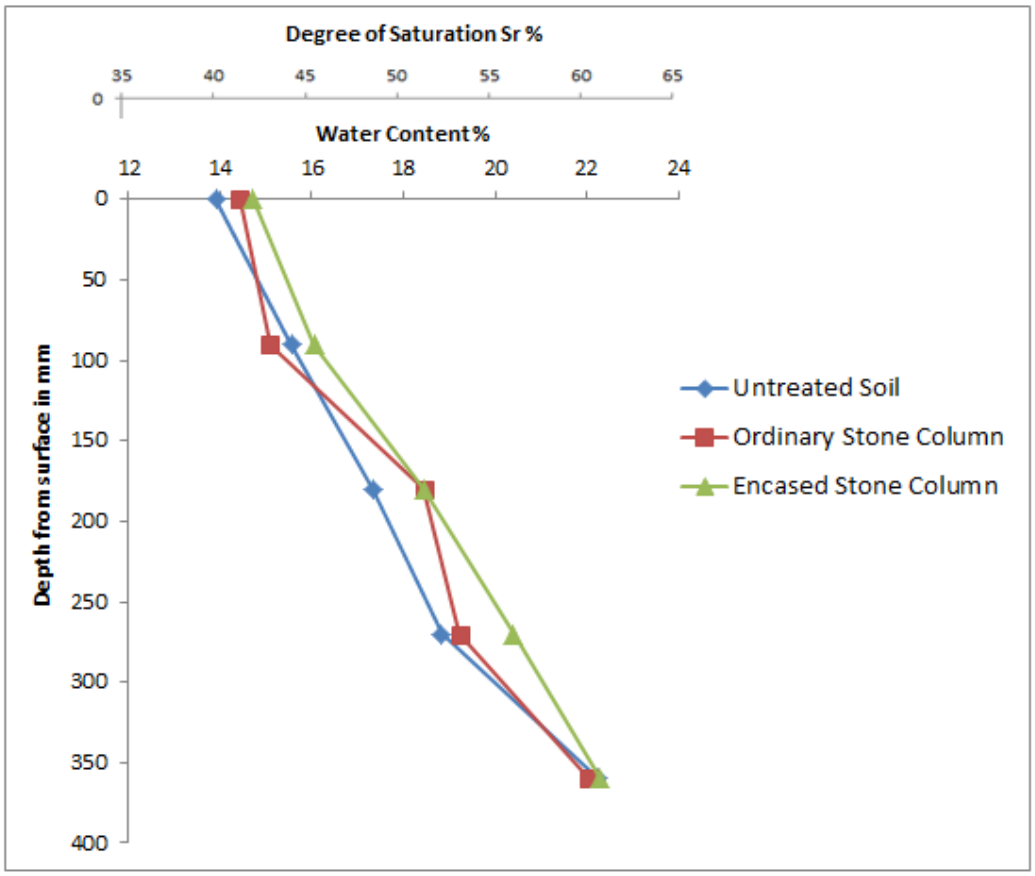

Figure 6.18: The change in water content after completing the test (initial wc=9.1%)

6.2.2.9. Investigating the Failure Profile of the Column after Completing the Tests (Wetting with 2.73 L of Water)

The failure profiles of the stone columns for those experiments series are shown in Fig. 6.19.The images indicated that the unreinforced columns bulged laterally into the upper layers. The maximum bulging showed an increase in column diameter of 15.7 mm. It is interesting to note that the obvious lateral bulging was contained within 120 mm length (the column length equals three times the diameter of the column), which was expected and lies within the range of 3-4 times the column diameter given by Hughes & Withers (1974), Black et al. (2007), and many other investigators.

The encased stone column showed a relatively consistent diameter over the entire length, due to the additional confinement provided by the generation of hoop stress by the mesh sleeve in a manner that agreed with work done by Black et al. (2007). Upon removal of the encased stone columns from the soil bed, no damage to the geotextile or the wires of the stitching was observed.

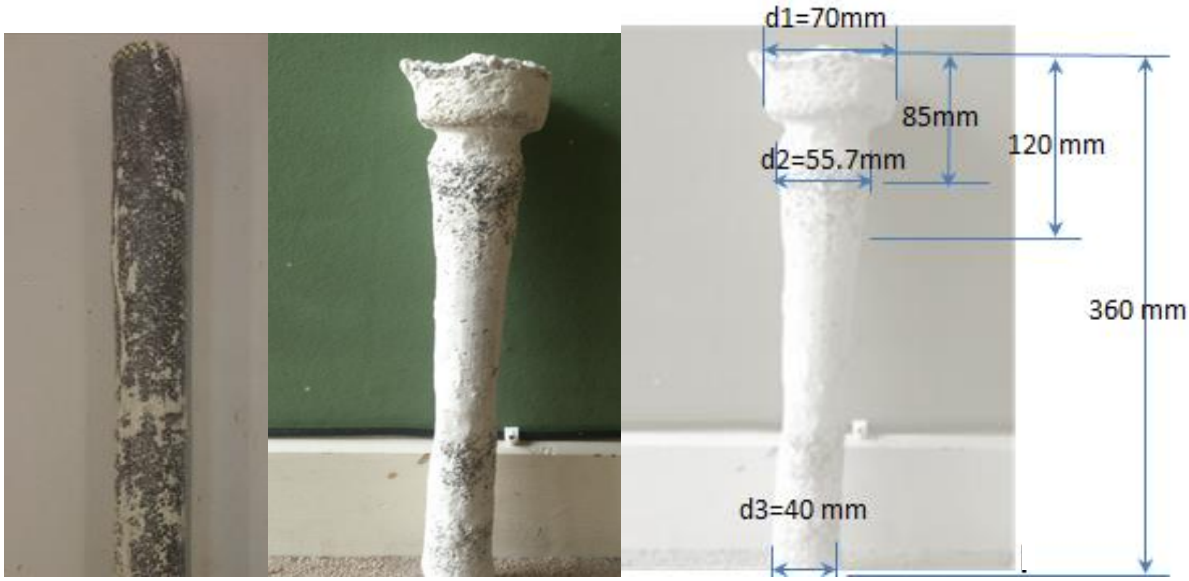

(a) (b) (C)

Figure 6.19: Failure profile under soaking with 2.73 L of water for (a) ESC (b) OSC (c) OSC with dimensions

6.2.3. Tests 7, 8, and 9 (Wetting the Test Cells with 6.15 L of Water: Wetting Prior to Loading)

6.2.3.1. Aim of Tests and General Description (Wetting with 6.15 L of Water)

These tests were conducted the same as previously, except that the wetting with water was increased to 6.15 L.

6.2.3.2. Checking the Homogeneity of the Host Ground (Wetting with 6.15 L of Water)

As with previous tests, the soil taken from the middle of the tanks to be replace with stones was checked for homogeneity. The results show a good consistency, as shown in Table 6-3.

Table 6-3: The homogeneity of the soil extruded to form the ordinary stone column or encased stone column for Test 8 and Test 9 (wetting with 6.15 L)

Test No.	Bore hole No.	Location	Average water content %	Average dry unit weight kN/m^3
Test 8	1	centre of the test cell of the stone column	9. 18	13.6
Test 9	2	centre of the test cell of the encased stone column	9.17	13.66

6.2.3.3. Admitting Water through the Soil Deposits (Wetting with 6.15 L of Water)

The water was introduced to the samples and after equilibrium was reached, with no more access to the water (see Section 4.10). The inundated cells were left until the next day to ensure complete saturation.

6.2.3.4. Time-Settlement and Stress-Settlement Characteristics of the Foundation (Wetting with 6.15 L of Water)

The next day, the dial gauges were observed and the corresponding data were collected. The readings from the dial gauges on foundation of tanks associated with untreated soil, treated with OSC, and treated with ESC recorded values 0.91, 0.62, and 0.52 mm respectively, and an average value of 0.84 mm was noticed for dial gauges on the surface of the three chambers.

After wetting, the loads were added in increments up to 300 kPa instead of 800 kPa in previous tests, this due to the high settlement observed which make the settlement under 800 kPa in such tests potentially unmeasured with the available gauges. The time intervals for increments of loads and the settlement induced are shown in Fig. 6.20.

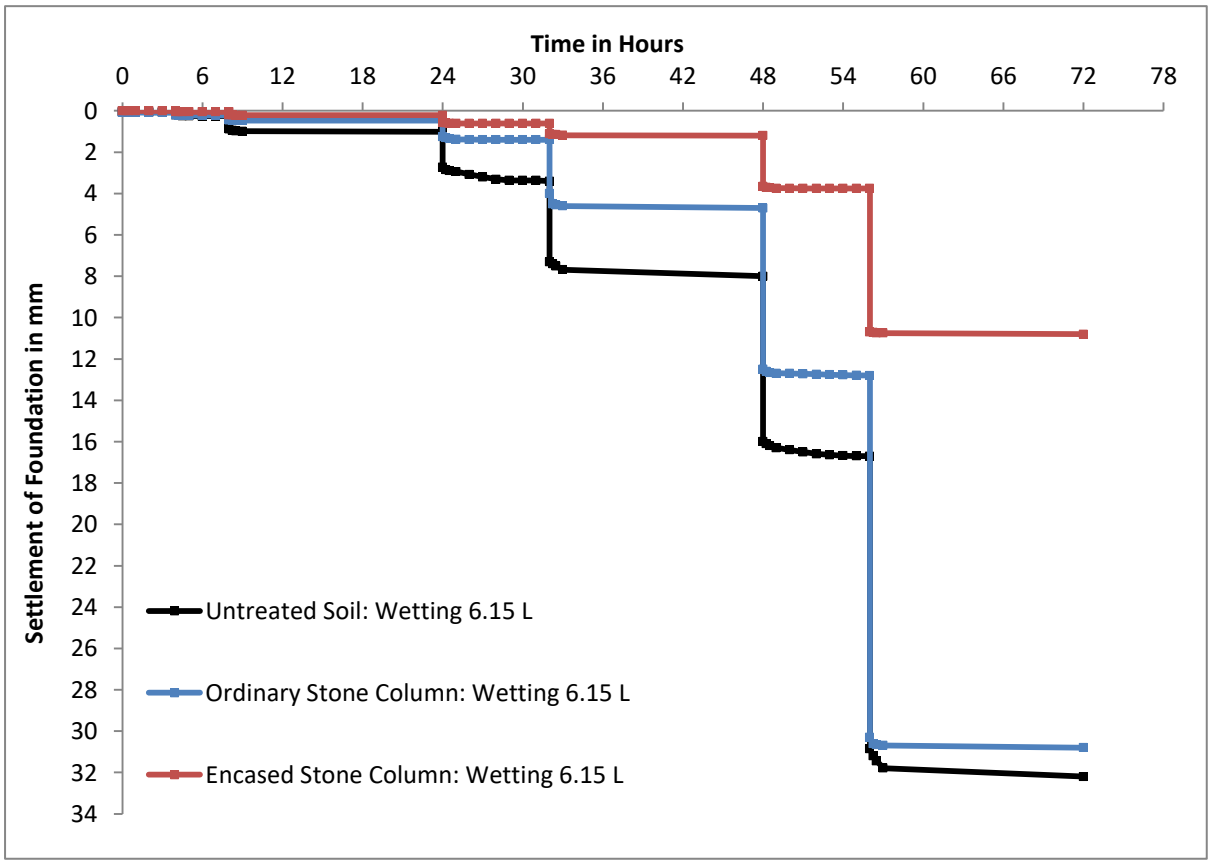

Figure 6.20: The time-settlement curve (soaking with 6.15 L)

The stress-settlement characteristics of the foundation resting on untreated artificial loess soil and treated with OSC and ESC are demonstrated in Fig. 6.21. It can be seen that the maximum bearing capacity at a strain of 10% of the diameter of the foundation was approximately 140, 168, and 248 kPa respectively. That means the improvement when treating the ground with the OSC achieves a ratio of 20%, while using the ESC achieves a capacity improvement of 77%.

The final settlement corresponding to 300 kPa for untreated soil, OSC, and ESC was 32.2, 30.8, and 10.8 mm respectively. The corresponding settlement improvement factor for using ESC recorded a ratio of 285%, against 105% for the ordinary stone column.

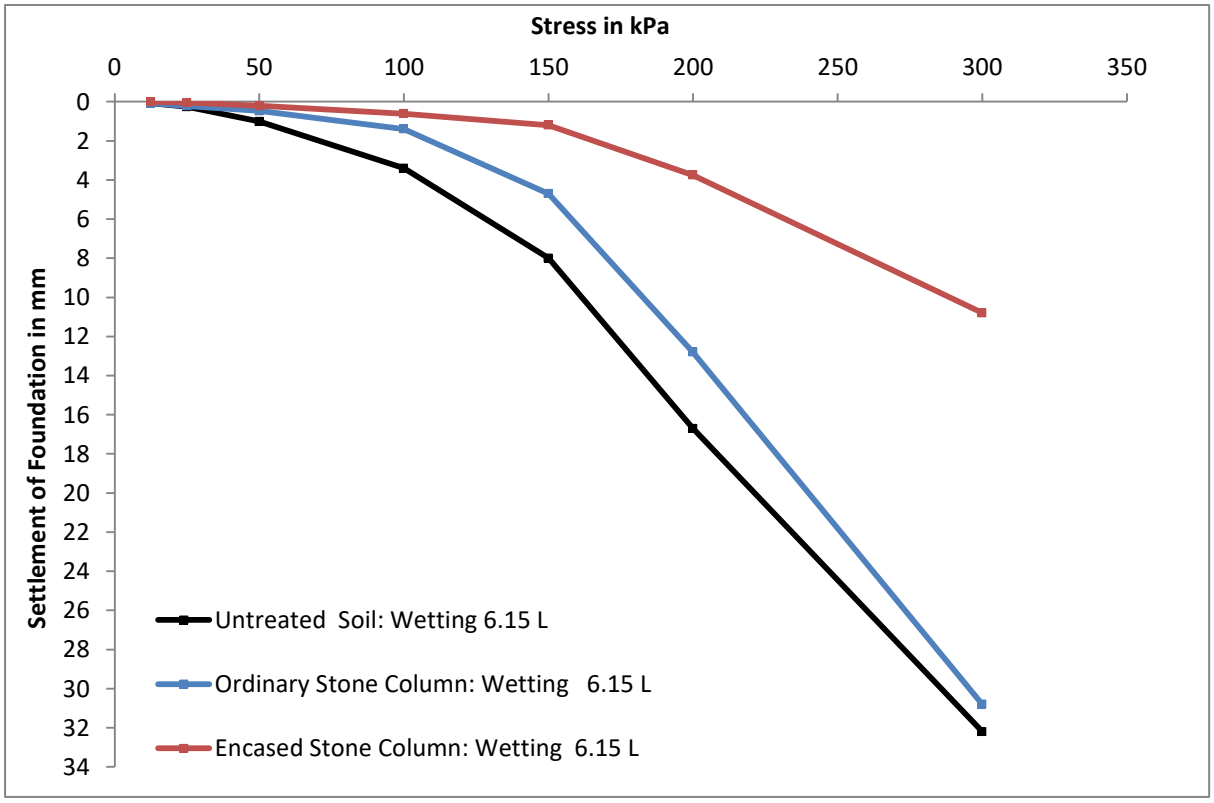

Figure 6.21: Stress-settlement behaviour (wetting with 6.15 L)

6.2.3.5. Deformation of the Soil Surface (Wetting with 6.15 L of Water)

In this series of tests, three dial gauges were fixed on one side of the foundation; they were arranged on the soil surface at distances of about 20, 60, and 100 mm respectively.

The readings of the closest to foundation showed the largest deflection and that was so outstanding for the test cell of the OSC, see Fig. 6.22. That was expected according to the variation of stresses in the surrounded ground in proportion to the distance from the column after the induced enlargement under loading.

Zahmatkesh & Choobbasti (2010) traced the new distribution of stresses that occur in the surrounding soil and quantified them by the ratio between effective horizontal and vertical stresses. They found that ratio with distance from column significantly decreases until it reaches the value of K_o (the coefficient of lateral earth pressure at rest). They found that the rest condition will happen when the ratio of the diameter of the cell to that of the column reaches 3.5. Similar observation points for soil only or ESC showed lower readings.

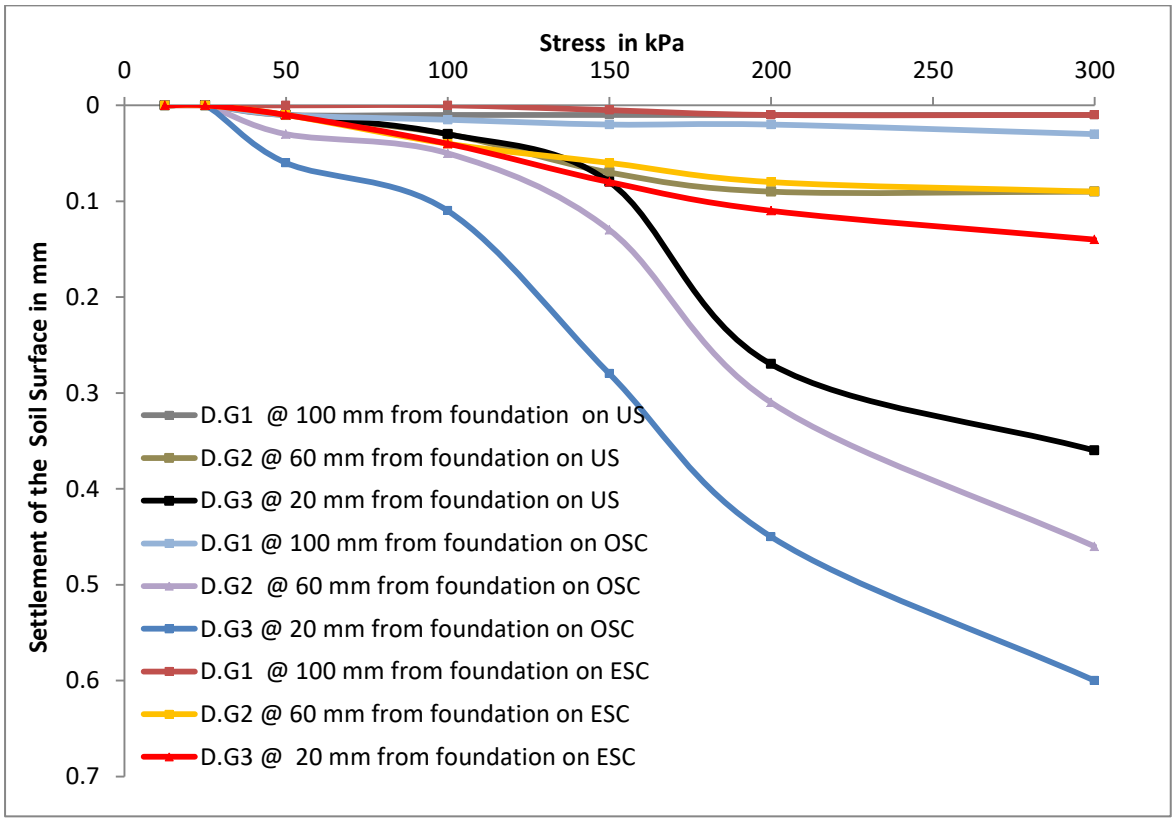

Figure 6.22: Readings from observation points on the soil surface at different distances from the foundation

6.2.3.6. Movement of the Tank (Wetting with 6.15 L of Water)

The lateral displacement of the sides of the tanks containing the stone columns, were monitored during Test 8 and Test 9. Under the final increments of load, the maximum movement reached values of 0.03 and 0.06 mm for the chambers with the OSC and ESC respectively. In comparison with the soil deformation, these values can be considered insignificant. Fig. 6.23 illustrates the displacement in the sides of the tanks with the OSC and ESC during loading.

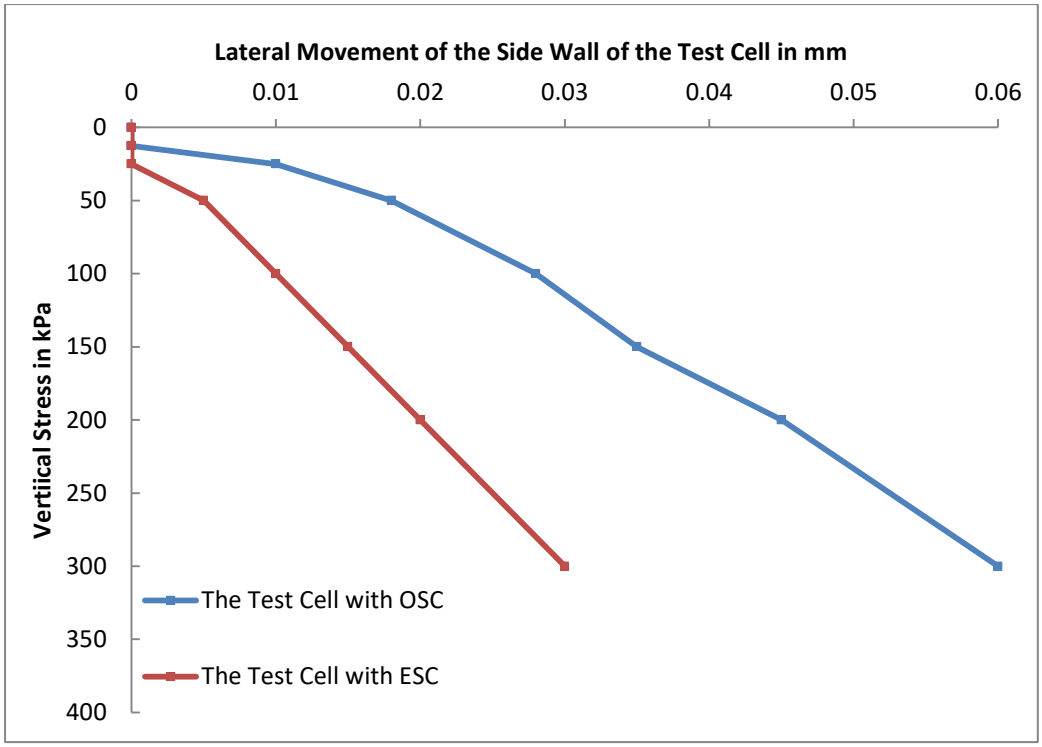

Figure 6.23: The lateral movement against vertical stress of the tanks associated with the OSC and ESC

6.2.3.7. Investigating the Soil Surface after Completing the Tests (Wetting with 6.15 L of Water)

After the test completion and removing the sand film at top, it was noticed that the untreated soil, OSC and ESC indicated no cracks in this case of adding 6.15 L.

6.2.3.8. Investigating the Water Profile after Completing the Tests (Wetting with 6.15 L of Water)

The water content profile after digging out the soil deposit was determined as shown in Fig. 6.24. The same procedure as in previous tests was followed, with the same number of samples positioned throughout the deposit. Obviously, the collected readings were higher than previous tests as a result of the larger amount of the water added. The minimum water content was recorded at the surface (22.7%), whereas the maximum water content was observed at the base of the tank (25.7%). It is worth mentioning that the water content at the soil base was consistent with the value of 25.0% found by Miller (2002). The average degree of saturation for the total deposit in this case was 69.0%, which fits well with the 70.0% computed by adding the theory value (62. 9%; calculated in Appendix (C)) and the 7.2% extra saturation from the filter layer, as explained in the previous section. The average degree of saturation for the total deposit in the tanks associated with the OSC and ESC was 71.0% and 74.0% respectively. The experimental values therefore fit the theoretical calculations, in addition to the estimated quantity of water coming from the filter layer. Although the quantity

of water was higher in this case, it was not enough to saturate the base of the soil; values were recorded of approximately 73.0% for untreated soil, 76.0% for the OSC, and 80.0% for the ESC.

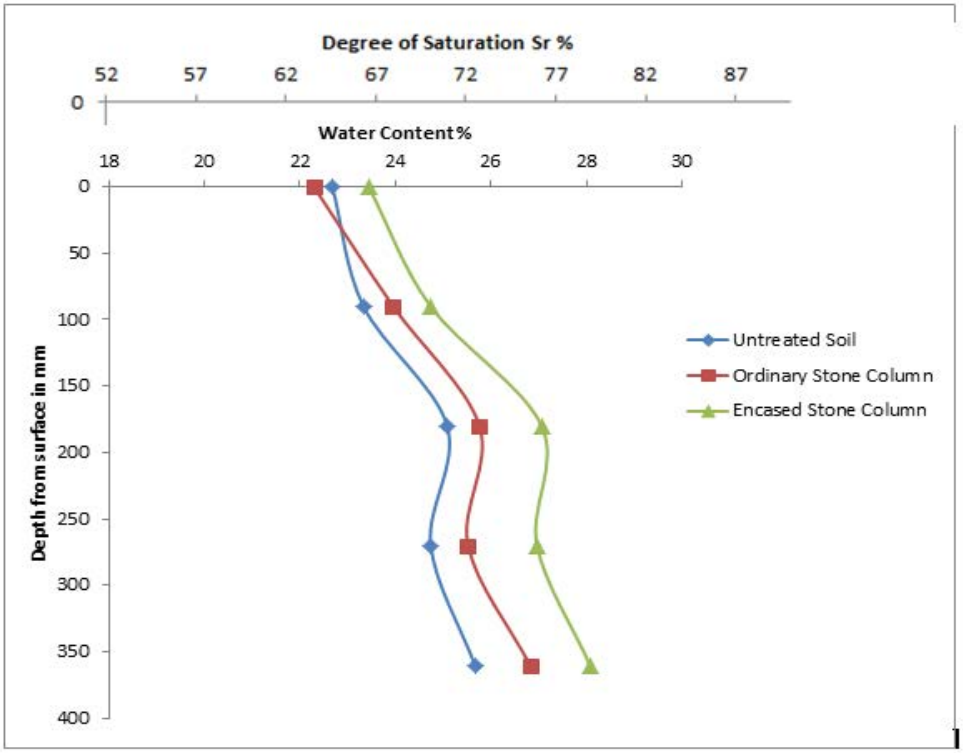

Figure 6.24 : Water content profile after digging out

6.2.3.9. Investigating the Failure Profile of the Column after Completing the Tests (Wetting with 6.15 L of Water)

The shapes of failure of Tests 8 and 9 are illustrated in Fig. 6.25. Regarding the OSC, it showed an expansion in the column diameter of more than that observed for Test 5, at the same depth. The column diameter increased by 17.3 mm at a depth of 85 mm. The lateral bulging was contained within 150 mm of the column length, which is more than that observed for Test 5. It can be understood that the affected bulging area is more than that observed for wetting with 2.73 L. It can be concluded that soil associated with a higher degree of saturation experiences a wider and deeper expansion as a result of a weakening of the shear strength of the soil. The reinforced stone column in Test 9 acted effectively to minimise the lateral expansion, as there no bulging was noticed. The encasement was checked and no damage was found.

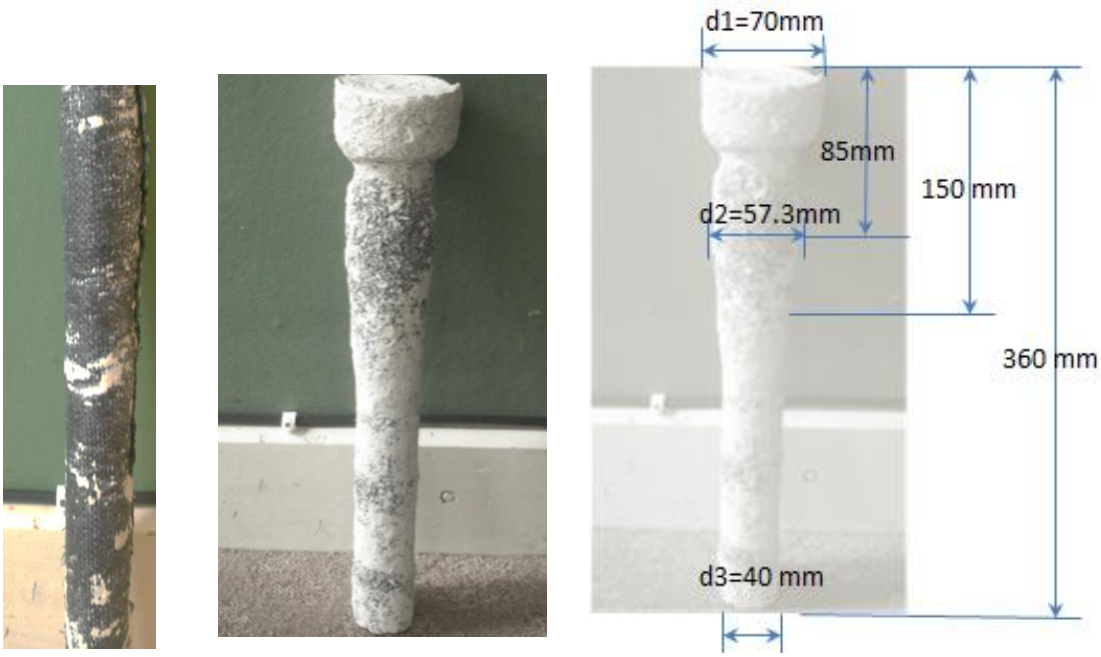

Figure 6.25: Failure profile under soaking with 6.15 L of water for (a) ESC, (b) OSC, (c) OSC with dimensions

6.2.4. Tests 10, 11, and 12 (Wetting the Test Cells with 6.15 L of Water: Wetting after Loading

6.2.4.1. Aim of Tests and General Description (Soaking after Stress of 100 kPa)

The aim of this series of physical tests was to investigate the effect of the soaking pattern on the bearing capacity of the artificial collapsible untreated soil, soil treated with an OSC, and soil treated with an ESC. The soil bed was prepared using the same procedure as for previous tests, by mixing with 12% water content and leaving each layer after compacting for 48 hours for bonds to develop.

6.2.4.2. Checking the Homogeneity of the Host Ground (Soaking after Stress of 100 kPa)

Table 6-4 shows the average water content and average dry unit weight of the extruded soil from the middle of the tanks in Test 11 and Test 12, which reflected a good convergence with the pilot and previous tests.

Table 6-4: The homogeneity of the soil extruded from the middle of the tanks with the OSC and ESC for Test 11 and Test 12 (soaking after stress with 100 kPa)

Test No.	Bore hole No.	Location	Average water content %	Average dry unit weight kN/m^3
Test 11	1	Centre of the test cell of the stone column	9.18	13.65
Test 12	2	Centre of the test cell of the encased stone column	9.25	13.62

6.2.4.3. Admitting Water through the Soil Deposits (Soaking after Stress of 100 kPa)

The water was added to the specimen in different scenario. The test cell was first loaded up to 100 kPa, and then water was admitted to the deposit using the method of wetting mentioned in Section 4.10. The quantity of water added to the reservoir was exactly the same as the previous tests (wetting with 6.15 L of water), and after equilibrium was reached, with no more access to the water, the inundated cells were left until the next day, to ensure the water had fully soaked in. Afterwards, the loading process was resumed up to 300 kPa.

6.2.4.4. Stress-Settlement Characteristics of the Foundation (Soaking after Stress of 100 kPa)

The deflection of the foundation at the centre of each test tank was monitored. Readings for settlement were recorded before and after inundation. The recorded stress-settlement curves of the three chambers were compared with those of tests run in a dry state, and tests where wetting was conducted before loading. Each increment of load was sustained until no vertical movement was observed, as for previous tests. See Figs 6.26, 6.27, and 6.28.

The results show behaviour consistent with the oedometer tests if we compare with the single and double collapse tests. For the same driving force acting on the foundation and the same degree of saturation of the host ground, soaking from the start or after a specific load is applied does not affect overall performance. These results are in line with the results found by Miller (2002) for soil only. In term of ultimate bearing capacity under soaking, after applying a stress of 100 kPa, tanks associated with untreated soil, OSC, and ESC reached values 144, 172, and 251 kPa respectively, while with soaking with water from the beginning of the test, they showed only slight differences with values of 140, 168, and 248 kPa respectively.

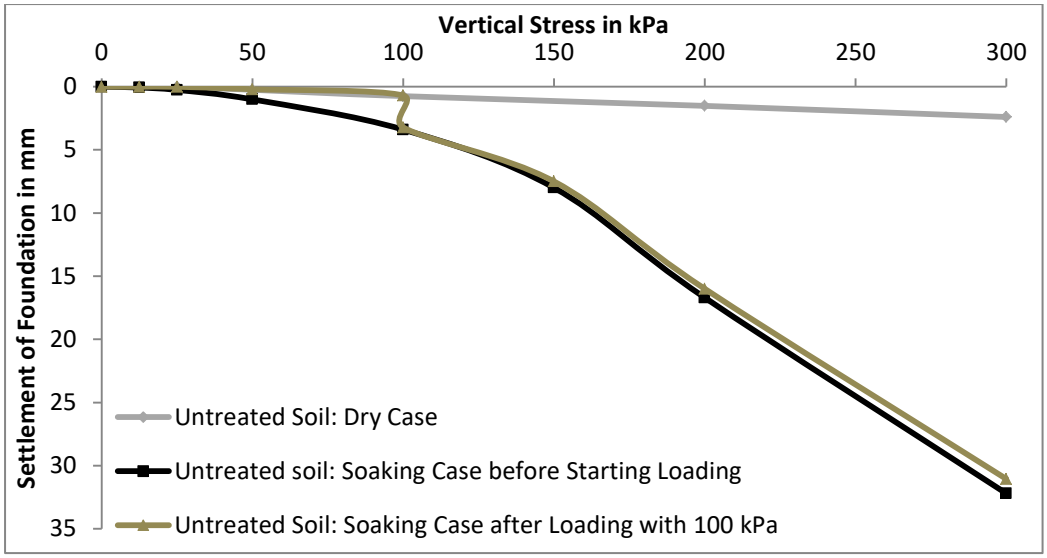

Figure 6.26: Different soaking patterns (test cell of untreated soil)

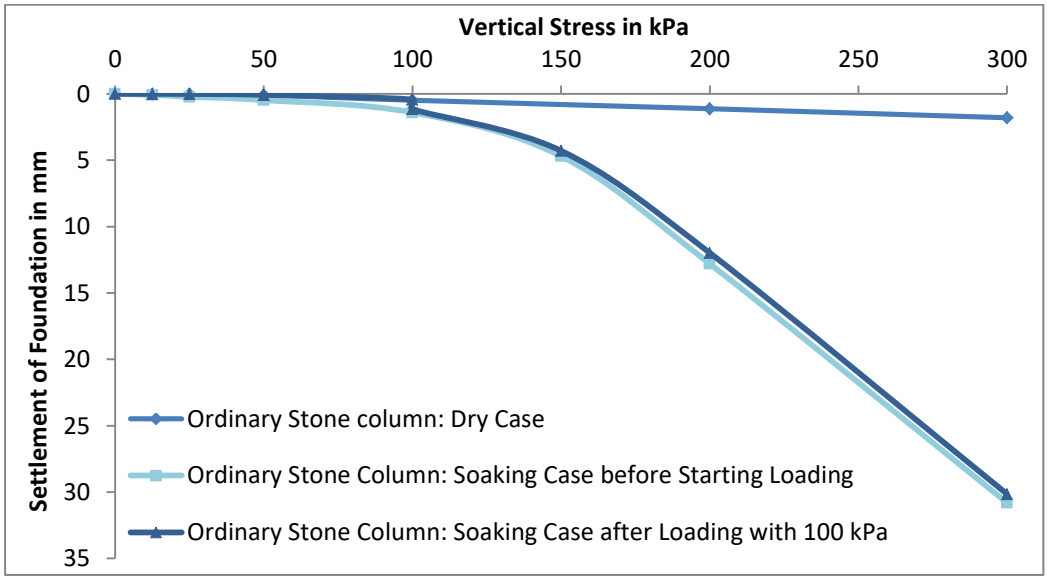

Figure 6.27: Different soaking pattern (test cell of OSC)

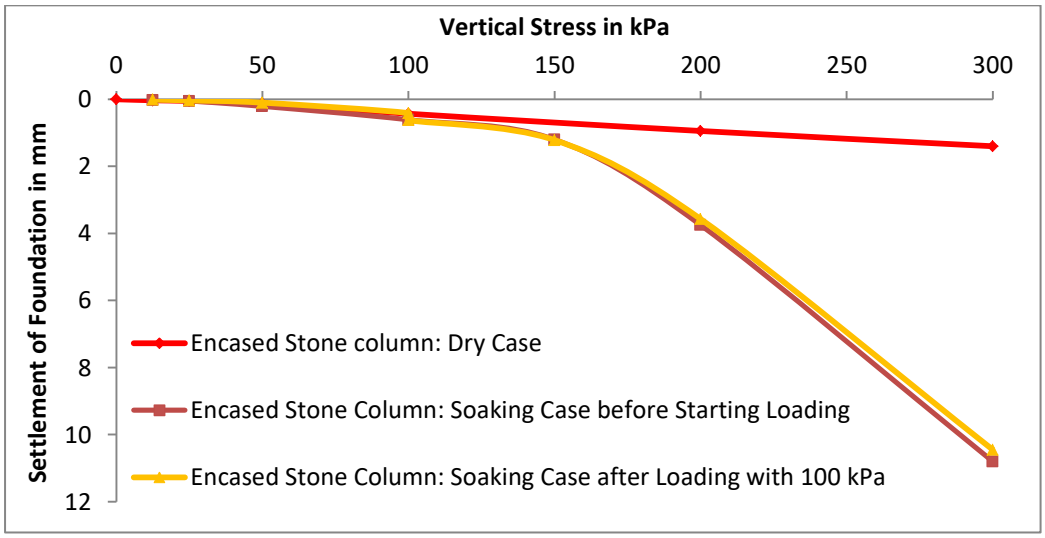

Figure 6.28: Different soaking patterns (test cell of ESC)

6.3. Results of the Geophysical Survey

The results of the geophysical investigation are presented, including both the circular arrangement and the vertical alignment of the electrodes.

6.3.1. Circular Configuration

The inversion results of the circular configuration using BERT software are presented in the following sections to show the distribution of the geophysical properties within the three chambers. Although the approach could leave the reader trying to visually identify zones with changes in colour for each test, the associated colour legend bar already reflects the values of ERT for any local point within the sample. By applying Clip or Slice tool of the ParaView software, the image of ERT values in any section and at any direction can be obtained. Another method for presenting and analysing the ERT measurements using plots of change from one physical condition to the next would be impractical due to the huge data gained.

6.3.1.1. General Trend of the Measurement of the Three Chambers

Figures 6.29, 6.30, and 6.31 demonstrate the inversion results for the three tanks, untreated soil and soil treated with the OSC and ESC, for different loading statuses. The outcomes for the three test chambers show that soil conductivity was very sensitive to load-induced and moisture-induced variations during collapse. Similar observations were made by Zourmpakis et al. (2006) on a metastable loess soil; the authors attributed such behaviour to the current conductivity passing through the clay bonds and bridges between the silt grains, which is highly affected by conditions of stress and inundation.

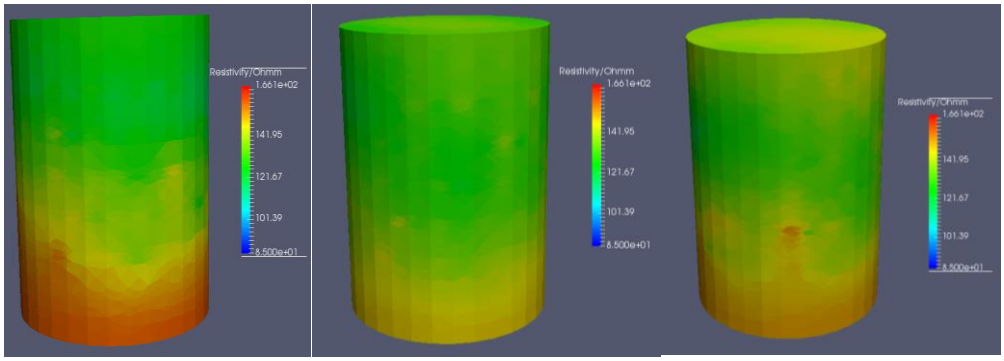

(No load) (25 kPa) (50 kPa)

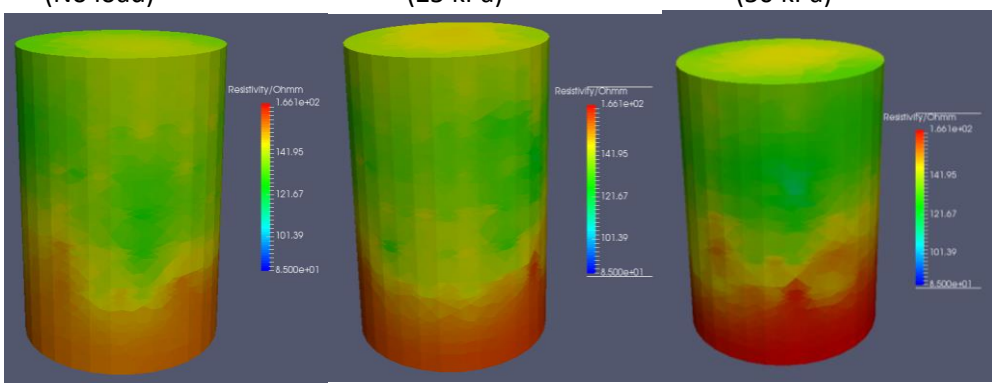

(100 kPa) (150 kPa) (300 kPa)

Figure 6.29: Inversion results for test tank with untreated soil at different loading stages

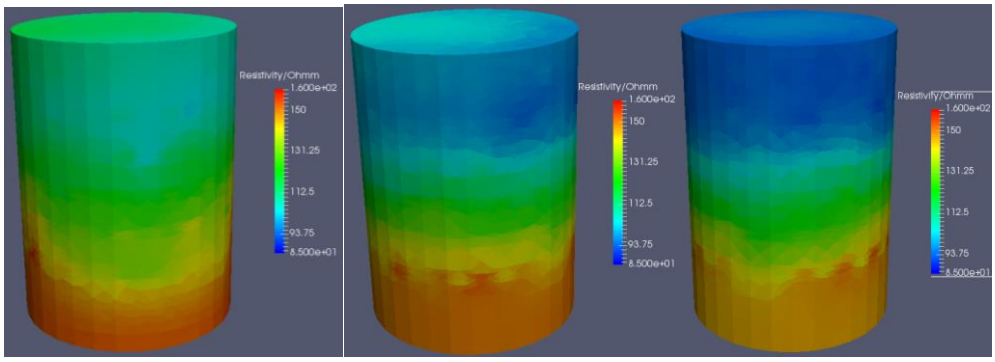

(No load) (25 kPa) (50 kPa)

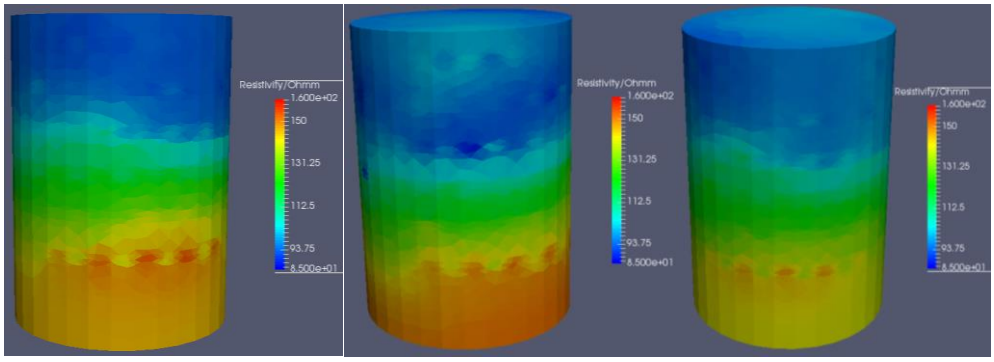

(100 kPa) (150 kPa) (300 kPa)

Figure 6.30: Inversion results for test tank with the OSC at different loading stages

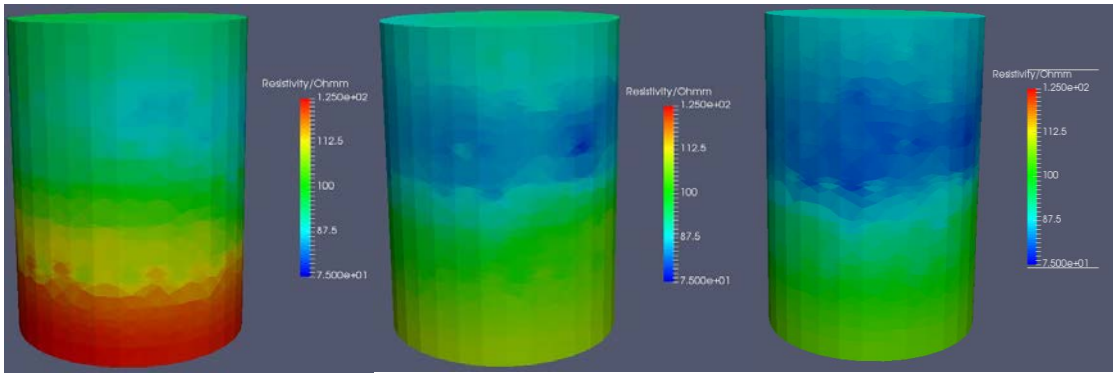

(No load) (25 kPa) (50 kPa)

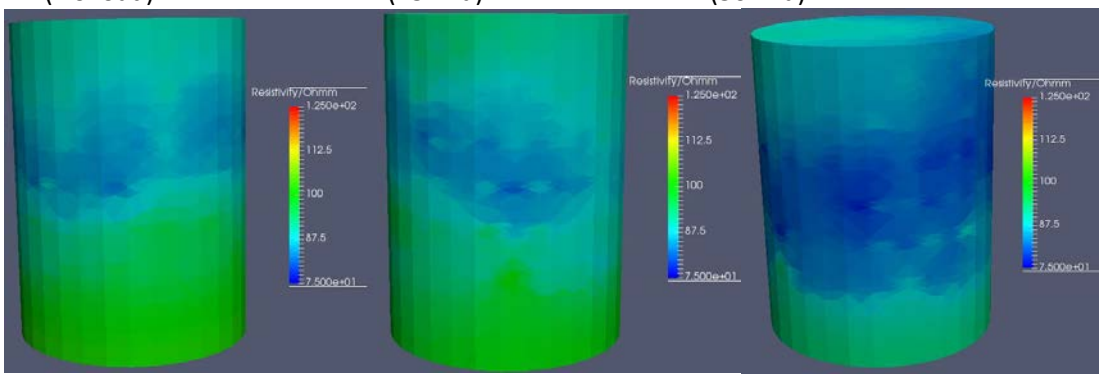

(100 kPa) (150 kPa) (300 kPa)

Figure 6.31: Inversion results for test tank with the ESC at different loading stages

The range of resistivity values gained for soil volume (characterised by a 0.93 void ratio), except for the tanks boundaries, reached magnitudes of between 90 and 150 Ohm.m; see the vertical slices through the tanks shown in Figs. 6.32, 6.33, and 6.34. They look very similar to those observed for artificial loess tested by Liu et al. (2014) of 100 to 160 Ohm.m where soil has void ratio of 1.15 and water content variations from 31% to 34%. The tank boundaries showed slightly lower values, which could be as a result of the disturbance from the electrodes, which create a path for more water to pass through the area between them and the soil in contact. The higher resistivity at the bottom of the tanks can be explained by the lower porosity of the gravel and thin sand layers, in comparison to the high porous soil layers above.

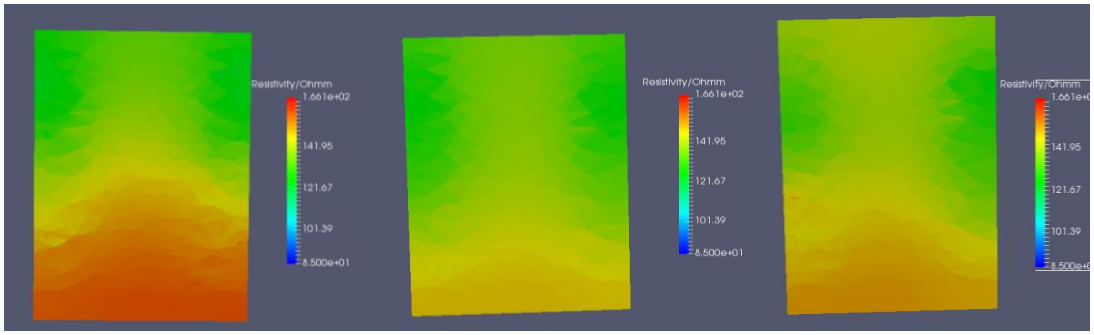

(No load) (25 kPa) (50 kPa)

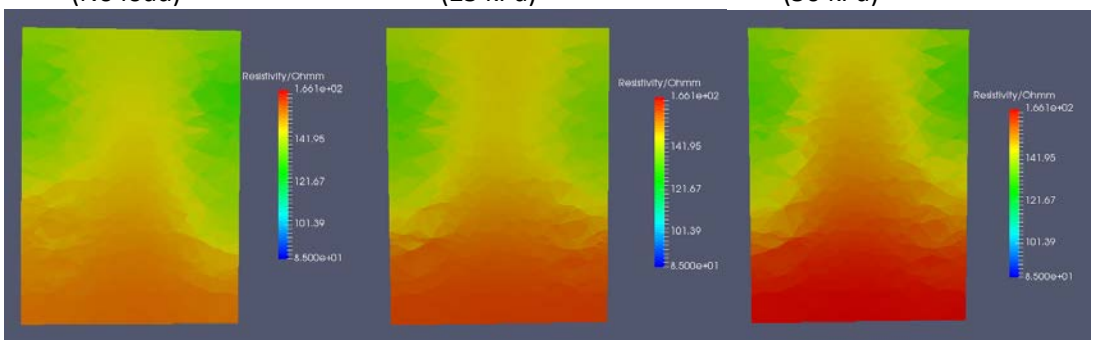

(100 kPa) (150 kPa) (300 kPa)

Figure 6.32: Vertical slice through the inversion results for the tank of untreated soil under loading up to 300 kPa

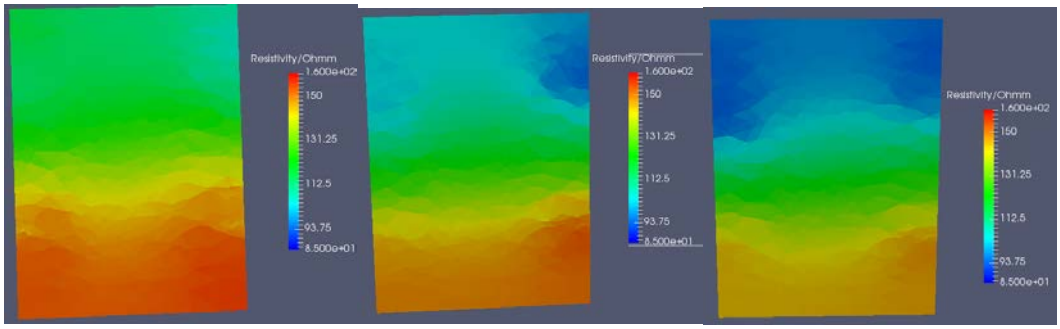

(No load) (25 kPa) (50 kPa)

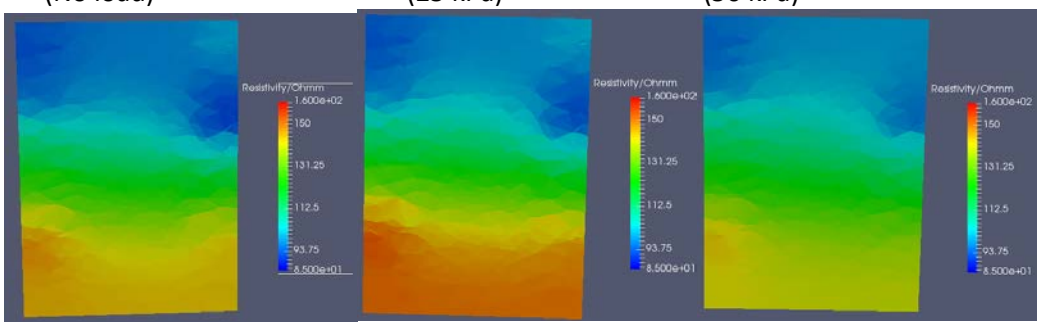

(100 kPa) (150 kPa) (300 kPa)

Figure 6.33: Vertical slice through the inversion results for the OSC tank under loading up to 300 kPa

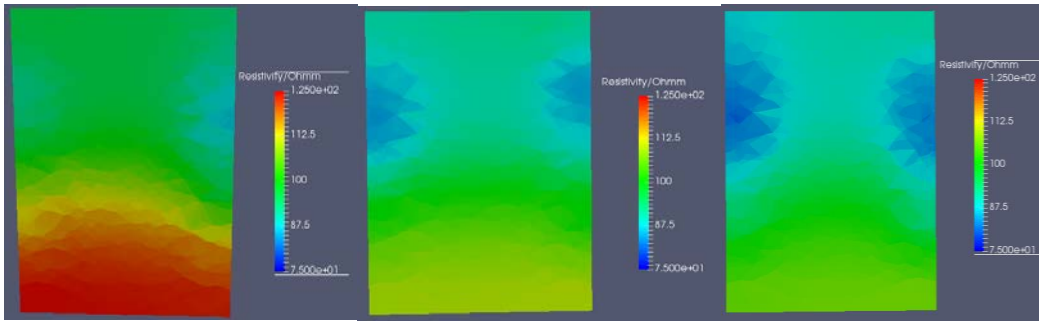

(No load) (25 kPa) (50 kPa)

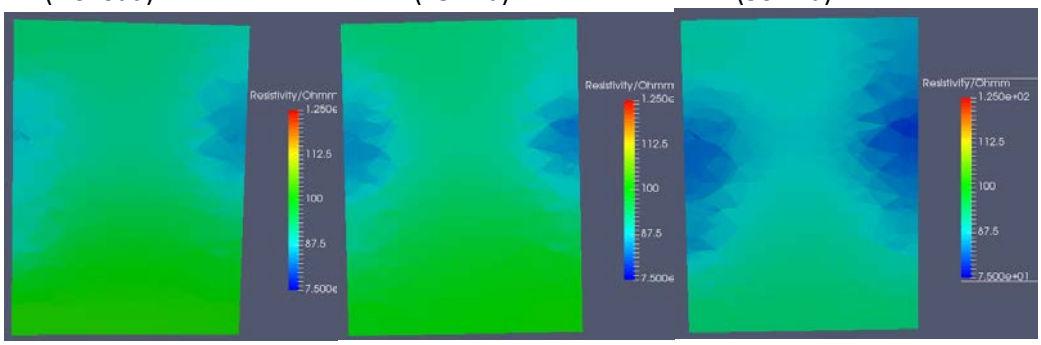

(100 kPa) (150 kPa) (300 kPa)

Figure 6.34: Vertical slice through the inversion results for the ESC tank under loading up to 300 kPa

6.3.1.2. The Data Corresponding to the Area Surrounding the Column of the Three Chambers

In the area surrounding the column, the results show that the electrical resistivity of the soil for the tank tested with untreated soil was higher than that observed for the tanks with OSC and ESC. See the vertical slices through the three chambers, which were shown in the previous section in Figs. 6.32, 6.33, and 6.34. This agrees with the observed variations in water content of the samples in the three tanks (69, 71, and 74%) after digging out, as stated in Section 6.2.3.8. The values were assessed theoretically with values taken from applying Archie"s law, considering a=0.7 (the value is normally taken for sandstone as the ground silica dominates) as recommended by Blenkinsop et al. (2000); m=1.33 is estimated according to the proportions of ground silica and kaolinite particles in the soil mixture and their corresponding factors, 1.2 for spheres (Jackson et al., 1978); 1.85 for platted particles, as recommended by Atkins & Smith 1961**;** B=1.64 for loess, as found by Zha et al. (2010). The error boundaries are demonstrated in the Table 6-5.

Table 6-5: The deviation from Archie's law for the soil in the three chambers

Description	Average degree of saturation %	Theoretical resistivity	Experimental Resistivity			
			Approximated Upper Limit	Deviation from Archie"s law %	Approximated Lower Limit	Deviation from Archie law %
Soil tank	69	145	139 141 130.5	-2.8	121	-16.6
OSC tank	71	139	131	-5.8	113	-18.0
ESC tank	74	130.5	95	-27.2	88	-32.6

6.3.1.3. Test 13 (Resistivity Measurements of the Test Chamber of Untreated Soil)

The results showed that measuring the ERT distribution of the investigated volume is effective in specifying variations in geophysical properties. See Figs. 6.29 and 6.32 in Section 6.3.1.1 for the tank filled with soil without a stone column at the centre. The images change noticeably with respect to load at the middle. Data for the electrical resistivity of the soil showed differentiations with respect to loading until it reached values ranging from about 122 to 166 Ω.m under 300 kPa (the last loading increment). That could be interpreted by the significant increase in resistivity readings due to high soil densification and water drainage at the top and bottom of the tank. Similar behaviour was seen in the oedometer sample under mechanical loading, as recorded by Comina et al. (2008), except that the bottom layer witnessed a decrease in resistivity because the drainage was only possible for the upper layer. An increase in resistivity as a result of drainage was also observed during oedometer testing by Ghorbani et al. (2012). The investigators ascribed that to salt crystallisation that occurs during drainage stage in the interstitial brine and causes an increase in the tortuosity of the soil, which leads to an increase in the value of resistivity. They also argued that this rise in the electrical resistivity is mitigated by a reduction in the concentrations of salts in the brine as a result of decreasing the volume of voids in the sample. For illustration, inversion results at each ring level during loading are shown in Figs. 6.35 to 6.40. It can be seen that rings 1 to 4 indicated a reduction in resistivity under loading 25 kPa; then they increased gradually with loading to reach the maximum value under the final increment of loading. That is likely to be associated with the continuous movement of water from the gravel layer at the base upward. However, after loading 50 kPa, the readings start to increase with loading because of the impact of the significant settlement.

Rings 5 and 6 were associated with a gradual increase in resistivity at all loading stages, as the stress concentration is higher in those upper rings in comparison to the other rings

because they are subjected to a higher vertical and horizontal effective stress, the outcomes of which are a higher decline of porosity and consequently a reduction in the conductivity of soil (Comina et al., 2008).

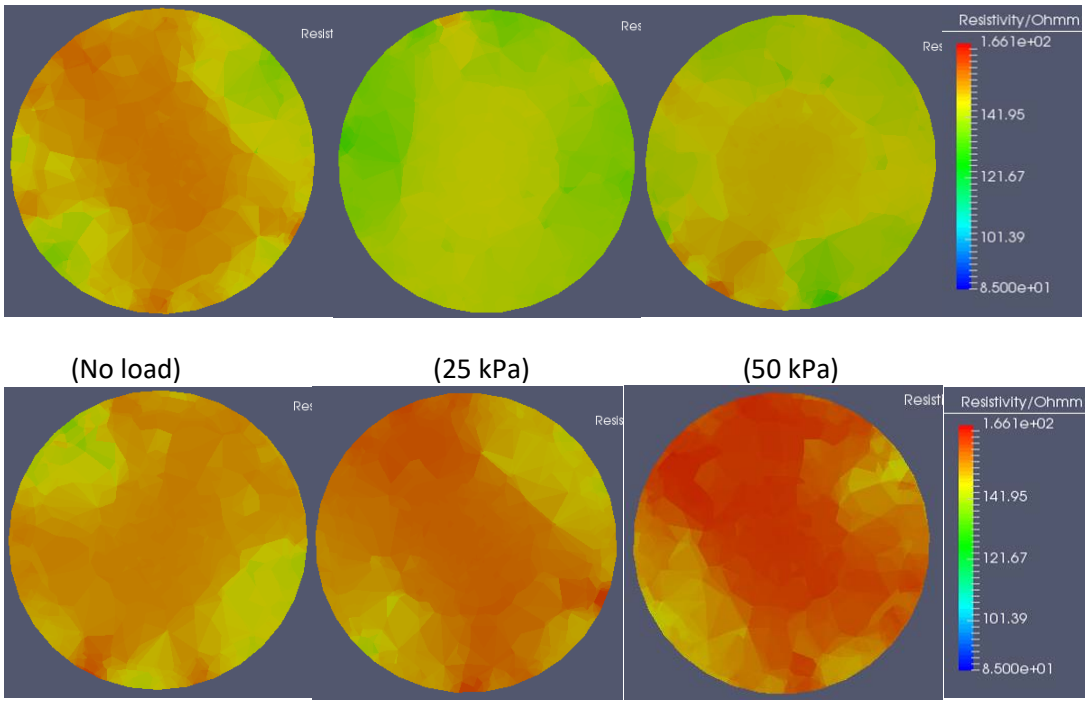

(No load) (25 kPa) (50 kPa)

(100 kPa) (150 kPa) (300 kPa)

Figure 6.35: Inversion results of Ring 1 for tank filled with untreated soil only under different loading stages

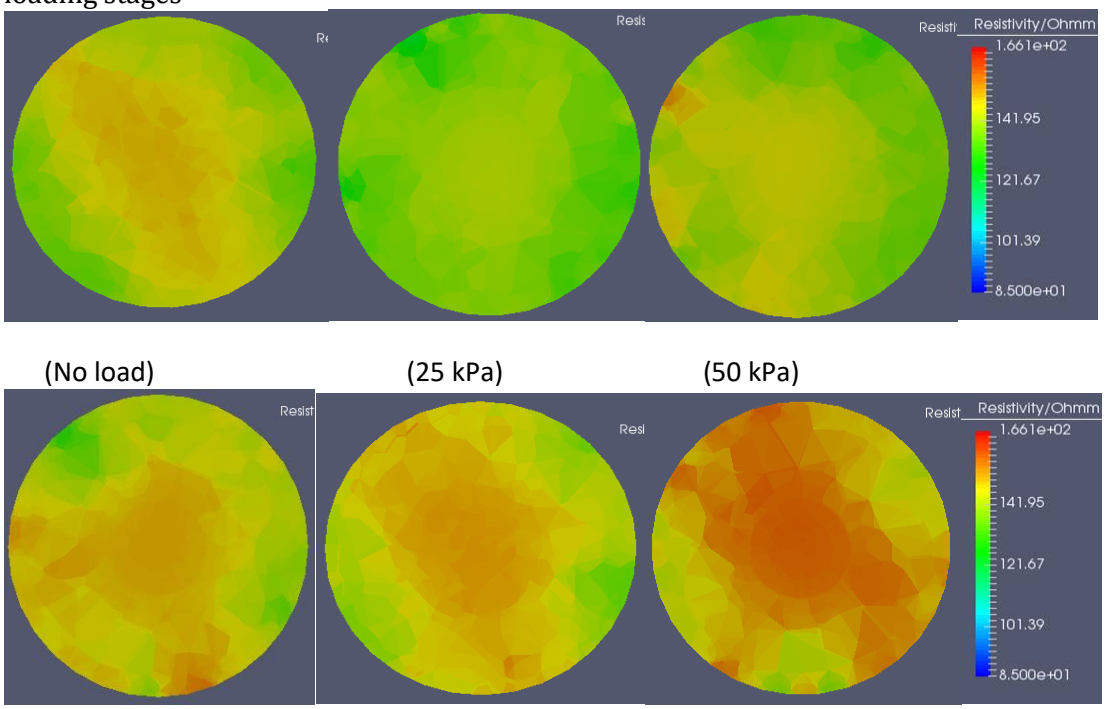

(No load) (25 kPa) (50 kPa)

(100 kPa) (150 kPa) (300 kPa)

Figure 6.36: Inversion results of Ring 2 for tank filled with untreated soil only under different loading stages

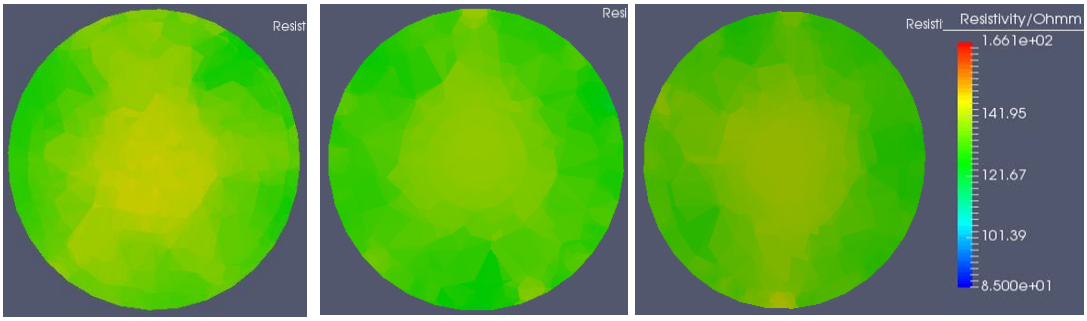

(No load) (25 kPa) (50 kPa)

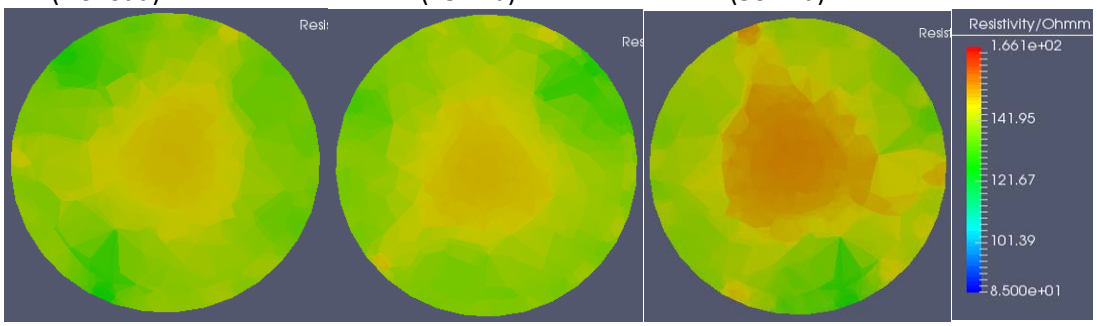

(100 kPa) (150 kPa) (300 kPa)

Figure 6.37: Inversion results of Ring 3 for tank filled with untreated soil only under different loading stages

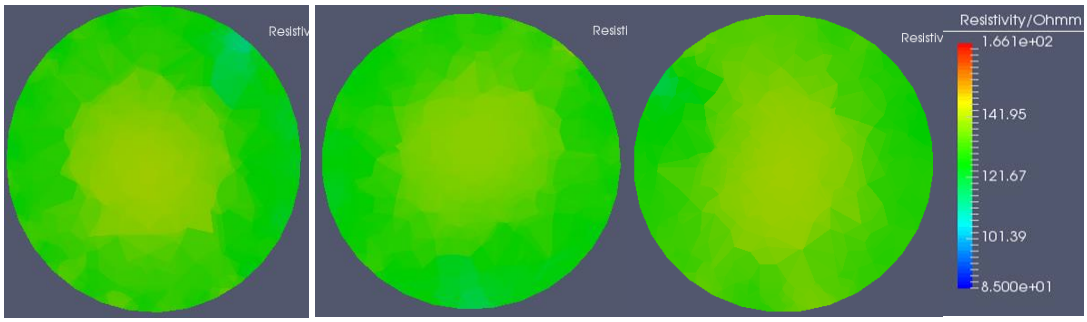

(No load) (25 kPa) (50 kPa)

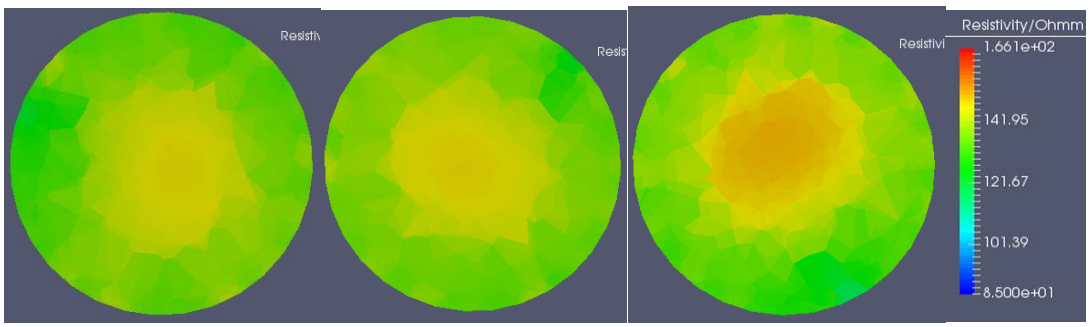

(100 kPa) (150 kPa) (300 kPa)

Figure 6.38: Inversion results of Ring 4 for tank filled with untreated soil only under different loading stages

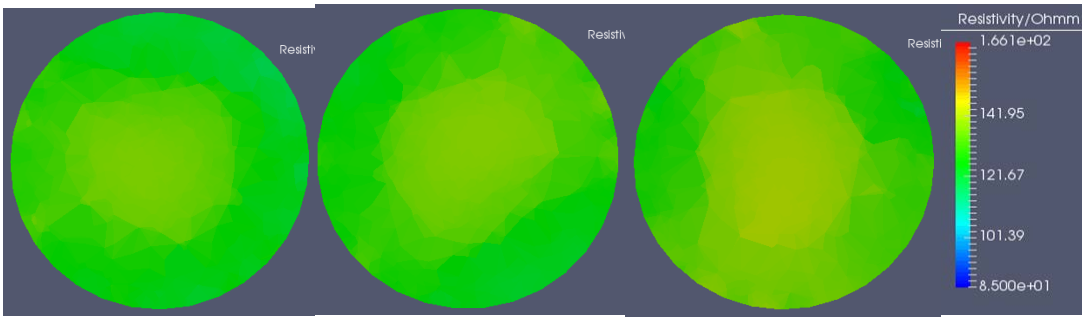

(No load) (25 kPa) (50 kPa)

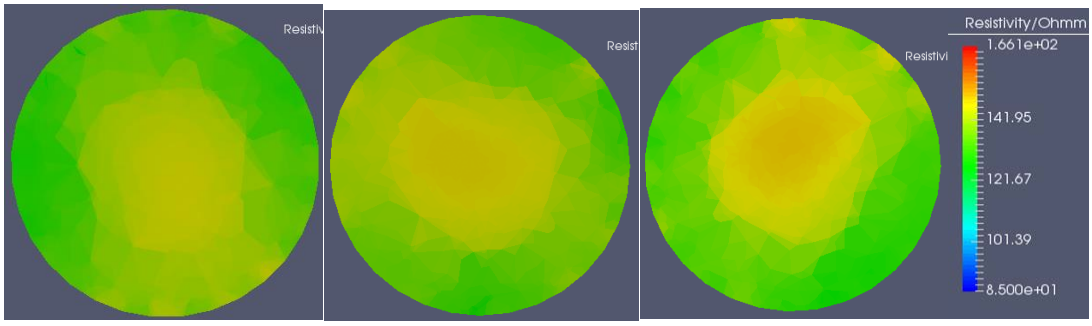

(100 kPa) (150 kPa) (300 kPa)

Figure 6.39: Inversion results of Ring 5 for tank filled with untreated soil only under different loading stages

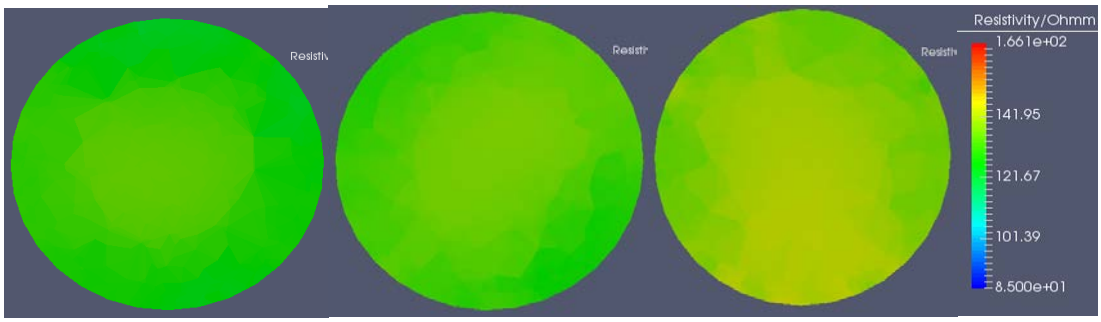

(No load) (25 kPa) (50 kPa)

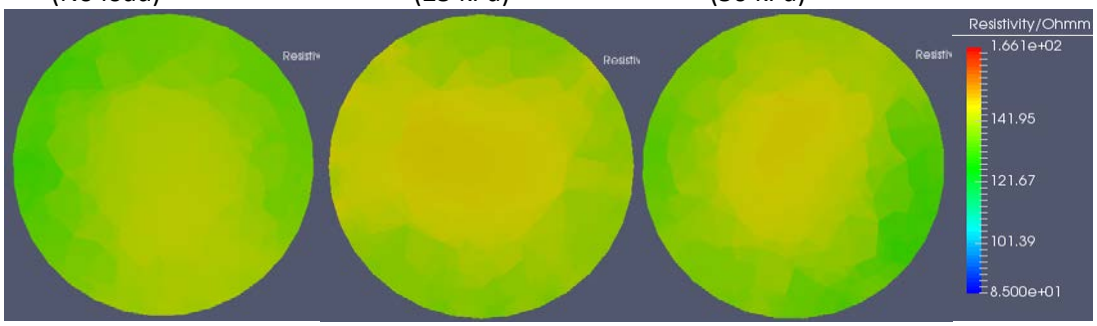

(100 kPa) (150 kPa) (300 kPa)

Figure 6.40: Inversion results of Ring 6 for tank filled with untreated soil only under different loading stages

6.3.1.4. Test 14, Resistivity Measurements for the OSC Test Chamber

As stated in Section 6.3.1.1, Figs 6.30 and 6.33 show the inversion results for the test cells that contained the OSC, while Figs 6.41 to 6.46 in this section show the readings from the rings around the tank. In the first stages of loading, it can be seen that the top three rings of the OSC cell indicated a decrease in resistivity values. That may be as a result of the continuous movement of water from the gravel layer at the base upward. However, after stress of 100 kPa, the readings started to increase, with loading at the middle. That may be due to the effect of the bulging within the stone column body in the upper layers and the resulting interaction between the soil and the column, which could activate the function of drainage in the stone column. The lower rings showed a gradual decrease in resistivity values, which could reflect an increase in soil saturation. Although this experimental trial produced a valuable insight into the system subjected to varying load and saturation conditions, the technique indicates a limitation in specifying the distinction of the column material at the middle of the test tank. This is probably because of the convergence of the electrical properties of the soil and the stone material used (lower limits for stone are found between 108 and 127 Ohm.m, and upper limits between 185 and 217 Ohm.m), or it could be as a result of the loss of the signal strength for the farthest electrode pairs, as this is the main disadvantage of using a dipole-dipole configuration, as confirmed by Holder et al. (2004).

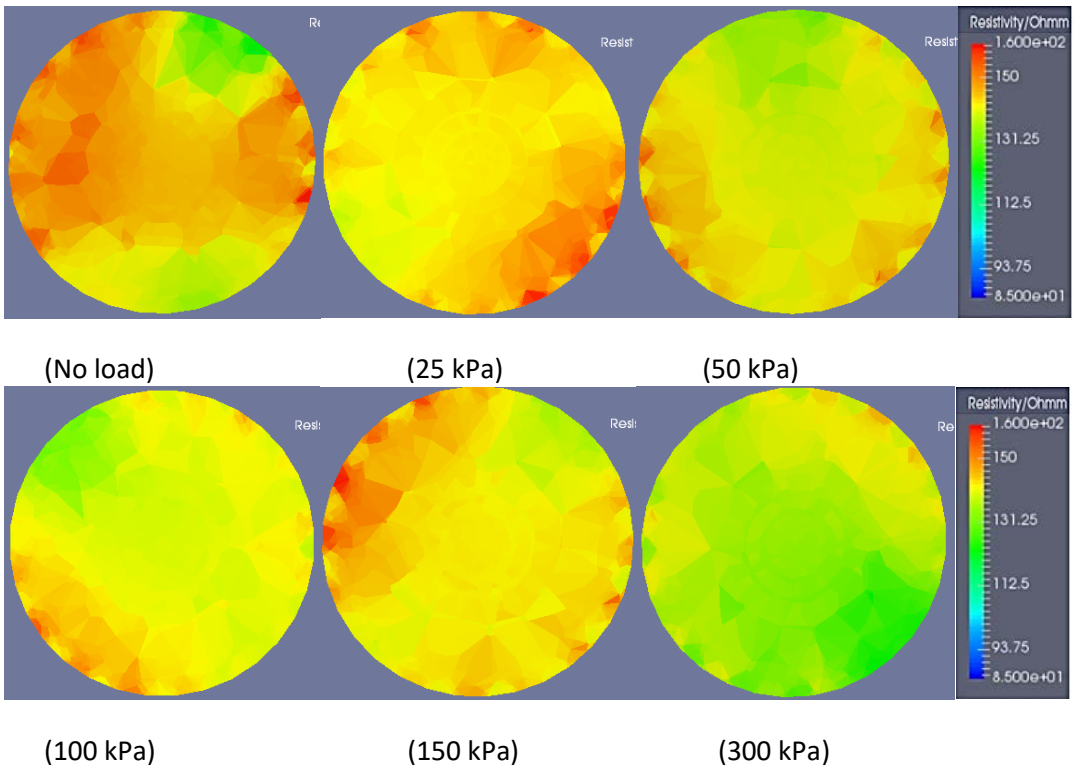

Figure 6.41: Inversion results of Ring 1 for tank filled with soil and OSC under different loading stages

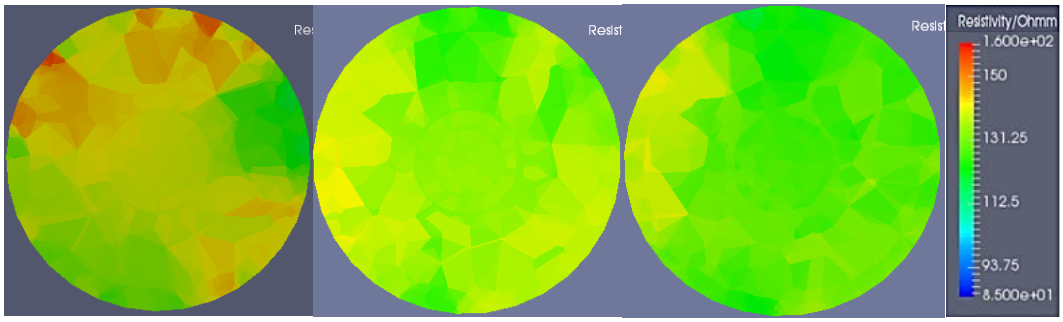

(No load) (25 kPa) (50 kPa)

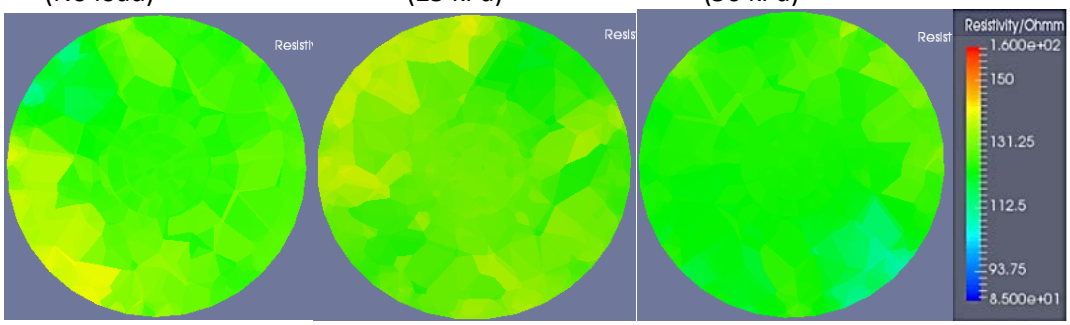

(100 kPa) (150 kPa) (300 kPa)

Figure 6.42: Inversion results of Ring 2 for tank filled with soil and OSC under different loading stages

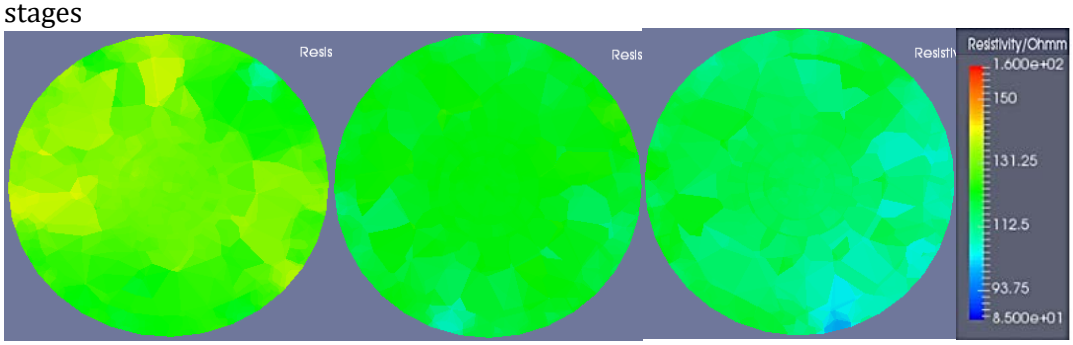

(No load) (25 kPa) (50 kPa)

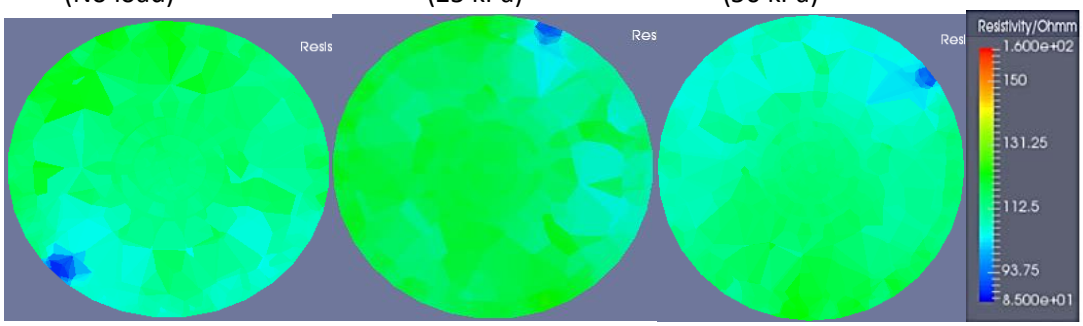

(100 kPa) (150 kPa) (300 kPa)

Figure 6.43: Inversion results of Ring 3 for tank filled with soil and OSC under different loading stages

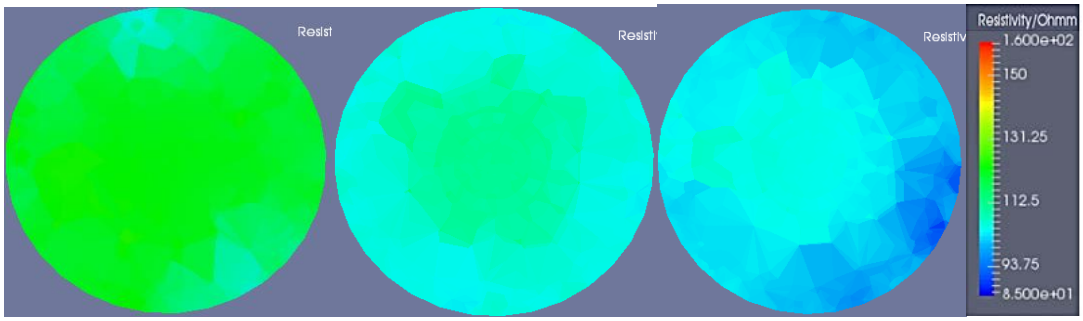

(No load) (25 kPa) (50 kPa)

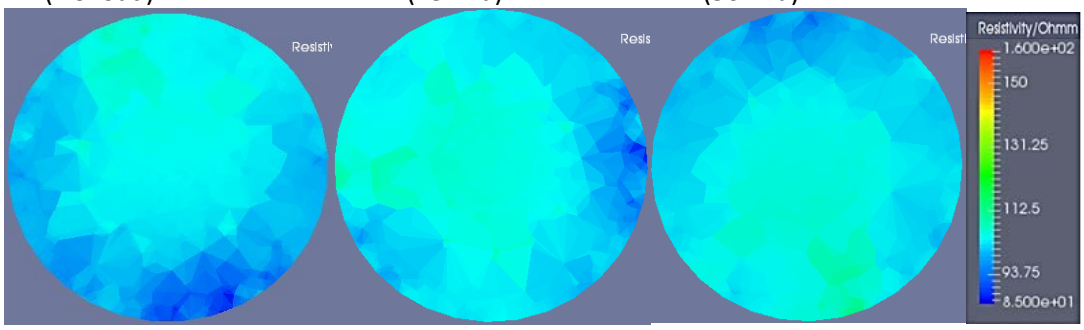

(100 kPa) (150 kPa) (300 kPa)

Figure 6.44: Inversion results of Ring 4 for tank filled with soil and OSC under different loading stages

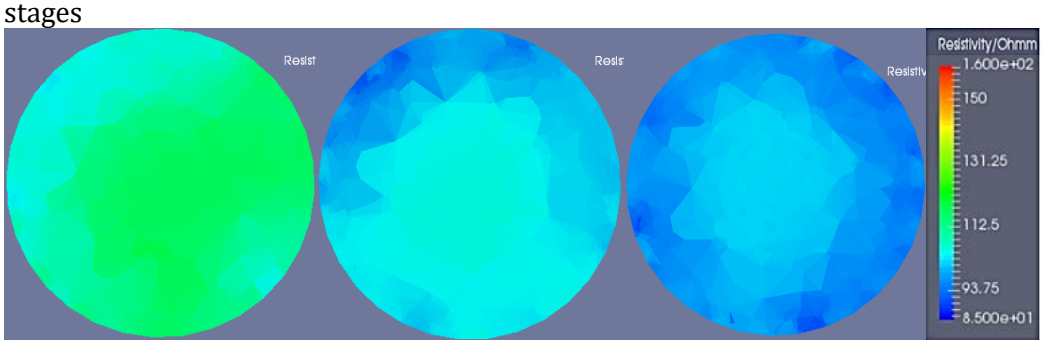

(No load) (25 kPa) (50 kPa)

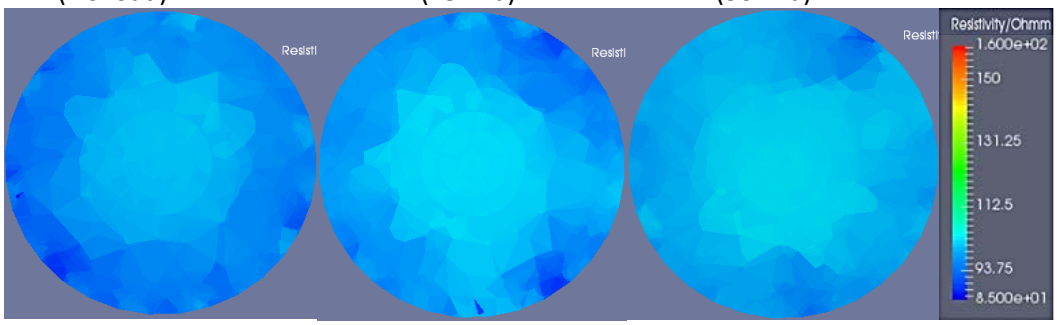

(100 kPa) (150 kPa) (300 kPa)

Figure 6.45: Inversion results of Ring 5 for tank filled with soil and OSC under different loading stages

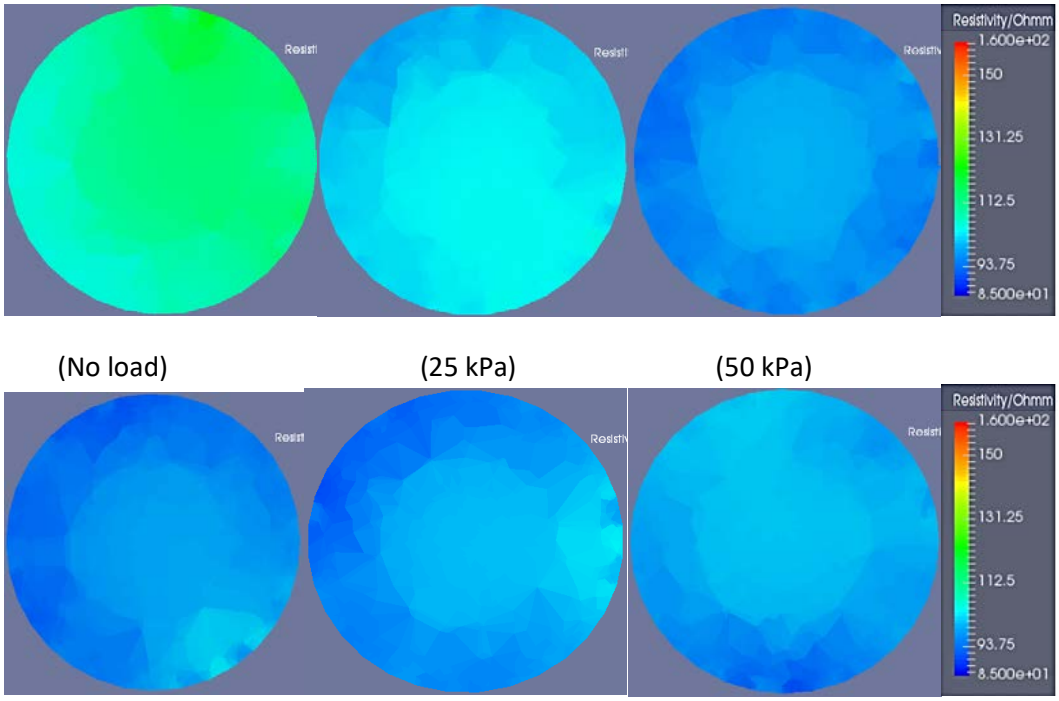

Figure 6.46: Inversion results of Ring 6 for tank filled with soil and OSC under different loading stages

6.3.1.5. Test 15, Resistivity Measurements for the ESC Test Chamber

In comparison to tank associated with OSC, imaging the physical properties of the ESC tank gave a different trend, as the resistivity magnitudes decreased with increasing load for all loading stages and all rings. That could be because of the enhancement achieved by the encasement with the geotextile, which makes the stress concentration collect more on the column than that on the surrounding soil and as a result limits the bulging effect. The low stress concentration on the soil makes the latter experiences less densification and in such case that would leads to less water moving around the soil particles, and so keeping the quantity of the fluid and the associated dissolved salts at in same concentration or even higher. This being associated with continous water movement upward the soil layers. The higher fluid volume and the associated salts changes, increase the measured conductivity and consequently decreasing the resistivity values.

Also, the lower ERT measured values of ESC chamber if compared to those of OSC chamber could be as a result to the higher degree of saturation of the soil surrounding the geotextile-column in comparison to that of the ordinary column as shown in the physical model, see Section 6.2.3.8. Figures 6.47 to 6.52 show the data corresponding to all six rings around the tank with respect to loading increments. Also, see Figs 6.31 and 6.34 in Section 6.3.1.1.

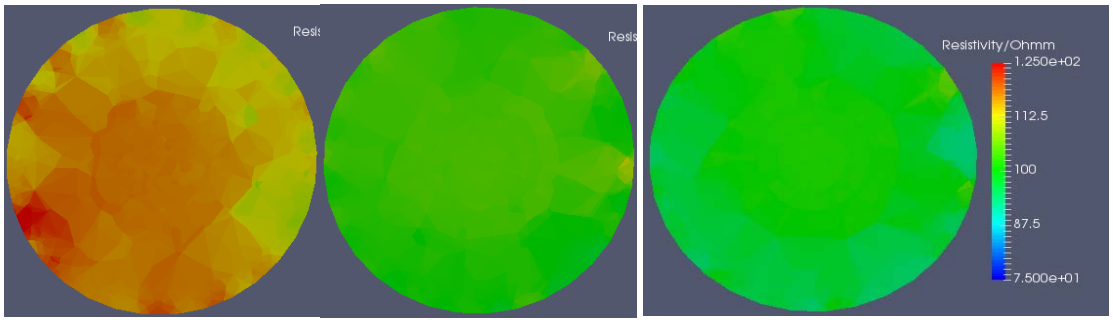

(No load) (25 kPa) (50 kPa)

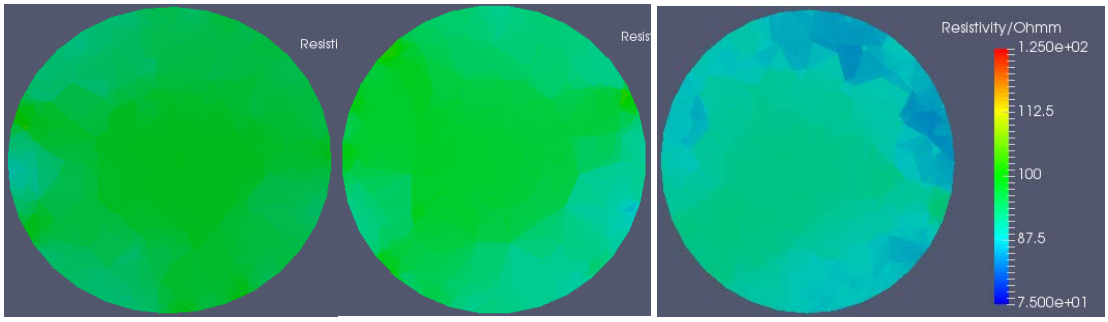

(1000 kPa) (150 kPa) (300 kPa)

Figure 6.47: Inversion results of Ring 1 for tank filled with soil and ESC under different loading stages

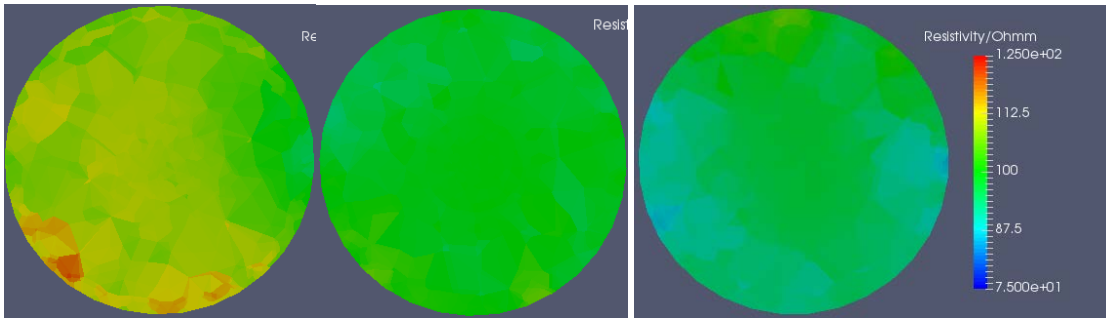

(No load) (25 kPa) (50 kPa)

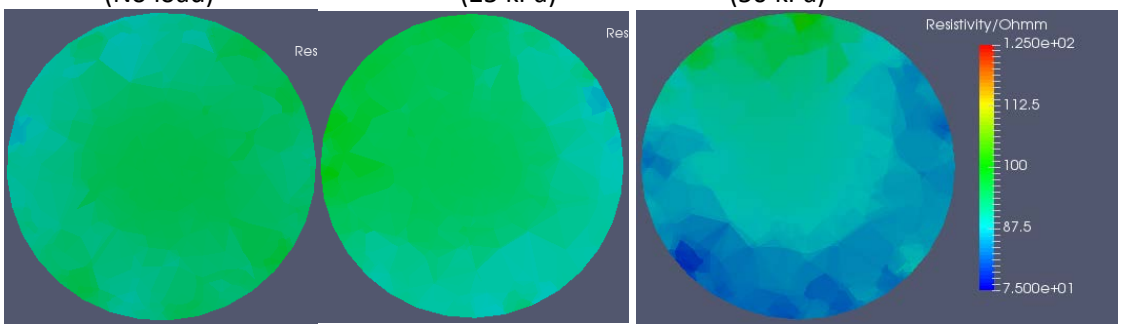

(100 kPa) (150 kPa) (300 kPa)

Figure 6.48: Inversion results of Ring 2 for tank filled with soil and ESC under different loading stages

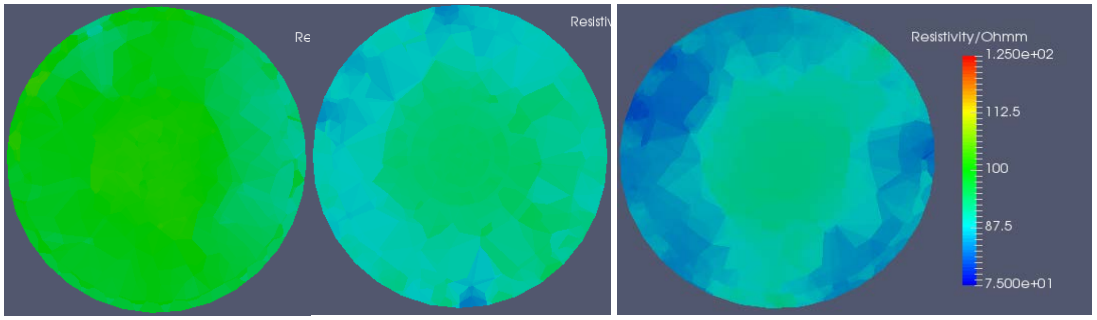

(No load) (25 kPa) (50 kPa)

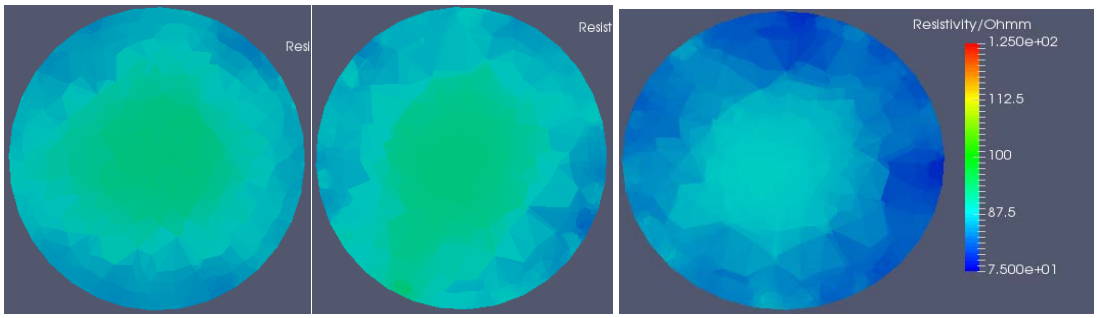

(100 kPa) (150 kPa) (300 kPa)

Figure 6.49: Inversion results of Ring 3 for tank filled with soil and ESC under different loading stages

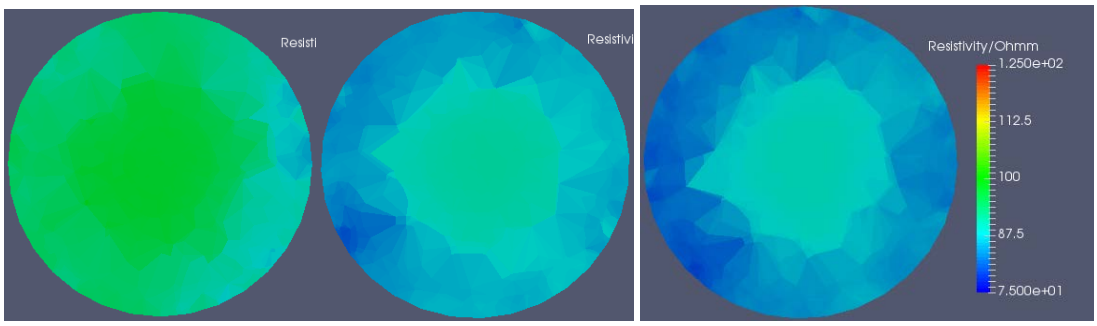

(No load) (25 kPa) (50 kPa)

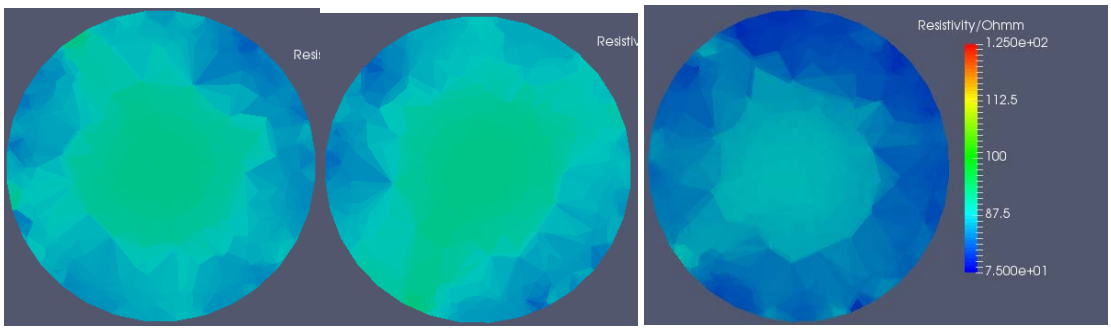

(100 kPa) (150 kPa) (300 kPa)

Figure 6.50: Inversion results of Ring 4 for tank filled with soil and ESC under different loading stages

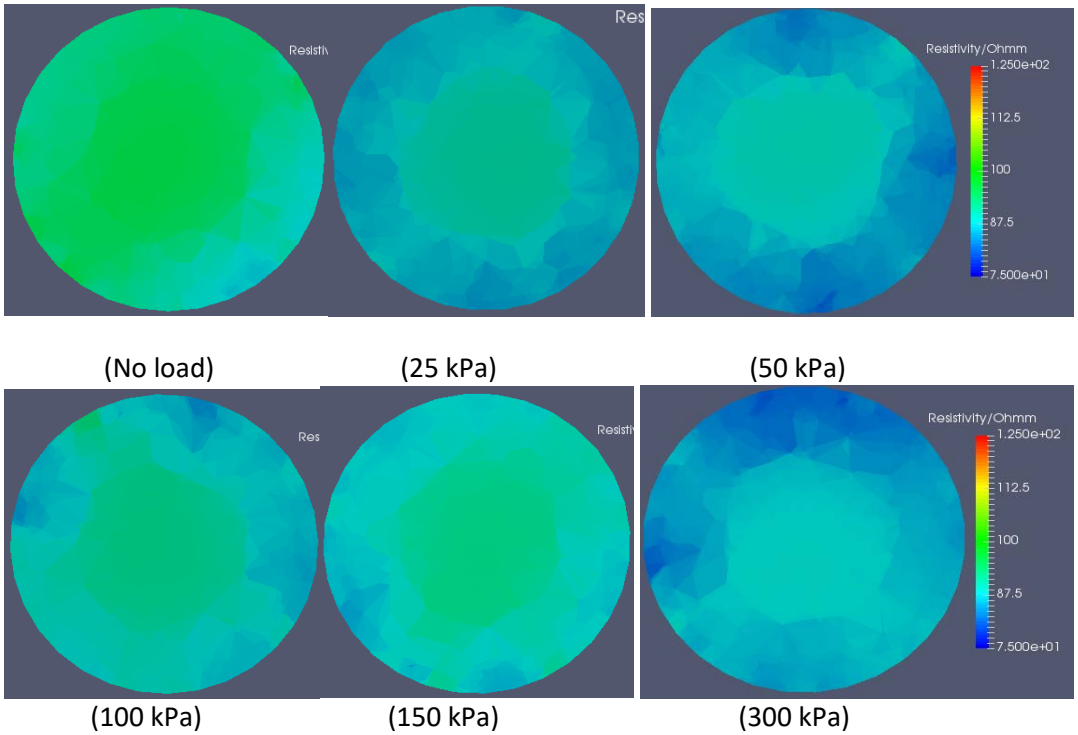

Figure 6.51: Inversion results of Ring 5 for tank filled with soil and ESC under different loading stages

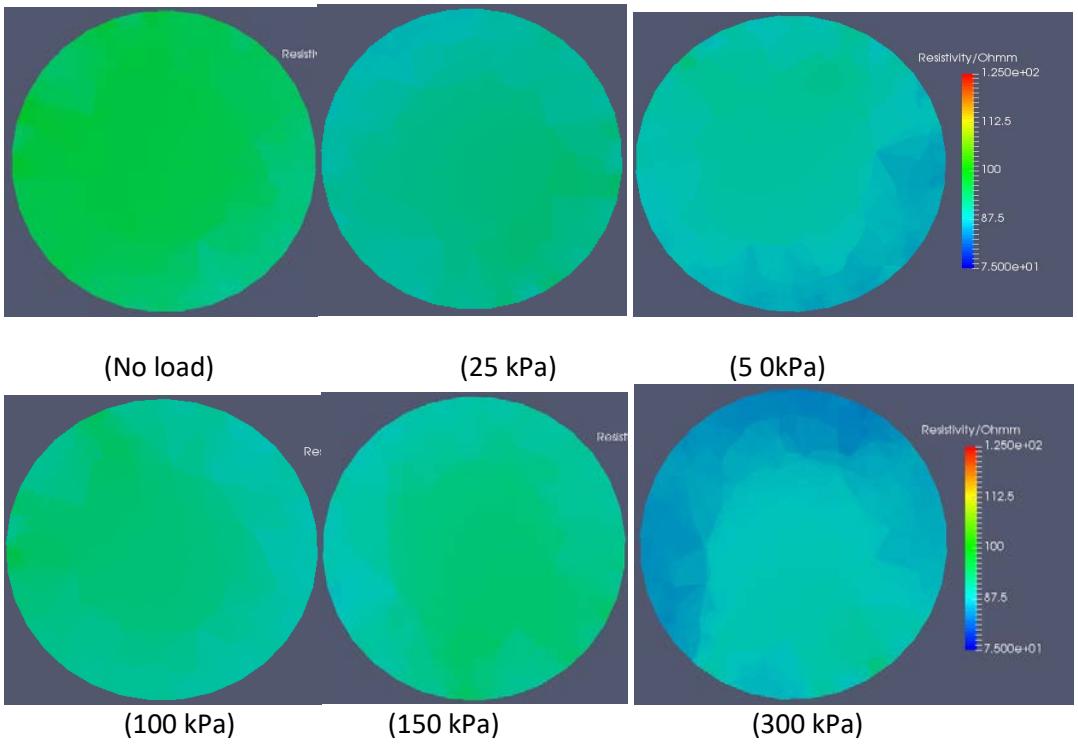

Figure 6.52: Inversion results of Ring 6 for tank filled with soil and ESC under different loading stages

6.3.2. Vertical Arrays

The results of the electrical resistivity are deduced based on the second configuration of the sixteen electrodes fixed in two vertical arrays along each test chamber, as was explained in Section 5.3. As those configurations did not follow the standard layout recommended in BERT, it was not possible to perform the corresponding inversion. Under such circumstances, the outcomes have not been inverted, but they were displayed as a function of the apparent resistivity instead. The resistivity of the soil in each tank, against the number of the reading (see Table D-2 in Appendix D), is presented in Fig. 6.53. For most readings, and as a general trend, it was observed that the resistivity increased with increasing stress, except at some points which reflect, according to their patterns, the physical properties of the soil closest to the electrodes. The results for the three chambers at the start of the test (under no load) and at the end (under a stress of 300 kPa) are shown in Fig. 6.54. It can be seen that the resistivity of the ESC tank recorded the lowest values; while those for the US and the OSC tank were higher. Such behaviour matches the water content profile obtaining at the end of the experiment and could be attributed to the higher degree of saturation of the surrounded host ground of ESC in comparison to US or OSC.

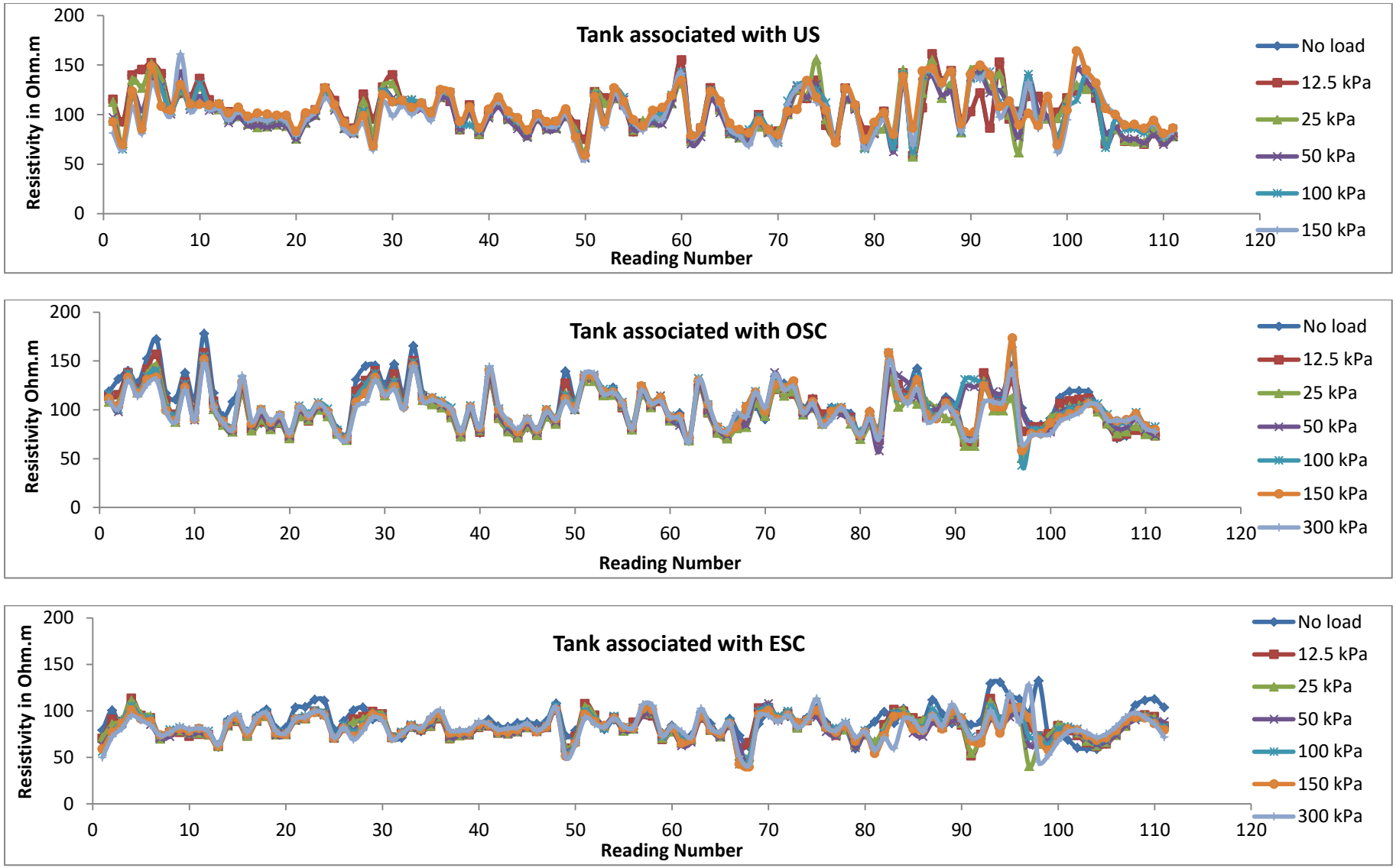

Figure 6.53: Resistivity values in the three chambers according to the configuration of the vertical arrays

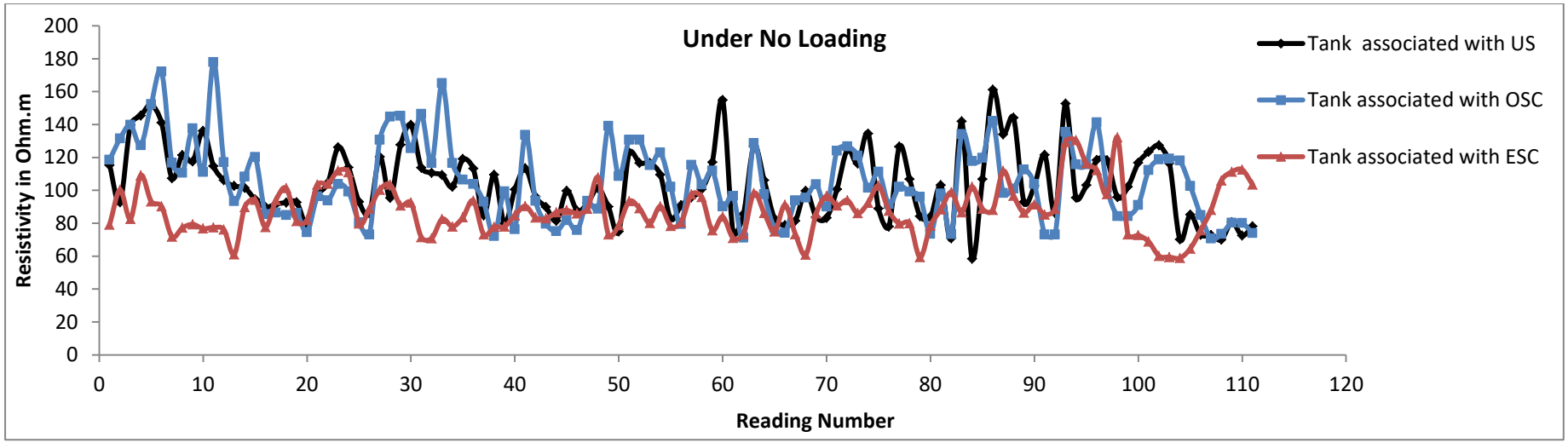

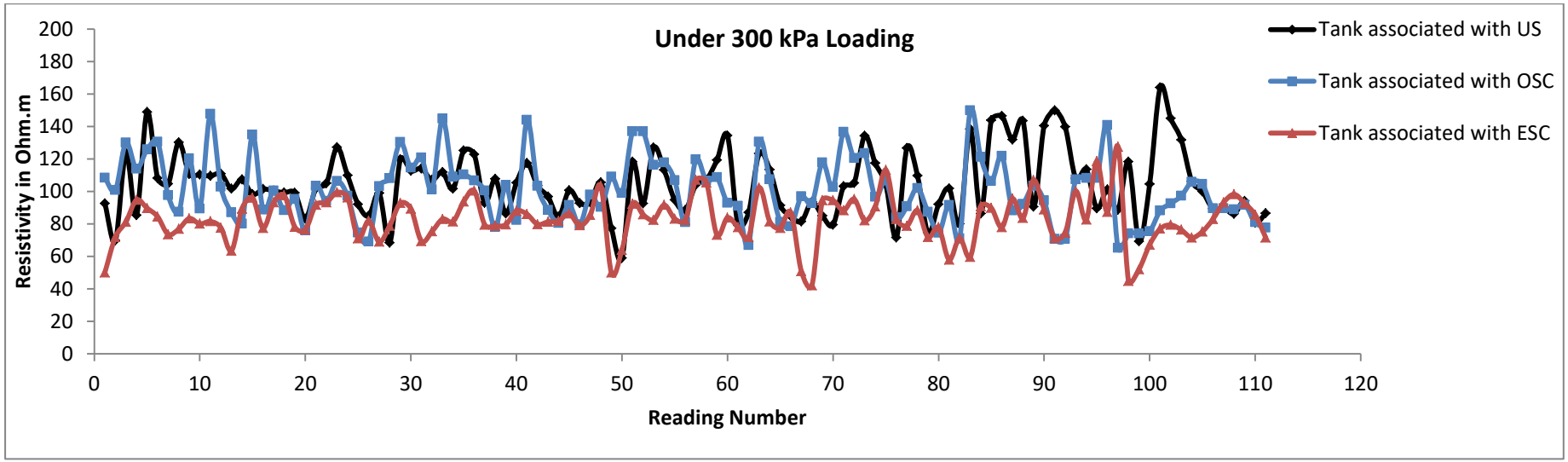

Figure 6.54 : Resistivity of the three chambers under no stress and stress of 300 kPa (vertical arrays)

6.4. Summary

Results and observations of the physical model and the geophysical investigation were presented and discussed in the previous sections of this chapter. The results showed that the behaviour of untreated collapsible soil US, soil treated with an OSC, and soil treated with an ESC under different loading and wetting conditions.

The physical model showed that OSC enhanced the stress- settlement behaviour of the treated collapsible soil in dry conditions. However, it was unsuccessful in supporting the inundated host soil as a result of loss the required confinement. In the dry conditions when no water was introduced to the composite cell of the soil and column, the drop in settlement of the OSC foundation in comparison to that of US reached a value of 150%. Upon flooding the system with 2.73 L and 6.15 L, the enhancement in the ultimate bearing capacity was insignificant such that it reported values of 14% and 20% respectively.

In addition to this, the physical model indicated a remarked improvement upon using ESC as geotextile increases the ultimate bearing capacity significantly, under any soaking conditions with or without flooding with water. At the dry state, the decrease in settlement in of the ESC foundation in comparison to US foundation was 230%. This was greater than that noticed for the OSC. By adding water to the system with 2.73 L and 6.15 L, the enhancement in the ultimate bearing capacity of the ESC was significant if compared to that of US foundation, it reached values of 49% and 77% respectively. Under the same soaking conditions, the settlement features were improved considerably upon encasing with the geotextile, such that the improvement factor increased to 216% and 285% respectively.

The failure profile of the physical model at the end of the experiment indicated that OSC expanded laterally into the upper stratums. At the higher degree of saturation of the host soil, the affected bulging zone extended more. However, a relatively consistent diameter along the column length was noticed, the column expanding was limited because of presence of the geotextile.

Also according to the physical model laboratory experiments, the improvement in load settlement behaviour obtained from using OSC or ESC did not vary if soaking occurred prior or post loading. Upon inundation at stress of 100 kPa, the ultimate bearing capacity of foundation of US, OSC, and ESC recorded 144, 172, and 251kPa respectively in comparison

to 140, 168, and 248 kPa respectively reported when the flooding with water occurred at the beginning of the test.

For the same physical model on the soil surface, the vertical deflection of the nearest observation points to the foundation recorded the largest deflection for OSC foundation while the lowest were for ESC foundation. The variations in values between them attributed to the stress concentration on the soil which is greater in case of OSC.

Results of the geophysical model showed that soil collapsibility upon wetting influenced the resistivity values due to associated variations in soil densification and water content. Conditions of stress and inundation affected the current passing through the clay bonds and bridges between the soil particles. The resistivity of soil under a stress increases, when the clay bridges to break, while it decreases with increasing the degree of saturation due to increasing the volume of voids occupied by the water.

During drainage stage, the resistivity increases, this is attributed, to the salt crystallisation which causes an increase in the tortuosity of the soil, or could also be due to decrease in in the dissolved salts.

Imaging the geophysical properties of the ESC tank showed decreasing in resistivity magnitudes for all loads and rings. This could be as a result of the encasement, which limits the bulging effect, and to the higher degree of saturation of the soil.

The measurement of the vertical arrays demonstrated an increasing in resistivity values with respect to increasing the applied stresses, excluding some points which reflect the geophysical properties of the soil nearest to the sensors. Also, Resistivity measurements in US and OSC tanks showed higher values in comparison to ESC tank because of the degree of saturation of the soil.

Mapping geophysical properties of the soil, in combination with conventional laboratory procedures, have the potential to be a valuable scientific procedure. However, to consider it as a standard tool, further investigations and modifications are required.

CHAPTER SEVEN

THE ANALYTICAL MODEL

7.1. Introduction

This chapter summarises the derivation of the adopted analytical model to compute the ultimate bearing capacity of the encased stone column installed in collapsible soil. The influence of the matric suction and the degree of saturation of the soil are considered. The latter effects for different properties that are likely effect the response of the encasement are assessed by running a code in Matlab, which has been developed for this purpose and to validate the experimental lab results.

7.2. The Adopted Analytical Model

Due to its advantages, including its simplicity and applicability for showing the influence of several factors governing a solution, the analytical approach has been widely adopted and preferred over an empirical or a purely numerical approach (Ayadat, 1990).In this study, an analytical solution was adopted and developed for the prediction of the ultimate bearing capacity for an encapsulated stone column installed into partially saturated collapsible soil, because previous work adopted a model suitable for saturated cases, while the impact of the severity of the soil collapsibility on overall behaviour was not adequately addressed, especially regarding the effect of matric suction on the shear strength of the treated collapsible soil after soaking with water. Moreover, the degree of saturation, or the level to which the underground water would be expected to rise through the soil, had not been taken into account.

7.3 Basic Theory behind the Derivation of the New Analytical Model

Greenwood (1970) produced an equation to calculate the ultimate vertical stress taken by a stone column installed into soil, assuming plain strain loading, as follows:

$$\sigma_v = k_p(F_i.\ \tau + \sigma'_{ro}) \qquad (7.1)$$

Where σ_v is the vertical stress of the soil and k_p is the Rankine passive pressure coefficient for the column material

$$k_p = tan^2\left(\frac{\pi}{4} + \frac{\phi'_c}{2}\right) \qquad (7.2)$$

Where ϕ_c' is the effective angle of shearing resistance of the stone column material and F_i is the factor of influence which equals 4, according to Hughes & Withers (1974). τ is the shear strength of the soil, in many studies this has been taken as undrained shear strength, see Hughes & Withers (1974). This is because it was calculated based on the total shear stress. However, if drained tests to be carried out, it is derived from effective shear strength parameters using Terzaghi"s equation (Terzaghi (1936)) below, see Ayadat (1990) who used triaxial consolidated drained test and used the following equation:

$$\tau = c' + (\sigma_n - u_w)\, tan\emptyset' \qquad (7.3)$$

Where c' and $\emptyset'$ are the soil effective shear strength parameters, (σ_n-u_w) is the effective normal stress, and σ'_{ro} is the effective lateral soil stress, which can be computed as follows:

$$\sigma'_{ro} = k_o(\gamma h) \qquad (7.4)$$

Where k_o is the coefficient of lateral earth pressure at rest (1-sinϕ'), γ is the unit weight of soil, and h is the soil depth.

To model a stone column reinforcing a collapsible soil in the potential presence of water, it was crucial to develop a reliable equation that represents such a situation, taking into consideration the following points:

1- The fact that collapsible soil is unsaturated soil, in which matric suction pressure is the governing force and plays a significant role in the collapse mechanism (Brink, 2011).
2- Depending on whether the soil is dry, wet, or partially saturated, as shown in Fig. 7.1, the inundation conditions should be considered.
3- The lateral stress of the geosynthetic should be added.

Based on the aforementioned points, it is appropriate to use the equation produced by Bishop (1959). He developed Tarzaghi"s equation (eq. (7.3)) for determining the drained shear strength of unsaturated or partially saturated soil, based on two independent stress state variables: the normal stress (σ_n-u_w) and the matric suction stress (u_a-u_w), as follows:

$$\tau = c' + (\sigma_n - u_w)tan\phi' + (u_a - u_w)xtan\phi' \quad (7.5)$$

Where x is a parameter that depends on the degree of saturation, ranging from 0 for fully saturated soil to 1 for totally dry soil. Also, the lateral soil stress should be computed

according to the case of inundation, which will be sensitive to the depth of soaking and the corresponding unit weight of soil, represented by the dry unit weight in the case of no soaking, or by γ_s (submerged unit weight of soil, which equals the difference between the saturated unit weight of soil and the unit weight of water = γ_{sat} - γ_w), in the case of soaking. The encasement effect: according to Castro & Sagaseta (2011), the unit cell is compressed in a vertical direction, and the encasement can only take tension because it is a flexible membrane, so the encasement acts only in the radial direction, and, as a result of equilibrium and the compatibility conditions, the radial encasement pressure can be calculated from the following equation:

$$\sigma_{encasement} = \frac{T_s t}{{r_c}^2} \qquad (7.6)$$

Where T_s is the tensile strength, t is the thickness of the geotextile, and r_c is the radius of the stone column. So, if we add eq. (7.6) to the term corresponding to the lateral stress of the soil, considering an additional lateral stress as was given by Ayadat and Hanna (2005) into eq. (7.1), and by substituting eq. (7.5) into eq. (7.1) too, it yields:

$$\sigma_v = k_p[F_i[c' + (\sigma_n - u_w)tan\phi' + (u_a - u_w)xtan\phi'] + \sigma'_{ro} + \frac{T_s t}{{r_c}^2}] \qquad (7.7)$$

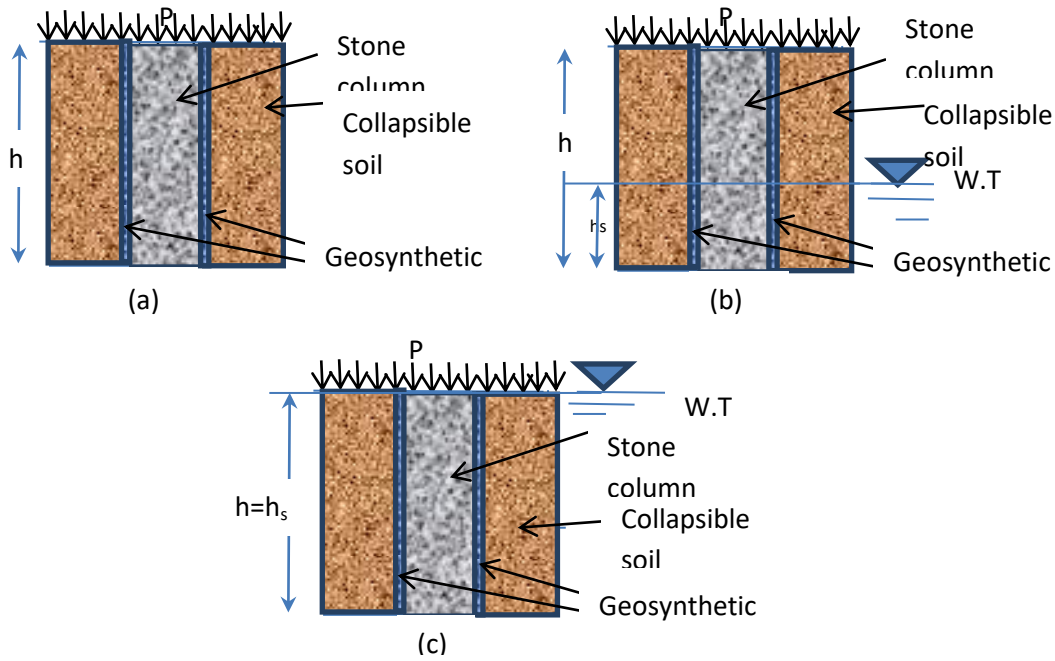

Figure 7.1: Unit cell model of encased stone column installed in collapsible soil (a) dry condition (b) partial saturation (c) full saturation

7.4 MATLAB Code

A piece of code in MATLAB was developed to compute the bearing capacity of the combined cell, including the stone column and surrounding soil (eq. (7.7)), in the previous section. The variations in the ultimate bearing capacity were calculated with respect to different suction and soaking conditions. The parameters related to the soil, stone, and geosynthetic that are used in this script; the corresponding symbols, are listed in Table 7-1. The full MATLAB script is presented in Appendix (E).

Table 7-1: Parameter values and symbols used in the MATLAB script

Soil	Symbol in the Matlab Script	Definition and Units	Value
	phi_sat	Effective angle of internal shear resistance of the soil in case of saturation in degrees	28.9^o
	c_sat	Effective cohesion of the soil in saturated case in kPa	4
	T	Drained shear strength of the soil	
	gamma_d	Dry unit weight of soil in kN/m^3	13.7
	gamma_sat	Saturated unit weight of the soil in kN/m^3	18.5
	gamma_w	Unit weight of water in kN/m^3	10
	Gs	Specific gravity of the soil	2.64
	e	Void ratio of soil	0.93
Stone	d	Diameter of the stone column in m	0.04
	L	Length of the stone column in m	0.36
	phi_stone	Angle of internal shear resistance of the column fill material in degrees	39.0^o
Geosynthetics	Ts	Tensile strength of the geosynthetic in kN/m	17.2
	t	Thickness of geosynthetic in m	0.0005

7.5 Sensitivity of the Analytical Model

By running the code, the model of the metastable soil reinforced with geosynthetic was tested to assess its sensitivity to the main parameters likely to affect the magnitude of the ultimate bearing capacity of the treated foundation under different soaking conditions. The influence the depth of inundation and the matric suction were investigated for both unreinforced and reinforced stone columns. The degree of saturation is linked to depth of the inundation in the

soil profile such that $s=h_s/h$; where s: degree of saturation, h_s: the inundated depth of the soil, and h: the total soil depth. The matric suction ranges corresponding to the water content were deduced from the soil water characteristic curve obtained from the filter paper experiment described in Section 3.14. The outcomes confirmed that using an encased stone column instead of the conventional one improves system behaviour and increases the bearing capacity, to an outstanding degree when soaking the soil layer with a large amount of water.

The ultimate bearing capacity decreases with increasing water depth through the soil layer. This is due to the dropping shear strength, which decreases significantly as a result of water inclusion. Conversely, the ultimate bearing capacity increases dramatically when the initial suction of the soil increases, as in cases of partial saturation; this is shown in Fig. 7.2 and Fig. 7.3. Factors that are likely to affect the response of the encasement, such as the tensile strength of the geotextile, the diameter of the reinforced column, and the angle shear resistance of the column material, were assessed. The corresponding results and their analyses are entirely presented in the following sections (7.5.1 to 7.5.3)

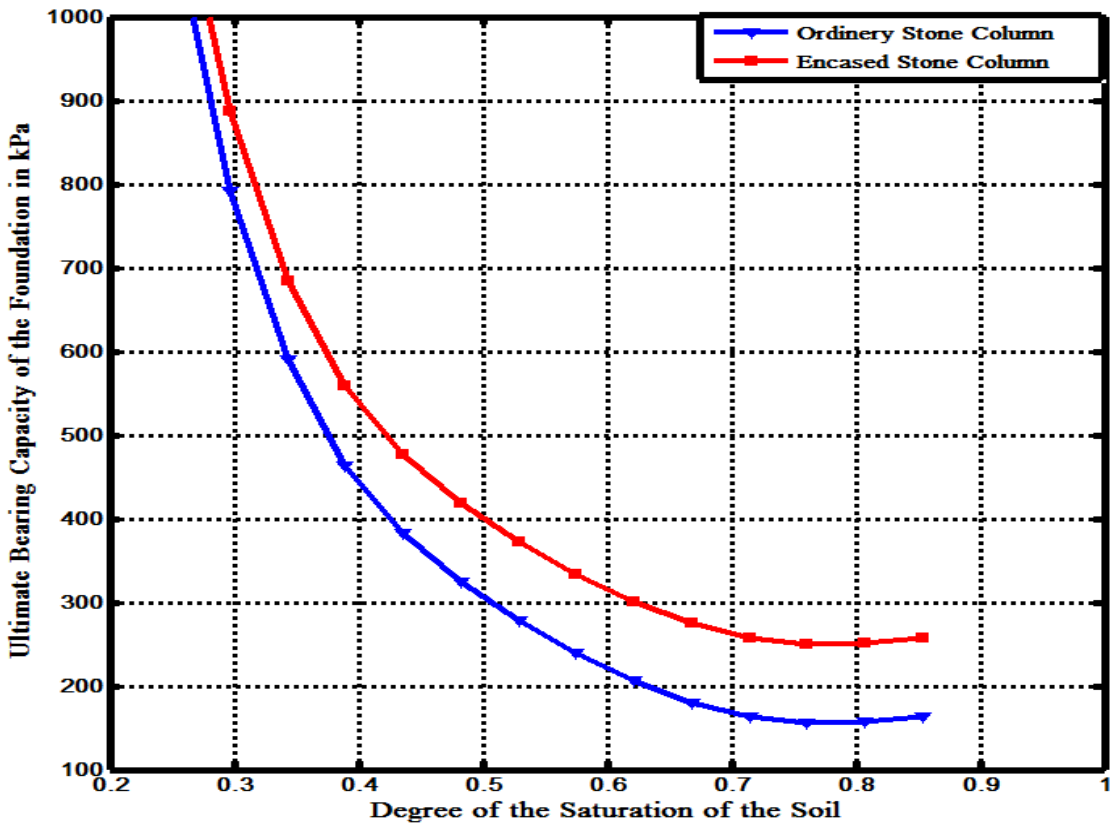

Figure 7.2: Bearing capacity of OSC and ESC for different degrees of saturation

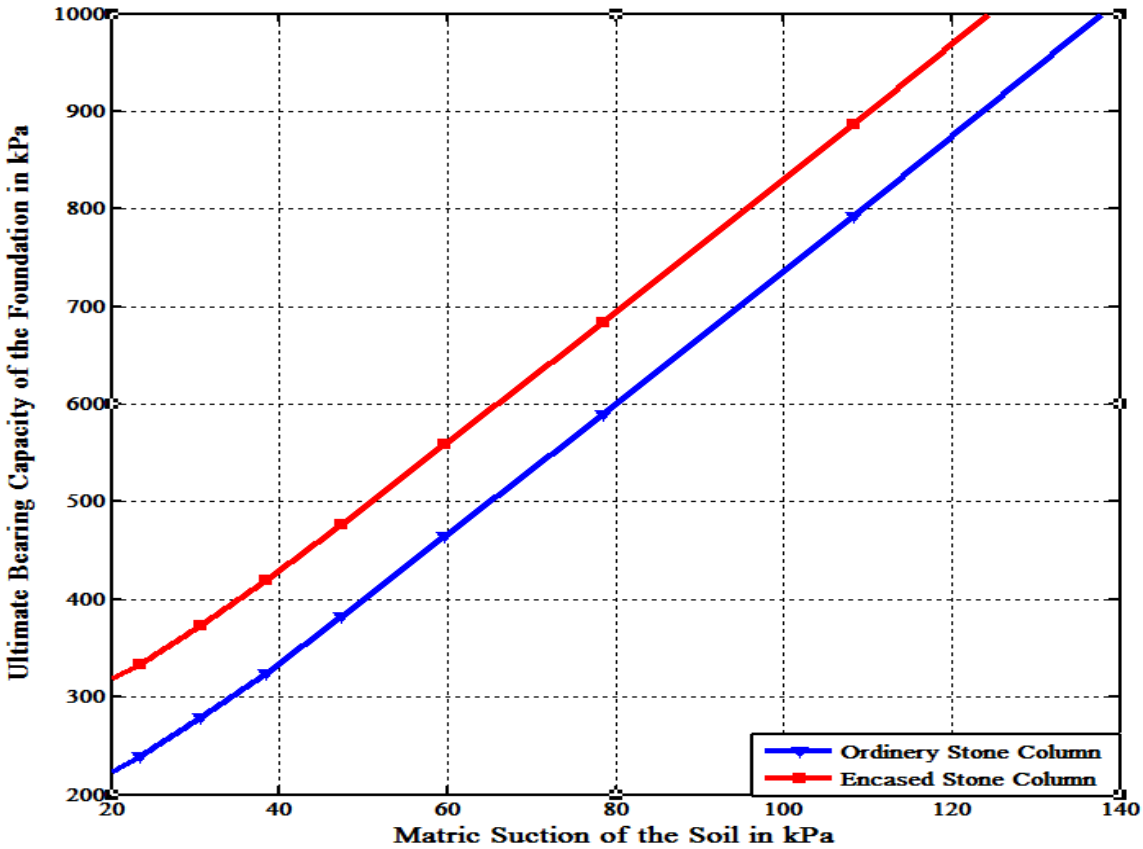

Figure 7.3: Bearing capacity of OSC and ESC for different degrees of saturation

7.5.1. Influence of the Tensile Strength of the Geotextile on the Ultimate Bearing Capacity of the Encased Foundation

For different magnitudes of geosynthetic tensile strength, the ultimate bearing capacity against degree of saturation and matric suction are determined as shown in Figs. 7.4 and 7.5 respectively. The outcomes indicated that increasing the tensile strength of the geotextile improves the ultimate bearing capacity. This is in agreement with the work done by Ayadat and Hanna (2005) on an encased stone column inserted into sandy collapsible soil. In this study, the enhancement was proportional to the degree of saturation of the soil in a nonlinear trend. A greater improvement is achieved under a higher degree of saturation, while for the same degree of matric suction, the ultimate bearing capacity of the reinforced foundation increased with increasing tensile strength (linear trend).

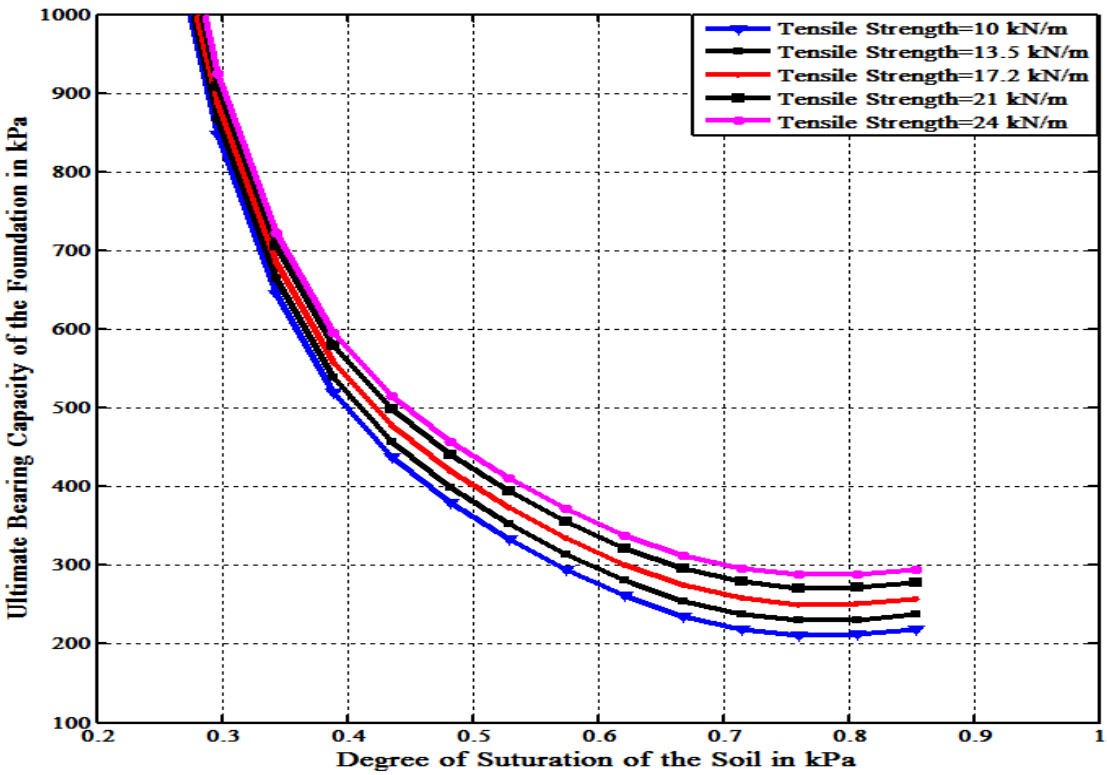

Figure 7.4: Bearing capacity of the foundation reinforced with a geotextile versus tensile strength of the geotextile (for different degrees of saturation)

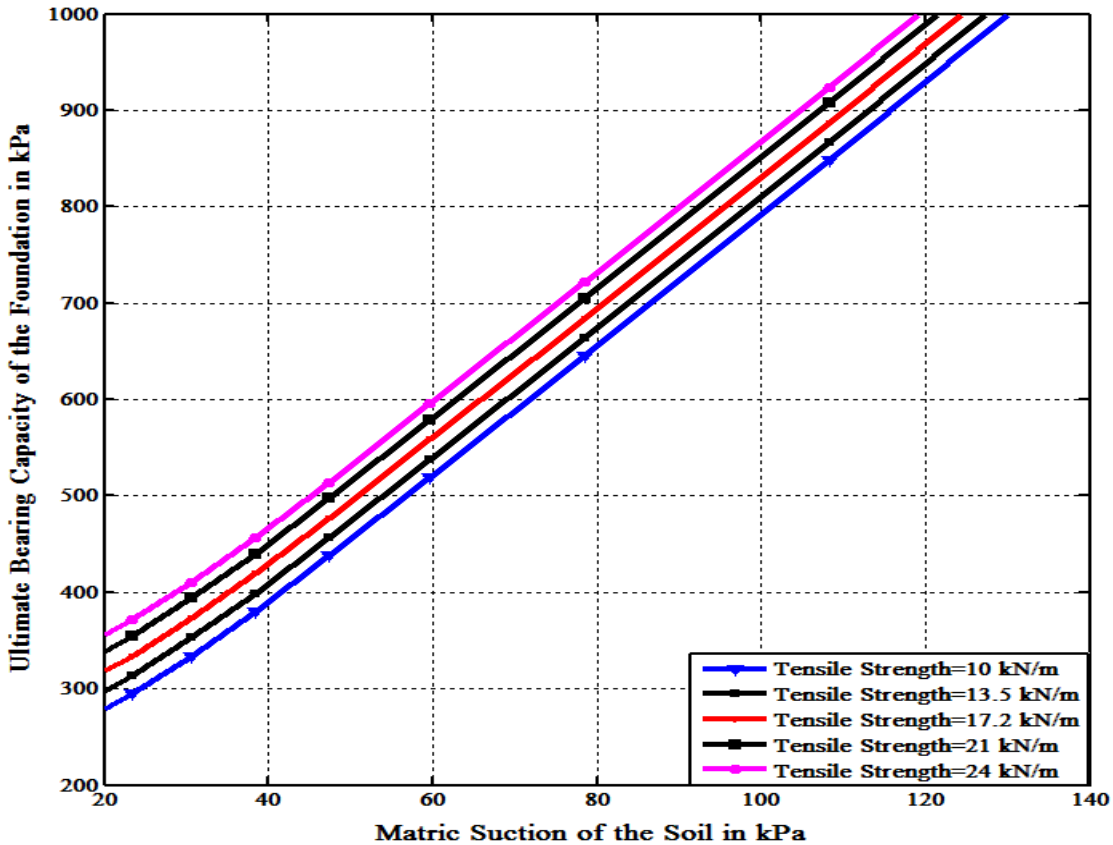

Figure 7.5: Bearing capacity of the foundation reinforced with a geotextile versus tensile strength of the geotextile (for different suction)

7.5.2. Influence of the Stone Column Diameter on the Ultimate Bearing Capacity of the Encased Foundation

For the same degree of saturation or matric suction, smaller diameters show superior performance in increasing the bearing capacity. The reason for this is the development of larger additional confining stresses in smaller diameter reinforced columns; see the relationship between the encasement confining stress and the column‟s radius (equation 7.6). This agrees with most laboratory studies that have looked at the influence of the diameter of the encased stone column when treating soft soil (e.g. Ali et al., 2010; Uttam et al., 2013). For data corresponding to an individual diameter, increasing the degree of saturation of the host ground leads to a decrease in the ultimate load carrying capacity, while increasing matric suction causes an increase in the bearing capacity of the foundation. See Figs. 7.6 and 7.7.

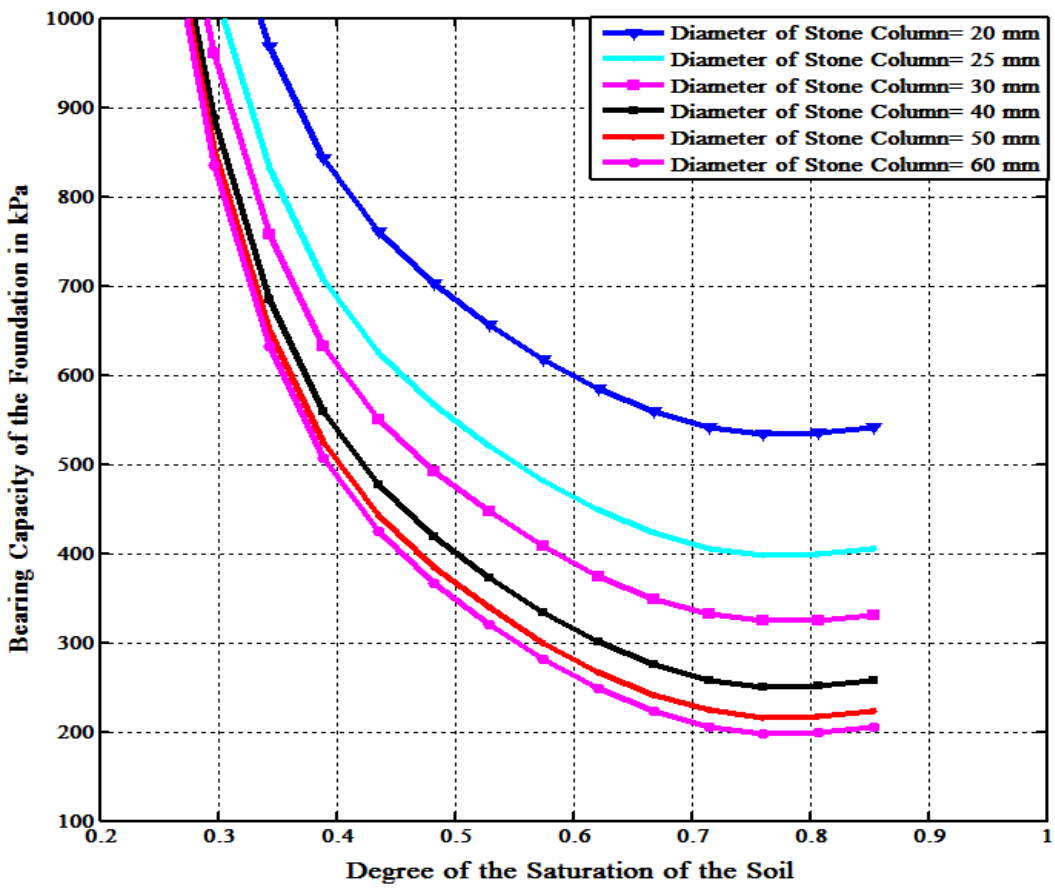

Figure 7.6: Bearing capacity of the foundation reinforced with a geotextile versus degree of saturation (for different column diameters)

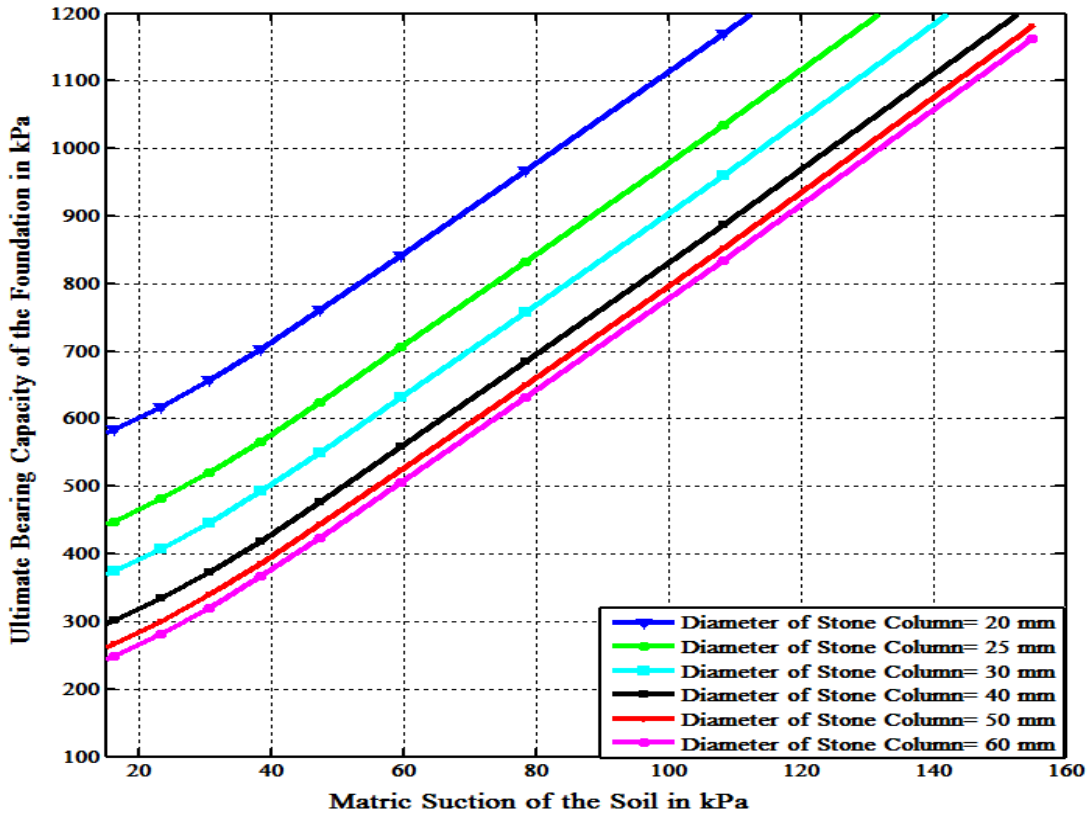

Figure 7.7: Bearing capacity of the foundation reinforced with geotextiles versus matric suction (for different column diameters)

7.5.3. The Influence of the Angle of Internal Shear Resistance of the Column Material on the Ultimate Bearing Capacity of the Encased Foundation

The general trend of the results indicated that increasing the angle of the column material led to an increase in the bearing capacity of the reinforced foundations. This has been established by many investigators, the most famous being Priebe (1995), who related the improvement in the stone column foundation to both the internal shear angle of the fill material and the replacement ratio. In this research, it was found that for a certain angle of internal shear resistance, increasing the degree of saturation to a certain value causes a remarkable decline in bearing capacity, while above that certain value of saturation, the bearing capacity showed a levelled trend. Conversely, the ultimate bearing capacity of the foundation increased with increasing matric suction, and was outstanding at higher suction. See Figs. 7.8 and 7.9.

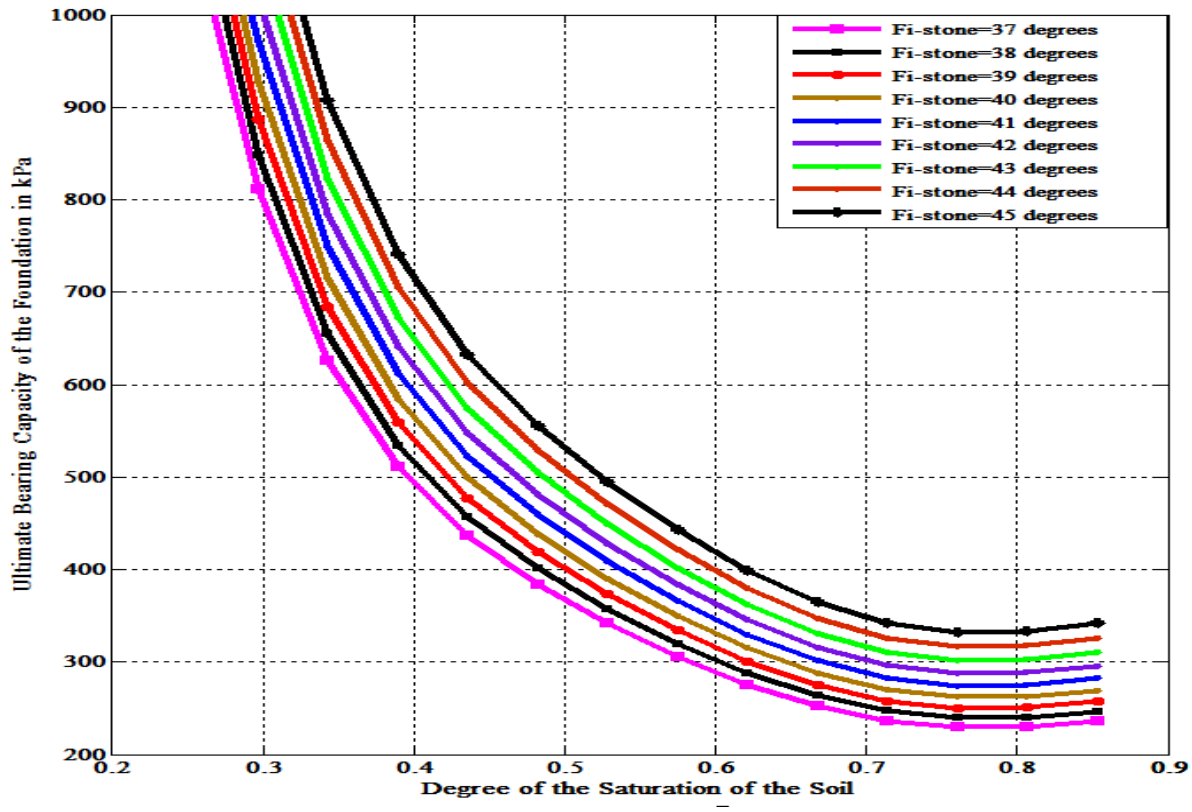

Figure 7.8: Bearing capacity of the foundation reinforced with a geotextile versus degree of saturation (for different angles of internal friction of the stone column)

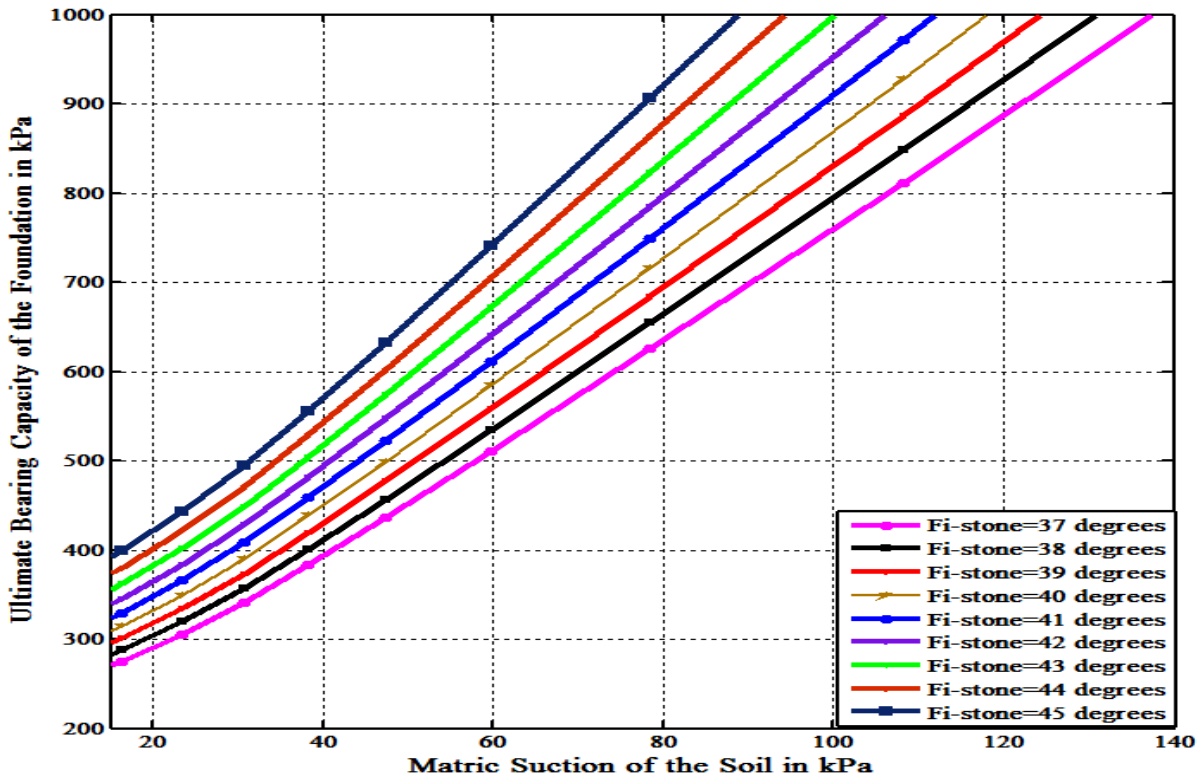

Figure 7.9: Bearing capacity of the foundation reinforced with a geotextile versus matric suction (for different angles of internal friction of the stone column)

7.6. Validation of the Experimental Results

Equation 7.1 which is developed in this study to give the new analytical solution, was used already by many investigators to predict the bearing capacity for full scale tests in field when the loaded area is only applied on the effective diameter of the column and surrounding soil according to a specific spacing pattern, see Greenwood (1970) and Hughes & Withers (1974). So, the computed results from the analytical solution developed, which was illustrated in the previous sections, could be compared directly to the results of the laboratory tests when the physical model was subjected to load partially over the soil surrounding the column as same as field situations. It was shown that there was an acceptable convergence between experimental and theoretical results. The error bounds were between -15% and +11%.

Table 7-2: Comparison between the experimental results and the theoretical calculations

Lab Test No.	Type of stone column *	Degree of saturation of the soil	Inundation pattern with respect to loading	Resistivity measurem-ents	Bearing capacity of the foundation		Error percen tage %
					Theoretical values	Experimental values	
No.5	OSC	0.5	Prior	Not taken	322	355	+10
No.6	ESC	0.5	Prior	Not taken	414	460	+11
No.8	OSC	0.69	Prior	Not taken	196	168	-14
No.9	ESC	0.69	Prior	Not taken	288	248	-14
No.11	OSC	0.69	After 100 kPa	Not taken	196	172	-12
No.12	ESC	0.69	After 100 kPa	Not taken	288	251	-13
No.14	OSC	0.69	Prior	taken	196	168	-14
No.15	ESC	0.69	Prior	taken	288	244	-15

7.7. Summary

The previous sections of this chapter showed the development of the analytical solution adopted to determine the ultimate carrying capacity of collapsible soil reinforced with an encased stone column. The model was tested for different degrees of saturation and matric suction. The results indicated that bearing capacity increases when using an encased stone column under varying degrees of soaking with water, increasingly so at higher levels, whilst the ultimate carrying capacity showed a remarked increase when increasing the initial suction of the soil. The effects of the tensile strength of the geotextile, the diameter of the reinforced column, and the angle of shear resistance of the column material on the bearing capacity of the encased stone column were studied. Outcomes stated that the bearing capacity for a specific degree of saturation or initial matric suction increases when increasing the geotextile tensile strength, decreasing the column diameter, and increasing the angle of shear resistance of the fill material. Moreover, results established satisfactory agreement between experimental and theoretical results; the error bounds recorded values between -15% and +11%. However, the analytical method was associated with some constraints specifically it does not take the effect of the soil outside the effective diameter of the loaded soil and column. There are no restrictions to the column geometry in relation to spacing pattern, for example bearing capacity increases with decreasing the column‟s diameter, the model does not have a look value of the diameter, instead that should be figure out according to area replacement ratio in advance.

CHAPTER EIGHT

CONCLUSIONS AND RECOMMENDATIONS

8.1. Introduction

This research presented a detailed study highlighting key aspects affecting the performance and monitoring the internal profile of composite system of the encased stone column within host artificial collapsible loess soil, under different wetting and loading conditions. The aim was to provide a better understanding of the behaviour of the reinforced foundation when inserted into a collapsible soil. To fulfil this aim, the investigations included four main tasks: modelling the host collapsible ground, conducting a conventional lab testing programme, performing a geophysical inspection, and developing an analytical solution. After accomplishing the aforementioned tasks individually, obtaining corresponding results, and analysing and integrating them, the conclusions and recommendations are summarised in the following sections (8.2 and 8.3).

8.2. Conclusions

8.2.1. Conclusions from Material Development

The developed loessial deposits were formed artificially in the laboratory, by compacting the ground silica which had already been mixed with clay, with dry-of-optimum water content, and then leaving the compacted sample to be dried off so that bonds were able to form. The method was demonstrated to be a process of creating a large uniform loess model. A series of single and double oedometer tests were conducted to examine the collapse behaviour of the artificial loess.

Results showed that the collapsibility of silica flour increases when increasing clay content, void ratio, and period of drying. The ideal water content preparation was found to be 12%. The collapse behaviour of the mixture was compared to another mixture of silty soil of a limestone geological origin, and had almost the same size of ground silica particles; it was found that soil consisting of ground silica and clay was the closest in behaviour to a reference natural collapse deposit before and after soaking. It was reported that considering the particle loess size alone can cause a misleading and untruthful indicator of the collapse mechanism of a meta-stable soil. So, the key conclusion is the importance of taking geological origin into consideration.

The representation of the host ground was achieved by mixing 80% ground silica with 20% English China clay at 12% water content, giving a 5.1% collapse potential.

8.2.2. Conclusions from the Physical Model

The performance and failure mechanism of a footing-type foundation resting on untreated collapsible soil US, soil treated with an OSC, and soil treated with an ESC has been examined under different soaking and loading conditions. Such observations have not been considered previously for fine metastable soil associated with a relatively high capillary rise.

The outcomes have highlighted important aspects in the behaviour of a stone column reinforced with geosynthetics in a loess deposit. The following key findings were revealed by the experimental programme:

The OSC improved the ultimate bearing capacity of the collapsible soil in dry conditions. However, it failed to support such a soil when inundation was introduced. For the dry case, under the final increment of stress 800 kPa, the foundation of the OSC did not reach its settlement failure criteria but the reduction in settlement in comparison to the untreated soil reached a value of 150%. When amounts of 2.73 L and 6.15 L of water were introduced to the cell, the improvement in the ultimate bearing capacity achieved (at settlement equalling 10% of the diameter of the foundation) was only 14% and 20% respectively.

Encasing the stone column within a collapsible soil with a geotextile improves the ultimate bearing capacity significantly, with or without the presence of water. For dry cases, and under the final increment of stress 800 kPa, the ESC system did not reach its settlement failure criteria, but the reduction in settlement in comparison to the untreated soil was higher than that observed for the OSC, such that the value of the enhancement of bearing capacity reached 230%. It was noticed that the improvement in bearing capacity provided by the encasement increased when increasing the amount of water added to the soil cell. It reached values of 49% and 77% when adding 2.73 L and 6.15 L of water respectively.

The settlement characteristics were enhanced significantly upon introducing the geotextile reinforcement. The settlement improvement factor increased to 216% and 285% when adding 2.73 L and 6.15 L of water respectively.

The degree of saturation and the matric suction of the soil govern the enhancement achieved for both the OSC and the ESC. The improvement in load settlement characteristics is noticeable at a higher degree of saturation and a lower amount of suction.

The shape of failure indicated that unwrapped columns bulged laterally into the upper layers. The affected bulging area increased when increasing the degree of saturation of the surrounding soil. The encased stone column showed a relatively consistent diameter along its entire length. The bulging of the column was restricted because of the confinement delivered by the geotextile.

Whether soaking occurred before or after loading did not affect the enhancement achieved by the OSC or the ESC. In terms of ultimate bearing capacity, under soaking after 100 kPa, the tanks associated with the US, OSC, and ESC, reached values of 144, 172, and 251kPa respectively, while when soaking with water at the beginning of the test, they showed only slight differences, with values of 140, 168, and 248 kPa respectively.

The readings of vertical deflection on the soil surface showed the largest deflection at the nearest position to the foundation, and that was so clear in the OSC foundation, which could reflect the variation in stresses in the surrounding ground in proportion to the distance from the column, after the induced enlargement when loading occurs. Conversely, when using the ESC, the value of vertical deflection was much lower because the stress concentration was on the encasement, not on the soil.

8.2.3. Conclusions from the Geophysical Survey

An automated electrical resistivity tomography (ERT) system was set up. The system was employed as a monitoring tool for discovering the homogeneity and geophysical characteristics of the composite cell of soil and column under loading. Using a geophysical survey to observe a stone column‟s foundation has not been considered previously.

The outcomes of the three tested chambers, untreated soil US, soil treated with an OSC, and soil treated with an ESC, showed that soil conductivity was very sensitive to load-induced and moisture-induced variations during collapse. It is believed that such behaviour is due to the current passing through the clay bonds and bridges between the silt grains, which are highly affected by conditions of stress and inundation. Applying load causes these bridges to break, increasing resistivity, while increasing the degree of saturation increases both particle-

to-particle contact and the volume of pores filled with water, causing a reduction in measured resistivity.

An increase in resistivity as a result of drainage was observed, which could be as result of the salt crystallisation in the interstitial brine that occurs during the drainage stage, and which causes an increase in the tortuosity of the soil, leading to an increase in its resistivity value and a reduction in the concentration of salts in the brine, as a result of a decrease in the volume of the voids in the sample.

In contrast, imaging the geophysical properties of the ESC tank provided a different trend, as the resistivity magnitudes decreased with increasing load for all loading stages and all rings. This could be as a result of the encasement, which limits the bulging effect, and to the higher degree of saturation of the soil caused by introducing the water to the tank.

Resistivity measurement from the vertical arrays indicated increasing in values upon increasing of the applied stresses, except at some points which reflect, according to their patterns, the geophysical properties of the soil closest to the electrodes. Also, resistivity of the ESC tank recorded the lowest values; while those for the US and the OSC tank were higher. This behaviour matches the degree of saturation of the soil obtained from the physical model.

In conclusion, the experimental trial produced valuable insights into the system subjected to varying loads and saturation conditions. However, the technique indicates a limitation in specifying the distinction of the column material at the middle of the test tank. This is probably because of the convergence of the electrical properties of the soil and the stone material used, or it could be as a result of the loss of signal strength for the farthest electrode pairs, as this is one of the main disadvantages of using a dipole-dipole configuration.

Also, it could be seen that mapping the geophysical properties of the soil in combination with conventional laboratory procedures has the potential to be a valuable scientific approach. However, before considering it to be a standard tool, further investigations and modifications are required.

8.2.4. Conclusions from the Analytical Model

The development of an analytical equation was undertaken in this study. The drained shear strength of the soil in this equation was calculated as being the same as that for unsaturated or partially saturated soil, which was not the same for previous studies of stone columns, where

a saturated state was adopted. In the equation developed, c_u was related to two independent stress state variables, the effective normal stress (σ_n-u_w) and the matric suction stress (u_a-u_w). Also, the lateral soil stress was computed according to a case of inundation that will be sensitive to the depth of soaking and the corresponding unit weight of the soil. The encasement effect was also included in the calculations.

The analytical model set out in this research showed how variations in the degree of saturation and matric suction could affect the performance of a foundation reinforced by an encased stone column when it was inserted into a collapsible soil. The improvement increased when increasing the tensile strength of the geotextile and the angle of internal shear resistance of the column fill material. However, the improvement decreased when expanding the diameter of the column. The theoretical results demonstrated strong consistency with the experimental results.

8.3. Recommendations for Future Work

Although this study has provided insights into the general behaviour of a reinforced stone column in a loess deposit, subjected to a variety of load and inundation situations, there are still essential areas that require further investigation.

For the physical model, these are recommended below:

- Field investigations are required to validate the laboratory findings established in this study.
- The performance of the system in such a metastable soil for a variety of column geometry, fill material, geosynthetic stiffness, and partial encasement patterns should be tested.
- An investigation into the behaviour under different loading conditions such as cyclical or lateral loading is advised for future work, in order to highlight performance under corresponding applications of an encased granular column inserted into collapsible soil.
- The performance of similar tests with more instrumentation is recommended, especially for measuring the matric suction force during the test, TDR probes could be employed for this purpose when it is arranged vertically on the soil surface and horizontally through the wall of the test chamber. Also, measuring pore water pressure through sensors positioned at specific locations of the chamber could offer valuable information of the system.

For the electrical resistivity system, the recommendations are below:

- Further configurations are required, such as inserting electrodes into the soil surface and at the intersection between the column and the host ground, in order to overcome the problem of the loss of signal strength.
- Although temperature change is considering insignificant in comparison to the reported resistivity values according to the low level of variation in temperature in the lab, measuring variations in temperature through the sample itself in future work is highly recommended for obtaining precise results.
- The electrical resistivity cells used in this study to assess the performance of the encased stone column could be extended and employed for different types of ground improvement.

REFERENCES

Abelev, Y. M. (1948).The essentials of designing and building on microporous soils. *Stroitel Naya Promyshelmast*, No.*10*.

Abidin, M. H. Z., Ahmad, F., Wijeyesekera, D. C., & Saad, R. (2014). The influence of basic physical properties of soil on its electrical resistivity value under loose and dense condition. *Journal of Physics: Conference Series*, 495, 012014, 1-13.

Adli, Z. H., Musa, M. H., & Arifin, M. N. K. (2010). Electrical resistivity of subsurface : field and laboratory assessment. *International Journal of Environmental, Chemical, Ecological, Geological and Geophysical Engineering*, *4*(9), 799–802.

Afshar, J. N., & Ghazavi, M. (2014). Experimental studies on bearing capacity of geosynthetic reinforced stone columns. *Arabian Journal for Science and Engineering*, 39(3), 1559–1571.

Alexiew, D., Brokemper, D., & Lothspeich, S. (2005). Geotextile encased columns (GEC): load capacity, geotextile selection and pre-design graphs. In *Proceedings of Geo- Frontiers* (pp. 497–510). Austin, Texas, US.

Ali, K., Sgahu, J. T., & Sharma, K. G. (2010). Behaviour of reinforced stone columns in soft soils : an experimental study. In *Indian Geotechnical Conference, GEOtrendz* (pp. 620–628). IGS Mumbai Chapter & IIT Bombay.

Al-Mosawe, M. J., Abbas, A. J., & Majieed, A. H. (1985). Prediction of ultimate capacity of a single and groups of stone columns. In *Iraqi conference on Engineering ICE 85 Vol.1* (pp. 61–68). Baghdad.

Al-Obaidy, N. K. (2000). Full scale tests on stone piles. *M. Sc thesis*, University of Baghdad, Baghdad, Iraq.

Ambily, A. P., & Gandhi, S. R. (2007). Behaviour of stone columns based on experimental and FEM analysis. *Journal of Geotechnical and Geoenvironment Engineering*, 133(4), 405–415.

Amini, R. (2014). Physical modelling of vibro stone column using recycled aggregates. *PhD thesis*, University of Birmingham, UK.

Araujo, G. L. S., Palmeira, E. M., & Cunha, R. P. (2009). Behaviour of geosynthetic-encased granular columns in porous collapsible soil. *Geosynthetics International*, *16*(6), 433–451.

Archie, G. E. (1941). The electrical resistivity log as an aid in determining some reservoir characteristics. *Dallas Meeting*, (October), 54–62.

Ashour, S. (2015). The response of stone columns under cyclic loading. *PhD thesis*, University of Birmingham, UK.

Assallay, A. M. (1998). Structure and hydrocollapse behaviour of loess. *PhD thesis*, Loughborough University of Technology, UK.

Assallay, A. M., Rogers, C. D. F., & Smalley, I. J. (1997). Formation and collapse of metastable particle packings and open structures in loess deposits. *Engineering Geology*, 48, 101–115.

Atkins, E. R., & Smith, G. H. (1961). The significance of particle shape in formation resistivity factor-porosity relationships. *Journal of Petroleum Technology*, *13*(3), 285–291.

Ayadat, T. (1990). Collapse of stone column foundations due to inundation. *PhD thesis*, University of Sheffield, UK.
Ayadat, T., A. M. Hanna, A. M., & Hamitouche, A. (2008). Soil improvement by internally reinforced stone columns. In *Proceedings of the ICE - Ground Improvement* (pp. 55–63).

Ayadat, T., Hanna, A., & Etezad, M. (2008). Failure process of stone columns in collapsible soils. *IJE Transactions B: Applications*, 21(2), 135–142.

Ayadat, T., & Hanna, A. M. (2005). Encapsulated stone columns as a soil improvement technique for collapsible soil. *Ground Improvement*, 9(4), 137–147.

Balaam, N. P., & Booker, J. R. (1981). Analysis of rigid rafts supported by granular piles. *International Journal for Numerical and Analytical Methods in Geomechanics*, 5(4), 379–403.

Balaam, N. P., & Booker, J. R. (1985). Effect of Stone Column Yield on Settlement of Rigid Foundations in Stabilized Clay. *International Journal of Numerical Methods in Engineering*, 9(4), 331–351.

Balaam, N. P., & Poulos, H. G. (1983). The behaviour of foundations supported by clay stabilized by stone columns. In *Proceeding of the 8th European Conference on Soil Mechanics and Foundation Engineering* (pp. 199–204). Helsinki.

Balaam, N. P., Poulos, H. G., & Brown, P. T. (1978). Settlement analysis of soft clays reinforced with granular piles. In *Proc., 5th Asian Conf. on Soil Engineering* (pp. 81–92). Bangkok, Thailand.

Bally, R. E. N. J. (1988). Some specific problems of wetted lossial soils in civil engineering. *Engineering Geology*, *25*, 303–324.

Barden, L., McGown, A., Collins, K. (1973). The collapse mechanism in partly saturated soil. *Engineering Geology*, *7*, 49–60.

Barksdale, R.D. and Bachus, R. C. (1983). Design and construction of stone columns. *FHWA/RD-83/026, Federal Highway Administration,* Washington, D.C. Springfield.

Basack, S., Indraratna, B., & Rujikiatkamjorn, C. (2016). Modeling the performance of stone column – reinforced soft ground under static and cyclic Loads. *Journal Of Geotechnical and Geoenvironmental Engineering*, 142(2), 1–15.

Bishop, A. W. (1959). The principal of effective stress. *Technische Ukebland*, 106(39), 859–863.

Black, J.A., Sivakumar, V., Madhav, M.R. and McCabe, B. A., Sivakumar, V., Madhav, M. R., & Hamill, G. A. (2007). Reinforced stone columns in weak deposits : laboratory model study. *Journal Of Geotechnical and Geoenvironmental Engineering*, 133(September), 1154–1161.

Black, J. A., Sivakumar, V., & Bell, A. (2011). The settlement performance of stone column foundations. *Geotechnique*, 61(11), 909–922.

Blenkinsop, T. G., Kruhl, J. H., & Kupková, M. (2000). Fractals and dynamic systems in geoscience. *Publisher Birkhäuser Basel*, 196 pages.

Borsic, A., Comina, C., Foti, S., Lancellotta, R., & Musso, G. (2005). Imaging heterogeneities with electrical impedance tomography : laboratory results. *Geotechnique*, 55(7), 539–547.

Briaud, J. L. (1991). The pressuremeter: some special applications. In *Proceedings of the Geotechnical Engineering Congress, Boulder, CO, ASCE Geotechnical Special Publication* (pp. 26–37).

Brink, G. E. (2011). The influence of soil suction on the collapse settlement of different soils in South Africa. *Master Thesis*, the Faculty of Natural and Agricutural Sciences, University of Pretoria, Pretoria.

Burland, J., Chapman, T., Skinner, H., & Brown, M. (2012). Geotechnical design, construction and verification. *ICE Manual of Geotechnical Engineering*, *2*.

Calamita, G., Brocca, L., Perrone, A., Piscitelli, S., Lapenna, V., Melone, F., & Moramarco, T. (2012). Electrical resistivity and TDR methods for soil moisture estimation in central Italy test-sites. *Journal of Hydrology*, 454-455, 101–112.

Castro, J., & Sagaseta, C. (2011). Deformation and consolidation around encased stone columns. *Geotextiles and Geomembranes*, 29(3), 268–276.

Chambers, J. E., Gunn, D. A., Wilkinson, P. B., Meldrum, P. I., Haslam, E., Holyoake, S., Kirkham, M., Kuras, O., Merritt, A., Wragg, J. (2014). 4D electrical resistivity tomography monitoring of soil moisture dynamics in an operational railway embankment. *Near Surface Geophysics*, 12, 61–72.

Chambers, J. E., Gunn, D. A., Wilkinson, P. B., Ogilvy, R. D., Ghataora, G. S., Burrow, M. P. N., & Smith, R. T. (2008). Non-invasive time-lapse imaging of moisture content changes in earth embankments using electrical resistivity tomography (ERT), *Advances in Transportation Geotechnics – Ellis,Yu, McDowell, Dawson & Thom (eds) © 2008 British Geological Survey,* Nottingham, (pp. 475–480).

Chambers, J. E., Loke, M. H., Ogilvy, R. D., & Meldrum, P. I. (2004). Noninvasive monitoring of DNAPL migration through a saturated porous medium using electrical impedance tomography. *Journal of Contaminant Hydrology*, 68(1-2), 1–22.

Cimentada, A., Da Costa, A., Cañizal, J., & Sagaseta, C. (2011). Laboratory study on radial consolidation and deformation in clay reinforced with stone columns. *Canadian Geotechnical Journal*, 48(1), 36–52.

Comina, C., Foti, S., Musso, G., & Romero, E. (2008). EIT oedometer: An advanced cell to monitor spatial and time variability in soil with electrical and seismic measurements. *Geotechnical Testing Journal*, 31(5), 404–412.

Cosenza, P., & Tabbagh, A. (2004). Electromagnetic determination of clay water content: role of the microporosity. *Applied Clay Science*, 26, 21–36.

Costa, J. E., & Baker, V. R. (1981). Surficial geology: building with the earth. John Wiley and Sons, New York, U. S. A.

Cunningham, M. R., Ridley, A. M., Dineen, K., & Burland, J. J. (2003). The mechanical behaviour of a reconstituted unsaturated silty clay. *Géotechnique*, 53(2), 183–194.

Dafalla, M. A. (2013). Effects of clay and moisture content on direct shear tests for clay-sand mixtures. *Hindawi Publishing Corporation Advances in Materials Science and Engineering*, 1–8.

Das, B. M. (2014). Foundations on difficult soils. In *Chapter Eleven, Principles of Foundation Engineering* (8th ed.). Boston, USA: Global Engineering.

Das, P., & Pal, S. K. (2013). A study of the behavior of stone column in local soft and loose layered soil. *EJGE, Bund. I*, *18*, 1777–1786.

Dash, S. K., & Bora, M. C. (2013). Influence of geosynthetic encasement on the performance of stone columns floating in soft clay. *Canadian Geotechnical Journal*, 50(April), 754–765.

Datye, K., & Nagaraju, S. (1981). Design approach and field control for stone columns. In *Proceeding,10th International Conference on Soil Mechanics and Foundation Engineering* (Vol. 3, pp. 637–640). Stockholm.

de Mello, L. G., Mondolfo, M., Montez, F., Tsukahara, C. N., & Bilfinger, W. (2008). First use of geosynthetic encased sand columns in South America. In *Proceedings of First Pan-American Geosynthetics Conference, Cancun* (pp. 1332–1341). Murugesan.

Deb, K., & Mohapatra, S. R. (2013). Analysis of stone column-supported geosynthetic-reinforced embankments. *Applied Mathematical Modelling*, 37(5), 2943–2960.

Demir, A., & Sarici, T. (2016). Bearing capacity and bulging behaviour of geogrid encased stone columns. *Selcuk University Journal of Engineering Science and Technology*, 4(2), 131–143.

Demir, A., Sarıcı, T., Laman, M., Bağrıaçık, B., & Ok, B. (2013). An experimental study on behaviour of geosynthetic reinforced stone columns. In *2nd International Balkans Conference on Challenges of Civil Engineering* (pp. 23–25). Tirana, Albania.

Derbyshire, E., & Mellors, T. W. (1988). Geological and geotechnical characteristics of some loess and loessic soils from China and Britain: a comparison. *Engineering Geology*, 25, 135–175.

Dheerendra Babu, M. R., Nayak, S., & Shivashankar, R. (2013). A critical review of construction, analysis and behaviour of stone columns. *Geotechnical and Geological Engineering*, 31(1), 1–22.

di Prisco, C., & Galli, A. (2011). Mechanical behaviour of geo-encased sand columns: small scale experimental tests and numerical modelling. *Geomechanics and Geoengineering*, 6(4), 251–263.

Dibben, S. (1998). A microstructural Model for collapsing soils. *Unpublished PhD thesis*, Nottingham Trent University, UK.

Dobson, T., & Slocombe, B. (1982). Deep densification of granular fills. In *2nd Geotechnical Conference and Exhabit on Design and Construction* (pp. 26–28). Las Vegas Nevada.

Elshazly, H. a., Hafez, D. H., & Mossaad, M. E. (2008). Reliability of conventional settlement evaluation for circular foundations on stone columns. *Geotechnical and Geological Engineering*, 26(3), 323–334.

Elshazly, H., Elkasabgy, M., & Elleboudy, A. (2007). Effect of inter-column spacing on soil stresses due to vibro-installed stone columns: interesting findings. *Geotechnical and Geological Engineering*, 26(2), 225–236.

Engelhardt, K., & Golding, H. C. (1975). Field testing to evaluate stone column performance in a seismic area. *Geotechnique*, 25(1), 61–69.

Erol, O. A., & EL-Ruwaih, I. A. (1982). Collapse behaviour of desert loess. In *Proc. 6th Congress International Association of Engineering Geology* (pp. 443–448).

Esring, M. I., & Bachus, R. C. (1991). Deep foundation improvements: design, construction and testing, *ASTM Special Technical Publication*. Philadephia: American Society for Testing & Materials.

Fattah, M. Y., & Majeed, Q. G. (2012). Finite element analysis of geogrid encased stone columns. *Geotechnical and Geological Engineering*, 30(4), 713–726.

Fattah, M. Y., Zabar, B. S., & Hassan, H. A. (2016). Experimental analysis of embankment on ordinary and encased stone Columns. *International Journal of Geomechanics*, 16(4), 1–13.

Frikha, W., Bouassida, M., & Canou, J. (2013). Observed behaviour of laterally expanded stone column in soft soil. *Geotechnical and Geological Engineering*, 31(2), 739–752.

Gao, G. (1996). The distribution and geotechnical properties of loess soils, lateritic soils and clayey soils in China. *Engineering Geology*, 42(1), 95–104.

Garakani, A. A. (2013). Laboratory assessment of the hydro-mechanical behavior of unsaturated undisturbed collapsible soils – case study: Gorgan loess. *Dissertation for the Doctoral Degree*, Sharif University of Technology, Tehran, Iran.

Gazdek, M., Strelec, S., & Rezo, M. (2011). Estimation of vibro replacement by compression seismic waves. *Tehnicki Vjesnik*, 18(2), 243–252.

Ghazavi, M., & Afshar, J. N. (2013). Bearing capacity of geosynthetic encased stone columns. *Geotextiles and Geomembranes*, *38*, 26–36.

Ghorbani, A., Cosenza, P., Badrzadeh, Y., & Ansari, A. (2012). Changes in the electrical resistivity of arid soils during oedometer testing. *European Journal of Environmental and Civil Engineering*, 17(February 2015), 84–98.

Gniel, J., & Bouazza, A. (2009). Improvement of soft soils using geogrid encased stone columns. *Geotextiles and Geomembranes*, 27(3), 167–175.

Gniel, J., & Bouazza, A. (2010). Construction of geogrid encased stone columns: A new proposal based on laboratory testing. *Geotextiles and Geomembranes*, 28(1), 108–118.

Goughnour, R. R., & Bayuk, A. A. (1979). Field study of long-term settlement of loads supported by stone columns in soft ground. In *Conf. Soil Reinforcement, Vol. 1* (pp. 279–286). Paris.

Greenwood, D. A. (1970). Mechanical improvement of soils below ground surfaces. In *Proceedings of the ground engineering conference, Institution of Civil Engineers* (pp. 11–22). London.

Greenwood, D. A. (1975). Vibroflotation: Rationale for design and practice, methods of treatment of unstable ground. Ed. By Bell, F. G., Newnes-Butterworths, London, 189–209.

Greenwood, D. A., & Kirsch, K. (1983). Specialist ground treatment by vibratory and dynamics methods. In *Proceedings, international conference on piling and ground treatment* (pp. 17–45).

Günther, T., & Rücker, C. (2013). Boundless Electrical Resistivity Tomography BERT 2 – the user tutorial (version 2).

Günther, T., Rücker, C., & Spitzer, K. (2006). Three-dimensional modelling and inversion of dc resistivity data incorporating topography - II. Inversion. *Geophysical Journal International*, 166(2), 495–505.

Haeri, S. M., & Garakani, A. A. (2016). Hardening behavior of a hydro collapsible loessial soil. *Japanese Geotechnical Society Special Publication ,The 15th Asian Regional Conference on Soil Mechanics and Geotechnical Engineering*, 253–257.

Han, J., Oztoprak, S., Parsons, R. L., & Huang, J. (2007). Numerical analysis of foundation columns to support widening of embankments. *Computers and Geotechnics*, 34(6), 435–448.

Hassan, A. A. (2014). Electrical resistivity method for water content characterisation of unsaturated clay Soil. *PhD thesis*, Geotechnical Group School of Engineering and Computing Sciences, Durham University, UK.

Hataf, N., & Nabipour, N. (2013). Experimental investigation on bearing capacity of geosynthetic encapsulated stone columns. In *Proceedings of the 18th International Conference on Soil Mechanics and Geotechnical Engineering* (pp. 2493–2496). Paris.

Head, K. H. (1994). Manual of soil laboratory testing: permeability, shear strength and compressibility tests (Volume 2). Halsted Press.

Head, K. H. (2006). Manual of soil laboratory testing: soil classification and compaction tests (Volume 1). Scotland, UK, Whittles Publishing.

Heaney, B. M. (2003). Electrical Conductivity and resistivity. Boca Raton, CRC Press , *Ch7 Electrical Measurement, Signal Processing, and Displays* (pp. 1–14).

Holder, E. D., Lionheart, W., Polydorides, N., & Borsic, A. (2004). Part 1 of Electrical Impedance Tomography: methods, history and applications. Institute of Physics Publishing, 3-64.

Hong, Y.-S. (2012). Performance of encased granular columns considering shear-induced volumetric dilation of the fill material. *Geosynthetics International*, 19(6), 438–452.

Hosseinpour, I., Almeida, M. S. S., & Riccio, M. (2016). Ground improvement of soft soil by geotextile-encased columns. ICE Proceedings, *Ground Improvement*, 169(GI4), 297-305.

Houston, S. L., Houston, W. N., & Zapata, C. E. (2001). Geotechnical engineering practice for collapsible soils. *Geotechnical and Geological Engineering*, 19, 333–355.

Hu, W. (1995). Physical modelling of group behaviour of stone column foundations. *PhD thesis*, University of Glasgow, Scotland, UK.

Hughes, J. M. O., & Withers, N. J. (1974). Reinforcing of soft cohesive soils with stone columns. *Ground Engineering*, 1(3), 42–49.

Hughes, J. M. O., Withers, N. J., & Greenwood, D. A. (1975). A field trial of the reinforcing effect of a stone column in soil. *Geotechnique*, 25(1), 31–44.

Jackson, P. D., Northmore, K. J., Entwisle, D. C., Gunn, D. A., Milodowski, A. E., Boardman, D., Zourmpakis, A., Rogers, C.D.F., Jefferson, I., Dixon, N. (2006). Electrical resistivity monitoring of a collapsing meta-stable soil. *Quarterly Journal of Engineering Geology and Hydrogeology,* 39, 151–172.

Jackson, P. D., Northmore, K. J., Meldrum, P. I., Gunn, D. A., Hallam, J. R., Wambura, J., Wangusi, B., Ogutu, G. (2002). Non-invasive moisture monitoring within an earth embankment: a precursor to failure. *NDT & E International*, *35*(2), 107–115.

Jackson, P. D., Smith, D. T., & Stanford, P. N. (1978). Resistivity-porosity-particle shape relationships for marine sands. *Geophysics*, 43(6), 1250–1268.

Jefferson, I., Klukanova, A., Evstatiev, D., Angelova, R., & Smalley, I. (2000). Improving metastable loess ground. In *International Symposium, Melbourne, Australia* (Vol. November, pp. 19–24).

Jefferson, I., O'Hara-Dhand, K. A., & Serridge, C. J. (2008). Assessment of the ground improvement of problematical soils. In *In Proceedings of the 3rd International Conference on Site Charac- terization, Taipei, Taiwan, April 2008*.

Jefferson, I., Serridge, C. J., Thomas, a. M., & Gaterell, M. (2010). Emissions assessment related to vibro stone columns. *Proceedings of the ICE - Ground Improvement*, 163(1), 71–77.

Jennings, J. E. and Knight, K. (1957). The Additional settlement of foundations due to collapse of sandy soils on wetting. In *the 4th International Conference on Soil Mechanics and Foundation Engineering* (Vol. 1, pp. 316–319).

Jennings, J. E., & Knight, K. (1975). A guide to construction on or with materials exhibiting additional settlement due to collapse of grain structure. In *In Proceeding of the 6th African Conference on Soil Mechanics and Foundation Engineering* (pp. 99–105). South Africa.

Jiang, M., Hu, H., & Liu, F. (2012). Summary of collapsible behaviour of artificially structured loess in oedometer and triaxial wetting tests. *Canadian Geotechnical Journal*, 49(10), 1147–1157.

Jotisankasa, A. (2005). *Collapse behaviour of a compacted silty clay*. Department of Civil and Environmental Engineering Imperial College London, London.

Kalhor, A. (2012). The shear strength analyses of soil with various compactions under vertical load in direct shear test. *International Research Journal of Applied and Basic Sciences*, 3, 2815–2821.

Kameshwar, R. T., Golait, Y. S., & Ashwini, S. Z. (2011). Improvement of bearing capacity of soft soil using stone column with and without encasement of geosynthetics. *International Journal of Science and Advanced Technology*, 1(7), 50–59.

Khabbazian, M., Kaliakin, V. N., & Meehan, C. L. (2015). Column Supported Embankments with Geosynthetic Encased Columns: Validity of the Unit Cell Concept. *Geotechnical and Geological Engineering*, 33(3), 425–442.

Kibria, G., Hossain, M. S., Hossain, J., & Khan, M. . (2012). Determination of moisture content and unit weight of clayey soil using Resistivity Imaging (RI). In *GeoCongress 2012 © ASCE 2012* (Vol. 3, pp. 3398–3407).

Killeen, M. M., & McCabe, B. A. (2014). Settlement performance of pad footings on soft clay supported by stone columns: A numerical study. *Soils and Foundations*, 54(4), 760–776.

Kowalczyk, S., Maślakowski, M., & Tucholka, P. (2014). Determination of the correlation between the electrical resistivity of non-cohesive soils and the degree of compaction. *Journal of Applied Geophysics*, 110, 43–50.

Kruse, G. A. M., Dijkstra, T. A., & Schokking, F. (2007). Effects of soil structure on soil behaviour: Illustrated with loess, glacially loaded clay and simulated flaser bedding examples. *Engineering Geology*, 91(1), 34–45.

Kumar, R., & Jain, P. K. (2013). Expansive Soft Soil Improvement by Geogrid Encased. *International Journal on Emerging Technologies*, 4(1), 55–61.

Kuo, J. (2014). Practical design calculations for groundwater and soil remediation. Press, (2nd Edition).

Ladd, R. S. (1978). Prepation test specimens using under compaction. *ASTM Geotechnical Testing Journal*, 1(1), 16–23.

Langroudi, A. A. (2014). Micromechanics of collapse in loess, PhD thesis, University of Birmingham, UK.

Langroudi, A. A., & Jefferson, I. (2013). Collapsibility in calcareous clayey loess. *International Journal of GEOMATE*, 5(1), 620–627.

Lee, D., Yoo, C., Park, S., & Jung, S. (2008). Field load tests of geogrid encased stone columns in soft ground. In *Proceeding of the Eighteenth International Offshore and Polar Engineering Conference* (Vol. 8, pp. 521–524). Vancouver, BC, Canada.

Lee, D.-Y., & Yoo, C.-S. (2011). Laboratory investigation on construction method of geogrid encased stone column. *Journal of the Korean Geotechnical Society*, 27(2), 73–80.

Liu, Z., Liu, F., Ma, F., Wang, M., Bai, X., Zheng, Y., Yin, H., Zhang, G. (2016). Collapsibility, composition, and microstructure of a loess in China. *Canadian Geotechnical Journal*, 53, 673–686.

Liu, Z., Liu, S., Ma, X., & Wu, C. (2014). Electrical resistivity behavior of loess specimens during Unconfined Compression Test. *Advances in Transportation Geotechnics and Materials for Sustainable Infrastructure GSP 250 © ASCE 2014*, 40–47.

Loke, M. H. (2012). Tutorial : 2-D and 3-D electrical imaging surveys. *Course Notes ,Copyright (1996-2011)*.

Lutenegger, A. J., & Saber, R. T. (1988). Determination of collapse potential of soils. *Geotechnical Testing*, 11(3), 173–178.

Madun, A. (2012). *Seismic evaluation of vibrostone column*. PhD thesis, School of Civil Engineering, University of Birmingham.

Madun, A., Jefferson, I., Foo, K. Y., Chapman, D. N., Culshaw, M. G., & Atkins, P. R. (2012). Characterization and quality control of stone columns using surface wave testing. *Canadian Geotechnical Journal*, 49(12), 1357–1368.

Malarvizhi, & Ilampararuthi. (2007). Comparative study on the behavior of encased stone column and conventional stone column. *Soils and Foundations Japanese Geotechnical Society*, 47(5), 873–885.

Malarvizhi, S. N., & Ilamparuthi, K. (2004). Load versus settlement of clay bed stabilized with stone & reinforced stone columns. In *Proceedings of the 3 rd Asian Regional Conference on Geosynthetics, GEOASIA* (pp. 322–329). Seoul, Korea.

Malarvizhi, S. N., & Ilamparuthi, K. (2010). Mechanism of geogrid encased stone column. *Indian Geotechnical Conference*, *16*(18), 949–952.

McCabe, B. a., Egan, D., & Nimmons, G. J. (2009). A review of field performance of stone columns in soft soils. *Proceedings of the ICE - Geotechnical Engineering*, *162*(6), 323–334.

McCabe, B. A., McNeill, J. A., & Black, J. A. (2007). Ground improvement using the vibro-stone column technique. *Paper Presented at the Joint Meeting of Engineers Ireland West Region and the Geotechnical Society of Ireland, NUI Galway*, 1–12.

McKelvey, D., & Sivakumar, V. (2000). A review of the performance vibro stone column foundations. In *3rd International Conference on Ground Improvement Techniques* (pp. 245–254). Singapore.

McKelvey, D., Sivakumar, V., Bell, A., & Graham, J. (2004). Modelling vibrated stone columns in soft clay. In *Proceedings of the institute of civil engineers geotechnical engineering* (Vol. 157, pp. 137–149).

Medero, G. M., Schnaid, F., & Gehling, W. Y. Y. (2009). Oedometer behavior of an artificial cemented highly. *Geotech. Geoenviron. Eng.*, 135(June), 840–843.

Miller, H. (2002). *Modelling the collapse of metastable loess soils*. PhD thesis, The Nottingham Trent University, UK.

Miranda, M., & Da Costa, A. (2016). Laboratory analysis of encased stone columns. *Geotextiles and Geomembranes*, 44(3*), 269–277.*

Mitchell, J. ., & Huber, T. R. (1985). Performance of a stone column foundation. *Journal of Geotechnical Engineering, ASCE,* 111(2), 205–223.

Mitchell, J. M., & Jardine, F. M. (2002). *A guide to ground treatment*. *Book*, Ed.C573, CIRIA, London.

Munoz-Castelblanco, J. A., Pereira, J. M., Delage, P., & Cui, Y. J. (2012). The influence of changes in water content on the electrical resistivity of natural unsaturated loess, 35(1), 11–17.

Muñoz-Castelblanco, J. A., Pereira, J. M., Delage, P., & Cui, Y. J. (2012). The water retention properties of a natural unsaturated loess from northern France. *Géotechnique*, 62(2), 95–106.

Murugesan, S., & Rajagopal, K. (2009). Experimental and numerical investigations on the behaviour of geosynthetic encased stone columns. *IGC*, 480–484.

Najjar, S. S. (2013). A state-of-the-art review of stone/sand-column reinforced clay systems. *Geotechnical and Geological Engineering*, 31(2), 355–386.

Najjar, S. S., Sadek, S., & Maakaroun, T. (2010). Effect of sand columns on the undrained load response of soft clays. *Journal of Geotechnical and Geoenvironmental Engineering*, 136(9), 1263–1277.

Nayak, N. (1996). Foundation design manual (4th ed.). Dhanapathi Rai publications (P) Ltd.

Nayak, N. V. (1987). The recent advances in Indian practice of ground improvement by stone columns. In *Proceeding, 5th International Geotechnical Seminar Organized by Nayany, Technology Institute* (pp. 235–244). Singapore.

Northmore, K., Jefferson, I., Jackson, P., Entwisle, D., Milodowski, A., Raines, M., Gunn, D., Boardman, D.I., Zourmpakis, A., Nelder, L.M., Rogers, C.D.F, Dixon, N., Smalley, I. J. (2008). On-site characterisation of loessic deposits in Kent, UK. *Geotechnical Engineering*, 161(GEI), 3–17.

Pereira, J. H. F., & Fredlund, D. G. (2000). Volume change behaviour of collapsible compacted Gneiss soil. *Journal of Geotechnical and Geoenvironmental Engineering*, *126*(October), 907–916.

Poulos, H. G., & Davis, E. R. (1975). Prediction of down-drag forces in end-bearing piles. *Journal Of Geotechnical Engineering*, 101(GT2), 189–204.

Prasad, S. G., & Satyanarayana, P. V. V. (2016). Improvement of soft soil performance using stone columns improved with circular geogrid discs. *Indian Journal of Science and Technology*, 9(30), 1-6.

Priebe, H. J. (1995). The design of vibroreplacement. *Technical Paper; Reprint from: Ground Engineering*, 1–16.

Raithel, M., Kirchner, A., Schade, C., & Leusink, E. (2008). Foundation of constructions on very soft soils with geotextile encased columns - state of the art. *GSP 136 Innovations in Grouting and Soil Improvement*, 1–11.

Redgers, J. D., Moxhay, A. L., Ghataora, G. S., & Jefferson, I. (2008). Case histories of settlement performance comparisons on ground improvement using soil stiffness seismic wave and traditional methods. In *Sixth International Conference on Case Histories in Geotechnical Engineering* (pp. 1–8).

Rogers, C. D. F., Dijkstra, T. a., & Smalley, I. J. (1994). Hydroconsolidation and subsidence of loess: Studies from China, Russia, North America and Europe. *Engineering Geology*, 37(2), 83–113.

Saad, R., Nawawi, M. N. M., & Mohamad, E. T. (2012). Groundwater detection in alluvium using 2-D electrical resistivity tomography (ERT). *Electronic Journal of Geotechnical Engineering*, 17 D, 369–376.

Salih, N. B. (2003). Field models on gypseous soils reinforced with stone columns stabilized with asphalt and lime. *M.Sc. thesis*, University of Technology, Baghdad, Iraq.

Samouëlian, A., Cousin, I., Tabbagh, A., Bruand, A., & Richard, G. (2005). Electrical resistivity survey in soil science : a review. *Soil and Tillage Research*, 83(2), 173–193.

Seladji, S., Cosenza, P., Tabbagh, a., Ranger, J., & Richard, G. (2010). The effect of compaction on soil electrical resistivity: a laboratory investigation. *European Journal of Soil Science*, 61(6), 1043–1055.

Serridge, C. (2005). Achieving sustainability in vibro stone column techniques. In *Proceedings of the Institution of Civil Engineers – Engineering Sustainability,* vol.158*,* No.4 (pp. 211–222).

Serridge, C. J. (2006). Some applications of ground improvement techniques in the urban environment. *The Geological Society of London*, 1–14.

Serridge, C. J. (2013). An evaluation of partial depth dry bottom - feed vibro stone columns to support shallow footings in deep soft clay deposits. *PhD thesis*, Anglia Ruskin University, UK.

Shahu, J. T., Madhav, M. R., & Hayashi, S. (2000). Analysis of soft ground–granular pile–granular mat system. *Computers and Geotechnics*, 27(1), 45–62.

Sharma, R. S., Kumar, B. R. P., & Nagendra, G. (2004). Compressive load response of granular piles reinforced with geogrids. *Canadian Geotechnical Journal*, 41, 187–192.

Shihada, H., Hossain, M. S., Kemler, V., & Dugger, D. (2013). Estimating moisture content of landfilled municipal solid waste without drilling-Innovative approach. *Journal of Hazardous, Toxic, and Radioactive Waste*, 17(4), 317–330.

Shivashankar, R., Dheerendra Babu, M. R., Nayak, S., & Manjunath, R. (2010). Stone columns with vertical circumferential nails: laboratory model study. *Geotechnical and Geological Engineering*, 28(5), 695–706.

Sivakumar, V, Mckelvey, D, Graham, J., & Hughes, D. (2004). Triaxial tests on model sand columns in clay. *Canadian Geotechnical Journal*, 41, 299–312.

Sivakumar, V., Boyd, J. L., Black, J. a., & McNeil, J. a. (2010). Effects of granular columns in compacted fills. *Proceedings of the ICE - Geotechnical Engineering*, 163(4), 189–196.

Sondermann, W., & Wehr, W. (2004). Deep vibro technique. In M. P. Moseley & K. Kirsch (Eds.), *Ground Improvement* (2nd ed., pp. 57–92). London and New York: Taylor & Francis Group.

Sudha, K., Israil, M., Mittal, S., & Rai, J. (2009). Soil characterization using electrical resistivity tomography and geotechnical investigations. *Journal of Applied Geophysics*, 67, 74–79.

Tadepalli, R., & Fredlund, D. G. (1991). The collapse behavior of a compacted soil during inundation. *Canadian Geotechnical Journal*, 28(4), 477–488.

Tandel, Y. k., Solanki, C. H., & Desai, A. K. (2012). Numerical modelling of encapsulated stone column-reinforced ground. *International Journal of Civil, Structural, Environmental and Infrastructure Engineering*, 2(1), 82–96.

Tandel, Y. K., Solanki, C. H., & Desai, A. K. (2013). Laboratory experimental analysis on encapsulated stone column. *Archives of Civil Engineering*, *LIX*(3), 359–379.

Taube, M. G., P.G., P. E., & Herridge, J. R. (2002). Stone columns for industrial fills. Nicholson Construction Company, Cuddy, Pennsylvania.

Tavenas, F., Mieussens, C., & Bourges, F. (1979). Lateral displacements in clay foundations under embankments. *Canadian Geotechnical Journal*, 16(3), 523–550.

Taylor, J. R. (1982). An introduction to error analysis. *The study of uncurtainties in the physical measurments* (Second Ed.).

Taylor, J. R. (1997). An introduction to error analysis: The study of uncertainties in physical measurements (Second Ed.).

Terzaghi, K. (1936). the shear resistance of saturated soils. In *Proceedings of the First International Conference of Soil Mechanics and Foundation Engineering, vol.1* (pp. 54–56). Cambridge, M.A.

Tigre Manual Rev E 0506", 2006. Retrieved from http://www.allied-associates.co.uk/wp-content/uploads/2016/06/Manual-Tigre.pdf.

Tognon, A. R., Rowe, R. K., & Brachman, R. W. I. (1999). Evaluation of side wall friction for a buried pipe testing facility. *Geotextiles and Geomembranes*, 17(4), 193–212.

Trofimov, V. T. (1990). Loess subsidence models. *Moscow University Geology Bulletin*, 45, 5–18.

Uttam, K., Tandel, Y. K., & Solanki, C. H. (2013). Effect of Geosynthetic Encasement on Sand Column. *International Journal of Structural and Civil Engineering Research*, 2(3), 1–8.

Van Impe, W., & Silence, P. (1986). Improving of the bearing capacity of weak hydraulic fills by means of geotextile. In *Proceedings of the 3rd International Conference on Geotextiles, Vienna, Austria* (pp. 1411–1416).

Ward, M. R. (1971). Electrical engineering science. New York: Published by McGraw-Hill Book Co, New York.

Weber, T. M., Laue, J., & Springman, S. (2006). Centrifuge modelling of sand compaction piles in soft clay under embankment load. In *Proceedings of the 6th International Conference on Physical Modelling in Geotechnics, Kowloon, Hong Kong (pp. 603-606).*

Wehr, J. (2006). The undrained cohesion of the soil as criterion for the column installation with a depth vibrator. In *Proceedings of the international symposium on vibratory pile driving and deep soil Vibratory compaction* (pp. 157–162). Paris.

Wen, B. P., & Yan, Y. J. (2014). Influence of structure on shear characteristics of the unsaturated loess in Lanzhou, China. *Engineering Geology*, *168*, 46–58.

Wood, D. (2000). Group effects in stone column foundations: model tests. *Geotechnique*, 50(6), 689 –698.

Wu, C.-S., Hong, Y.-S., & Lin, H.-C. (2009). Axial stress–strain relation of encapsulated granular column. *Computers and Geotechnics*, 36(1-2), 226–240.

Yan, M., Miao, L., & Cui, Y. (2012). Electrical resistivity features of compacted expansive soils. *Marine Georesources & Geotechnology*, 30(2), 167–179.

Zahmatkesh, A., & Choobbasti, A. J. (2010). Settlement evaluation of soft clay reinforced by stone columns, considering the effect of soil compaction. *IJRRAS*, 3(2), 159–166.

Zha, F., Liu, S., Du, Y., Cui, K., & Xu, L. (2010). Characterization of compacted loess by electrical resistivity method. In *GeoShanghai 2010 International Conference* (pp. 68–73).

Zhang, L., & Zhao, M. (2015). Deformation Analysis of Geotextile-Encased Stone Columns. *Int. J. Geomech*, 15(3), 1–10.

Zourmpakis, A., Boardman, D. I., Rogers, C. D. F., Jefferson, I., Gunn, D. A., Jackson, P. D.,Northmore, K. J., Entwisle, D. C., Nelder, L. M., Dixon, N. (2006). Case study of a loess collapse field trial in Kent, SE England. *Quarterly Journal of Engineering Geology and Hydrogeology*, 39, 131–150.

APPENDIX (A)

A1. The Published Paper

Treatment of Iraqi collapsible soil using encased stone columns

N. Al-Obaidy[i), ii)], I. Jefferson[iii)] and G. Ghataora[iv)]

i) Doctoral researcher, School of Civil Engineering, University of Birmingham, Edgbaston, Birmingham, B15 2TT, UK, e-mail: nka229@bham.ac.uk,
ii) Assistant Professor, Civil Engineering Department, College of Engineering, University of Thi-Qar, Iraq.
iii) Professor in Geotechnical Engineering, School of Civil Engineering, University of Birmingham, Edgbaston, Birmingham, B15 2TT, UK,e-mail: i.jefferson@bham.ac.uk.
iv) Senior Lecturer in Geotechnical Engineering, School of Civil Engineering, University of Birmingham, Edgbaston, Birmingham, B15 2TT, UK, e-mail: g.s.ghataora@bham.ac.uk.

ABSTRACT

Stone columns are widely used globally due to theirversatility and relative wide applicability to treat different soil and foundation situations but much of the research undertaken to date has focused on their use in soft soils. In countries like Iraq the use of stone columns is still limited from a practical point of view, chiefly as many other soil conditions are commonly encountered. These include collapsible soils: soils that are prone to relatively rapid volume compressions (through collapse of metastable fabrics) that occur due to the action of load and/or increases in water content. Recent work has opened up the possibility to use stone columns in these soils by the use of encasement, thereby overcoming the impact of loss of lateral support when collapse occurs.Area of potential will be discussed; why stone columns could be beneficial for use in Iraq and how employing them as an alternative to conventional ground improvement techniques in number of Iraqi projects would be cost saving and has other benefits.Also, a review of soil conditions in Iraq will be presented and focusing how to treat collapsible soil by encasing the individual stone column by geofabrics illustrating the scope for developing a reliable design approach which suits Iraqi soils. An evidence of their potential applicability in Iraqi soils will be presented. Moreover, the installation technique, facts regarding failure, factors control the behaviour of encased stone columns, calculation of bearing capacity and settlement and some previous related laboratory work will be reviewed as well as recommendations regarding the proposal work in this field are produced with this paper.

Keywords: Collapsible soils, Iraqi Problematic soils, encased stone columns, Ground improvement

A2. The Submitted Paper to IEEE Conference in Iraq

Modelling an Artificial Loess Soil; Assessing Its Collapsibility Behaviour through Conventional and Geophysics Testing

Nesreen Al-Obaidy
Civil Engineering, College of Engineering, University of Thi-Qar, Thi-Qar, Iraq

Ian Jefferson
Civil Engineering, School of Engineering University of Birmingham Birmingham, UK

Nigel Cassidy
Civil Engineering, School of Engineering University of Birmingham Birmingham, UK

Gurmel Ghataora
Civil Engineering, School of Engineering University of Birmingham Birmingham, UK

Abstract—this paper describes the method used to prepare small and large artificial loess samples. The silt and clay particles of the natural collapse soil were modeled in the laboratory by mixing a certain type of silica flour with different percentages of English China clay. A series of single and double oedometer tests have been conducted, the aim was to find out the collapse potential ranges obtained and how the artificial soil mimics the behaviour of natural deposits. Results compared with a natural loess sample and showed a good agreement. Another soil that has almost the same range of ground silica particles, but is from different geologic origin was tested too but it failed in producing the target collapsible soil. From this, the right mixture and method for developing a medium scale collapse sample were chosen. The physical model is tested under different soaking and loading conditions. The hidden surfaces of the soil are monitored by taking resistivity measurement to characterize the geophysical and hydraulical properties. Outcomes revealed that collapse is controlled by the degree of the saturation; soil resistivity was very sensitive to loading and wetting conditions during collapse.

Keywords—collapsible soil ;artificial loess; loess; resistivity; geophysics

APPENDIX (B)

B1. Calculations of Specific Gravity Gs for Soil (A), Soil (B) , and (ECC)

Table B-1: Specific gravity of Soil (A)

Bottle	1	2	3
Mass of bottle in g (w1)	48.17	47.81	48.55
Mass of bottle and dry soil in g (w2)	58.15	57.8	58.55
Mass of bottle, soil and water in g (w3)	112.13	112.38	112.84
Mass of bottle and water in g (w4)	105.95	106.15	106.6
w2-w1	9.98	9.99	10.0
w4-w1	57.78	58.34	58.05
w3-w2	53.98	54.58	54.29
Gs=(w2-w1)/((w4-w1)-(w3-w2))	2.63	2.66	2.66
Average	2.65		

Table B-2: Specific gravity of Soil (B)

Bottle	1	2	3
Mass of bottle in g (w1)	47.85	48.59	47.45
Mass of bottle and dry soil in g (w2)	57.85	58.59	57.45
Mass of bottle, soil and water in g (w3)	112.7	112.38	112.6
Mass of bottle and water in g (w4)	106.48	106.15	106.37
w2-w1	10	10	10
w4-w1	58.63	57.56	58.92
w3-w2	54.85	53.79	55.15
Gs=(w2-w1)/((w4-w1)-(w3-w2))	2.645503	2.65252	2.65252
Average	2.65		

Table B-3: Specific gravity of English china Clay (ECC)

Bottle	1	2	3
Mass of bottle in g (w1)	47.45	47.83	48.58
Mass of bottle and dry soil in g (w2)	55.45	55.82	56.56
Mass of bottle, soil and water in g (w3)	109.81	110.13	111.52
Mass of bottle and water in g (w4)	104.86	105.18	106.62
w2-w1	8	7.99	7.98
w4-w1	57.41	57.35	58.04
w3-w2	54.36	54.31	54.96
Gs=(w2-w1)/((w4-w1)-(w3-w2))	2.62	2.63	2.59
Average	2.61		

B2. Liquid Limit Calculations and corresponding curves for Soil (A), Soil (B) , and (ECC)

Table B-4: Liquid Limit calculations of Soil (A)

Sample No.	Trial No.	penetration in (mm)			Average penetration in (mm)	Mass of empty container (m1) in g	Mass of container and wet soil (m2) in g	Mass of container and dry soil (m3) in g	Mass of solid (ms) in g mw=m3-m1	Mass of water (mw) in g ms=m3-m1	Water content % =(mw/ms)* 100	Liquid Limit L.L at 20 mm	Average L.L
		Try (1)	Try (2)	Try (3)									
1	1	15.2	15.6		15.4	5.5	17.79	15.2	9.7	2.59	26.70103	28.2	≈28
	2	18.8	18.2	18.5	18.5	5.3	17.82	15.1	9.8	2.72	27.7551		
	3	19.5	20.2	19.7	19.8	4.8	16.21	13.7	8.9	2.51	28.20225		
	4	20.5	20.9		20.7	4.7	17.36	14.56	9.86	2.8	28.39757		
	5	23	23.4		23.2	5.6	18.36	15.5	9.9	2.86	28.88889		
	6	24.4	25.1	24.9	24.8	5.66	17.12	14.52	8.86	2.6	29.34537		
2	1	15.3	15.7		15.5	3.99	15.71	13.25	9.26	2.46	26.56587	27.8	
	2	17.3	17.9	18.2	17.8	4.44	16.71	14.09	9.65	2.62	27.15026		
	3	19.1	19.8	19.6	19.5	3.92	15.92	13.32	9.4	2.6	27.65957		
	4	20.1	20.5		20.3	5.65	17.29	14.75	9.1	2.54	27.91209		
	5	21.9	21.2	21.7	21.6	3.39	16.2	13.38	9.99	2.82	28.22823		
	6	23.7	24.1		23.9	5.01	16.98	14.31	9.3	2.67	28.70968		

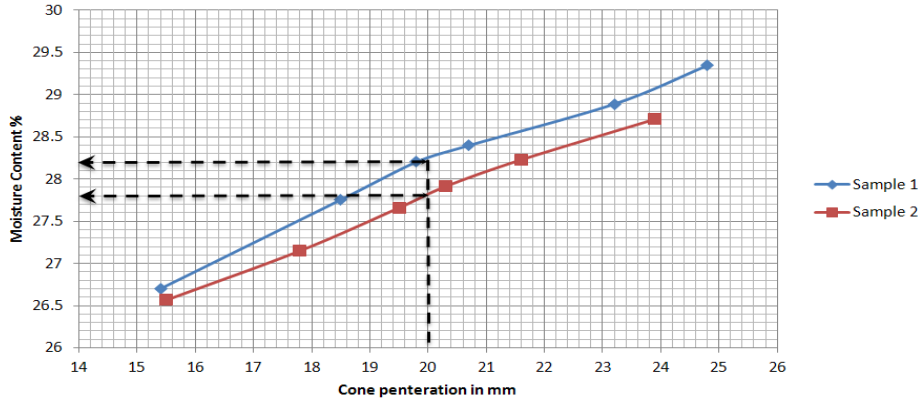

Figure B.1: Liquid Limit curve of Soil (A)

Table B-5: Liquid Limit calculations of Soil (B)

Sample No.	Trial No.	penetration in (mm)			Average penetration in (mm)	Mass of empty container (m1) in g	Mass of container and wet soil (m2) in g	Mass of container and dry soil (m3) in g	Mass of solid (ms) in g mw=m3-m1	Mass of water (mw) in g ms=m3-m1	Water content % =(mw/ms)* 100	Liquid Limit L.L at 20 mm	Average L.L
		Try (1)	Try (2)	Try (3)									
1	1	15.2	14.8		15	5.36	17.7	15.4	10.04	2.3	22.90837	24.4	≈24
	2	18	18		18	3.48	15.88	13.5	10.02	2.38	23.7525		
	3	20	20.6	20.3	20.3	5.5	17.9	15.46	9.96	2.44	24.49799		
	4	22.6	22	22.3	22.3	5.66	18.1	15.6	9.94	2.5	25.15091		
	5	23.8	24.4	23.8	24	5.6	18	15.48	9.88	2.52	25.50607		
	6	25	25.4		25.2	5.45	18.02	15.44	9.99	2.58	25.82583		
2	1	15.4	14.8	14.5	14.9	24.85	37.01	34.8	9.95	2.21	22.21106	24	
	2	17.6	18		17.8	24.24	36.76	34.4	10.16	2.36	23.22835		
	3	18.7	18.9		18.8	30.02	41.12	39	8.98	2.12	23.60802		
	4	20.7	21.3	21.3	21.1	33	45.29	42.89	9.89	2.4	24.26694		
	5	22.9	22.5		22.7	30.12	42.33	39.92	9.8	2.41	24.59184		
	6	25.4	24.7	24.9	25	5.66	17.06	14.76	9.1	2.3	25.27473		

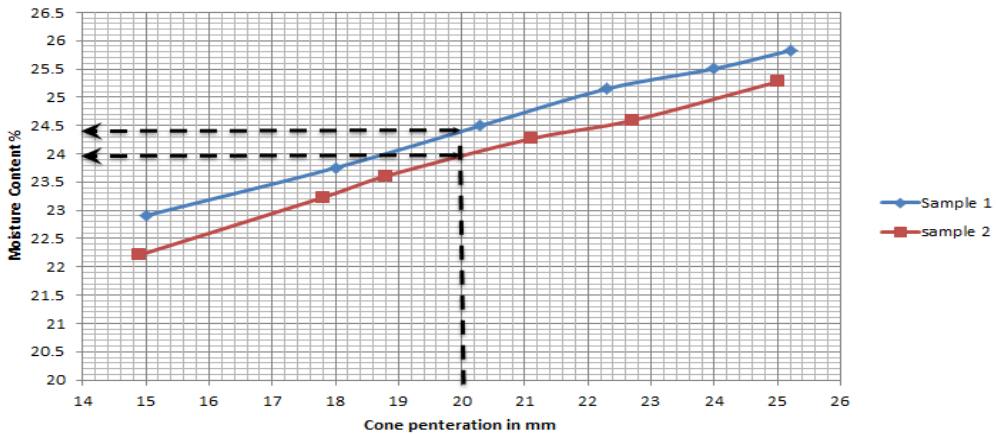

Figure B.2: Liquid Limit curve of Soil (B)

Table B-6: Liquid Limit calculations of English China Clay

Sample No.	Trial No.	penetration in (mm)		Average penetration in (mm)	Mass of empty container (m1) in g	Mass of container and wet soil (m2) in g	Mass of container and dry soil (m3) in g	Mass of solid (ms) in g mw=m3-m1	Mass of water (mw) in g ms=m3-m1	Water content % =(mw/ms)*100	Liquid Limit L.L at 20 mm	Average L.L
		Try (1)	Try (2)									
1	1	14.9	15.3	15.1	3.38	17.53	12.91	9.53	4.62	48.5	57.7	≈58
	2	18.2	17.8	18	4.09	18.66	13.55	9.46	5.11	54.0		
	3	19.6	20	19.8	5.65	21.35	15.63	9.98	5.72	57.3		
	4	20.3	20.7	20.5	5.66	22.4	16.22	10.56	6.18	58.5		
	5	23.4	23.6	23.5	4.85	19.63	13.92	9.07	5.71	63.0		
	6	24.9	24.7	24.8	4.09	18.93	13.12	9.03	5.81	64.0		
2	1	14.8	15.2	15	5.49	20.3	15.43	9.94	4.87	49.0	58.4	
	2	17.2	17.4	17.3	4.78	19.23	14.17	9.39	5.06	53.9		
	3	19.2	19.4	19.3	5.66	19.81	14.67	9.01	5.14	57.0		
	4	20.1	20.5	20.3	3.47	18.02	12.62	9.15	5.4	59.0		
	5	22.3	22.6	22.45	4.84	19.66	13.98	9.14	5.68	62.1		
	6	24	24.4	24.2	5.01	20.25	14.29	9.28	5.96	64.2		

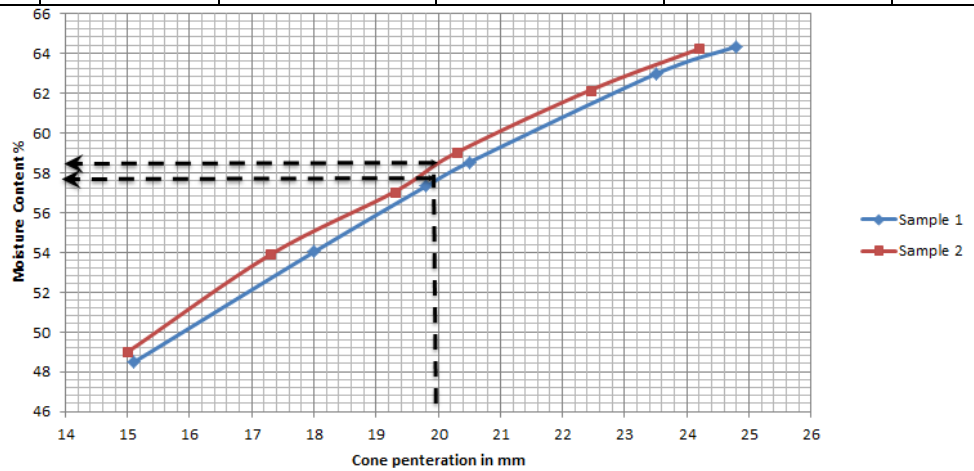

Figure B.3: Liquid Limit Curve of English China Clay (ECC)

B3. Plastic Limit Calculations for Soil (A), Soil (B) , and (ECC)

Table B-7: Plastic Limit calculations of Soil (A)

Sample No.	Trial No.	Mass of empty container (m1) in g	Mass of container and wet soil (m2) in g	Mass of container and dry soil (m3) in g	Mass of solid (ms) in g mw=m3-m1	Mass of water (mw) in g mw=m3-m1	Water content % =(mw/ms)*100	Plastic Limit P.L	Average P.L
1	1	4.48	6.9	6.5	2.02	0.4	19.8	20.1	≈20
	2	9.48	11.81	11.42	1.94	0.39	20.1		
	3	9.5	11.82	11.43	1.93	0.39	20.2		
	4	3.88	6.44	6.01	2.13	0.43	20.2		
2	1	5.65	8.27	7.83	2.18	0.44	20.2	20.1	
	2	4.85	7.3	6.89	2.04	0.41	20.1		
	3	3.47	6.12	5.68	2.21	0.44	19.9		
	4	5.66	8.11	7.7	2.04	0.41	20.1		

Table B-8: Plastic Limit calculations of Soil (B)

Sample No.	Trial No.	Mass of empty container (m1) in g	Mass of container and wet soil (m2) in g	Mass of container and dry soil (m3) in g	Mass of solid (ms) in g mw=m3-m1	Mass of water (mw) in g mw=m3-m1	Water content % =(mw/ms)*100	Plastic Limit P.L	Average P.L
1	1	6.36	8.61	8.33	1.97	0.28	14.21	14.09	≈14
	2	6.01	8.14	7.88	1.87	0.26	13.90		
	3	5.89	8.3	8	2.11	0.3	14.22		
	4	5.03	7.39	7.1	2.07	0.29	14.01		
2	1	4.87	7.09	6.81	1.94	0.28	14.43	14.34	
	2	3.48	5.62	5.35	1.87	0.27	14.44		
	3	5.67	8.19	7.87	2.2	0.32	14.54		
	4	4.86	7.15	6.87	2.01	0.28	13.93		

Table B-9: Plastic Limit calculations of English China Clay (ECC)

Sample No.	Trial No.	Mass of empty container (m1) in g	Mass of container and wet soil (m2) in g	Mass of container and dry soil (m3) in g	Mass of solid (ms) in g mw=m3-m1	Mass of water (mw) in g mw=m3-m1	Water content % =(mw/ms)*100	Plastic Limit P.L	Average P.L
1	1	3.38	6.36	5.64	2.26	0.72	31.9	32.1	≈32
	2	5.66	8.24	7.61	1.95	0.63	32.3		
	3	3.47	6.02	5.4	1.93	0.62	32.1		
	4	30.01	32.68	32.03	2.02	0.65	32.2		
2	1	25.4	28.79	27.97	2.57	0.82	31.9	32.0	
	2	4.08	6.52	5.93	1.85	0.59	31.9		
	3	15.33	18.16	17.47	2.14	0.69	32.2		
	4	13.7	16.21	15.6	1.9	0.61	32.1		

B4. Compaction Test Data for Soil (A), Soil (B) , and (ECC)

Table B-10: Compaction test data for Soil (A)

Trials No.	Sam -ple No.	Mass of empty container (m1) in g	Mass of container and wet soil (m2) in g	Mass of container and dry soil (m3) in g	Mass of water (mw) in g ms=m3-m1	Mass of solid (ms) in g mw=m3-m1	Water content % =(mw/ms) *100	Mass of empty mould (m4) in g	Mass of mould and wet soil (m5) in g	Mass of wet in soil (m6) in g m6=m5-m4 in g	Volume of Mould (v) in m^3	Mass of wet soil in kN	Wet unit weight of soil in kN/m γ_{wet} =m6/v	Dry unit weight of soil in kN/m γ_{dry} =γ_{wet} /(1+w)
1	1	5.48	30.79	29.86	0.93	24.38	3.81	3582	4944.2	1362.2	0.000991	0.013359	1.35E+01	1.30E+01
	2	5.67	32.91	30.96	1.95	25.29	7.71	3582	5049.4	1467.4	0.000991	0.01439	1.45E+01	1.35E+01
	3	5.45	30.81	28.25	2.56	22.8	11.23	3582	5153.2	1571.2	0.000991	0.015408	1.55E+01	1.40E+01
	4	4.8	29.09	26	3.09	21.2	14.58	3582	5244.2	1662.2	0.000991	0.016301	1.64E+01	1.44E+01
	5	3.48	28.38	24.33	4.05	20.85	19.42	3582	5405.06	1823.06	0.000991	0.017878	1.80E+01	1.51E+01
	6	24.14	49.39	44.82	4.57	20.68	22.10	3582	5429.67	1847.67	0.000991	0.018119	1.83E+01	1.50E+01
2	1	5.07	30.72	29.75	0.97	24.68	3.93	3582	4944.11	1362.11	0.000991	0.013358	1.35E+01	1.30E+01
	2	5.65	30.6	28.85	1.75	23.2	7.54	3582	5046.43	1464.43	0.000991	0.014361	1.45E+01	1.35E+01
	3	3.47	26.59	24.2	2.39	20.73	11.53	3582	5155.78	1573.78	0.000991	0.015434	1.56E+01	1.40E+01
	4	25.4	49	45.96	3.04	20.56	14.79	3582	5249.54	1667.54	0.000991	0.016353	1.65E+01	1.44E+01
	5	5.66	30.6	26.5	4.1	20.84	19.67	3582	5407.97	1825.97	0.000991	0.017907	1.81E+01	1.51E+01
	6	5.49	29.72	25.3	4.42	19.81	22.31	3582	5432.4	1850.4	0.000991	0.018146	1.83E+01	1.50E+01

Table B-11: Compaction test data for Soil (B)

Trials No.	Sam -ple No.	Mass of empty container (m1) in g	Mass of container and wet soil (m2) in g	Mass of container and dry soil (m3) in g	Mass of water (mw) in g ms=m3-m1	Mass of solid (ms) in g mw=m3-m1	Water content % =(mw/ms) *100	Mass of empty mould (m4) in g	Mass of mould and wet soil (m5) in g	Mass of wet in soil (m6) in g m6=m5-m4 in g	Volume of Mould (v) in m^3	Mass of wet soil in kN	Wet unit weight of soil in kN/m γ_{wet} =m6/v	Dry unit weight of soil in kN/m γ_{dry} =γ_{wet} /(1+w)
1	1	5.66	30.67	29.9	0.77	24.24	3.18	4278	5776.23	1498.23	0.000931	0.014693	1.58E+01	1.53E+01
	2	5.47	30.94	29.2	1.74	23.73	7.33	4278	5900.11	1622.11	0.000931	0.015907	1.71E+01	1.59E+01
	3	22.29	46.95	45	1.95	22.71	8.59	4278	6010.03	1732.03	0.000931	0.016985	1.82E+01	1.68E+01
	4	30	54.75	52	2.75	22	12.5	4278	6145.44	1867.44	0.000931	0.018313	1.97E+01	1.75E+01
	5	5.65	29.97	26.5	3.47	20.85	16.64	4278	6177.65	1899.65	0.000931	0.018629	2.00E+01	1.72E+01
	6	30.01	56.64	52.22	4.42	22.21	19.90	4278	6152.99	1874.99	0.000931	0.018387	1.98E+01	1.65E+01
2	1	3.47	28.78	28	0.78	24.53	3.18	4278	5780.9	1502.9	0.000931	0.014738	1.58E+01	1.53E+01
	2	5.07	30.77	29	1.77	23.93	7.40	4278	5903.32	1625.32	0.000931	0.015939	1.71E+01	1.59E+01
	3	3.07	28.38	26.4	1.98	23.33	8.49	4278	6013	1735	0.000931	0.017015	1.83E+01	1.68E+01
	4	5.65	30.8	28	2.8	22.35	12.53	4278	6142.08	1864.08	0.000931	0.01828	1.96E+01	1.74E+01
	5	5.65	32.9	29	3.9	23.35	16.70	4278	6188.1	1910.1	0.000931	0.018732	2.01E+01	1.72E+01
	6	3.47	29.21	24.94	4.27	21.47	19.89	4278	6160.64	1882.64	0.000931	0.018462	1.98E+01	1.65E+01

Table B-12: Compaction test data for English China Clay (ECC)

Trials No.	Sam -ple No.	Mass of empty container (m1) in g	Mass of container and wet soil (m2) in g	Mass of container and dry soil (m3) in g	Mass of water (mw) in g ms=m3-m1	Mass of solid (ms) in g mw=m3-m1	Water content % =(mw/ms) *100	Mass of empty mould (m4) in g	Mass of mould and wet soil (m5) in g	Mass of wet in soil (m6) in g m6=m5-m4 in g	Volume of Mould (v) in m^3	Mass of wet soil in kN	Wet unit weight of soil in kN/m γ_{wet} =m6/v	Dry unit weight of soil in kN/m γ_{dry} =γ_{wet} /(1+w)
1	1	3.87	31.54	27.5	4.04	23.63	17.10	4268	5773.12	1505.12	0.000931	0.01476	1.59E+01	1.35E+01
	2	3.47	33.45	28.22	5.23	24.75	21.13	4268	5855.32	1587.32	0.000931	0.015566	1.67E+01	1.38E+01
	3	24.7	52.98	47.35	5.63	22.65	24.86	4268	6000.05	1732.05	0.000931	0.016986	1.82E+01	1.46E+01
	4	30.01	61.3	54.21	7.09	24.2	29.30	4268	6052.29	1784.29	0.000931	0.017498	1.88E+01	1.45E+01
	5	5.66	33.31	26.3	7.01	20.64	33.96	4268	6020.32	1752.32	0.000931	0.017184	1.85E+01	1.38E+01
	6	5.06	34.96	26.7	8.26	21.64	38.17	4268	6017.54	1749.54	0.000931	0.017157	1.84E+01	1.33E+01
2	1	9.87	33.52	30.1	3.42	20.23	16.91	4268	5776	1508	0.000931	0.014788	1.59E+01	1.36E+01
	2	6.66	33.22	28.6	4.62	21.94	21.06	4268	5863.54	1595.54	0.000931	0.015647	1.68E+01	1.39E+01
	3	5.66	31.61	26.4	5.21	20.74	25.12	4268	6008.76	1740.76	0.000931	0.017071	1.83E+01	1.47E+01
	4	3.48	35.09	28	7.09	24.52	28.92	4268	6065.08	1797.08	0.000931	0.017623	1.89E+01	1.47E+01
	5	24.8	55.05	47.33	7.72	22.53	34.27	4268	6032.75	1764.75	0.000931	0.017306	1.86E+01	1.38E+01
	6	33.09	63.12	54.8	8.32	21.71	38.32	4268	6009.87	1741.87	0.000931	0.017082	1.83E+01	1.33E+01

B5. Technical Properties of Soil (A), Soil (B) , and English China Clay (ECC)

Table B-13: Technical Properties of Soil A (Ground Silica M10)

Supplier: Minerals Marketing Silverbond Range

Source Dessel, Belgium
Description High purity quartz sand dry ground and classified
Colour White

M10			Method
Control Sieve >63*u*m	2	%	Alpine
D10	4	*u*m	Malvern
D50	23	*u*m	Malvern
D90	60	*u*m	Malvern
Density	2.65	kg/dm^3	
Bulk Density	0.9	kg/dm^3	
Specific Surface	0.9	m^2/g	BET
Oil Absorption	17.5	g/100g	
Hardness	7	Mohs	
pH	7		
Loss on Ignition	0.12	%	
Colour L*	91		Minolta
a*	0.74		
b*	3.57		
Refractive Index	1.55		

Chemical Analysis

SiO_2	99.5
Fe_2O_3	0.03
Al_2O_3	0.20
TiO_2	0.03
K_2O	0.04
CaO	0.02

Table B-14: Technical Properties of Soil B (Ground Calcium Carbonate)

B6. Calculations of the Compaction Effort

Compaction Energy=(Weight of hammer*Height of drop of hammer*Number of blows per layer*Number of layers)/volume of mould

Mass of hammer=0.535 kg

Height of drop of hammer=0.03 m

Number of Layers=3

Number of blows per layer=25

Volume of the Oedometer ring (19.15 mm height and 74.74 mm inner diameter) = 8.46E-05 m^3

Weight = mass*acceleration

Acceleration=9.81 m/s^2

1 kg $(m/s)^2$= 1 $(kg.m2)/s^2$=J

KJ=1000J

Compaction Energy =[0.535 (kg)* 9.81 (m/s^2) *0.03m*3*25]/ 8.46E-05 m^3

= 139580.4159J/m^3 = 139.6 kJ/m^3

B7. Calculations of Specific Gravity Gs for Soil (A) mixed to different percentages of English China Clay

Table B-16: Specific Gravity of different mixture of Ground Silica M10 (Soil A) and English China Clay (ECC)

Soil	M10 =100% ECC=0%			M10 =95% ECC=5%			M10 =90% ECC=10%			M10 =85% ECC=15%			M10 =80% ECC=10%			M10 =75% ECC=25%		
Bottle	1	2	3	1	2	3	1	2	3	1	2	3	1	2	3	1	2	3
W1	48.17	47.81	48.55	46.89	47.82	48.48	47.43	46.9	47.83	48.58	46.47	47.82	48.17	47.83	46.9	46.47	47.82	46.87
W2	58.15	57.8	58.55	56.88	57.82	58.48	57.4	56.88	57.81	58.58	56.45	57.81	58.17	57.82	56.9	56.47	57.82	56.87
W3	112.13	112.38	112.84	111.98	112.27	112.8	112.18	112.07	112.8	112.83	112.24	112.85	112.23	112.82	112.12	112.23	112.27	112.13
W4	105.95	106.15	106.6	105.74	106.05	106.6	105.95	105.86	106.6	106.6	106.05	106.64	106	106.65	105.89	106	106.05	105.95
w2-w1	9.98	9.99	10.0	9.99	10	10	9.97	9.98	9.98	10	9.98	9.99	10	9.99	10	10	10	10
w4-w1	57.78	58.34	58.05	58.85	58.23	58.12	58.52	58.96	58.77	58.02	59.58	58.82	57.83	58.82	58.99	59.53	58.23	59.08
w3-w2	53.98	54.58	54.29	55.1	54.45	54.32	54.78	55.19	54.99	54.25	55.79	55.04	54.06	55	55.22	55.76	54.45	55.26
Gs	2.63	2.66	2.66	2.66	2.65	2.63	2.67	2.65	2.64	2.65	2.63	2.64	2.65	2.62	2.65	2.65	2.65	2.62
Average	2.65			2.65			2.65			2.64			2.64			2.64		

W1,w2,w3,w4, and Gs as defined and calculated in the Table above

B8. Liquid Limit calculations and corresponding curves for different mixture of ground silica Soil (A) and (ECC)

Table B-17: Calculations of liquid limit for different mixture of ground silica Soil (A) and (ECC)

Description	Sample No.	Trial No.	penetration in (mm)			Average penetration in (mm)	Mass of empty container (m1) in g	Mass of container and wet soil (m2) in g	Mass of container and dry soil (m3) in g	Mass of solid (ms) in g mw=m3-m1	Mass of water (mw) in g ms=m3-m1	Water content % =(mw/ms)*100	Liquid Limit L.L at 20 mm	Average L.L
			Try (1)	Try (2)	Try (3)									
100% M10	1	1	15.2	15.6		15.4	5.5	17.79	15.2	9.7	2.59	26.70	28.2	≈28
		2	18.8	18.2	18.5	18.5	5.3	17.82	15.1	9.8	2.72	27.76		
		3	19.5	20.2	19.7	19.8	4.8	16.21	13.7	8.9	2.51	28.20		
		4	20.5	20.9		20.7	4.7	17.36	14.56	9.86	2.8	28..40		
		5	22.9	23.4	23.3	23.2	5.6	18.36	15.5	9.9	2.86	28.89		
		6	24.4	25.1	24.9	24.8	5.66	17.12	14.52	8.86	2.6	29.35		
	2	1	15.3	15.7		15.5	3.99	15.71	13.25	9.26	2.46	26.57	27.8	
		2	17.3	17.9	18.2	17.8	4.44	16.71	14.09	9.65	2.62	27.15		
		3	19.1	19.8	19.6	19.5	3.92	15.92	13.32	9.4	2.6	27.66		
		4	20.1	20.6	20.2	20.3	5.65	17.29	14.75	9.1	2.54	27.91		
		5	21.9	21.2	21.7	21.6	3.39	16.2	13.38	9.99	2.82	28.23		
		6	23.7	24.1		23.9	5.01	16.98	14.31	9.3	2.67	28.71		
95%M10 + 5% ECC		1	15.4	16	16	15.8	30.01	41.39	38.98	8.97	2.41	26.9	28.4	≈28
		2	18.9	19.6	18.8	19.1	29.98	41.68	39.11	9.13	2.57	28.1		
		3	20.6	21.2	20.6	20.8	32.12	43.49	40.97	8.85	2.52	28.5		
		4	22.7	22.3		22.5	33.01	43.82	41.4	8.39	2.42	28.8		
		5	24	24.4		24.2	30.21	42.14	39.44	9.23	2.7	29.3		
		6	24.7	25.3	25.3	25.1	30.13	42.06	39.32	9.19	2.74	29.8		
		1	15.4	15.6		15.5	5.66	17.85	15.3	9.64	2.55	26.5	28.1	
		2	17.3	18	18.1	17.8	5.65	16.62	14.25	8.6	2.37	27.6		
		3	19.3	18.9		19.1	5.48	17.35	14.76	9.28	2.59	27.9		
		4	21.5	20.9	21.8	21.4	3.48	15.49	12.83	9.35	2.66	28.4		
		5	23.1	22.5	22.8	22.8	3.47	16.21	13.37	9.9	2.84	28.7		

		6	24.4	25	25.3	24.9	5.36	16.92	14.3	8.94	2.62	29.3		
90%M10 + 10% ECC		1	15.4	15.8		15.6	4.48	17.15	14.45	9.97	2.7	27.1	28.8	≈29
		2	18	18.4		18.2	9.78	22.77	19.9	10.12	2.87	28.4		
		3	20.2	19.6	19.6	19.8	9.77	22.96	20.01	10.24	2.95	28.8		
		4	21.5	22.1	21.8	21.8	5.01	17.88	14.97	9.96	2.91	29.2		
		5	23.2	23.8	23.8	23.6	5.66	18.58	15.62	9.96	2.96	29.7		
		6	24.4	25	24.1	24.5	5.66	18.12	15.24	9.58	2.88	30.1		
		1	14.9	15.5	15.2	15.2	3.47	16.04	13.4	9.93	2.64	26.6	28.5	
		2	16.8	17.4	17.4	17.2	3.85	16.53	13.8	9.95	2.73	27.4		
		3	19.1	19.5		19.3	4.87	17.69	14.86	9.99	2.83	28.3		
		4	21.5	21.9		21.7	5.65	18.52	15.64	9.99	2.88	28.8		
		5	23	23.4		23.2	3.66	16.52	13.6	9.94	2.92	29.4		
		6	25	24.4	25	24.8	3.65	16.52	13.57	9.92	2.95	29.7		
85%M10 + 15% ECC		1	15	15.5	15.1	15.2	9.87	22.55	19.82	9.95	2.73	27.4	29.3	≈29
		2	16.6	17		16.8	8.89	21.65	18.85	9.96	2.8	28.1		
		3	19.3	19.7		19.5	5.66	18.56	15.65	9.99	2.91	29.1		
		4	20.6	21		20.8	4.85	17.76	14.82	9.97	2.94	29.5		
		5	22.5	23	22.6	22.7	3.47	16.49	13.5	10.03	2.99	29.8		
		6	24.4	25	24.7	24.7	24.7	37.65	34.65	9.95	3	30.2		
		1	15.5	15.7		15.6	9.45	22.04	19.35	9.9	2.69	27.2	28.7	
		2	17.6	18.3	18.1	18	6.3	19.03	16.24	9.94	2.79	28.1		
		3	19	19.5	19.1	19.2	6.33	19.19	16.34	10.01	2.85	28.5		
		4	21	20.5	20.6	20.7	4.65	17.57	14.67	10.02	2.9	28.9		
		5	22.3	21.9		22.1	5.65	18.52	15.6	9.95	2.92	29.3		
		6	24.7	24.3		24.5	3.86	16.74	13.79	9.93	2.95	29.7		
80%M10 + 20% ECC		1	14.7	15.1		14.9	5.03	17.74	15.01	9.98	2.73	27.4	29.5	≈29
		2	16.9	16.7		16.8	5.65	18.43	15.62	9.97	2.81	28.2		
		3	19.3	19.9	19.9	19.7	5.66	18.57	15.64	9.98	2.93	29.4		
		4	20.5	21.1	20.5	20.7	5.85	18.81	15.85	10	2.96	29.6		
		5	22.3	21.7	22.3	22.1	5.07	18.13	15.12	10.05	3.01	30.0		
		6	24.8	24.4		24.6	5.1	18.13	15.09	9.99	3.04	30.4		
		1	15.5	14.9	14.9	15.1	3.47	16.23	13.51	10.04	2.72	27.1	28.8	

		2	17.6	16.9	17.1	17.2	3.85	16.6	13.81	9.96	2.79	28.0		
		3	19.2	18.8		19	3.9	16.7	13.86	9.96	2.84	28.5		
		4	20.6	21.2	20.9	20.9	3.87	16.82	13.9	10.03	2.92	29.1		
		5	22.8	23.2		23	3.91	16.92	13.96	10.05	2.96	29.5		
		6	24.8	25		24.9	3.55	16.56	13.57	10.02	2.99	29.8		
75%M10 + 25% ECC		1	15.7	15.3		15.5	3.45	16.2	13.4	9.95	2.8	28.1	29.7	≈29
		2	17.4	18	17.4	17.6	5.66	18.48	15.61	9.95	2.87	28.8		
		3	19.3	19.5		19.4	3.87	16.78	13.84	9.97	2.94	29.5		
		4	20.7	21.1		20.9	5.89	18.81	15.83	9.94	2.98	30.0		
		5	22.8	23.4	23.4	23.2	5.03	17.98	14.95	9.92	3.03	30.5		
		6	25	24.6		24.8	5.55	18.05	15.1	9.55	2.95	30.9		
		1	15.2	15.6		15.4	5.67	18.32	15.6	9.93	2.72	27.4	29	
		2	16.8	16.2	17.1	16.7	5.6	18.21	15.45	9.85	2.76	28.0		
		3	18.4	19	19	18.8	3.85	16.59	13.75	9.9	2.84	28.7		
		4	21	21.2		21.1	3.54	16.44	13.51	9.97	2.93	29.4		
		5	23	22.3	22.5	22.6	4.5	17.42	14.45	9.95	2.97	29.8		
		6	24.6	25.2	24.6	24.8	3.55	16.49	13.49	9.94	3	30.2		

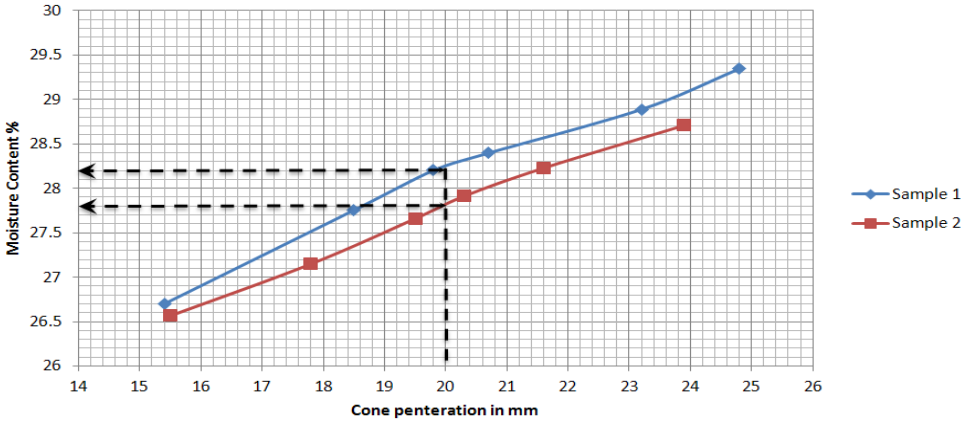

Figure B.4: Liquid Limit Curve of soil 100% ground silica M10

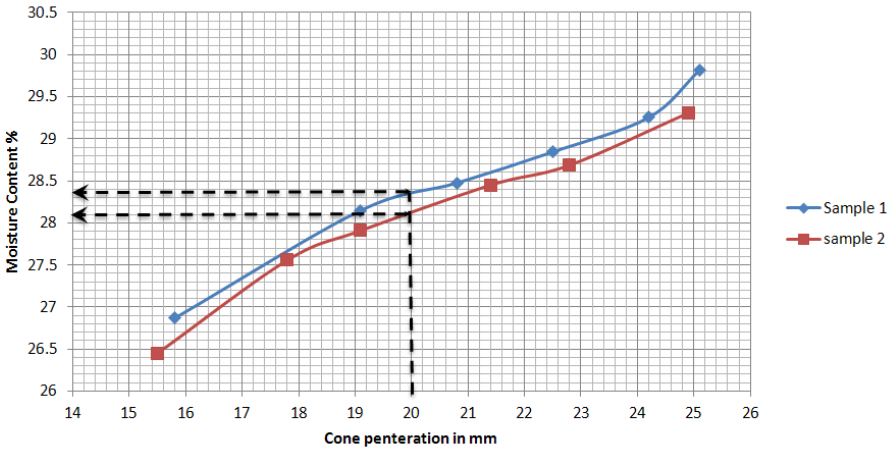

Figure B.5: Liquid Limit Curve of soil 95% ground silica M10 + 5% ECC

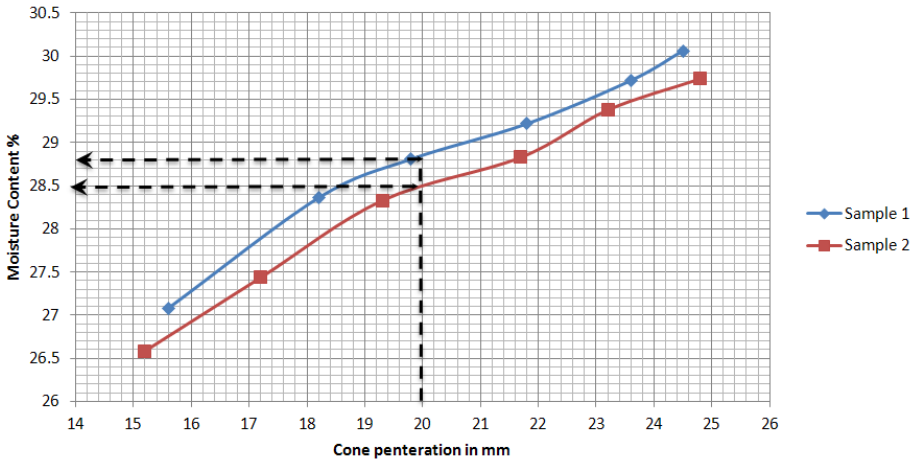

Figure B.6: Liquid Limit Curve of soil 90% ground silica M10 + 10% ECC

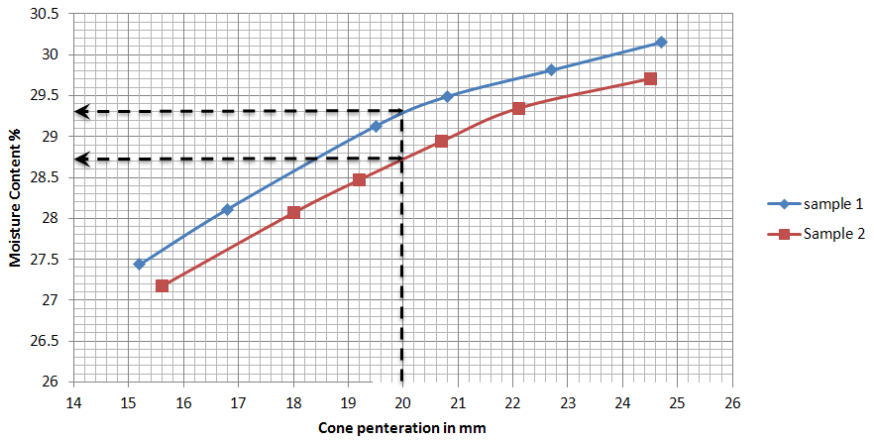

Figure B.7: Liquid Limit Curve of soil 85% ground silica M10 + 15% ECC

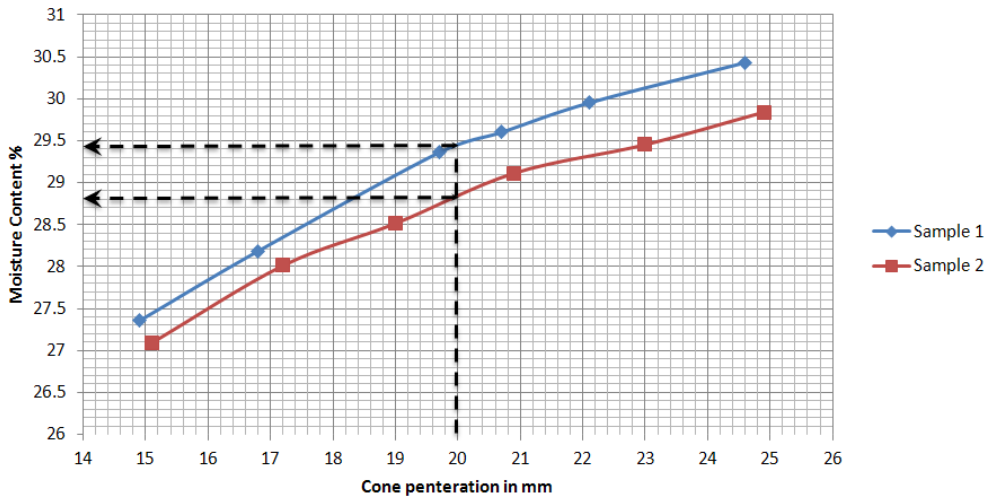

Figure B.8: Liquid Limit Curve of soil 80% ground silica M10 + 20% ECC

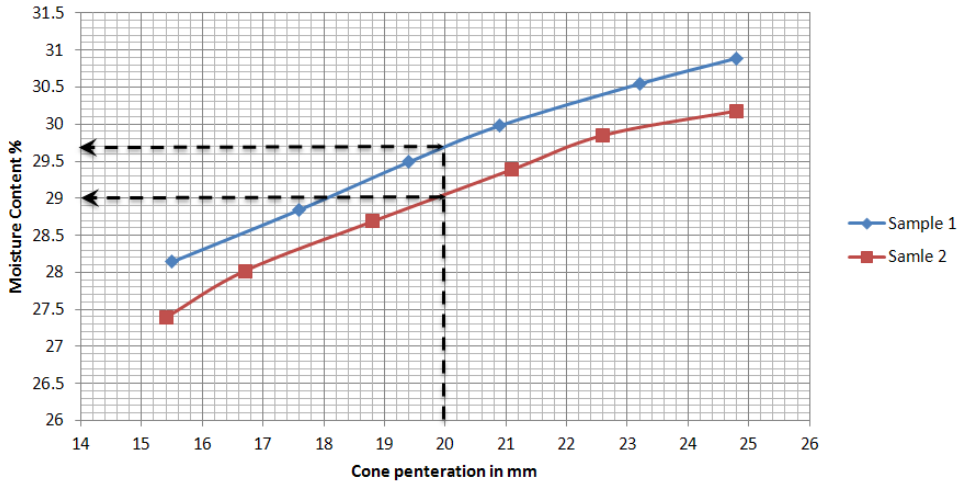

Figure B.9: Liquid Limit Curve of soil 75% ground silica M10 + 25% ECC

B9. Plastic Limit calculations for different mixture of ground silica Soil (A) and (ECC)

Table B-18: Calculations plastic limit for different mixture of ground silica Soil (A) and (ECC)

Description	Sample No.	Trial No.	Mass of empty container (m1) in g	Mass of container and wet soil (m2) in g	Mass of container and dry soil (m3) in g	Mass of solid (ms) in g mw=m3-m1	Mass of water (mw) in g mw=m3-m1	Water content % =(mw/ms)*100	Plastic Limit P.L	Average P.L
100% M10	1	1	4.48	6.9	6.5	2.02	0.4	19.8	20.1	≈20
		2	9.48	11.81	11.42	1.94	0.39	20.1		
		3	9.5	11.82	11.43	1.93	0.39	20.2		
		4	3.88	6.44	6.01	2.13	0.43	20.2		
	2	1	5.65	8.27	7.83	2.18	0.44	20.2	20.1	
		2	4.85	7.3	6.89	2.04	0.41	20.1		
		3	3.47	6.12	5.68	2.21	0.44	19.9		
		4	5.66	8.11	7.7	2.04	0.41	20.1		
95% M10 + 5% ECC	1	1	24.78	27.17	26.77	1.99	0.4	20.1	20.2	≈20
		2	30.01	32.37	31.97	1.96	0.4	20.4		
		3	30.11	32.38	32	1.89	0.38	20.1		
		4	29.98	32.66	32.21	2.23	0.45	20.2		
	2	1	24.8	27.18	26.78	1.98	0.4	20.2	20.0	
		2	32.4	34.91	34.49	2.09	0.42	20.1		
		3	33.01	35.73	35.28	2.27	0.45	19.8		
		4	27.8	30.14	29.75	1.95	0.39	20.0		
90% M10 + 10% ECC	1	1	5.65	8.1	7.68	2.03	0.42	20.7	20.7	≈21
		2	5.66	8.06	7.65	1.99	0.41	20.6		
		3	3.47	5.93	5.51	2.04	0.42	20.6		
		4	9.85	12.23	11.82	1.97	0.41	20.8		
	2	1	5.01	7.57	7.13	2.12	0.44	20.8	20.6	

		2	3.85	6.21	5.81	1.96	0.4	20.4		
		3	3.9	6.25	5.85	1.95	0.4	20.5		
		4	5.81	8.3	7.87	2.06	0.43	20.9		
85% M10 + 15% ECC	1	1	30.01	32.44	32.02	2.01	0.42	20.9	20.9	≈21
		2	30	32.38	31.97	1.97	0.41	20.8		
		3	24.25	26.62	26.21	1.96	0.41	20.9		
		4	9.87	12.23	11.82	1.95	0.41	21.0		
	2	1	33	35.46	35.04	2.04	0.42	20.6	20.7	
		2	30.87	33.32	32.9	2.03	0.42	20.7		
		3	30.03	32.4	31.99	1.96	0.41	20.9		
		4	30	32.5	32.07	2.07	0.43	20.8		
80% M10 + 20% ECC	1	1	24.7	27.11	26.67	1.97	0.44	22.3	22.2	≈22
		2	30.1	32.57	32.12	2.02	0.45	22.3		
		3	30.09	32.54	32.1	2.01	0.44	21.9		
		4	30	32.43	31.99	1.99	0.44	22.1		
	2	1	33.01	35.6	35.13	2.12	0.47	22.2	22.2	
		2	30.11	32.64	32.18	2.07	0.46	22.2		
		3	24.85	27.24	26.81	1.96	0.43	21.9		
		4	24.24	26.7	26.25	2.01	0.45	22.4		
80% M10 + 20% ECC	1	1	5.66	8.22	7.75	2.09	0.47	22.5	22.5	≈22
		2	5.65	7.95	7.53	1.88	0.42	22.3		
		3	5.66	8.03	7.59	1.93	0.44	22.8		
		4	5.48	8.16	7.67	2.19	0.49	22.4		
	2	1	5.47	7.99	7.54	2.07	0.45	21.7	22.2	
		2	5.33	8.02	7.53	2.2	0.49	22.3		
		3	5.84	8.26	7.82	1.98	0.44	22.2		
		4	5.67	8.08	7.65	1.98	0.43	21.7		

B10. Compaction test calculations for different mixture of ground silica Soil (A) and (ECC)

Table B-19: Compaction test data for mixture of 95% ground silica M10 and 5% English China Clay (ECC)

Trials No.	Sam -ple No.	Mass of empty container (m1) in g	Mass of container and wet soil (m2) in g	Mass of container and dry soil (m3) in g	Mass of water (mw) in g ms=m3-m1	Mass of solid (ms) in g mw=m3-m1	Water content % =(mw/ms) *100	Mass of empty mould (m4) in g	Mass of mould and wet soil (m5) in g	Mass of wet in soil (m6) in g m6=m5-m4 in g	Volume of Mould (v) in m^3	Mass of wet soil in kN	Wet unit weight of soil in kN/m γ_{wet} =m6/v	Dry unit weight of soil in kN/m γ_{dry} =γ_{wet} /(1+w)
1	1	3.48	29.32	28.3	1.02	24.82	4.11	3582	4966.4	1384.4	0.000931	0.013576	1.37E+01	1.32E+01
	2	3.48	28.67	26.75	1.92	23.27	8.25	3582	5083.75	1501.75	0.000931	0.014727	1.49E+01	1.37E+01
	3	5.65	30.11	27.47	2.64	21.82	12.10	3582	5189.87	1607.87	0.000931	0.015768	1.59E+01	1.42E+01
	4	4.8	30.2	26.68	3.52	21.88	16.09	3582	5320.25	1738.25	0.000931	0.017046	1.72E+01	1.48E+01
	5	5.47	31.54	27.4	4.14	21.93	18.88	3582	5425.5	1843.5	0.000931	0.018079	1.82E+01	1.53E+01
	6	5.65	37	31.33	5.67	25.68	22.08	3582	5445.1	1863.1	0.000931	0.018271	1.84E+01	1.51E+01
2	1	24.15	49.15	48.2	0.95	24.05	3.95	3582	4968.99	1386.99	0.000931	0.013602	1.37E+01	1.32E+01
	2	25.4	50.41	48.6	1.81	23.2	7.80	3582	5076.3	1494.3	0.000931	0.014654	1.48E+01	1.37E+01
	3	25.41	50.7	48.01	2.69	22.6	11.90	3582	5192.8	1610.8	0.000931	0.015797	1.59E+01	1.42E+01
	4	5.66	30.63	27.2	3.43	21.54	15.92	3582	5314.7	1732.7	0.000931	0.016992	1.71E+01	1.48E+01
	5	3.47	28.97	24.89	4.08	21.42	19.05	3582	5409.7	1827.7	0.000931	0.017924	1.81E+01	1.52E+01
	6	5.47	30.58	26.04	4.54	20.57	22.07	3582	5439.26	1857.26	0.000931	0.018213	1.84E+01	1.51E+01

Table B-20: Compaction test data for mixture of 90% ground silica M10 and 10% English China Clay (ECC)

Trials No.	Sam -ple No.	Mass of empty container (m1) in g	Mass of container and wet soil (m2) in g	Mass of container and dry soil (m3) in g	Mass of water (mw) in g ms=m3-m1	Mass of solid (ms) in g mw=m3-m1	Water content % =(mw/ms) *100	Mass of empty mould (m4) in g	Mass of mould and wet soil (m5) in g	Mass of wet in soil (m6) in g m6=m5-m4 in g	Volume of Mould (v) in m^3	Mass of wet soil in kN	Wet unit weight of soil in kN/m γ_{wet} =m6/v	Dry unit weight of soil in kN/m γ_{dry} =γ_{wet} /(1+w)
1	1	5.47	28.8	27.5	1.3	22.03	5.90	3582	5040.7	1458.7	0.000991	0.014305	1.44E+01	1.36E+01
	2	5.65	30.5	28.2	2.3	22.55	10.20	3582	5153.2	1571.2	0.000991	0.015408	1.55E+01	1.41E+01
	3	25.3	51.07	47.54	3.53	22.24	15.87	3582	5335	1753	0.000991	0.017191	1.73E+01	1.50E+01
	4	5.66	30.3	26.51	3.79	20.85	18.18	3582	5413.5	1831.5	0.000991	0.017961	1.81E+01	1.53E+01
	5	5.89	33.93	28.49	5.44	22.6	24.07	3582	5473.1	1891.1	0.000991	0.018545	1.87E+01	1.51E+01
2	1	3.48	27.85	26.45	1.4	22.97	6.09	3582	5043	1461	0.000991	0.014328	1.45E+01	1.36E+01
	2	5.47	30.31	28.1	2.21	22.63	9.77	3582	5150.35	1568.35	0.000991	0.01538	1.55E+01	1.41E+01
	3	5.64	30.42	27	3.42	21.36	16.01	3582	5345.1	1763.1	0.000991	0.01729	1.74E+01	1.50E+01
	4	5.65	31.4	27.5	3.9	21.85	17.85	3582	5408.3	1826.3	0.000991	0.01791	1.81E+01	1.53E+01
	5	5.64	30.5	25.7	4.8	20.06	23.93	3582	5477.5	1895.5	0.000991	0.018589	1.88E+01	1.51E+01

Table B-21: Compaction test data for mixture of 85% ground silica M10 and 15% English China Clay (ECC)

Trials No.	Sam -ple No.	Mass of empty container (m1) in g	Mass of container and wet soil (m2) in g	Mass of container and dry soil (m3) in g	Mass of water (mw) in g ms=m3-m1	Mass of solid (ms) in g mw=m3-m1	Water content % =(mw/ms) *100	Mass of empty mould (m4) in g	Mass of mould and wet soil (m5) in g	Mass of wet in soil (m6) in g m6=m5-m4 in g	Volume of Mould (v) in m^3	Mass of wet soil in kN	Wet unit weight of soil in kN/m γ_{wet} =m6/v	Dry unit weight of soil in kN/m γ_{dry} =γ_{wet} /(1+w)
1	1	33.7	59.1	58.1	1	24.4	4.10	3582	5000.05	1418.05	0.000991	0.013906	1.40E+01	1.35E+01
	2	33	55.4	53.4	2	20.4	9.80	3582	5168.22	1586.22	0.000991	0.015556	1.57E+01	1.43E+01
	3	32	54.58	51.5	3.08	19.5	15.79	3582	5379.54	1797.54	0.000991	0.017628	1.78E+01	1.54E+01
	4	32.9	60.68	55.7	4.98	22.8	21.84	3582	5455.13	1873.13	0.000991	0.018369	1.85E+01	1.52E+01
2	1	32.03	57.39	56.44	0.95	24.41	3.89	3582	4994.76	1412.76	0.000991	0.013854	1.40E+01	1.35E+01
	2	33.68	57.31	55.1	2.21	21.42	10.32	3582	5175.7	1593.7	0.000991	0.015629	1.58E+01	1.43E+01
	3	33.03	57.4	54	3.4	20.97	16.21	3582	5393.04	1811.04	0.000991	0.01776	1.79E+01	1.54E+01
	4	32	57.65	53	4.65	21	22.14	3582	5462.36	1880.36	0.000991	0.01844	1.86E+01	1.52E+01

Table B-22: Compaction test data for mixture of 80% ground silica M10 and 20% English China Clay (ECC)

.	Sam -ple No.	Mass of empty container (m1) in g	Mass of container and wet soil (m2) in g	Mass of container and dry soil (m3) in g	Mass of water (mw) in g ms=m3-m1	Mass of solid (ms) in g mw=m3-m1	Water content % =(mw/ms) *100	Mass of empty mould (m4) in g	Mass of mould and wet soil (m5) in g	Mass of wet in soil (m6) in g m6=m5-m4 in g	Volume of Mould (v) in m^3	Mass of wet soil in kN	Wet unit weight of soil in kN/m γ_{wet} =m6/v	Dry unit weight of soil in kN/m γ_{dry} =γ_{wet} /(1+w)
1	1	13.5	39.46	38.01	1.45	24.51	5.92	3582	5068.5	1486.5	0.000931	0.014578	1.47E+01	1.39E+01
	2	20.1	45.77	43.4	2.37	23.3	10.17	3582	5212.35	1630.35	0.000931	0.015988	1.61E+01	1.46E+01
	3	23.7	55.98	51.5	4.48	27.8	16.12	3582	5443.2	1861.2	0.000931	0.018252	1.84E+01	1.59E+01
	4	15.4	39.74	35.7	4.04	20.3	19.90	3582	5495.4	1913.4	0.000931	0.018764	1.89E+01	1.58E+01
	5	22.2	48.95	44.1	4.85	21.9	22.15	3582	5502.5	1920.5	0.000931	0.018834	1.90E+01	1.56E+01
2	1	24.5	49.95	48.47	1.48	23.97	6.17	3582	5072.1	1490.1	0.000931	0.014613	1.47E+01	1.39E+01
	2	33.68	57.21	55.1	2.11	21.42	9.85	3582	5198.1	1616.1	0.000931	0.015849	1.60E+01	1.46E+01
	3	33	58.5	55	3.5	22	15.91	3582	5450	1868	0.000931	0.018319	1.85E+01	1.59E+01
	4	5.67	33.59	28.9	4.69	23.23	20.19	3582	5505.13	1923.13	0.000931	0.018859	1.90E+01	1.58E+01
	5	5.47	32.2	27.4	4.8	21.93	21.89	3582	5509	1927	0.000931	0.018897	1.91E+01	1.56E+01

Table B-23: Compaction test data for mixture of 75% ground silica M10 and 25% English China Clay (ECC)

Trials No.	Sam -ple No.	Mass of empty container (m1) in g	Mass of container and wet soil (m2) in g	Mass of container and dry soil (m3) in g	Mass of water (mw) in g ms=m3-m1	Mass of solid (ms) in g mw=m3-m1	Water content % =(mw/ms) *100	Mass of empty mould (m4) in g	Mass of mould and wet soil (m5) in g	Mass of wet in soil (m6) in g m6=m5-m4 in g	Volume of Mould (v) in m^3	Mass of wet soil in kN	Wet unit weight of soil in kN/m γ_{wet} =m6/v	Dry unit weight of soil in kN/m γ_{dry} =γ_{wet} /(1+w)
1	1	5.67	31.27	29.8	1.47	24.13	6.09	3582	5079.01	1497.01	0.000991	0.014681	1.48E+01	1.40E+01
	2	5.35	30.26	28	2.26	22.65	9.98	3582	5212.72	1630.72	0.000991	0.015992	1.61E+01	1.47E+01
	3	5.68	32.15	28.5	3.65	22.82	15.99	3582	5463.9	1881.9	0.000991	0.018455	1.86E+01	1.61E+01
	4	5.47	31.34	27	4.34	21.53	20.16	3582	5530	1948	0.000991	0.019103	1.93E+01	1.60E+01
	5	5.8	34.7	29	5.7	23.2	24.57	3582	5523.88	1941.88	0.000991	0.019043	1.92E+01	1.54E+01
2	1	5.68	32.09	30.6	1.49	24.92	5.98	3582	5085.25	1503.25	0.000991	0.014742	1.49E+01	1.40E+01
	2	3.47	29.5	27.1	2.4	23.63	10.16	3582	5222.3	1640.3	0.000991	0.016086	1.62E+01	1.47E+01
	3	3.24	28.5	25	3.5	21.76	16.08	3582	5471.8	1889.8	0.000991	0.018533	1.87E+01	1.61E+01
	4	5.01	33.65	28.9	4.75	23.89	19.888	3582	5515	1933	0.000991	0.018956	1.91E+01	1.60E+01
	5	5.17	32.6	27.4	5.2	22.23	23.39	3582	5499.23	1917.23	0.000991	0.018802	1.90E+01	1.54E+01

APPENDIX (C)

C1. Calculations the Deformation of the Footing Plate

plate diameter	a	=	70.000	mm	0.070	m
Plate thickness	t	=	14.500	mm	plate radius =	0.035 m
Modulus of elasticity (mild steel)=			212	Gpa		

Using equation presented by Oberg et al. 2000 the thickness of the plate is not greater than one-quarter the least width of the plate

d=0.22Wr2/Et3 when d=deflection of the plate

area= 0.003848 m^2 =

Maximum deflection at centre for fixed edges , and load at centre (p)

Stress in kPa	Load in N	Load in kN	maximum deflection in mm	Deflection in m
100	385	0.385	1.60539E-07	0.000160539
200	770	0.77	3.21077E-07	0.000321077
300	1155	1.155	4.81616E-07	0.000481616
400	1540	1.54	6.42155E-07	0.000642155
800	1925	1.925	8.02693E-07	0.000802693

C2. Calculation of Void Ratio and Porosity of the Filter Layer (Gravel and Sand) and the Soil

C2.1 Porosity of the Gravel Layer (90 mm Depth from the Base of the Tank)

Volume of the gravel layer [349 mm (the inner diameter of the tank)*90 mm (the depth of the layer)] =Vt=$8.613x10^{-3}m^3$

Mass of soil to fill the layer (ms) = 18kg

Volume of solid (Vs) =Ms/(Gs*ρ_w)

Gs: Particle density of soil =2.67

ρ_w: denity of water =1000 kg/m^3

Vs=18/(2.67*1000)= $5.243x10^{-3}$ m^3

Vv= Vt-Vs =$8.163x10^{-3}$-$5.243x10^{-3}$=$3.370x10^{-3}$

Void ratio (e) = Vv/Vs

$e=3.37x10^{-3}/5.243x10^{-3}$

e=0.64

Porosity (n) = Vv/Vt

$n=3.370x10^{-3}/8.613x10^{-3}$

n=39%

C2.2 Porosity of the Thin Layer of the Sand above the Gravel (10 mm Depth above the Gravel Layer)

Volume of the layer [349 mm (the inner diameter of the tank)*10 mm (the depth of the layer)] $=Vt=9.574x10^{-4}\ m^3$

Mass of soil to fill the layer (Ms) = 2 kg

Volume of solid (Vs) $=Ms/(Gs*\rho_w)$

Gs: Particle density of soil =2.65

ρ_w: denity of water $=1000\ kg/m^3$

$Vs=2/(2.65*1000)=7.547x10^{-4}$ m3

$Vv= Vt-Vs =2.020x10^{-4}$

Void ratio (e) = Vv/Vs

$e=2.020x10^{-4}/7.547x10^{-4}$ m3

e=0.27

Porosity (n) = Vv/Vt

$n=2.020x10^{-4}/9.574x10^{-4}$

n=22%

C3. Calculations of the Compaction Effort

Compaction Energy = (Weight of hammer*Height of drop of hammer*Number of blows per layer*Number of layers)/Volume of mould

To calculate Compaction energy for one soil layer of height of 60 mm

Mass of hammer=2.5 kg

Height of drop of hammer=0.125 m

Initial Height of drop of hammer to avoid dust =0.02 m

Number of Layers=3

Number of blows per layer=75

Volume of the compacted soil layer (60 mm height in tank of 349 mm inner diameter)= 0.00574 m^3

Weight = mass*acceleration

Acceleration=9.81 m/s^2

1 kg $(m/s)^2$= 1 $(kg.m^2)/s^2$=J

KJ=1000J

Energy of compaction one layer of soil=[2.5 (kg)* 9.81 (m/s^2) *0.125m*3*75]/0.00574m^3 +[2.5 (kg)* 9.81 (m/s^2) *0.02m*3*75]/0.00574m^3

= 139.5 kJ/m^3

C4. Calculations of Void Ratio, Porosity, and Dry Density of the Soil

Volume of one layer of soil [349 mm (the inner diameter of the tank)*60 mm (the depth of the layer)] =Vt=5.74x10^{-3} m^3

Mass of soil to fill one layer (Ms)= 7.85 kg

Volume of solid (vs) =Ms/(Gs*ρ_w)

Gs: Particle density of soil =2.64

ρ_w: denity of water in kg/m^3

Vs=7.85/(2.64*1000)=2.97x10^{-3} m^3

Volume of void (vv)=Vt-Vs

Vv=2.77x10^{-3}

Void ratio (e) = Vv/Vs

e=2.77x10^{-3}/2.97x10^{-3}

e=0.93

Porosity (n) = Vv/Vt

n=2.77x10^{-3}/5.74x10^{-3}

n=48.3%

Bulk (Dry) Density =Ms/Vt

γ dry=7.85/5.74x10^{-3} =13.7 kN/m^3

C5. Calculations of Water Required to Fill Voids in the Filter Layer

Volum of voids in gravel layer (Vv gravel)=3.37x10^{-3} m^3

Volum of voids in sand layer (Vv sand)= 0.20x10^{-3} m^3

Volum of voids in the whole filter layer (Vv filter)= Vv gravel + Vv sand = 3.57x10^{-3} m^3 =3.57 L

C6. Calculations of water required to saturate the half of the tank (volume of 180 mm layer depth of the soil)

Total volume (Vt) for 180 mm soil depth in tank of 349 mm diameter

Vt= 17.219x10^{-3} m^3

Volume of solid (Vs)=Ms/Gs(2.64)*1000(ρ_w)in kg/m^3

Ms = 23.55 kg

Vs=23.55/2.64*1000

Vs= 8.92x$10^{-3}m^3$

Vv=Vt-Vs

Vv=8.299x10^{-3} m^3

but Vv=Vair+Vwater

Vwater=weight water/γw

Weight of soil occupy 180 mm depth=23.55 kg

Weight water from 9. 13% water content (from feasibility test) in soil weight 23.55 kg

=2.143 kg, so Vwater= 2.140x10^{-3} m^3

V_{air}=Vv-Vw

V_{air}=8.299x10^{-3}-2.140x10^{-3} =6.150x$10^{-3}m^3$=6.15 L

So adding 6.15 L of water to the soil will fill air voids cover the depth 180 mm (half the tank)

Saturation after soaking with 6.15 litres

Since Vv for 60 mm depth=2.77 $x10^{-3}$ m^3

Total Vv in the whole tank=2.77 $x10^{-3}$ *6= 16.595$x10^{-3}$ m^3

V_w= 6.15 $x10^{-3}$ m^3+4.286$x10^{-3}$ m^3 (9.1%wcontent whole the tank)= 10.436$x10^{-3}m^3$====

S=10.436$x10^{-3}$/16.595$x10^{-3}$ = 62. 9%

C7. Calculating the saturated soil depth resulting from adding 2.73L of water

Since adding 6.15 L of water will saturate 180 mm depth of soil, then adding 2.73 L of water will be enough to saturate a soil depth of 79.77 mm only.

Weight of the soil to fill79.77 mm depth = 10.44 kg

V_s= 10.44/(2.64*1000)= 3.950$x10^{-3}$ m^3

e=V_v/V_s leads V_v= e.V_s then V_v=0.93*3.950$x10^{-3}$ = 3.677$x10^{-3}$ m^3

but V_v=V_{air}+V_{water} that yields

V_{water}=weight $_{water}/\gamma_w$

Weight of water for 9. 13% water content (from feasibility test) in soil weight 10.44 kg=

0.95004 kg so V_{water}= 0.95$x10^{-3}$ m^3 , V_{air}=V_v-V_w

V_{air}=3.677$x10^{-3}$ m^3-0.95$x10^{-3}$ m^3= 2.727$x10^{-3}m^3$ ==2.73 Litre per 79.77 mm depth

So 2.73=equal depth of 79.77 mm

V_w=V_w from adding water+ V_w from (9.13% wc) for the remaining depth of the tank 280.23 mm

Weight of water corresponding to the remaining weight of soil = 3.82 kg

V_w for 280.23 mm depth =3.82$x10^{-3}$ m^3

V_w= 2.727$x10^{-3}m^3$+ 3.82$x10^{-3}$ m^3= 6.55$x10^{-3}$ m^3

S = V_w/V_v × 100%

Since V_v for 60 mm depth=2.77$x10^{-3}$ m^3

Total Vv in the whole tank= 2.77$x10^{-3}$ *6= 16.595$x10^{-3}$ m^3

Vv =16.595$x10^{-3}$ m^3

S=6.55$x10^{-3}$ /16.595$x10^{-3}$ == 40%

APPENDIX (D)

Table C-1: The configuration of the thirty two electrodes over one ring, 128 measurements, C1 and C2: current electrodes, P1 and p2: Potential electrodes

Readings No.	C1	C2	P1	P2
1	1	2	3	4
2	5	6	7	8
3	9	10	11	12
4	13	14	15	16
5	17	18	19	20
6	21	22	23	24
7	25	26	27	28
8	29	30	31	32
9	1	2	5	6
10	7	8	9	10
11	11	12	13	14
12	15	16	17	18
13	19	20	21	22
14	23	24	25	26
15	27	28	29	30
16	1	2	7	8
17	3	4	5	6
18	9	10	13	14
19	11	12	15	16
20	13	14	17	18
21	19	20	23	24
22	21	22	25	26
23	27	28	31	32
24	1	2	9	10
25	17	18	21	22
26	3	4	7	8
27	5	6	9	10
28	21	22	31	32
29	11	12	17	18
30	19	20	29	30
31	3	4	13	14
32	1	2	21	22
33	5	6	29	30
34	11	12	31	32
35	1	2	17	18
36	7	8	23	24
37	5	6	17	18
38	25	26	31	32
39	5	6	23	24

40	3	4	19	20
41	7	8	15	16
42	9	10	23	24
43	3	4	11	12
44	7	8	19	20
45	13	14	25	26
46	7	8	29	30
47	17	18	27	28
48	1	2	29	30
49	9	10	17	18
50	3	4	25	26
51	9	10	21	22
52	15	16	27	28
53	1	2	25	26
54	13	14	31	32
55	9	10	15	16
56	11	12	25	26
57	1	2	31	32
58	7	8	21	22
59	15	16	23	24
60	9	10	31	32
61	1	2	15	16
62	25	26	29	30
63	11	12	21	22
64	17	18	31	32
65	7	8	17	18
66	13	14	21	22
67	23	24	29	30
68	11	12	19	20
69	1	2	27	28
70	3	4	29	30
71	13	14	19	20
72	21	22	29	30
73	7	8	31	32
74	5	6	13	14
75	21	22	27	28
76	9	10	19	20
77	3	4	17	18
78	23	24	27	28
79	13	14	23	24
80	5	6	11	12
81	15	16	19	20
82	23	24	31	32
83	1	2	13	14

84	15	16	29	30
85	19	20	25	26
86	1	2	11	12
87	15	16	21	22
88	17	18	29	30
89	3	4	9	10
90	11	12	29	30
91	19	20	31	32
92	17	18	25	26
93	7	8	13	14
94	19	20	27	28
95	17	18	23	24
96	5	6	15	16
97	13	14	27	28
98	3	4	21	22
99	15	16	31	32
100	1	2	19	20
101	9	10	29	30
102	15	16	25	26
103	11	12	27	28
104	3	4	31	32
105	9	10	25	26
106	3	4	15	16
107	7	8	25	26
108	3	4	27	28
109	13	14	29	30
110	5	6	19	20
111	1	2	23	24
112	9	10	27	28
113	5	6	25	26
114	11	12	23	24
115	5	6	27	28
116	3	4	23	24
117	7	8	11	12
118	5	6	21	22
119	7	8	27	28
120	5	6	31	32
121	1	4	9	12
122	17	20	25	28
123	1	8	17	24
124	1	4	17	20
125	9	12	25	28
126	1	4	25	28
127	9	16	25	32

128	9	12	17	20

Table D-2: The configuration of the thirty two electrodes over the two vertical arrays, 111 measurements, C1 and C2: current electrodes, P1 and p2: Potential electrodes

Readings No.	C1	C2	P1	P2
1	1	2	3	4
2	32	31	30	29
3	2	3	4	5
4	31	30	29	28
5	3	4	5	6
6	30	29	28	27
7	4	5	6	7
8	29	28	27	26
9	5	6	7	8
10	28	27	26	25
11	6	7	8	9
12	27	26	25	24
13	7	8	9	10
14	26	25	24	23
15	8	9	10	11
16	25	24	23	22
17	9	10	11	12
18	24	23	22	21
19	10	11	12	13
20	23	22	21	20
21	11	12	13	14
22	22	21	20	19
23	12	13	14	15
24	21	20	19	18
25	13	14	15	16
26	20	19	18	17
27	1	2	5	6
28	32	31	28	27
29	2	3	6	7
30	31	30	27	26
31	3	4	7	8
32	30	29	26	25
33	4	5	8	9
34	29	28	25	24
35	5	6	9	10
36	28	27	24	23
37	6	7	10	11
38	27	26	23	22
39	7	8	11	12

40	26	25	22	21
41	8	9	12	13
42	25	24	21	20
43	9	10	13	14
44	24	23	20	19
45	10	11	14	15
46	23	22	19	18
47	11	12	15	16
48	22	21	18	17
49	1	2	7	8
50	32	31	26	25
51	2	3	8	9
52	31	30	25	24
53	3	4	9	10
54	30	29	24	23
55	4	5	10	11
56	29	28	23	22
57	5	6	11	12
58	28	27	22	21
59	6	7	12	13
60	27	26	21	20
61	7	8	13	14
62	26	25	20	19
63	8	9	14	15
64	25	24	19	18
65	9	10	15	16
66	24	23	18	17
67	1	2	9	10
68	32	31	24	23
69	2	3	10	11
70	31	30	23	22
71	3	4	11	12
72	30	29	22	21
73	4	5	12	13
74	29	28	21	20
75	5	6	13	14
76	28	27	20	19
77	6	7	14	15
78	27	26	19	18
79	7	8	15	16
80	26	25	18	17
81	1	2	11	12
82	32	31	22	21
83	2	3	12	13

84	31	30	21	20
85	3	4	13	14
86	30	29	20	19
87	4	5	14	15
88	29	28	19	18
89	5	6	15	16
90	28	27	18	17
91	1	2	13	14
92	32	31	20	19
93	2	3	14	15
94	31	30	19	18
95	3	4	15	16
96	30	29	18	17
97	1	2	15	16
98	32	31	18	17
99	32	29	1	4
100	31	28	2	5
101	30	27	3	6
102	29	26	4	7
103	28	25	5	8
104	27	24	6	9
105	26	23	7	10
106	25	22	8	11
107	24	21	9	12
108	23	20	10	13
109	22	19	11	14
110	21	18	12	15
111	20	17	13	16

APPENDIX (E)

```
clear

% Matlab Code to determine ultimate bearing capacity

%d=diameter of stone column in m

%l=length of stone column in m

%phi_stone=angle of internal shear resistance of the column fill material in degrees

prompt1 = 'Input the stone column properties and geometry values in [d, l, phi_stone] format?;

 result1=input(prompt1);

d = result1(1);

l = result1(2);

phi_stone= result1(3)*(pi/180);

%phi_sat=effective angle of internal shear resistance of the soil in case of saturation in degrees

%c_sat= effective cohesion of soil in kPa

%gamma_d=dry unit weight of soil in kN/cubic meter

%gamma_sat=saturated unit weight of soil in kN/cubic meter

%gamma_w=unit weight of water in kN/cubic meter

%Gs=specific gravity of soil

%e=void ratio of soil

prompt2 = 'Input the Soil properties values in [phi_sat, c_sat, gamma_d, gamma_sat, gamma_w, Gs,
e] format? ';

result2=input(prompt2);

phi_sat=result2(1)*(pi/180);

c_sat=result2(2);

gamma_d=result2(3);

gamma_sat=result2(4);

gamma_w=result2(5);

Gs=result2(6);

e=result2(7);
```

```
phi_sat=24.88*(pi/180);

%Ts=tensile strength of the geosynthetic in KN/m

%t=thickness of the geosynthetic in m

prompt3 = 'Input Geotextile properties values in [Ts,t] format? ';

result3=input(prompt3);

Ts=result3(1);

t=result3(2);

prompt4 = ' Input 1 if there is an encasement otherwise 0 ?';

result4= input(prompt4);

delta_enc=result4;

prompt5= 'Input the depth of inundation hs? ';

result5=input(prompt5);

hs=result5;

prompt6= 'Input the total depth of the soil layer h? ';

result6=input(prompt6);

h=result6;

prompt6= 'Input the matric suction from the soil water characteristics suction? ';

%kp=coefficient of passive earth pressure of the stone column material

%ko=coefficient of earth pressure at rest of the soil

kp=(tan((pi/4)+(phi_stone/2)))^2;

ko= 1-sin(phi_sat);

%s=degree of saturation

s= hs/h;

%w=water content

w=(s*100*e)/Gs;

% Suction equation from soil water characteristic curve (SWCC)

  p1 =  -0.0001144;
```

```
    p2 =    0.01548;
    p3 =    -0.7774;
    p4 =      18.66;
    p5 =     -221.8;
    p6 =       1105;
suction=p1*w^5+ p2*w^4+ p3*w^3+p4*w^2+p5*w+p6;
%uw=pore water pressure
%x=Coefficient of inundation
%T=drained shear strength of the soil
%sigma_n=effective normal stress
%sigma_ro=effective lateral stress
%sigma_v= effective vertical stress
%delta_geosynthetic=stress provided by encasement
% sigma_vf =Ultimate bearing capacity of the foundation
if  (hs==0 && hs~=h)
uw=0;
h=h-hs;
gamma=gamma_d;
sigma_v=(gamma*(h));
 sigma_ro=ko*(gamma*(h));
    x=1;
   sigma_n=(sigma_v+sigma_ro)/2;
   T=c_sat+(sigma_n-uw)*tan(phi_sat)+suction*x*tan(phi_sat);
     if delta_enc==1
      delta_geosynthetic=(Ts*t)/((d/2)^2);
      sigma_vf=kp*(4*T+sigma_ro+delta_geosynthetic);
      disp('Ultimate Bearing Capacity=');disp(sigma_vf);
```

```
        else
      delta_geostnthetic=0;
      sigma_vf=kp*(4*T+sigma_ro);
            disp('Ultimate Bearing Capacity=');disp(sigma_vf);
    end
elseif hs~=h
    x=1-(hs/h);
    uw=hs*gamma_w;
    gamma=gamma_sat-gamma_w;
    sigma_v=(gamma_d*(h-hs))+(gamma*(hs));
    sigma_ro=ko *((gamma_d*(h-hs)))+ko*(gamma*(hs));
    sigma_n=(sigma_v+sigma_ro)/2;
    T=c_sat+(sigma_n-uw)*tan(phi_sat)+suction*x*tan(phi_sat);
       if delta_enc==1
      delta_geosynthetic=(Ts*t)/((d/2)^2);
      sigma_vf=kp*(4*T+sigma_ro+delta_geosynthetic);
      disp('Ultimate Bearing Capacity=');disp(sigma_vf);
        else
      delta_geosynthetic=0;
      sigma_vf=kp*(4*T+sigma_ro);
      disp('Ultimate Bearing Capacity');disp(sigma_vf);
    end
     else
    gamma=gamma_sat-gamma_w;
    h=hs;
    x=0;
    uw=h*gamma_w;
```

```
sigma_v=(gamma*(h));
sigma_ro=ko*(gamma*(h));
sigma_n=(sigma_v+sigma_ro)/2;
 T=c_sat+(sigma_n-uw)*tan(phi_sat)+suction*x*tan(phi_sat);
    if delta_enc==1
   delta_geosynthetic=(Ts*t)/((d/2)^2);
   sigma_vf=kp*(4*T+sigma_ro+delta_geosynthetic);
   disp('Ultimate Bearing Capacity');disp(sigma_vf);
else
   delta_geosynthetic=0;
   sigma_vf=kp*(4*T+sigma_ro);
   disp('Ultimate Bearing Capacity');disp(sigma_vf);
end
```